Thermodynamic and Dynamic Modeling of Atmospheric Aerosols

Thesis by

Zhaoyue Meng

In Partial Fulfillment of the Requirements

for the Degree of

Doctor of Philosophy

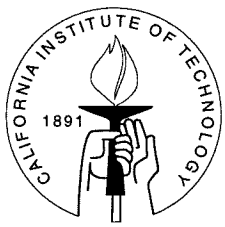

California Institute of Technology

Pasadena, California

1997

(Submitted March 6, 1997)

Acknowledgments

First, I would like to express my sincere gratitude to my advisor, Professor John H. Seinfeld, for his guidance, support, and encouragement throughout my graduate study at Caltech. His creativity and scientific insights have been my constant inspiration.

I am grateful to Professors Glen R. Cass, Richard C. Flagan, Michael R. Hoffmann, and Yuk L. Yung, for sacrificing their valuable time to be involved in my advisory committee. I am particularly thankful to Professor Cass; as the Option Representative of Environmental Engineering Science, he has helped me in many aspects of my graduate life at Caltech. I thank our librarians, Rayma Harrison and Susan Leising, for their patience with my constant bothering. I should also thank Fran Matzen, Shirley A. Anderson, Andrea Wilson, Linda L. Scott, Marta Goodman, Jennifer S. Packman, and Marlys M. Murray for their secretarial assistance and helps.

Many thanks go to the various past and present members of the "Air Pollution/Aerosols Group" family, Yong Pyo Kim, Donald Dabdub, Spyros Pandis, Jay Odum, Chris Pilinis, and Frank M. Bowman, for providing their valuable ideas and discussions. Dr. Kim has helped me in aerosol thermodynamic modeling. Dr. Dabdub has given me tremendous helps while we have been working together closely on airshed modeling. I would also like to thank Suresha Guptha at Caltech for providing computing assistance and Laurel DeHaan at University of California at Irvine for helping in visualization of our 3-D aerosol dynamic model. I am also indebted to Dr. Pradeep Saxena at Electric Power Research Institute for the support and insightful suggestions.

I would like to thank my parents for their love, encouragement, and understanding. They have never failed to support me throughout my career.

Finally and most importantly, my deep gratitude goes to my wife, Xiaohua, and my daughter, Karen. Without their enduring and fullhearted love, support, and caring, I would lose some of the very meaning of my life, not to mention reaching this goal.

The research described in this dissertation was mostly sponsored by the Electric Power Research Institute. Its financial support is gratefully acknowledged.

To Xiaohua and Karen

A journey of a thousand li[*]

begins at one's feet. – Lao Tzu

[*] 1 li ≈ 1/3 mile

Abstract

This dissertation investigates thermodynamic and dynamic modeling of urban and regional atmospheric aerosols. A rigorous and efficient aerosol thermodynamic model, SCAPE2, is developed. The model considers the inorganic aerosol system of sulfate, nitrate, ammonium, chloride, sodium, potassium, calcium, magnesium, carbonate, and water. SCAPE2 can be used to predict either the equilibrium gas/aerosol partition of volatile inorganic species or the particle surface vapor concentrations if applied to the aerosol phase only. It has also the option of predicting the equilibrium or metastable aerosol water content.

A three-dimensional, size- and chemically-resolved aerosol dynamic model is developed by incorporating the aerosol thermodynamic model, SCAPE2, into an urban airshed model (CIT model). The model includes advection, turbulent diffusion, condensation/evaporation, nucleation, emissions, and dry deposition. Gas-to-particle conversion is represented by dynamic mass transfer between the gas and aerosol phases. The model employs an absorption approach in dynamically modeling production of secondary organic aerosols. A calculation method for dry deposition of aerosol particles is proposed.

The aerosol model is applied to simulate gas and aerosol behavior in the 27-29 August episode in the 1987 Southern California Air Quality Study (SCAQS). Simulation results are compared systematically against SCAQS measurements, and general good

agreement is observed. The assumption that volatile inorganic species such as NH_4NO_3 are at instantaneous, local equilibrium is examined and it is found that, in many instances, gas/aerosol mass transfer limits the rate of gas-to-particle conversion.

Table of Contents

List of Tables

Chapter 1

Chapter 2

Chapter 3

Chapter 4

Chapter 5

Chapter 6

Chapter 7

List of Figures

Chapter 2

Chapter 3

Chapter 4

Chapter 5

Chapter 6

Chapter 7

Chapter 1

Introduction

Atmospheric aerosols are of paramount importance in urban air pollution control. The particulates can cause health problems, affect visibility, and lead to acid deposition. Atmospheric aerosols typically consist of three modes, the nucleation mode (0.01-0.1 μm diameter), the accumulation mode (0.1-1.0 μm diameter), and the coarse mode (>1 μm diameter). Freshly formed aerosols can frequently deviate from the general atmospheric aerosol size distribution; for instance, ambient measurements in South Coast Air Basin have shown that two distinct modes can exist in the 0.1 - 1.0 μm diameter range (see Chapter 2).

Chemical components of atmospheric aerosols include elemental and organic carbon and a variety of inorganic compounds. The inorganic substances, typically comprising 25-50% of the total aerosol mass (Gray et al., 1986; Heintzenberg, 1989), include sulfate, nitrate, chloride, ammonium, sodium, and crustal species such as aluminum, silicon, calcium, and iron. In the Los Angeles area, particulate carbon accounts for about 40% of the fine particulate mass concentration.

Developing mathematical models of air pollution is extremely useful to study how the pollutants form and transport in the atmosphere. It helps us better understand the interactions among all the physical and chemical aspects that govern the behavior of atmospheric pollutants. Using mathematical models to predict the fate of atmospheric aerosols also facilitates policy makers to assess control strategies. A state-of-the-science model employs the currently best understanding of physics and chemistry; it can be used to predict the response of the ambient air pollution levels to different emission control strategies.

1. Thermodynamic Aerosol Models

The first generation of thermodynamic gas/aerosol equilibrium models can be dated back to 1983, when Bassett and Seinfeld (1983) and Saxena et al. (1983) independently developed two thermodynamic equilibrium models. Earlier works studying aerosol-phase chemistry include those of Peterson and Seinfeld (1979, 1980), Beyak and Peterson (1980), and Orel and Seinfeld (1977). These earlier models treated aerosols as single-phase systems, and considered time-dependent condensation and/or aerosol-phase oxidation of sulfur dioxide. Russell et al. (1983) considered ammonium nitrate in equilibrium with its gas-phase precursors in modeling the formation and transport of ammonium nitrate aerosol. This might be the first effort ever in coupling a gas-phase air quality model to an aerosol equilibrium calculation. The model developed by Saxena et al. (1983) treats aerosols as containing an insoluble core, a soluble solid shell and an aqueous film. The chemical composition of the aerosol phase is governed by the chemical equilibria between the ambient gas and the aerosol liquid phases and between the aerosol liquid and the soluble solid phases. H_2SO_4 is solely controlled by the diffusion-limited condensation process. The liquid-phase chemical reactions of SO_2 are also considered. At about the same time, a more rigorous equilibrium model (EQUIL) was developed by Bassett and Seinfeld (1983). This model set up the basic framework that has influenced all the subsequent equilibrium models.

The model EQUIL is a pure thermodynamic equilibrium model. The partition of all the species, including sulfate, among the gas, liquid and solid phases is solely

controlled by thermodynamic equilibria. Aerosol particles are assumed to be mono-dispersed. Note that a transport calculation for sulfate has to be performed if a particle size distribution is considered. The model uses Kusik and Meissner (1978) (K-M) method to estimate multicomponent activity coefficients and the polynomial regression to estimate binary activity coefficients. It is one of the few equilibrium models that consider the temperature dependence of activity coefficients. Water activity is calculated by the K-M method also. This model only considers three species in the aerosol phase (sulfate, nitrate, and ammonium) and their counterparts in the gas phase (sulfuric acid, nitric acid, and ammonia) besides water. EQUIL is an accurate and robust model that is free from a priori approximation on species concentrations. The negligible species concentrations are calculated and converged too. The model predictions agree well with measurements. Subsequently, Bassett and Seinfeld (1984) extended EQUIL to deal with the particle size distribution and considered the Kelvin effect. This subsequent version of EQUIL is termed as KEQUIL. In KEQUIL the sulfate size distribution has to be a fixed priori because, as noted earlier, thermodynamics does not control the sulfate distribution. It is worth mentioning that inclusion of the Kelvin effect does not necessarily lead to a better improvement of a model's performance. The reason lies in the time scale for mass transfer between particles of different sizes due to the Kelvin effect. For particles larger than 1 μm, the Kelvin effect is generally not important, and the time scale for the equilibrium state to be reached with respect to the Kelvin effect is so long that it may never materialize. EQUIL and KEQUIL demand large computing time as a result of its rigorous treatment of the equilibrium state.

Based on the model EQUIL and a major concern of computational efficiency, Saxena et al. (1986) presented another equilibrium model, MARS (Model for an Aerosol Reacting System), that was intended for incorporation into large-scale air quality models. MARS is basically a simplified version of EQUIL. Given the total concentrations of sulfate, nitrate, and ammonium, MARS first determines which species in the system are important and which are not. The calculation domain is divided according to the molar ratio of total ammonia to sulfate, which is important in determining the chemical composition of the system, and the ambient relative humidity (RH), which determines whether or not a specific solid phase exists. For example, in an ammonia-rich environment ($[NH_3] > 2[H_2SO_4]$) and RH larger than 80%, the model will assume that all the species exist in an aqueous phase and $[HSO_4^-] = 0$ (the stoichiometric sulfate compound is $(NH_4)_2SO_4(aq)$ only). Note that in reality, the equilibrium $H^+ + SO_4^{2-} = HSO_4^-$ will always produce some HSO_4^- in the aerosol solution. These simplifications enable MARS to be very computationally efficient; it is about 400 times faster than KEQUIL and 60 times faster than EQUIL. The disagreement is generally smaller than 5% between the predictions of MARS and EQUIL, and 10% between those of MARS and KEQUIL.

EQUIL, KEQUIL and MARS only consider sulfate, nitrate, and ammonia, the simplest chemical composition of an aerosol system. Ambient measurements have shown that chloride and sodium may also be important in the aerosols, especially in the coastal regions (Russell and Cass, 1984; Orsini et al., 1986; John et al., 1988). Moreover the marine aerosol particles can lose their chloride completely by reaction with sulfuric

acid and/or nitric acid (Hitchcock et al., 1980), shifting the chloride to the gas phase or the smaller sized particles.

Considering the importance of NaCl in aerosols, Pilinis and Seinfeld (1987) developed the equilibrium model SEQUILIB that deals with the gas/aerosol system containing sulfate, nitrate, chloride, sodium, and ammonium. The model uses Bromley (1973) method to estimate multicomponent activity coefficients and the Pitzer method (Pitzer and Mayorga, 1973) to estimate the binary activity coefficients. Temperature dependence of the activity coefficients is not considered in the model. Water activity is estimated by the ZSR method (Robinson and Stokes, 1965). The model is assumed to be able to predict the aerosol size distribution in equilibrium with the gas-phase compounds. In doing so, it requires the given size distributions of non-volatile species (i.e., sulfate and sodium). In some cases, however, thermodynamic equilibria cannot uniquely determine the aerosol size distribution (see Chapter 6); therefore, the model is not expected to be capable of predicting the equilibrium aerosol size distributions in these cases. The technical approach in SEQUILIB is similar to that used in MARS. The full calculation domain is divided according to the ratio of ammonia plus sodium over sulfate molar concentrations and the ambient relative humidity. The unimportant species identified are generally assumed to be zero. The detailed determination of calculation domain has been proven to be very useful in speeding up the computations. In general, SEQUILIB is seven times slower than MARS and five times faster than EQUIL when dealing with the sulfate/nitrate/ammonium only system. SEQUILIB gives results similar to those of EQUIL and MARS when applicable and it successfully predicted the amount of the

aerosol nitrate, ammonium, and chloride existing at Long Beach, California, during the episode of 30-31 August 1982. SEQUILIB has been used as an inorganic aerosol module to calculate the quantities of ammonium, chloride, nitrate, and water contained in atmospheric particles in a size-resolved secondary organic aerosol model (SRSOAM) (Pandis et al., 1993).

Several assumptions used in SEQUILIB may lead to limitations of the model's application. These assumptions are: (1) in sulfate poor cases, H^+ and HSO_4^- are assumed not to exist; (2) in sulfate rich cases, gas-phase ammonia, $NH_3(g)$, is assumed to be zero; (3) in sulfate extremely rich cases (the ammonia plus sodium to sulfate ratio is smaller than 1), SO_4^{2-} is assumed to be zero; (4) if RH is lower than the lowest deliquescence point of the mixture's possible binary salts, aerosol water content is assumed to be zero. Also, SEQUILIB uses the thermodynamic data from a variety of sources, which may not be internally consistent. The first three assumptions in SEQUILIB perhaps do not greatly alter the major species concentrations in the gas phase and liquid phase, but it causes estimation of the H^+ concentration inaccurate. The fourth assumption is not correct theoretically; the deliquescence point of a multicomponent salt is generally lower than the lowest deliquescence point of the mixture's binary salts. And the temperature independence of the deliquescence points assumed in SEQUILIB may lead to even larger inaccuracy. Wexler and Seinfeld (1991) showed that SEQUILIB can considerably underestimate aerosol water content at low RHs.

Considering the weaknesses of SEQUILIB, Kim et al. (1993a, b) developed a second-generation aerosol equilibrium model SCAPE (Simulating Composition of

Atmospheric Particles at Equilibrium). The original goal of developing this model was to maintain the computational efficiency as well as eliminating the ad hoc assumptions that may prevent an accurate prediction of aerosol acidity. Also considering that the previous models have arbitrarily used the activity coefficient estimation methods without an evaluation first, in SCAPE all the three most widely used activity coefficient estimation methods (i.e., Bromley, K-M, and Pitzer) are adopted as options and the guidance of choosing them is given. The ZSR method is used to estimate water activity because of its computational efficiency and acceptable accuracy. The fourth assumption in SEQUILIB is released so that aerosol water content can exist at any humidity in SCAPE only if the equilibrium state is satisfied. The temperature dependency of deliquescence points is also calculated.

The computational approach in SCAPE is as follows. The first step is devoted to calculate the initial concentrations that can serve as a starting point for the iterative solution of the full equilibrium problem. This initial guess of concentrations is actually the one-size version of SEQUILIB. The next step is to calculate the full equilibrium concentrations of the gas and liquid phases without neglecting any species. The equilibrium relations together with the mass balance and electroneutrality equations are then reduced to one equation that includes only the hydrogen ion concentration as the independent variable. After the hydrogen ion concentration is obtained, the entire species concentrations in the gas and liquid phases can then be calculated. Aerosol water content is used as a constraint in this step. After gaseous and aqueous species concentrations are obtained, solid concentrations in the aerosol phase are then calculated. In SCAPE one

has the option to calculate the negligible solid concentrations or not. The solid concentrations are then used as constraints and the full process is iterated until these constraints are satisfied. This computational approach can make SCAPE very accurate.

Some limitations of SCAPE should be mentioned. First, SCAPE does not consider temperature dependence of activity coefficients. This temperature effect has yet to be evaluated. Second, SCAPE has convergence problems at low relative humidities because of use of Newton's method, which is fast but not so robust and its convergence depends on closeness of the initial guess. Third, SCAPE is slow at high nitrate-to-sulfate loadings and low RH's. Finally, SCAPE is a bulk gas/aerosol equilibrium model, which cannot be installed in an airshed photochemical model without modifications.

Another second-generation inorganic aerosol model developed prior to SCAPE is AIM (Aerosol Inorganics Model) (Wexler and Seinfeld, 1991). AIM is actually not a pure aerosol thermodynamic equilibrium model. It first calculates the species surface partial vapor pressures around aerosol particles based on equilibria only in the aerosol phase, then calculates mass transfer between the aerosol and gas phases if the species surface vapor pressures are not equal to those in the bulk gas phase. Therefore, AIM is a model coupling aerosol dynamics and thermodynamics in view of the fact that sometimes thermodynamics cannot uniquely determine the aerosol size distribution. The capability of AIM to predict the particle surface vapor pressures is most useful for it to be coupled in an aerosol dynamic model. AIM is rigorous but computational time consuming. AIM's slow convergence is a result of its rigorous treatment of chemical equilibria; it uses the Gibbs free energy minimization method, which generally requires large computing

time. Kim et al. (1993b) compared the computing times required for several cases by SCAPE and AIM and found that SCAPE is generally considerably faster than AIM. Another weakness of AIM is its neglect of bisulfate ion, HSO_4^-. This makes the model most inaccurate under atmospheric conditions with a large generation of sulfate and insufficient aerosol sodium or ammonium to neutralize the sulfate.

A brief summary of the attributes of the different models is presented in Tables 1.1 and 1.2. It should be noted that SCAPE here is implied as the original version; since then SCAPE has experienced considerable modifications. Description of the current version of SCAPE, termed as SCAPE2, which is developed to be incorporated into an urban/regional aerosol dynamic model, is given in Chapter 7.

2. Three-Dimensional Comprehensive Aerosol Models

Pandis et al. (1992, 1993) used a trajectory model to study the dynamics of secondary organic aerosols. The trajectory aerosol model, as is the case for most of the general Lagrangian air pollution models, assumes simplified turbulent diffusion and no flow convergence/divergence and wind shear. For three-dimensional modeling of complex nonlinear atmospheric chemistry and transports, the Eulerian approach is required (Peters et al., 1995).

Based on an urban airshed model (i.e., CIT model) for gaseous pollutants, Pilinis and Seinfeld (1988) constructed the first 3-D comprehensive aerosol model coupled with the gas phase. The model was applied to the South Coast Air Basin of California and

provided the first 3-D predictions of the concentrations and size distribution of inorganic and organic aerosol species over an urban airshed.

Currently available 3-D comprehensive aerosol models are those developed by Pilinis and Seinfeld (1988); Wexler et al. (1994) and Lurmann et al. (1997); and Binkowski and Shankar (1995). Most of the aerosol models have been developed as modules to be merged with previously developed gas-phase air quality models. The important physical and chemical processes for urban aerosols are advection, turbulent diffusion, emission, sedimentation and deposition, nucleation, coagulation, and condensation/evaporation. All the currently available 3-D aerosol models assume gas-aerosol equilibrium for the volatile inorganic compounds although it has been shown that equilibrium cannot be established under certain conditions (Wexler and Seinfeld, 1990; Meng and Seinfeld, 1996). A more thorough assessment of the 3-D comprehensive aerosol models is given in Chapter 7.

This dissertation consists of eight chapters. Chapter 1 (this chapter) introduces the general background of aerosol thermodynamic and 3-D airshed aerosol modeling. The research works presented in Chapters 2 to 6 have already been published, and can be read independently. In Chapter 2, the mechanisms of formation of the droplet mode in addition to the three typical modes (i.e., nucleation, accumulation, and coarse) of atmospheric aerosols are examined. The most plausible explanation for formation of the droplet mode in aerosol size distribution is proposed. In Chapter 3, aerosol water content and acidity associated with the inorganic fraction of $PM_{2.5}$ and PM_{10} mass in South Coast

Air Basin are evaluated by using a thermodynamic gas/aerosol equilibrium model (SCAPE) and the measured aerosol composition data from the 1987 Southern California Air Quality Study (SCAQS). Chapter 4 is devoted to develop the data and correlations for incorporating carbonate and bicarbonate salts into a gas/aerosol equilibrium model. The species of importance for atmospheric aerosols are considered. Chapter 5 investigates the gas/aerosol distribution of formic and acetic acids for typical sulfate/nitrate/ammonium/sodium/chloride/water aerosols. Chapter 6 studies the time scales to achieve gas-aerosol equilibrium for volatile atmospheric species. This study demonstrates the necessity of dynamic approach in calculating mass transport between the gas and aerosol phases under certain conditions. In Chapter 7, we incorporate a thermodynamic model (SCAPE2) into an urban airshed model (CIT). The episode of 27-29 August in the 1987 SCAQS is simulated with a dynamic approach for the gas-aerosol interaction. Model predictions are compared against SCAQS measurements. Chapter 8 presents summary and conclusions of this thesis research.

REFERENCES

Bassett, M. and Seinfeld, J.H. (1983). *Atmos. Environ.* 17:2237-2252.

Bassett, M. and Seinfeld, J.H. (1984). *Atmos. Environ.* 18:1163-1170.

Beyak, R.A. and Peterson, T.W. (1980). *Ann. N.Y. Acad. Sci.* 338:174-189.

Binkowski, F. S. and Shankar, U. (1995). *J. Geophys. Res.* 100: 26191-26209.

Bromley, L.A. (1973). *AIChE J.* 19:313-320.

Gray, H.A., Cass, G.R., Huntzicker, J.J., Heyerdahl, E.K. and Rau, J.A. (1986). *Envir. Sci. Technol.* 20: 580-589.

Heintzenberg, J. (1989). *Tellus* 41B:149-160.

Hitchcock, D.R., Spiller, L.L. and Wilson, W.E. (1980). *Atmos. Environ.* 14:165-182.

John, W., Wall, S.M. and Ondo, J.L. (1988). *Atmos. Environ.* 22:1627-1635.

Kim, Y.P., Seinfeld, J.H. and Saxena, P. (1993a). *Aerosol Sci. Technol.* 19:157-181.

Kim, Y.P., Seinfeld, J.H. and Saxena, P. (1993b). *Aerosol Sci. Technol.* 19:182-198.

Kusik, C.L. and Meissner, H.P. (1978). *AIChE Symp. Series.* 173:14-20.

Lurmann, F.W., Wexler, A.S., Pandis, S.N., Musarra, S., Kumar, N. and Seinfeld, J.H. (1997). Submitted to *Atmos. Environ.*

Meng, Z. and Seinfeld, J. H. (1996). *Atmos. Environ.* 30: 2889-2900.

Orel, A.E. and Seinfeld, J.H. (1977). *Envir. Sci. Technol.* 11:1000-1007.

Orsini, C.Q., Tabacnicks, M.H., Artaxo, P., Andrade, M.F. and Kerr, A. S. (1986). *Atmos. Environ.* 20:2259-2269.

Pandis, S. N., Harley, R. A., Cass, G. R. and Seinfeld, J. H. (1992). *Atmos. Environ.* 26: 2269-2282.

Pandis, S. N., Wexler, A. S. and Seinfeld, J. H. (1993). *Atmos. Environ.* 27: 2403-2416.

Peters, L. K., Berkowitz, C. M., Carmichael, G. R., Easter, R. C., Fairweather, G., Ghan, S. J., Hales, J. M., Leung, L. R., Pennell, W. R., Potra, F. A., Saylor, R. D. and Tsang, T. T. (1995). *Atmos. Environ.* 29: 189-222.

Peterson, T.W. and Seinfeld, J.H. (1979). *AIChE J.* 25:831-838.

Peterson, T.W. and Seinfeld, J.H. (1980). *Adv. Envir. Sci. Technol.* 10:125-180.

Pilinis, C. and Seinfeld, J.H. (1987). *Atmos. Environ.* 21:2453-2466.

Pilinis, C. and Seinfeld, J. H. (1988). *Atmos. Environ.* 22: 1985-2001.

Pitzer, K.S. and Mayorga, G. (1973). *J. Phys. Chem.* 77:2300-2308.

Robinson, R.A. and Stokes, R.J. (1965). *Electrolyte Solutions.* 2nd ed. Butterworth, London.

Russell, A.G. and Cass, G.R. (1984). *Atmos. Environ.* 18:1815-1827.

Russell, A.G., McRae, G.J. and Cass, G.R. (1983). *Atmos. Environ.* 17:949-964.

Saxena, P., Hudischewskyj, A.B., Seigneur, C. and Seinfeld, J.H. (1986). *Atmos. Environ.* 20:1471-1483.

Saxena, P., Seigneur, C. and Peterson, T.W. (1983). *Atmos. Environ.* 17:1315-1329.

Wexler, A.S., Lurmann, F.W. and Seinfeld, J.H. (1994). *Atmos. Environ.* 28A:531-546.

Wexler, A.S. and Seinfeld, J.H. (1990). *Atmos. Environ.* 24A:1231-1246.

Wexler, A.S. and Seinfeld, J.H. (1991). *Atmos. Environ.* 25A:2731-2748.

Table 1.1. Comparison of thermodynamic treatments in gas-aerosol equilibrium models

	EQUIL, KEQUIL	MARS	SEQUILIB	AIM	SCAPE
Temperature dependence	μ, K, γ, a_w	K	K	μ, *RHD*	K, *RHD*
Binary activity coefficient	Polynomial regression	Pitzer	Pitzer	K-M	K-M
Multicomponent activity coefficient	K-M	Bromley	Bromley	K-M	Bromley, K-M, Pitzer
Water activity	K-M	ZSR	ZSR	ZSR	ZSR
Kelvin effect	Yes	No	No	No	No

[a] μ, K, γ, a_w, and *RHD* are chemical potential, equilibrium constant, activity coefficient, water activity, and relative humidity at deliquescence, respectively.

Table 1.2. Comparison of the attributes of different gas-aerosol equilibrium models

	Model attributes
EQUIL, KEQUIL	Pros: rigorous, accurate, including Kelvin effect Cons: only sulfate/nitrate/ammonium system, slow
MARS	Pros: fast, simple Cons: only sulfate/nitrate/ammonium system, a priori approximation on concentrations, inaccurate in predicting aerosol acidity and aerosol water content at low RH's, RHD's are temperature independent
SEQUILIB	Pros: fast, size resolved Cons: a priori approximation on concentrations, inaccurate in predicting aerosol acidity and aerosol water content at low RH's, RHD's are temperature independent, unique problem in predicting aerosol size distribution under certain conditions
AIM	Pros: rigorous, size resolved, capable of calculating particle surface vapor pressures at any time Cons: slow, exclusion of bisulfate ion, inaccurate in predicting aerosol acidity
SCAPE	Pros: accurate, free of approximation on any species concentrations, fast except in extreme cases Cons: not size resolved, convergence problem at low RH's and high nitrate-to-sulfate ratios

Chapter 2

On The Source of The Submicron Droplet Mode of Urban and Regional Aerosols

[The text of this chapter appears in: Meng Z. and Seinfeld J. H. (1994) *Aerosol Science and Technology* **20**, 253-265.]

ABSTRACT

While atmospheric aerosols are typically described as consisting of three modes, the nucleation mode (0.01-0.1 μm diameter), the accumulation mode (0.1-1.0 μm diameter), and the coarse mode (>1 μm diameter), ambient measurements have shown that two distinct modes can exist in the 0.1 - 1.0 μm diameter range. These modes are referred to as the condensation mode (approximate aerodynamic diameter of 0.2 μm) and the droplet mode (approximate aerodynamic diameter of 0.7 μm). It has been postulated that the droplet mode results from aqueous-phase chemistry (Hering and Friedlander, 1982; John et al., 1990). In this work we examine the mechanisms of formation of the droplet mode. It is shown that growth of condensation mode particles by accretion of water vapor or by gas-phase or aerosol-phase sulfate production cannot explain the existence of the droplet mode. Activation of condensation mode particles to form fog or cloud drops followed by aqueous-phase chemistry and fog evaporation is shown to be a plausible mechanism for formation of the droplet mode.

1. Introduction

Atmospheric aerosols have been described by a trimodal size distribution; the three modes are commonly designated as the nucleation (0.01-0.1 μm), accumulation (0.1-1.0 μm) and coarse (>1 μm) modes (Whitby, 1978; Whitby and Sverdrup, 1980). Several recent measurements of inorganic as well as organic aerosol size distributions, however, have shown that two distinct modes can exist in the 0.1 - 1 μm diameter range. Based on data from the low pressure impactor, Hering and Friedlander (1982) reported two distinct types of fine particle sulfur size distributions in Los Angeles, with mass median aerodynamic diameters of 0.2 μm and 0.54 μm. The larger mode was observed to be associated with heavy sulfate loadings, as much as 52 μg m^{-3}. During the 1980 PEPE-NEROS study near Columbus, Ohio, McMurry and Wilson (1983) found that more sulfur was observed to accumulate in particles larger than 0.5 μm than that which could be accounted for from gas phase reactions alone. More recently, Wall et al. (1988) and John et al. (1990) observed two modes in the 0.1 - 1 μm diameter range for inorganic aerosols in the 1987 Southern California Air Quality Study (SCAQS). Wall et al. observed a bimodal nitrate distribution during both day- and night-time periods. Strong acid was found to be associated with the smaller sulfate mode. John et al. reported the two modes to have aerodynamic diameters of 0.2± 0.1 μm and 0.7±0.2 μm. Nitrate was observed to be internally mixed with sulfate in the aerosols; it has similar mode diameters as the sulfate. The submicron aerosol was almost neutral due to the near-balance of ammonium with sulfate and nitrate. Bimodal organic aerosol size distributions in the 0.1 - 1.0 μm diameter range were also measured during the SCAQS at Claremont (Pickle et

al., 1990; Mylonas et al., 1991). It is not clear from these measurements whether the organics are externally or internally mixed with the inorganic aerosol, but it appears that the existence of a bimodal size distribution for organics is due to secondary formation, associated with photochemical reactions. In a numerical study of the ambient secondary organic aerosol size distribution, Pandis et al. (1993) showed that a bimodal secondary organic aerosol size distribution can result only if there exist sufficient primary particles in the 0.5-1.0 μm diameter size range or if the condensable species have a strong preference (an accommodation coefficient difference of two orders of magnitude) for the 0.5-1.0 μm diameter particles. Similarly, the existence of the inorganic droplet-mode particles will, to some extent, influence or be influenced by the second peak of organics through condensation.

Whereas a number of studies have shown that the smaller mode at around 0.2 μm can be produced by nucleation and/or condensation, the formation mechanism of the observed mode in the 0.5 - 1.0 μm diameter range is not clear. Although it was postulated that the larger mode results from aqueous-phase chemistry (Hering and Friedlander, 1982; John et al., 1990), the precise mechanisms of generation of such a mode have not been examined quantitatively. It is the goal of this work to consider the possible mechanisms that could be responsible for the existence of the larger mode, which was termed the so-called droplet mode by John et al. (1990).

Hering and Friedlander (1982) observed that during the 15 days when the droplet-mode aerosols were measured in the South Coast Air Basin, morning fogs also appeared at the coast in 8 of the 15 days. In the 1987 summer SCAQS, only two fog episodes in the coastal areas were reported. However, low stratus clouds have been observed to cover much of the southern California coastal region during most of the extensive sampling days (see Table 2.1) and to penetrate about 10-15 miles inland. The typical height of these clouds is from 250 to 500 m, which is generally lower than the mixing height (Motallebi, 1993). Low clouds can play the same role as fogs to assist aerosol particles to grow. Although the droplet-mode aerosols were measured every day of the summer SCAQS by John et al. (1990) (droplet modes might not be observed in some individual sampling periods), fogs or clouds were not observed in every instance. It is worth pointing out that the summer sampling period was chosen to study conditions of high oxidant and particulate matter (Hering and Blumenthal, 1989). The meteorological conditions were fairly uniform on the SCAQS intensive sampling days. The existence of the droplet mode observed in the summer and fall SCAQS intensive days does not necessarily mean that such a mode would also exist under significantly different atmospheric conditions.

The possible formation mechanisms of the droplet mode include: (1) direct particle emissions, (2) growth out of the smaller mode, and (3) evaporation of larger droplets. Since the droplet mode has been found to be generally associated with higher relative humidities and higher sulfate/oxidant levels (Hering and Friedlander, 1982), it

cannot be explained as arising solely from primary emissions. Also, sulfate, nitrate, and ammonium are the major components in the droplet-mode particles, and generally they constitute secondary material. By eliminating the possibility of direct emission as the sole source of the droplet mode, we must examine growth out of a smaller mode or evaporation of larger droplets as potential mechanisms of formation. We first consider the possibility of growth from the smaller particles.

2. Growth From the Smaller Mode

Particles grow by coagulation, condensation of gaseous species, water accretion and water accretion followed by aqueous-phase chemistry. At ambient concentration levels formation of the droplet mode by coagulation of submicron particles can be shown to be too slow to account for the growth to the droplet mode within normal residence times available (Hering and Friedlander, 1982).

Water Accretion

Although water accretion alone cannot explain the appearance of the droplet mode simply because of the different chemical compositions of the two modes, it is important to know how large a dry particle can grow as a result solely of increasing ambient relative humidity. The growth of a dry particle of initial diameter D_0 by accretion of water to a diameter D can be expressed in terms of the volumes of its constituents as:

$$\frac{D}{D_0} = \left(\frac{V}{V_0}\right)^{1/3} = \left(1 + \frac{V_{H_2O}}{V_0}\right)^{1/3} \tag{1}$$

where V is the total volume, V_{H2O} is the volume of water in the particle, and the subscript "0" denotes the dry particle. Since the total volume of the dry particle, V_0, can consist in general of both soluble and insoluble constituents, we write V_0 as

$$V_0 = V_{sol} + V_{insol} = (1 + \beta) V_{sol} \tag{2}$$

where $\beta = V_{insol}/V_{sol}$ is the insoluble to soluble volume ratio of the original material. So we can rewrite Eq. (1) as

$$\frac{D}{D_0} = \left(1 + \frac{1}{1+\beta} \frac{M_{H_2O}}{M_{sol}} \frac{\rho_{sol}}{\rho_{H_2O}}\right)^{1/3} \tag{3}$$

where M_{H2O} and M_{sol} are the total mass concentrations of water and soluble materials (μg m^{-3}); and ρ_{H2O} and ρ_{sol} are the mass densities of water and the soluble component (g cm^{-3}).

Using these relations and typical observed aerosol compositions, we will now calculate the size change associated with water accretion. We will take the values of β

and M_{sol} as observed and calculate only M_{H2O} by the thermodynamic-equilibrium code SCAPE (Simulating Composition of Atmospheric Particles at Equilibrium), which determines the minimum of the total Gibbs free energy for a closed multiphase system given the total concentrations of sulfate, nitrate, ammonia, chloride, and sodium and the ambient temperature and relative humidity (Kim et al., 1993ab). The observed inorganic composition of condensation and droplet mode particles in the 1987 summer SCAQS is given in Table 2.2. Throughout the calculation, we fix the temperature to be 298 K. For a given relative humidity, we vary the total ambient ammonia concentration until we find the observed inorganic composition for D_0=0.2 μm particles as given in Table 2.2. We can then obtain from the equilibrium calculation the water M_{H2O} associated with the given inorganic composition for each relative humidity. We have used ρ_{H2O} = 1 g cm^{-3} and ρ_{sol} = 1.75 g cm^{-3}, which is between the density of ammonium sulfate (1.78) and ammonium nitrate (1.73) (Zhang et al., 1992). β was measured to decrease from 5 for particles of 0.04 μm in diameter to 0 for particles larger than 0.6 μm in diameter and was approximately 2 for particles of about 0.2 μm diameter in SCAQS (Zhang et al., 1992). M_{sol} was calculated to be 6.22 μg m^{-3} for the condensation mode from Table 2.2. Fig. 2.1 shows the calculated ratio of the wet particle diameter to the dry particle diameter as a function of relative humidity. Also shown is a data point for the dry 0.2 μm diameter particles in the 1987 SCAQS at Claremont, California. The datum was obtained by a tandem differential mobility analyzer and was averaged over 12 measurements (Zhang et al., 1992). The ratio for the aerodynamic diameters will be even smaller than the calculated values indicated by the curve in Figure 2.1 due to the

decrease of density when the particle absorbs water. Both the observation and theoretical calculations thus show that the condensation-mode particles observed in SCAQS can at best grow to twice their diameter from water accretion alone for relative humidities up to 95%.

Vapor Condensation

Condensation of gaseous species onto preexisting particles is another possible growth mechanism. First, we want to examine whether the observed amount of sulfate in the droplet mode can be produced in the gas phase by SO_2 oxidation within a time scale consistent with typical aerosol residence times.

SO_2 can be oxidized to sulfate in the atmosphere, and reaction with OH radicals is the major SO_2 gas-phase oxidation pathway in the urban environment (Middleton et al., 1980; Saxena and Seigneur,1987). The rate constant for this reaction at 298 K is 1.2×10^{-12} molecule^{-1}cm^{3}s^{-1} (NASA, 1990). Using a summer daytime OH concentration of 5×10^6 molecules cm^{-3} (Lin et al., 1983; Seinfeld, 1986), we can estimate the SO_2 conversion rate by OH radicals at 298 K to be about 2% hr^{-1}. For SO_2 concentrations of 1 and 10 ppb, the typical observed values, for example, in SCAQS at Long Beach, we estimate that the characteristic times required to produce the amount of sulfate in the droplet mode from the condensation mode (see Table 2.2) are 59 and 5.9 hours, respectively. The shorter time scale is attainable if the SO_2 concentration remains close to 10 ppb.

Although the observed total amount of sulfate in the droplet mode may be produced in the gas phase, the droplet-mode aerodynamic diameter of around 0.7 μm cannot be attained through the condensation process. Starting with a 0.32 μm mass median diameter aerosol with σ_g=2.16, Hering and Friedlander (1982) showed that the mass median diameter of the final aerosol size distribution is 0.26 μm for the added aerosol volume to be 30% of the total. They also showed that the mass median diameters for the added aerosol volume size distributions are 0.14-0.16 μm for the new aerosol volume to be 5-60% of the total. For the data we are using, the added aerosol volume is 83% of the total. Based on Hering and Friedlander's analysis, it is unlikely that the droplet-mode particles (~0.2 μm in aerodynamic diameter) can grow into the droplet mode (~0.7 μm) through the pure condensation.

Aerosol Phase Chemistry

Particles may grow as a result of aerosol-phase chemistry. The aqueous-phase oxidation of sulfur dioxide has been frequently studied (Penkett et al., 1979; Chameides, 1984; Jacob,1986), indicating the importance of aqueous phase conversion of SO_2 to SO_4^{2-} in fogs and clouds. However, investigations of the oxidation pathways of SO_2 in wet aerosols have shown that aerosol phase chemistry is not as important as a sulfate generation mechanism as the gas-phase pathway in daytime (Middleton et al., 1980; Peterson and Seinfeld, 1980; Saxena and Seigneur, 1987). Although atmospheric sulfate production is dominated by aqueous-phase paths at night, the overall sulfate production

rate is predicted to be an order of magnitude smaller at night than in the daytime (Saxena and Seigneur, 1987). Nevertheless, we will reexamine here the importance of aqueous-phase sulfate production in submicron aerosols using the recently developed thermodynamic computer code (SCAPE) (Kim et al., 1993ab). We seek to see if sufficient sulfate can be produced to account for growth from the smaller mode to the larger mode. We shall consider the reactions of SO_2 with O_3, H_2O_2, and O_2 catalyzed by Fe^{3+} and Mn^{2+}, since other chemical pathways appear to be insignificant (Saxena and Signeur, 1987). The conversion rate expressions are given in Table 2.3.

For the purpose of estimation, we choose p_{SO_2} = 10 ppb, p_{O_3} = 50 ppb, $p_{H_2O_2}$ = 1 ppb. The metal concentrations are $[Mn^{2+}] = 10^{-5}$ M, which is the typical concentration in the haze aerosols (Martin, 1984b), and $[Fe^{3+}]$ = 0.3 μM, which is the saturation value at pH 5.0 (Martin and Good, 1991). The water content and pH of the wet aerosols used are those for the droplet mode in Table 2.2. The predicted conversion rates are given in Table 2.4. Also given in Table 2.4 are the growth times required for particles starting with the amount of sulfate observed in the condensation mode to achieve the amount of sulfate in the droplet mode (see Table 2.2 for the compositions of the two different modes). The metal catalyzed oxidation mechanisms are predicted to be most influential. However, even for the transition-metal catalyzed pathway, the characteristic time for sulfate to increase from the amount typical of the condensation mode to that of the droplet mode is about 11 - 32 hours, which exceeds that corresponding to gas-phase chemistry at the same ambient SO_2 concentration. Also, since we assumed the water

content to be at its upper limit for the growing aerosols, the actual time needed is likely even longer.

The calculations of Saxena and Seigneur (1987) and our predictions indicate that, based on our current understanding of heterogeneous sulfate-forming reactions, gas-phase oxidation of SO_2 tends to be the dominant daytime sulfate production mechanism for RHs less than 100%. Uncertainties in the kinetics of SO_2 oxidation by O_2 and/or an underestimation of the liquid water available for SO_2 oxidation can affect this prediction. The latter does not seem to be a significant factor for this discrepancy since the normal relative humidity rarely exceeds 90%. In the early morning, the relative humidities can be close to or larger than 100%, and the larger droplets may be formed. We will treat this case later. Pathways of metal catalyzed SO_2 oxidation, indeed, are not well understood at high ionic strengths. Martin and Hill (1987) reported an inhibition effect of ionic strength on the rate of the manganese catalyzed oxidation of sulfur; this inhibition effect may be important for the aerosol-phase chemistry due to its high-ionic-strength characteristics. On the other hand, Berresheim and Jaeschke (1986) studied the removal of SO_2 directly in the presence of different aerosol systems. By using a metal concentration of 55 ng m^{-3} and RH=94%, they obtained an SO_2 removal rate of 2-5% hr^{-1} for $Mn(NO_3)_2$, 1.5% hr^{-1} and 0.09% hr^{-1} for $MnCl_2$ and $MnSO_4$, respectively, at pHs as low as 1.5. If we use 2.5% hr^{-1} as an upper limit of the metal catalyzed liquid-phase reaction rate, it is only comparable with that of the gas-phase chemistry as we have shown above.

General Considerations

Given the major compositions observed in both the condensation and droplet modes, we can estimate the relative growth factor of the diameter D/D_0 between the droplet and condensation modes regardless of the detailed mechanism. By assuming the number concentration is conserved, from Eq. (1) we obtain

$$\frac{D}{D_0} = \left(\frac{V}{V_0}\right)^{1/3} = \left\{\frac{(1+\beta)V_{sol} + V_{H_2O}}{(1+\beta)V_{sol,0}}\right\}^{1/3} \tag{4}$$

or

$$\frac{D}{D_0} = \left\{\frac{(1+\beta)M_{sol} + M_{H_2O}\,\rho_{sol} / \rho_{H_2O}}{(1+\beta_0)M_{sol,0}}\right\}^{1/3} \tag{5}$$

We assume the same β_0, ρ_{sol}, and ρ_{H_2O} as before. Since β drops to 0 for hygroscopic aerosols with diameters larger than 0.6 μm (Zhang et al., 1992), we choose β=0 for the droplet mode particles. M_{H_2O} is calculated by SCAPE given the composition in the droplet mode and the ambient relative humidity. In Figure 2.2, we show the calculated diameter ratio from Eq. (5) as a function of the droplet-mode sulfate, nitrate and chlorine concentration, respectively, while keeping concentrations of the other components at their observed mean values (Table 2.2). The calculated diameter ratio

between the droplet mode and the condensation mode is well below the observed mean value 4.2 in the summer SCAQS. The mean ratio 4.2 of the physical diameters is converted from the measured one, 3.5, of the aerodynamic diameters according to an assumed 80% relative humidity for the droplet-mode particles. Even increasing the sulfate or nitrate concentrations in the droplet mode well beyond those observed, the diameter ratio is still considerably below the observed mean value. The chloride concentration is the least reliable one among the measured species, but from Figure 2.2c we see that within the uncertainty in the chloride measurement the observed droplet-mode diameter also cannot be reproduced. The actual number concentration of the droplet-mode particles is much smaller than that of the condensation mode, implying that all of the condensation-mode particles do not grow to become droplet-mode particles. The above analysis suggests, in short, that the droplet-mode aerosols do not result from growth out of the condensation mode.

3. Fog-Assisted Particle Growth

Formation of small particles can result from a two-step process, the first step of which is the activation of the small particles to form fogs or clouds, followed by the evaporation of the droplets to give residual aerosol. Since aqueous-phase chemistry can occur inside the fog droplets, the residual particles resulting from evaporation can be altered in size and composition from the original cloud condensation nuclei. As noted earlier, high sulfate loadings in Los Angeles have been observed to be correlated with morning fogs (Cass, 1979).

The number concentration of the droplet-mode particles can be estimated from the measured total mass concentration M of droplet mode particles and the mean diameter of the droplet mode as

$$N = \frac{M}{\frac{\pi}{6}\rho D^3} \tag{6}$$

where ρ is the density of the individual droplet-mode particles,

$$\rho = \frac{M_{sol} + M_{H_2O}}{M_{sol}/\rho_{sol} + M_{H_2O}/\rho_{H_2O}} \tag{7}$$

From the data for the droplet mode in Table 2.2 at 80% relative humidity, the number concentration of the droplet-mode aerosols is estimated to be about 390 cm^{-3}. Number concentrations of fog droplets above 2 μm in diameter have been observed to range from 10 to a few hundred cm^{-3} (Garland, 1971). Waldman (1986) measured a fog number concentration of 738 cm^{-3} at 04:30, 11 June 1983 at Henninger Flats, California, with mass median diameter of 25.7 μm and observed an increase of the number concentration and decrease of the mass median diameter with increasing time. From some of the available data, therefore, it appears that the number concentration of the droplet mode is of the same order as that of fogs.

Activation of CCN

At a given supersaturation (RH>100%) particles larger than the critical size will be activated to form fog droplets. The relationship between the saturation ratios and the particle diameter can be written as (Seinfeld, 1986)

$$ln S = \frac{A}{D} - \frac{B}{D^3} \tag{8}$$

where $A = 4\sigma\overline{V}_w/RT$, $B = 6n_B\overline{V}_w/\pi$, σ is surface tension, $\overline{V}_w$ is the molar volume of water, and n_B is the number of moles of solute in the particle. The values of σ and $\overline{V}_w$ are found to be 72 dynes cm^{-1} and 18 cm^3 mol^{-1}, respectively, from CRC Handbook of Chemistry and Physics. n_B can be calculated from the data in Table 2.2. The so-called Köhler curves that result from Eq. (8) are given in Figure 2.3 for particles with the composition of the condensation-mode particles in Table 2.2. In Figure 2.4, we show the critical diameter as a function of the supersaturation ratio. It is predicted that the supersaturation needed to activate particles of the observed composition at 0.2 μm is 0.045%, and 0.025% at 0.3 μm.

To calculate the activated fraction of the particles, we assume an initial log-normal size distribution for the condensation-mode particles,

$$n(D_p) = \frac{N}{\sqrt{2\pi} D_p \ln\sigma} exp[-\frac{(\ln D_p - \ln D_{pg})^2}{2\ln^2 \sigma}] \quad (9)$$

$$n_m(D_p) = \frac{M}{\sqrt{2\pi} D_p \ln\sigma} exp[-\frac{(\ln D_p - \ln D_{pgm})^2}{2\ln^2 \sigma}] \quad (10)$$

where N and M are the total number and mass concentrations, respectively, σ is geometric standard deviation, and $\overline{D}_{pg}$ and $\overline{D}_{pgm}$ are the number and mass median diameters, respectively. $\overline{D}_{pgm}$ is related to $\overline{D}_{pg}$ by $\overline{D}_{pgm} = \overline{D}_{pg} \exp(3\ln^2 \sigma)$. The cumulative number distribution function can be expressed as

$$\frac{F(D_p)}{N} = \frac{1}{2} + \frac{1}{2}\text{erf}[\frac{\ln(D_p / \overline{D}_{pg})}{\sqrt{2}\ln\sigma}] \quad (11)$$

where erf(x) is the error function. The error function can be approximated by $\text{erf}(x) \approx (1 - e^{-4x^2/\pi})^{\frac{1}{2}}$ for x>0 (REA, 1991) . The absolute error for this approximation is smaller than 0.008, and goes to zero when x approaches zero or infinity. Thus, for a certain critical diameter D_{pc} the activated fraction of the total number concentration can be approximated as

$$1-\frac{F(D_{pc})}{N}\approx\frac{1}{2}-\frac{1}{2}\left\{1-exp\left[-\frac{4}{\pi}\left(\frac{ln(D_{pc}/\overline{D}_{pg})}{\sqrt{2}\,ln\,\sigma}\right)^2\right]\right\}^{1/2} \qquad (12)$$

Similarly, we can calculate the activated fraction for the mass concentration. The result is shown in Figure 2.5. For a supersaturation of 0.1%, at 298 K about one-half of the total number of condensation mode particles are predicted to be activated. When the supersaturation reaches 0.4%, all the condensation mode particles are predicted to be activated.

Aqueous-Phase Reaction

In order to calculate the aqueous-phase reactions, we need to know how many fog droplets are present and therefore how many of the condensation-mode particles are activated. Based on the observed data, only a small fraction of the condensation-mode particles should be activated. We do not know what the supersaturation value was under the observed conditions. Above we showed that a supersaturation of 0.1% leads to activation of about one-half of the particles. Since fewer than one-half appears to be activated, we need to assume a supersaturation value somewhat less than 0.1%. We will assume a supersaturation of 0.035%, which leads to about 4% of the condensation-mode particles being activated (see Fig. 2.5). The initial log-normal size distribution of the condensation-mode nuclei around 0.2 μm mass median diameter is used. We also assume that the final fog size is monodisperse, and that activation is essentially

instantaneous. The assumption of a single final fog droplet size leads to a simplification in the calculation. Although the actual fog droplets should be distributed in size, the difference among different droplet sizes should be small for the case considered here. For a supersaturation of 0.035%, the critical particle diameter is 0.24 μm (see Fig. 2.4). For the initial nuclei size distribution used here, all particles above 0.24 μm are activated. These particles constitute about 4% of the total number of particles. Only about 0.4% of the particles exceed 0.34 μm diameter. If we consider that the fog droplets form primarily from particles between 0.24 μm and 0.34 μm, the final fog droplet sizes resulting from particles in this range should be very similar. In a detailed fog formation study by Pandis et al. (1990), such a size range was put into one computational section and the final droplets were represented by one size within one section.

The pH of the fog droplets is used as 5.0 (Waldman, 1986) and the fog is assumed to exist for one hour. Aqueous-phase oxidation of SO_2 to sulfate inside fog droplets is treated similarly to that inside submicron particles except that we now use the aqueous-phase concentration of Fe^{3+} and Mn^{2+} in the fogs as 225 and 33 μg/L (Waldman, 1986) and neglect the oxidation by dissolved ozone (Pandis and Seinfeld, 1989). After fog evaporation, the diameter of the residual particles is calculated according to $D_p = \left(6m/\pi\rho\right)^{1/3}$, where m is the mass of the remaining material, which includes the original CCN mass, the added mass from aqueous-phase chemistry, and the associated water at equilibrium at the relative humidity prevailing after the fog. We present the diameter of the residual particles after evaporation as a function of the fog droplet

diameter in Figure 2.6. We have calculated only sulfate production; nitrate is assumed to be uniformly mixed with sulfate in the particles at an observed mean molar ratio 3.37 for the droplet mode. Ammonium is calculated based on thermodynamic equilibrium by assuming that there exists sufficient NH_3 present in the atmosphere to neutralize the sulfuric and nitric acids in the particles. This assumption seems justified since sulfuric and nitric acids were observed to be neutralized by ammonium in the droplet mode (the overall average ratio of the equivalent ammonium concentration to the sum of nitrate and sulfate measured in the three summer sites is 1.01 without taking into account sodium and chlorine ions). After the fog evaporates, the ambient relative humidity is assumed as 80%. For a given fog diameter at 5 μm, we obtain droplet modes at 0.6 and 0.8 μm diameter for SO_2 concentrations of 1 and 10 ppb, respectively. When the fog diameter is 10 μm, the corresponding droplet modes after evaporation can be as large as 0.9 and 1.5 μm in diameter, for the two SO_2 levels, respectively.

Figure 2.7 shows the total mass concentration of the droplet-mode particles predicted to result from fog evaporation as a function of the initial supersaturation. The assumptions made are the same as those for Figure 2.6. In the South Coast Air Basin of California, fog usually occurs at night or early morning, during which time the SO_2 concentration is around 1 ppb. The curve for 1 ppb SO_2 concentration and 5 μm fog diameter gives a droplet-mode aerosol mass concentration comparable to those measured. In Figure 2.7 we see that the mass concentration saturates when the supersaturation ratio is sufficiently large. This occurs because beyond a certain value of the supersaturation

ratio, all the available CCN are activated. Since the fog diameter is assumed to be fixed, further increase of the supersaturation does not alter the conversion rate of SO_2 to sulfate. Under ambient conditions, the increase of supersaturation will also increase the rate of particle growth, so the fog diameter will itself increase.

4. Conclusions

The important mechanisms that may contribute to particle growth from the atmospheric aerosol condensation mode (about 0.2 μm aerodynamic diameter) to the droplet mode (about 0.7 μm aerodynamic diameter) have been studied. Water accretion alone cannot account for the growth of droplet-mode particles from the condensation mode. Aerosol-phase chemistry as currently understood and gas-phase sulfate formation do not appear to be capable of explaining the existence of the droplet mode as resulting from growth of the condensation mode. The number concentration of droplet mode particles is generally less than that of the condensation mode, also suggestive of mechanisms other than direct growth of the condensation mode.

Activation of condensation mode particles to form fogs or clouds followed by aqueous-phase sulfate formation and fog evaporation is shown to be a plausible mechanism for formation of the urban and regional aerosol droplet mode.

Acknowledgments

This work was supported by the Electric Power Research Institute under agreement RP3189-03.

REFERENCES

Appel, B. R., Tokiwa, Y., Wu, Y., Povard, V. and Kothny, E. L. (1987). *Southern California Air Quality Study - Summer Phase.* Final report, California Air Resources Board, Sacramento, California.

Berresheim, H. and Jaeschke, W. (1986). *J. Atmos. Chemistry.* 4:311-334.

Cass, G. R. (1979). *Atmos. Environ.* 13:1069-1084.

Chameides, W. L. (1984). *J. Geophys. Res.* 89:4739-4755.

Garland, J. A. (1971). *Quart. J. R. Met. Soc.* 97:483-494.

Hering, S. V., and Blumenthal, D. L. (1989). *Southern California Air Quality Study (SCAQS) - Description of Measurement Activities.* Final report, California Air Resources Board, Sacramento, California.

Hering, S. V. and Friedlander, S. K. (1982). *Atmos. Environ.* 16:2647-2656.

Hoffmann, M. R. and Calvert, J. G. (1985). *Chemical Transformation Modules For Eulerian Acid Deposition Models, Vol. 2, The Aqueous-phase Chemistry.* EPA/600/3-85/017, U.S. Environ. Prot. Agency, Research Triangle Park, N. C.

InstaWeather, Inc. (1989). *A Weather Satellite Documentation of the 1987 SCAQS Intensive Days.* InstaWeather, Inc., Ontario, California.

Jacob, D. J. (1986). *J. Geophys. Res.* 91:9807-9826.

John, W., Wall, S. M., Ondo, J. L. and Winklmayr, W. (1990). *Atmos. Environ.* 24A:2349-2359.

Kim, P. Y., Seinfeld, J. H. and Saxena, P. (1993a). *Aerosol Sci. Technol.* In press.

Kim, P. Y., Seinfeld, J. H. and Saxena, P. (1993b). *Aerosol Sci. Technol.* In press.

King, D., Wheeler, N., Wagner, K. and Patton, E. (1990). *Southern California Air Quality Study Modeling Data Archive.* California Air Resources Board, Sacramento, California.

Lin, X., Chameides, W. L., Kiang, C. S., Stelson, A. W. and Berresheim, H. (1992). *J. Geophys. Res.* 97:18,161-18,171.

Martin, L. R. (1984a). In *SO_2, NO And NO_2 Oxidation Mechanisms: Atmospheric Considerations* (J. G. Calvert, ed.). Ann Arbor Sci., Boston. p. 63.

Martin, L. R. (1984b). In *Conference on Gas-Liquid Chemistry of Neutral Waters.* Brookhaven National Laboratory, Upton, NY.

Martin, L. R. and Hill, M. W. (1987). *Atmos. Environ.* 21:2267-2270.

Martin, L. R. and Good, T. W. (1991). *Atmos. Environ.* 25A:2395-22399.

McMurry, P. H. and Wilson, J. C. (1983). *J. Geophys. Res.* 88:5101-5108.

Middleton, P., Kiang, C. S. and Mohnen, V. A. (1980). *Atmos. Environ.* 14:463-472.

Motallebi, N. (1993). California Air Resources Board, Sacramento, California. Personal communication.

Mylonas, D. T., Allen, D. T., Ehrman, S. H. and Pratsinis, S. E. (1991). *Atmos. Environ.* 25A:2855-2861.

NASA (1990) *Chemical kinetics and photochemical data for use in stratospheric modeling*, Evaluation 9.

Pandis, S. N. and Seinfeld, J. H. (1989). *J. Geophys. Res.* 94:12,911-12,923.

Pandis, S. N. and Seinfeld, J. H. (1990). *Atmos. Environ.* 24A:1957-1969.

Pandis, S. N., Wexler, A. S. and Seinfeld, J. H. (1993). Submitted to *Atmos. Environ.*

Penkett, S. A., Jones, M. R., Brice, K. A. and Eggleton, A. E. (1979). *Atmos. Environ.* 13:123-137.

Peterson, T. W. and Seinfeld, J. H. (1980). *Adv. Environ. Sci. Technol.* 10:125-180.

Pickle, T., Allen, D. T. and Pratsinis, S. E. (1990). *Atmos. Environ.* 24:2221-2228.

REA (Research & Education Association) (1991) *Handbook of Mathematical, Scientific, and Engineering Formulas, Tables, Functions, Graphs, Transforms.* Piscataway, New Jersey. p. 493.

Saxena, P. and Seigneur, C. (1987). *Atmos. Environ.* 21:807-812.

Seinfeld, J. H. (1986) *Atmospheric Chemistry and Physics of Air Pollution.* John Wiley, New York. p. 348.

Waldman, J. M. (1986) *Depositional aspects of pollutant behavior in fog*, Ph.D. thesis, Calif. Inst. of Technol., Pasadena.

Wall, S. M., John, W. and Ondo, J. L. (1988). *Atmos. Environ.* 22:1649-1656.

Whitby, K. T. (1978). *Atmos. Environ.* 12:135-159.

Whitby, K. T. and Sverdrup, G. M. (1980). In *The Character and Origins of Smog Aerosols* (C. M. Hidy et al., eds.). John Wiley, New York. p. 477.

Zhang, X. Q., McMurry, P. H., Hering, S. V. and Casuccio, G. S. (1992). Submitted to *Atmos. Environ.*

Table 2.1. Observation of fogs and low clouds over the coastal areas and the droplet-mode aerosols in the 1987 summer SCAQS†

Summer SCAQS Days	Fogs	Low Clouds (lower than 500 m)	Droplet Mode Aerosol
6/19	No	Yes	Yes
6/20	No	-	Yes
6/24	No	Yes	Yes
6/25	No	Yes	Yes
7/13	Yes	Yes	Yes
7/14	No	Yes	Yes
7/15	No	Yes	Yes
8/27	No	No	Yes
8/28	No	Yes	Yes
8/29	No	Yes	Yes
8/30	Yes	-	Yes
9/2	No	No	Yes
9/3	No	Yes	Yes

†The measurements of fogs and clouds shown here are only for the coastal areas. Two fog events reported here are inferred from the relative humidity data measured at Long Beach City College (Appel et al., 1987). Cloud measurements are obtained from the Weather Satellite Photos (InstaWeather, 1989) and *SCAQS Modeling Data Archive of California Air Resources Board (CARB) (King et al., 1990).* Droplet-mode aerosols were measured in all three sampling sites, Long Beach near the Pacific Coast, Claremont inland, and Rubidoux near the eastern end of the South Coast Air Basin, by John et al. (1990).

Table 2.2. Observed composition of condensation and droplet mode particles in the Southern California Air Quality Study (SCAQS) (John et al., 1990) and calculated water content and pH at thermodynamic equilibrium at different relative humidities

	Composition (neq/m^3)[a]					Calculated properties[b]			
						Water content (μg/m^3)		pH	
Mode	NH_4	NO_3	SO_4	Na	Cl	RH = 0.8	RH = 0.9	RH = 0.8	RH = 0.9
Condensation (0.2 μm)	75 ± 84	50 ± 90	24 ± 18	10 ± 0	10 ± 14	8.8	19	4.75	4.84
Droplet (0.7 μm)	352 ± 283	219 ± 238	129 ± 66	-	21 ± 12	36	81	4.43	4.55

[a] Data are from the 1987 summer SCAQS-Long Beach, Claremont and Rubidox, and the sizes given for the mode are the measured mean aerodynamic diameters (John et al., 1990).

[b] Data are calculated with the gas-aerosol equilibrium code SCAPE (Kim et al., 1993ab).

Table 2.3. SO_2 oxidation rate expressions[a]

O_3: $R_{O_3} = L\left\{k_0[SO_2(aq)] + k_1[HSO_3^-] + k_2[SO_3^=]\right\}[O_3(aq)]/[SO_2(gas)]$

$k_0 = 2.4\times10^4 M^{-1}s^{-1}$ at 298 K

$k_1 = 3.7\times10^5 M^{-1}s^{-1}$

$k_2 = 1.5\times10^9 M^{-1}s^{-1}$ Hoffmann and Calvert (1985)

H_2O_2: $R_{H_2O_2} = L\dfrac{k[H^+][HSO_3^-][H_2O_2(aq)]}{1+K[H^+]}\dfrac{1}{[SO_2(gas)]}$

$k = 7.45\times10^7 M^{-2}s^{-1}$ at 298 K

$K = 13M^{-1}$ Hoffmann and Calvert (1985)

Fe^{3+} & Mn^{2+}:

$$R_{metal} = L\left\{4.7[H^+]^{-1}[Mn^{2+}]^2 + 0.82[H^+]^{-1}[Fe^{3+}][S(IV)]\sigma\right\}/[SO_2(gas)]$$

$$\sigma = 1+\frac{1.70\times10^3[Mn^{2+}]^{1.5}}{6.31\times10^{-6}+[Fe^{3+}]}, \text{ for } [S(IV)]>10^{-4}M, \text{ pH } 0-4 \text{ and}$$

$$R_{metal} = L\left\{4.7[H^+]^{-1}[Mn^{2+}]^2 + 1\times10^7[Fe^{3+}][S(IV)]^2\right\}/[SO_2(gas)]$$

for $[S(IV)]>10^{-4}M$, pH $4-7$ Martin (1984a)

[a] L is water content expressed in μg m^{-3}, $[SO_2(gas)]$ is in units of nmol m^{-3} and the conversion rates are in units of s^{-1}.

Table 2.4. Aerosol-phase sulfate conversion rates and estimated times for particles with the composition of the condensation mode to grow to the composition of the droplet mode at 80% and 90% relative humidities

Mode	O_3	H_2O_2 RH=80%	Metal	O_3	H_2O_2 RH=90%	Metal
Conversion rates (%/hr)	0.0002	0.027	0.40	0.0007	0.06	1.19
Growth time (hr)	6.6×10^4	468	32	1.7×10^4	208	10.8

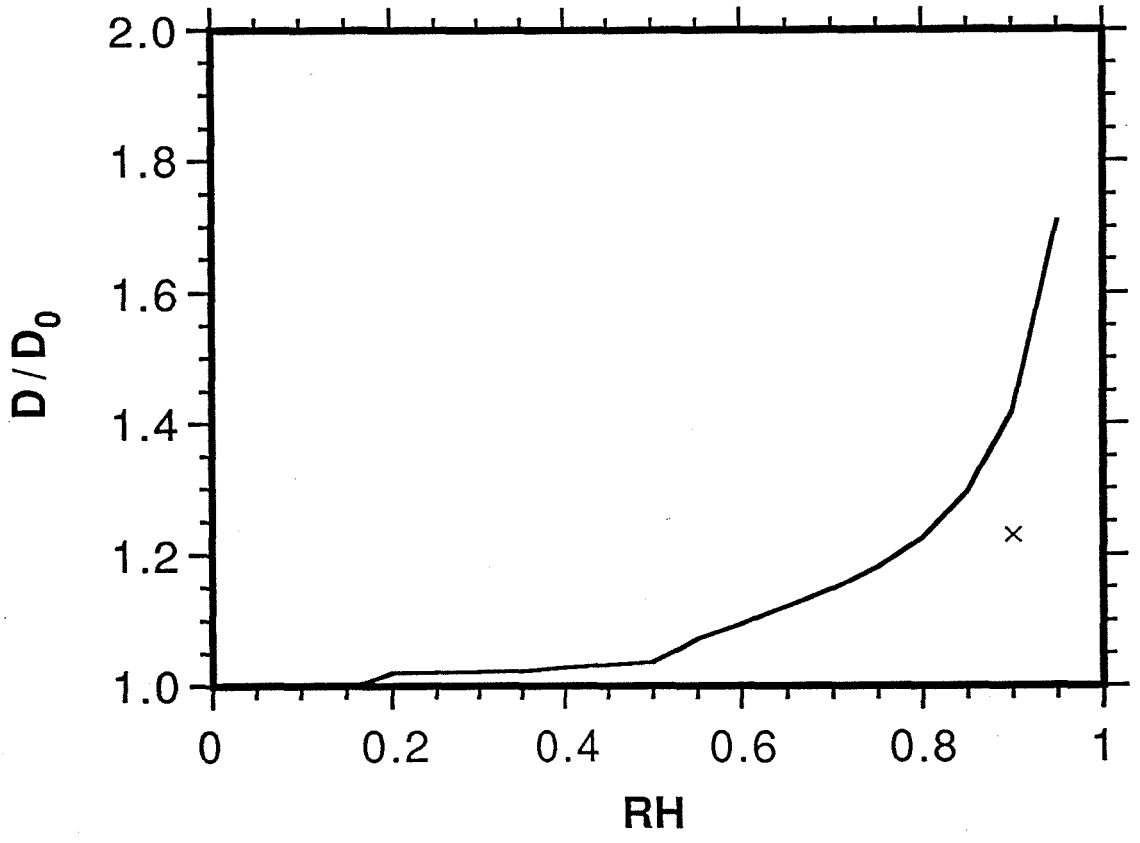

Fig. 2.1 The diameter growth factor as a function of the relative humidity for accretion of water by particles. The curve is calculated by the gas-aerosol equilibrium code SCAPE by assuming the mean condensation-mode composition of Table 2.2. The data point is the observed value at RH=80% in SCAQS at Claremont, CA.

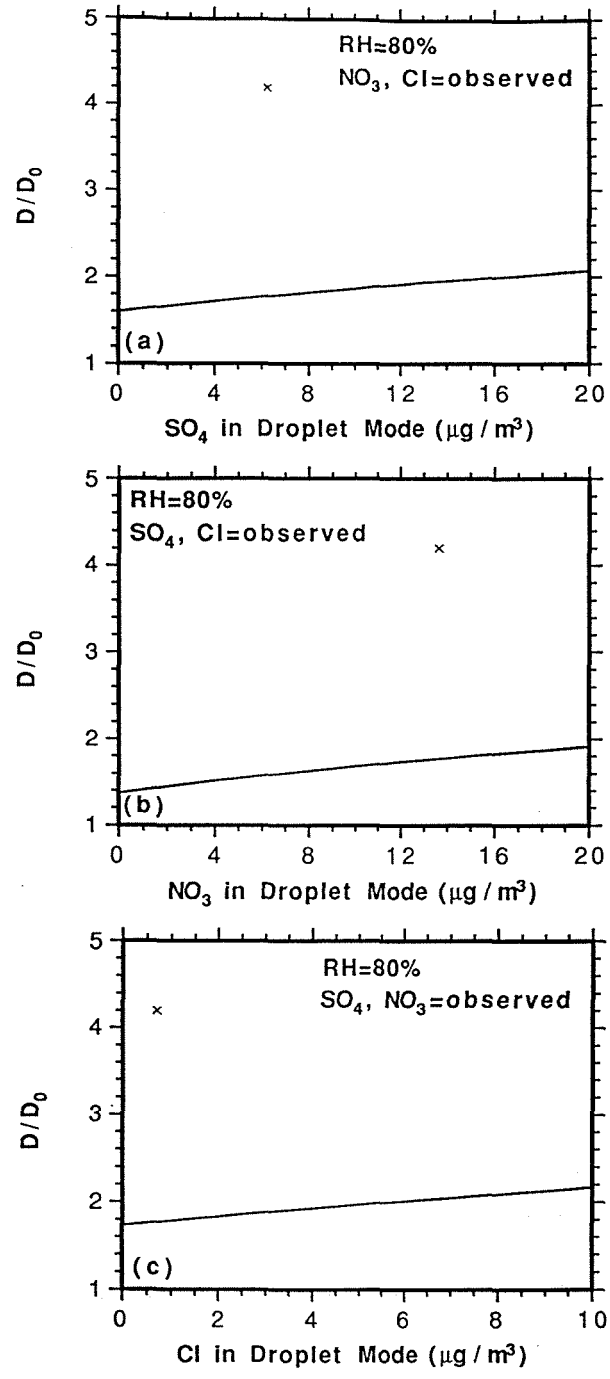

Fig. 2.2 Calculated diameter ratio of the droplet mode to the condensation mode as a function of (a) sulfate, (b) nitrate, and (c) chloride in droplet-mode particles at 80% relative humidity, with the concentrations of other components as observed. The data points are observed mean values in summer SCAQS.

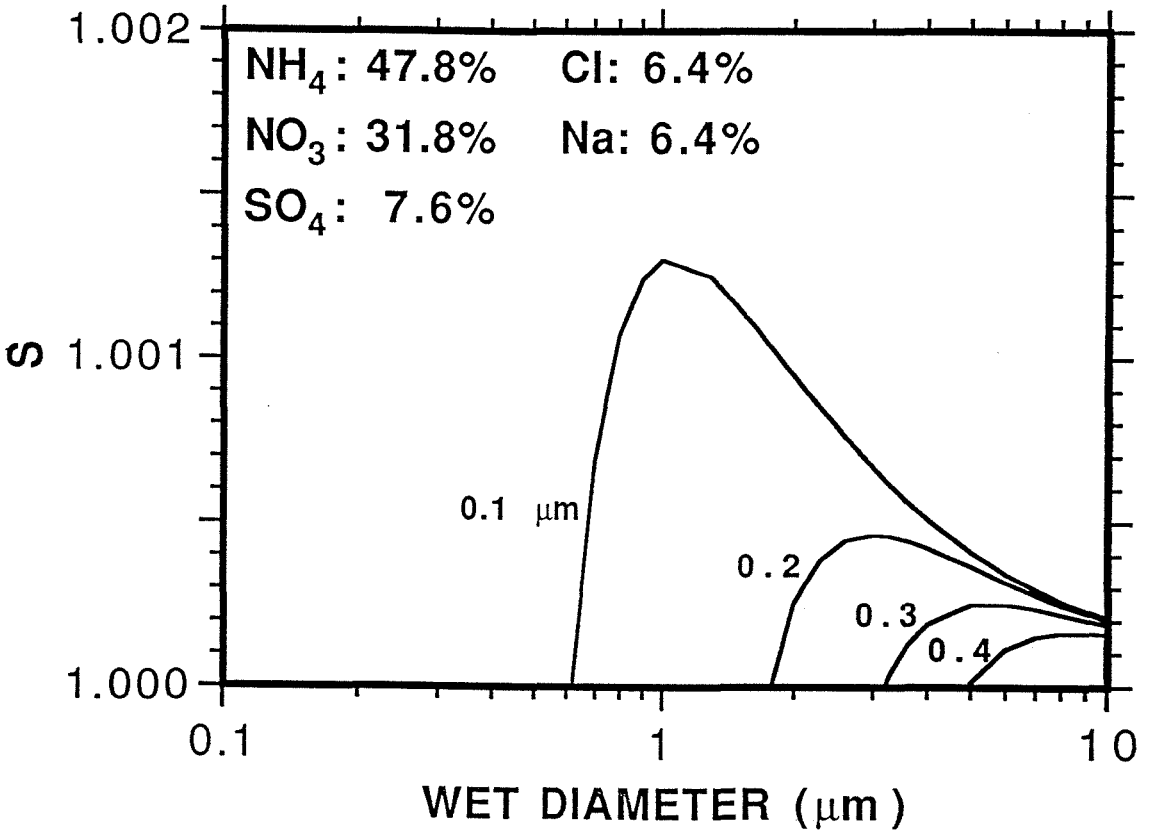

Fig. 2.3 Köhler curves for dry particles with the same composition as observed in the condensation mode.

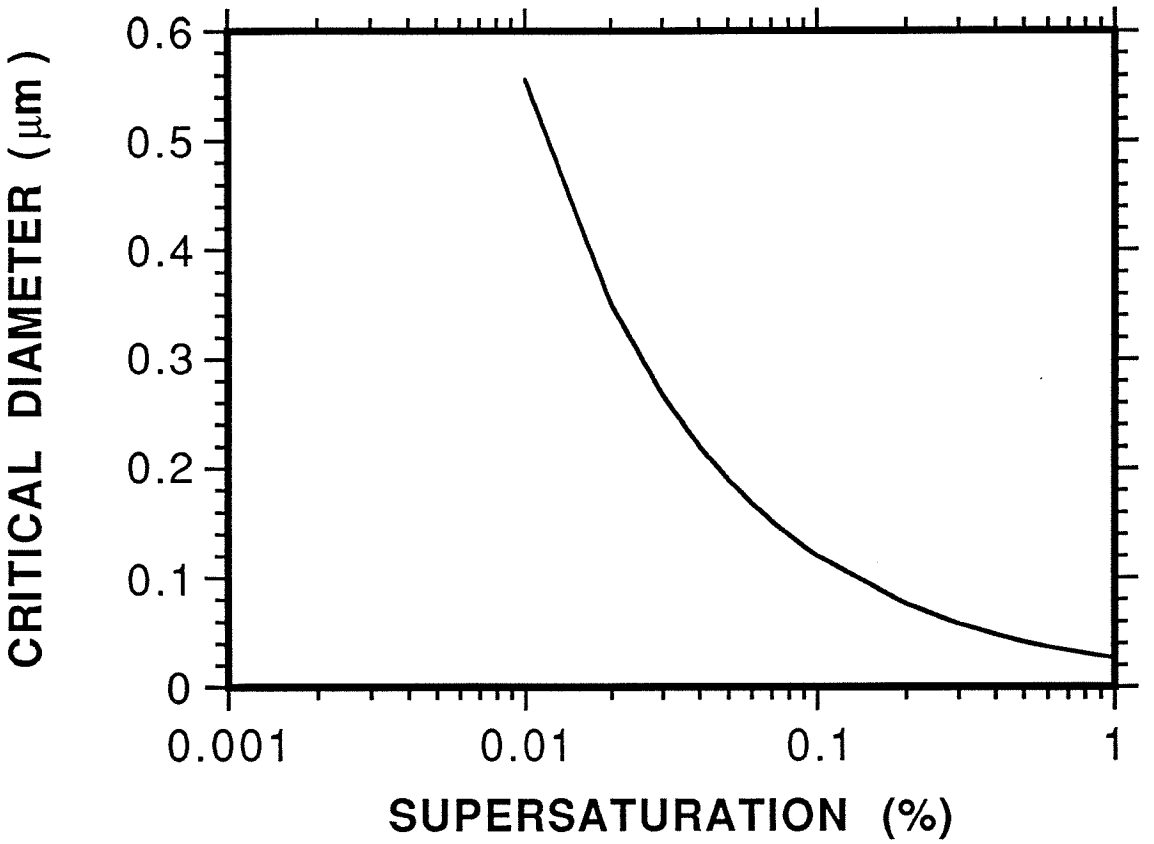

Fig. 2.4 Critical diameter above which the condensation mode particles will be activated as a function of the supersaturation.

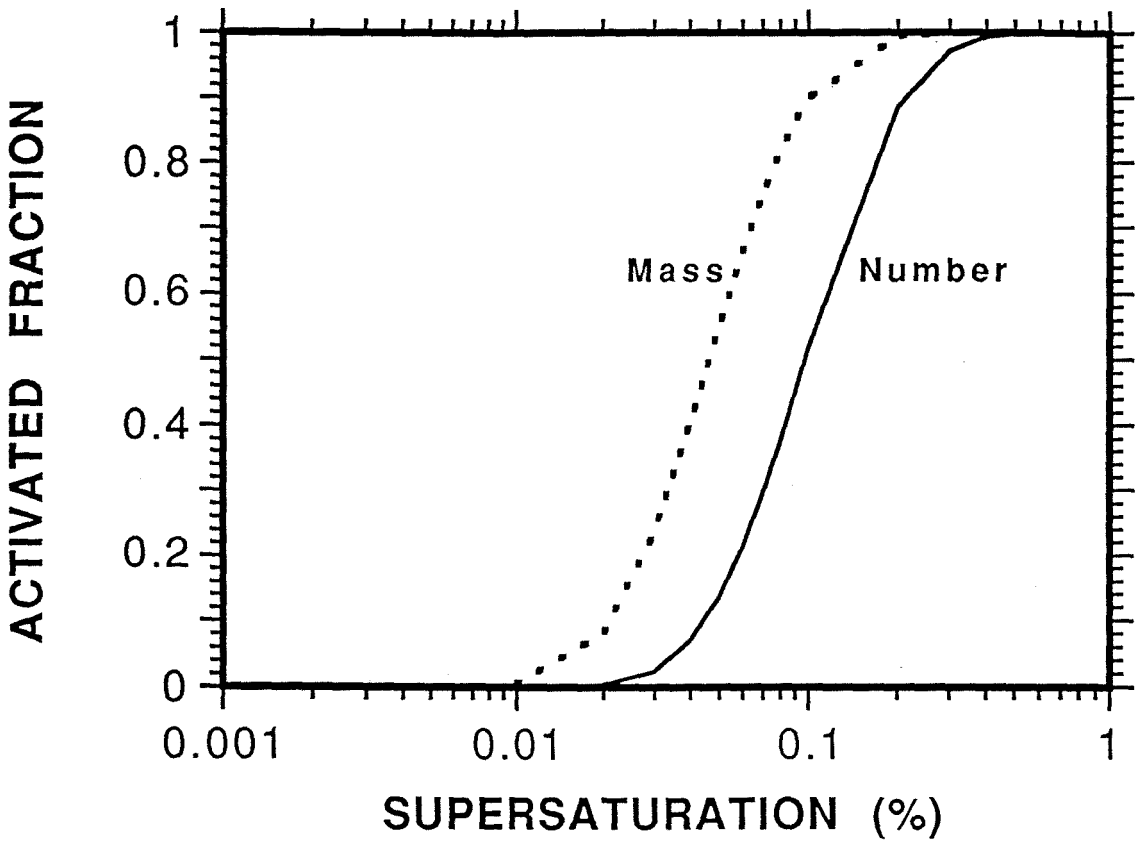

Fig. 2.5 Activated fractions of the number and mass concentrations as a function of the supersaturation for particles with the same composition as in Fig. 2.3, and lognormally distributed.

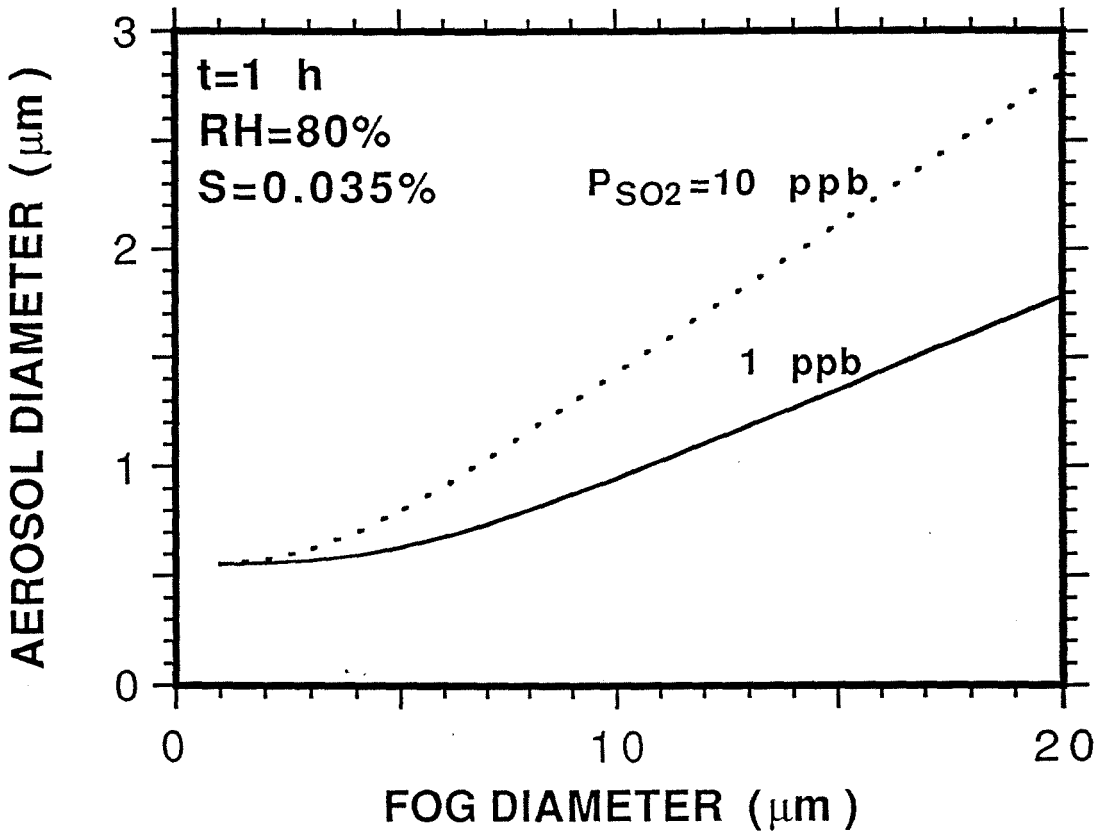

Fig. 2.6 Diameter of the aerosols at equilibrium with 80% relative humidity after fog evaporation as a function of the monodispersed fog diameter for 0.035% supersaturation and 1 hour fog.

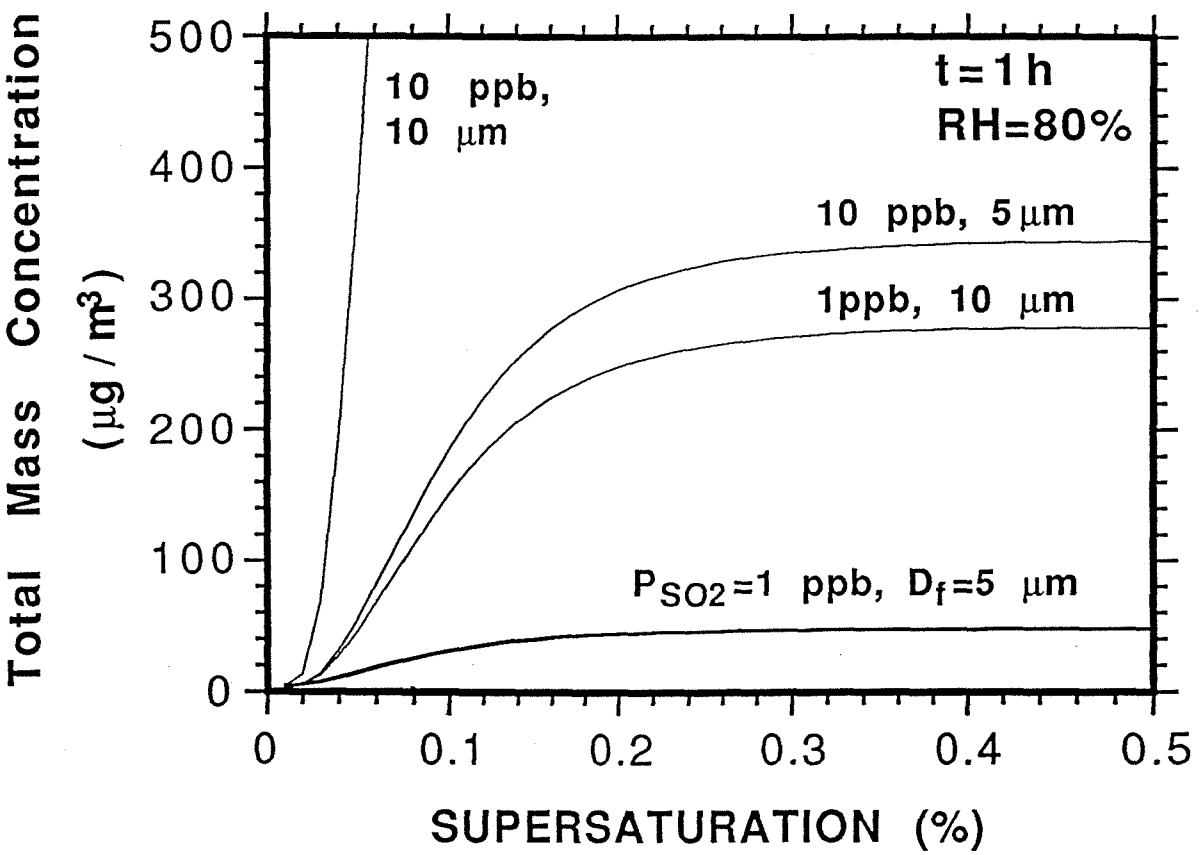

Fig. 2.7 Total particle mass concentration at equilibrium with 80% relative humidity after fog evaporation as a function of the supersaturation for 1 hour fog. The curves correspond to 5 and 10 μm fog diameter and 1 and 10 ppb SO_2 concentrations.

Chapter 3

Contribution of Water to Particulate Mass in the South Coast Air Basin

[The text of this chapter appears in: Meng Z., Seinfeld J. H., Saxena P., and Kim Y. P. (1995) *Aerosol Science and Technology* **22**, 111-123.]

ABSTRACT

Water content associated with the inorganic fraction of $PM_{2.5}$ and PM_{10} mass at San Nicolas Island, Long Beach, Burbank, and Riverside, California, has been estimated by using a thermodynamic gas/aerosol equilibrium model (SCAPE) and the measured aerosol composition data from the 1987 Southern California Air Quality Study (SCAQS). From midnight to the early morning, when the temperature is low and relative humidity is high, water is usually the predominant aerosol substance. Particulate water in the winter is estimated to be considerably larger than in the summer at each of the four sites. The estimated mass of aerosol water at high relative humidities is generally larger than that required to account for the total measured gravimetric aerosol mass, suggesting a loss of water in the measurement of total $PM_{2.5}$ and PM_{10} mass. Aerosol acidity was also estimated on the basis of the SCAQS data. Generally pH is estimated to be low for all the sampling sites, with the highest pH values at Riverside (2-4.5) and lowest at Long Beach and San Nicolas Island (-0.8-3.3) in the summer. Wintertime particles are estimated to be less acidic than those in the summer.

1. Introduction

Atmospheric aerosol frequently consists of an external mixture of non-hygroscopic and hygroscopic particles (Covert and Heintzenberg, 1984; Zhang et al., 1993). Hygroscopic particles are generally more abundant than the nonhygroscopic particles; nonhygroscopic particles in the size range between 0.05 μm and 0.4 μm observed at Claremont, California, and Grand Canyon, Arizona, generally consist of less than 30% of the total by number (Zhang et al., 1993). Aerosol samples collected in the summertime urban atmosphere of Nagoya, Japan, showed that hygroscopic particles comprised 70 to 80% of the total in the 0.1-0.7 μm diameter size range (Okada, 1985). The hygroscopicity of atmospheric particles is primarily determined by the presence of soluble substances; for instance, the water absorption properties of sulfate, nitrate, ammonium, sodium, and chloride are well known (Tang, 1976). The hygroscopicity of organics, on the other hand, is just beginning to receive attention (Rogers et al., 1991).

The hygroscopic properties of atmospheric particles are important in determining the ambient behavior of urban and regional aerosols. Atmospheric haze is most intense at high relative humidity (Ho et al., 1974; Covert et al., 1979; Sloane and Wolff, 1985; Takeda et al., 1986). A linear relationship between light scattering coefficient and liquid water content has been suggested (Ho et al., 1974) and a strong correlation between light scattering coefficient and relative humidity (RH) at high RH has been reported (Covert et

al., 1979; Rood et al., 1987). Strong particle acidity is controlled by the inorganic substances as well as by the water content of the particles (Saxena et al., 1993).

Direct measurement of aerosol water content has proven to be difficult because sampling and analytical techniques used for other aerosol species are inappropriate for measurement of water (McMurry and Stolzenburg, 1989). Water content can also include metastable water, which is that corresponding to a supersaturated solute concentration. In a study in 1983 of the hygroscopic properties of atmospheric particles in Riverside, California, Rood et al. (1987) found that metastable water contributed 5 to 20% of the total particle light scattering coefficient. Recently, the TDMA (Tandem Differential Mobility Analyzer) technique has been used to measure the sensitivity of particle size to RH (McMurry and Stolzenburg, 1989; Covert et al., 1991; Zhang et al., 1993).

Aerosol water content can be estimated on theoretical grounds by assuming that an equilibrium state holds between the gas and aerosol phases (Pilinis and Seinfeld, 1987). Once the particle chemical composition has been determined, the water content can be calculated from thermodynamic equilibrium. In this work, we employ the state-of-the-art gas/aerosol equilibrium model SCAPE (Kim et al., 1993ab) to estimate the liquid water content associated with $PM_{2.5}$ and PM_{10} aerosol particles during the 1987 Southern California Air Quality Study (SCAQS). We also present theoretical calculations of the daily as well as seasonal change of the aerosol acidity during the SCAQS at four sites, Burbank, Long Beach, Riverside, and San Nicolas Island.

2. Evaluation of Equilibrium Calculation

The 1987 Southern California Air Quality Study provides a data base of unprecedented quality for study of aerosol properties (Hering and Blumenthal, 1989). The SCAQS sampling systems for $PM_{2.5}$ and PM_{10} particles are described by Fitz and Zwicker (1989). Basically, $PM_{2.5}$ and PM_{10} samples were collected on Teflon and prefired quartz fiber filters that were then analyzed to determine aerosol mass, trace element, ionic species, and organic and elemental carbon. Aerosol total mass concentrations were determined by gravimetric techniques. The summer period included eleven sampling days: 19 June, 24 and 25 June, 13 to 15 July, 27 to 29 August, and 2 and 3 September. The fall and winter period included 11 to 13 November, 3 December, and 10 to 11 December. The particulate samples were taken five times per day at 0000, 0500, 0900, 1300, 1700 PST in the summer and 0000, 0600, 1000, 1400, 1800 PST in the winter, with sampling periods of four hours (daytime) and five to seven hours (nighttime) duration.

The input data of the SCAPE equilibrium calculation consist of total (gas and aerosol phase) concentrations of sulfate, nitrate, ammonium, sodium, and chloride, relative humidity, and temperature. All of the required data are available from the California Air Resources Board (Watson et al., 1993) except the gas phase hydrogen chloride concentrations. Because measurements of gas-phase HCl concentrations were unavailable, we did not compute gas-particle equilibrium for chloride. Instead, we

determined the total chloride concentration through iteration of the equilibrium calculation until the calculated particulate chloride concentration was within 10% of that measured. The calculated HCl concentrations in the gas phase then are generally within the annual average range (0.5-1.8 $\mu g\ m^{-3}$) reported by Eldering et al. (1991) in the same region in 1986. In a few cases, especially at low RH, the chloride calculation did not converge; consequently no results for these cases are presented.

The SCAPE calculations are based on the thermodynamic equilibrium between the gas and particle phases at the ambient temperature and RH. The calculated particulate concentrations based on equilibrium can be compared with those actually measured as a means of evaluating the validity of the equilibrium assumption.

The calculated concentrations of volatile substances (nitrate and ammonium) in the aerosol phase have been compared with those measured for the sites considered. Observed and estimated $PM_{2.5}$ and PM_{10} concentrations for nitrate and ammonium are shown in Figures 3.1 and 3.2 for the four sites considered and for both the summer and winter study periods in the 1987 SCAQS. Strong correlations between the calculated and measured nitrate and ammonium concentrations are displayed, implying a tendency to the equilibrium state of nitrate and ammonium in the $PM_{2.5}$ and PM_{10} particles in the South Coast Air Basin. The correlation coefficients between the calculated and the measured values are given in Table 3.1. The calculated PM_{10} nitrate and ammonium concentrations are more scattered around the measured values than those of the $PM_{2.5}$, and we can see

from Table 3.1 that the correlation coefficients for the PM_{10} particles (with all sites and both sampling periods considered) are smaller than those for the $PM_{2.5}$ particles. This behavior may be a consequence of the observation of Wexler and Seinfeld (1990) that the equilibration time is longer for larger particles. In some cases, which generally correspond to high temperatures and low humidities, little or no nitrate was estimated by SCAPE, but a considerable amount of nitrate was measured. Note that the measured filter concentrations were averaged for four to seven hours whereas the calculated concentrations are based on the temperature and RH at the inception of sampling. This may lead to an underestimate of the particulate nitrate if RH was low at the start of sampling and increased subsequently and/or the temperature was high at the start of sampling and decreased subsequently. We have examined these low estimated-nitrate cases and found that in many cases the RH and/or temperature changed over the sampling period. Another reason that may explain the measured nitrate concentrations exceeding those calculated is that the ambient aerosol particles contained supersaturated water. The presence of supersaturated water may result in more nitrate in the aerosol phase than the equilibrium model predicts. In Table 3.1 San Nicolas Island showed the least correlation between the measured and the calculated aerosol nitrate and ammonium concentrations. Wexler and Seinfeld (1990) argued that ammonium nitrate in the gas and aerosol phases is more likely to be in equilibrium under high concentration and warmer conditions. This may explain the deviation of the San Nicolas Island aerosols from the equilibrium state, because San Nicolas Island generally has lower pollutant concentrations and cooler temperatures.

Table 3.1 also shows that the winter aerosols were generally closer to equilibrium than those in the summer, although the temperatures in the winter were much lower than those in the summer. This is likely a consequence of the fact that the winter aerosols were generally more concentrated than those in the summer, and the temperatures in the winter were not low enough to reverse the equilibrium trend. The above analysis indicates that the equilibrium assumption for the SCAQS aerosol data is generally a good approximation in most of the cases, although in some cases (e.g., San Nicolas Island) the error incurred from the equilibrium assumption can be large.

3. Liquid Water Content in the South Coast Air Basin Aerosol

In SCAPE as well as in previous gas/aerosol equilibrium models, the ZSR method (Robinson and Stokes, 1965) is employed to calculate aerosol water content based on the soluble species concentrations in the aqueous phase that is determined by the equilibrium state for the gas/liquid (aerosol)/solid (aerosol) system. The ZSR method is computationally efficient and its performance is similar to other estimation methods (Kim et al., 1993a). In order to calculate aerosol water content, the ZSR method requires the saturation molalities of all the possible single salts that are present in the solution as ions at the ambient RH. Note that the aerosol particles frequently become concentrated solutions, and the necessary binary solution data are generally lacking at such high ionic strengths; this affects the accuracy of this method. SCAPE has used the up-to-date water

activity data, some of which are available up to very high ionic strengths. In our calculations, we used the convergence constraint of 1% for water content.

The gravimetric mass determinations from filters were generally made at 45% relative humidity (Countess, 1989), but the particulate mass concentration at ambient RH can be significantly larger than that measured gravimetrically at 45% RH. This is because (1) water makes a significant contribution to the total particulate mass at high RHs; and (2) volatile inorganic substances generally favor the particulate phase at high RHs.

Tables 3.2 and 3.3 show the 10th, 50th, and 90th percentile values of the calculated water content for $PM_{2.5}$ particles at Burbank, Long Beach, Riverside, and San Nicolas Island in the summer and winter periods of 1987 SCAQS. Also shown in the tables are the concentrations of each measured chemical species on which the percentiles of calculated water content are based. Tables 3.4 and 3.5 show similar results but for PM_{10} particles. The procedure of calculating the percentile values listed in Tables 3.2-3.5 is as follows. We first construct the cumulative frequency distribution of the calculated water content, as shown in Figure 3.3 for the $PM_{2.5}$ aerosols in the summer. From this plot we can identify the 10th, 50th, and 90th percentile values of the calculated water content at different sites; for instance the 50th percentile of $PM_{2.5}$ water content at Long Beach in the summer is 10.2 $\mu g\ m^{-3}$. The actual sample that corresponds to this amount of water content is then found; for this example, it was taken at 17:00 PST on 28 August 1987.

The measured concentrations of the other chemical species for this sample are then recorded in the 50th percentile column for Long Beach in Table 3.2. Note that since we only calculate the percentiles of water content and associate all the other measured chemical species to it, the measured species concentrations corresponding to the different percentiles of water do not correspond to the percentile values for these species. For instance, the measured sodium concentration corresponding to the 10th percentile of water content at Long Beach in Table 3.2 is even larger than that corresponding to the 50th percentile of water content. Note that all the species concentrations were actually measured except that the aerosol water content was calculated by SCAPE. The mass represented by "other" is the difference between the gravimetrically measured total mass at 45±5% RH and the summation of all the measured species excluding water.

A notable feature of the results shown in Tables 3.2-3.5 is that at all sites the 90th percentiles of the calculated mass of particulate water, which generally corresponds to high relative humidities, exceed the unidentified portion of the measured total mass concentration, suggesting a loss of water in measuring the gravimetric mass in these cases. On the other hand, the 10th percentiles of the particulate water at inland sites, which corresponds to very low relative humidities, are generally less than "other" concentrations, suggesting an overmeasurement of the total mass due to additional water condensation onto particles during the gravimetric measurements. At the coastal sites (i.e., Long Beach and San Nicolas Island) the 50th percentiles of water are generally larger than the 50th percentiles of the unidentified portion, whereas at the inland sites the

50th percentiles of water are less or comparable. In summary, measuring total gravimetric mass at a fixed RH of 45% leads to either loss or gain of liquid water compared to that under ambient conditions; furthermore, observations so derived can be corrected to the ambient RH by using SCAPE.

The gravimetrically measured total mass and the calculated average water content associated with $PM_{2.5}$ particles over the summer and winter intensive SCAQS sampling days are shown in Figure 3.4. Daytime averages (0900, 1300 and 1700) and nighttime averages (0000 and 0005 PST) are carried out separately. Water content for RH larger than 95% is not included in the averages because of the possibility of fog formation. Water is estimated to be the dominant particulate substance during most of the nighttime and early mornings. Aerosol mass concentrations during the summer SCAQS periods were largest at Riverside and smallest at San Nicolas Island. During the nighttime and early morning, excluding fog events, the aerosol at Riverside has the largest water content; Burbank and Long Beach particles are estimated to have similar amounts of water. During the daytime Riverside aerosol has the smallest water content due to low RHs, and Long Beach aerosol has the largest liquid water content. The aerosol liquid water content during daytime is smaller than that during nighttime and early morning at all locations. It is evident that water content in the winter is much larger than that in the summer, favored by the larger pollutant concentrations (mainly nitrate), the low temperature and higher average RH in the winter. Long Beach aerosol has the largest water content of the sites considered in the winter.

The daytime average water content in the summer was calculated to be 23% and 33% of the total gravimetric mass at 45% RH at the coastal sites of Long Beach and San Nicolas Island, and 6% and 3% at Burbank and Riverside, respectively. The nighttime water content in the summer was calculated to be from 30% to 40% for inland sampling sites and slightly larger for the near-coast sites. In the winter, for both daytime and nighttime, liquid water content relative to the total gravimetric mass at all sites was predicted to be slightly larger than that in the summer. In summary, for both seasons, daytime aerosol liquid water content constituted about 3% to 10% of the total gravimetric mass at inland sites and about one third of the total aerosol mass in the coastal areas on average while nighttime aerosol liquid water content ranged from 20% to 55% for sampling sites from at inland to at coastal areas.

Aerosol water content associated with PM_{10} particles generally exhibits similar features to that associated with $PM_{2.5}$ particles, but the PM_{10} water content is larger than the $PM_{2.5}$ water. We have observed that in most of the cases when ammonium is dominant in both $PM_{2.5}$ and PM_{10} particles, the water content of PM_{10} rarely exceeds 1.5 times that of $PM_{2.5}$ particles. However, in some cases where sodium is of equal importance with ammonium in the PM_{10} particles, for instance at 05:00 on June 19, at Burbank, the PM_{10} water is estimated to be more than twice the $PM_{2.5}$ water. This is because most of the ammonium in PM_{10} particles is actually distributed in $PM_{2.5}$ particles whereas most of the sodium is associated with PM_{10} particles.

4. Aerosol Acidity

The acidity (pH) associated with the $PM_{2.5}$ and PM_{10} aerosol particles has also been calculated by using SCAPE. We show the results for $PM_{2.5}$ and PM_{10} particles in Figures 3.5 and 3.6, respectively. pH here is defined according to the molality of H^+. Generally, the summer $PM_{2.5}$ particles are estimated to be quite acidic, with daytime particles being more acidic than the nighttime particles. The estimated summer aerosol pH ranged from 0.7 to 3.5 at Burbank, -0.7 to 2.5 at Long Beach, 2.0 to 4.5 at Riverside and -0.8 to 3.3 at San Nicolas Island (not shown). The median pH was around 1.5 at Burbank, 1.0 at Long Beach, 3.5 at Riverside and 0.6 at San Nicolas Island. The difference of chemical composition is primarily responsible for the pH difference at different locations. For comparison, for northeastern U.S., Ferek et al. (1983) estimated the particulate pH to range between -0.8 and 2.0 over 24 samples (April 1979-August 1980). The estimated low pH at San Nicolas Island (not shown) was due to the absence of basic compounds such as ammonium. Riverside particles have an estimated pH higher than that of other sites because of the prevalence of ammonium in that area. Aerosol acidity in the winter was less than that in the summer; this tendency is consistent with observations of aerosol acidity in St. Louis, Montana, and Kingston, Tennessee (Koutrakis et al., 1988). This is primarily a result of the low sulfate and relatively high ammonium concentrations in the winter. Another reason for this is that RH is generally higher in the winter than in the summer. At higher RHs water dilutes the concentrations of acidic compounds, such as

$(NH_4)_2SO_4$, NH_4HSO_4 and NH_4NO_3. The median estimated pH of the winter $PM_{2.5}$ aerosol particles was around 2.5 at Burbank and Long Beach, and 4.0 at Riverside. Note that the typical pH of fog droplets in this area is about 5.0 (Waldman, 1986); therefore, the particles are predicted to be considerably more acidic.

The pH of PM_{10} aerosol particles is expected generally to be larger than that of the corresponding $PM_{2.5}$ aerosol due to the presence of crustal basic species such as Na^+, Ca^{2+}, K^+, and Mg^{2+} (only Na^+ is considered in the current version of SCAPE) in the larger particles. Our results basically reflect this tendency, although sometimes the difference is small.

The aerosol acidities predicted by SCAPE are affected by accuracy of SCAPE's estimation of aerosol water content. The predictions are less accurate at low RHs when only a small amount of water is present in the particles. Since SCAPE is not a size segregated model, the calculated aerosol acidity is only a bulk property. Note that different sized particles generally have different chemical compositions; for example, most of sulfate is generally present in small particles and sodium generally exists in the coarse particles. Thus, in reality, sodium in the coarse particles cannot neutralize the sulfate in the fine particles, but unless we carry out a size-resolved equilibrium calculation, this size-distribution effect cannot be resolved. The acidities predicted by SCAPE should be viewed only as the average over all the applicable particles.

Saxena et al. (1993) pointed out that the acidity measured in an aqueous extract of collected particles does not necessarily correspond to the actual aerosol acidity; the suspended particle acidity is generally smaller than that implied by the total extract method. A rough estimate of the average hydrogen ion concentration in the summer at Burbank based on the median pH of 1.5 and water content of 7 $\mu g\ m^{-3}$ is 0.22 nmoles m^{-3}, which is considerably smaller than the mean hydrogen ion concentrations measured in Kingston, TN (36.1 nmoles m^{-3}), and St. Louis, MO (10.3 nmoles m^{-3}) (Koutrakis et al., 1988). To make a valid comparison, we estimate the total extractable aerosol acidity in SCAQS according to

$$\left[H^+\right] = 2\left[SO_4^{2-}\right] + \left[NO_3^-\right] + \left[Cl^-\right] - \left[NH_4^+\right] - \left[Na^+\right]$$

where all the ion concentrations are in units of nmol m^{-3}. We show the results in Table 3.6. The total estimated extractable aerosol acidity in the South Coast Air Basin is generally comparable with that measured in other locations.

5. Summary

The water content of atmospheric aerosols is important in determining aerosol properties such as light extinction and acidity. Aerosol water content is difficult to measure. Because of its volatility and high concentration in the atmosphere, water can generally be assumed to be in local equilibrium between the gas and particulate phases. Development

of the ability to predict aerosol water content given other atmospheric and aerosol parameters is important to predicting changes in $PM_{2.5}$ and PM_{10} mass and visibility that are likely to result from changes in emissions. In this work we have used a state-of-the-art gas/aerosol equilibrium model to estimate the water associated with the $PM_{2.5}$ and PM_{10} aerosol measured during the 1987 Southern California Air Quality Study (SCAQS) at San Nicolas Island, Long Beach, Burbank, and Riverside, California, for both the summer and winter phases of SCAQS. By comparing observed and estimated total aerosol mass, it is seen that most of the aerosol water was generally lost in measuring the total gravimetric mass at 45% relative humidity when the ambient RH was high. Acidity was estimated for the SCAQS aerosol. Generally, pH is estimated to be low for all the sampling sites, with the highest pH values at Riverside (2-4.5) and lowest at Long Beach and San Nicolas Island (-0.8-3.3) in the summer. Winter particles are less acidic than summer particles because of the smaller sulfate concentrations and larger water content. Detailed comparisons of estimated and observed aerosol compositions at the SCAQS sites generally validates the assumption of equilibrium between the gas and particulate phases for the volatile inorganic species.

Acknowledgment

This work was supported by the Electric Power Research Institute under agreement RP3189-03.

REFERENCES

Countess, R. J. (1989). *Southern California Air Quality Study Sampler Chemistry, Final Report.* Prepared for California Air Resources Board, Sacramento, California, February 1989, P4-2.

Covert, D. S., Hansson, H.-C., Winkler, P., Heintzenberg, J. (1991). The degree of mixing of hygroscopic properties in source and receptor locations in Northern Europe, Paper 9A.1 presented at the annual meeting of the American Association for Aerosol Research, Traverse City, MI, October 7-11.

Covert, D. S. and Heintzenberg, J. (1984). *Sci. Total Environ.* 36:347-352.

Covert, D. S., Waggoner, A. P., Weiss, R. E., Ahlquist, N. J. (1979). In *The Character and Origins of Smog Aerosols* (G. M. Hidy et al., eds.). John Wiley, New York. p. 559-581.

Eldering, A., Solomon, P. A., Salmon, L. G., Fall, T. and Cass, G. R. (1991). *Atmos. Environ.* 25A:2091-2102.

Ferek, R. J., Lazrus, A. L., Haagenson, P. L. and Winchester, J. W. (1983). *Environ. Sci. Technol.* 17:315-323.

Fitz, D. and Zwicker, J. (1989). *Design and Testing of the SCAQS Sampler for the SCAQS Study, 1987.* Final Report. California Air Resources Board, Sacramento, California.

Hering, S. V. and Blumenthal, D. L. (1989). *Southern California Air Quality Study (SCAQS) Description of Measurement Activities, Final Report.* California Air Resources Board, Sacramento, California.

Ho, W., Hidy, G. M. and Govan, R. M. (1974). *J. Appl. Meteorol.* 13:871-879.

Kim, Y. P., Seinfeld, J. H. and Saxena, P. (1993a). *Aerosol Sci. Technol.* 19:157-181.

Kim, Y. P., Seinfeld, J. H. and Saxena, P. (1993b). *Aerosol Sci. Technol.* 19:182-198.

Koutrakis, P., Wolfson, J. M. and Spengler, J. D. (1988). *Atmos. Environ.* 22:157-162.

McMurry, P. H. and Stolzenburg, M. R. (1989). *Atmos. Environ.* 23:497-507.

Okada, K. (1985) *Atmos. Environ.* 19:743-757.

Pilinis, C. and Seinfeld, J. H. (1987). *Atmos. Environ.* 21:2453-2466.

Robinson, R. A. and Stokes, R. J. (1965). *Electrolyte Solutions.* 2nd ed. Butterworth, London.

Rogers, C. F., Hudson, J. G., Zielinska, B., Tanner, R. L., Hallett, J. and Watson, J. G. (1991). Cloud Condensation Nuclei from Biomass Burning. In *Global Biomass Burning: Atmospheric, Climatic, and Biospheric Implications* (Joel S. Levine, Ed.). MIT Press, Cambridge, MA.

Rood, M. J., Covert, D. S., and Larson, T. V. (1987). *Tellus.* 39B:383-397.

Saxena, P., Muller, P. K., Kim, Y. P., Seinfeld, J. H. and Koutrakis, P. (1993). *Aerosol Sci. Technol*, 19:279-293.

Sloane, C. S. and Wolff, G. T. (1985). *Atmos. Environ.* 19:669-680.

Takeda, T., Wu, P. and Okada, K. (1986). *J. Met. Soc. Japan.* 64:957-965.

Tang, I. N. (1976). *J. Aerosol Sci.* 7:361-371.

Waldman, J. M. (1986). *Depositional aspects of pollutant behavior in fog*, Ph.D. thesis, Calif. Inst. of Technol., Pasadena.

Watson, J. G., Chow, J. C., Lu, Z., Gertler, A. W. (1993). *Particulate and Gaseous Organic Receptor Modeling for the Southern California Air Quality Study.* Draft Final Report, California Air Resources Board, Sacramento, California.

Wexler, A. S. and Seinfeld, J. H. (1990). *Atmos. Environ.* 24A:1231-1246.

Zhang, X. Q., McMurry, P. H., Hering, S. V. and Casuccio, G. S. (1993). *Atmos. Environ.* 27A:1593-1607.

Table 3.1. Correlation between the calculated and measured aerosol nitrate and ammonium concentrations during the 1987 SCAQS[a]

	Nitrate								Ammonium							
	Summer				Winter				Summer				Winter			
	R(F)	*k*(F)	*R*(T)	*k*(T)	*R*(F)	*k*(F)	*R*(T)	*k*(T)	*R*(F)	*k*(F)	*R*(T)	*k*(T)	*R*(F)	*k*(F)	*R*(T)	*k*(T)
Burbank	0.77	0.58	0.64	0.50	0.97	0.99	0.95	1.09	0.94	0.93	0.88	0.91	0.96	1.17	0.66	0.68
Long Beach	0.70	0.79	0.63	0.51	0.99	0.94	0.87	0.78	0.89	0.86	0.90	0.97	0.99	1.02	0.83	0.85
Riverside	0.83	0.78	0.62	0.89	1.00	0.94	0.92	0.96	0.61	0.91	0.66	1.20	0.97	1.17	0.82	1.30
San Nicolas Isl.	0.47	0.34	0.57	0.54					0.56	0.95	0.64	0.98				

	R(F)	*k*(F)	*R*(T)	*k*(T)	*R*(F)	*k*(F)	*R*(T)	*k*(T)
All sites and both periods	0.96	0.91	0.85	0.91	0.94	1.02	0.72	0.91

[a] The correlation analysis is based on linear regression with zero intercept. "*R*" and "*k*" denote the correlation coefficient and the regression slope, and the letter in the parentheses denotes either fine aerosol particles (F) or total PM_{10} aerosol particles (T).

Table 3.2. The 10th, 50th and 90th percentile values of the calculated water content and concentrations of each measured chemical species for $PM_{2.5}$ aerosols in the summer periods of 1987 SCAQS[a]

	Burbank (46)[b]			Long Beach (52)			Riverside (48)			San Nicolas Isl. (23)		
Observable	10th	50th	90th	10th	50th	90th	10th	50th	90th	10th	50th	90th
Na^+	0.20	0.02	0.00	0.40	0.19	0.17	0.03	0.01	0.00	0.36	0.28	0.10
NH_4^+	2.30	6.54	5.72	1.23	4.03	5.70	6.78	9.24	14.7	0.46	0.46	0.63
SO_4^{2-}	5.59	10.4	10.4	5.39	8.55	14.3	4.47	8.92	10.9	2.59	2.20	2.81
NO_3^-	1.17	9.67	7.31	0.81	1.75	1.76	18.9	19.5	37.1	0.21	0.30	0.49
Cl^-	0.00	0.03	0.11	0.00	0.00	0.00	0.00	0.27	0.39	0.51	0.76	0.00
Tot. carbon[c]	16.1	13.7	9.09	3.56	5.51	7.95	14.5	10.7	18.9	1.32	1.10	1.89
Crustal[d]	0.63	0.29	0.40	0.41	0.48	0.29	1.55	1.38	1.53	0.43	0.25	0.28
Tot. mass[e]	33.7	49.7	40.7	13.6	25.6	41.3	55.7	61.4	98.1	17.2	6.15	6.80
Other[f]	7.68	8.97	7.68	1.78	5.16	11.1	9.50	11.3	14.5	11.3	0.80	0.61
Water[g]	0.00	0.65	35.8	0.01	10.2	39.1	0.00	0.03	49.4	2.81	7.03	189
T (°C)	32.8	25.0	17.3	20.2	22.4	18.7	26.7	30.0	21.7	14.5	12.1	14.0
RH (%)	33	56	85	61	66	85	39	37	70	65	74	99

[a]Percentiles are calculated for water content only with the other chemical species linked to it. Only cases where a convergent SCAPE water calculation was obtained have been taken into account in the statistics. Units are in $\mu g/m^3$ for species.

[b]Number in the parentheses is the number of available cases used in the statistics.

[c]Total carbon is constructed as EC+1.4[OC], where [OC] is measured as carbon.

[d]Crustal mass is constructed as 1.67[Mg]+1.89[Al]+2.14[Si]+1.2[K]+1.4[Ca]+1.43[Fe]+trace elements. No weighting factors are applied to the trace elements, which have less mass concentrations than those given above.

[e]Gravimetric mass measured at 45% RH.

[f]Difference between the total mass and summation of the measured constituent mass excluding water.

[g]Calculated by SCAPE at ambient RH.

Table 3.3. The 10th, 50th and 90th percentile values of the calculated water content and concentrations of each measured chemical species for $PM_{2.5}$ aerosols in the winter periods of 1987 SCAQS[a]

	Burbank (28)[b]			Long Beach (29)			Riverside (23)		
Observable	10th	50th	90th	10th	50th	90th	10th	50th	90th
Na^+	0.09	0.07	0.03	0.02	0.24	0.04	0.02	0.09	0.05
NH_4^+	4.50	5.17	14.1	5.76	4.37	9.22	0.02	10.2	10.2
SO_4^{2-}	1.22	1.54	5.74	2.23	4.03	5.22	0.43	3.72	3.5
NO_3^-	14.9	16.5	45.7	17.6	8.55	22.7	0.00	36.1	34.4
Cl^-	0.00	0.52	1.64	0.15	0.91	2.86	0.00	0.57	1.24
Tot. carbon[c]	20.7	46.1	63.2	20.3	19.8	61.6	3.66	26.1	26.7
Crustal[d]	0.94	1.86	2.07	1.61	1.11	1.52	2.30	6.52	6.33
Tot. mass[e]	48.1	65.0	153.	44.8	45.4	126.	4.52	97.1	93.9
Other[f]	5.73	-6.79	20.8	-2.83	6.32	22.8	-1.91	13.9	11.5
Water[g]	0.00	1.92	59.3	0.13	25.0	174.	0.00	9.95	65.8
T (°C)	22.3	18.4	10.6	23.9	18.4	11.2	25.3	16.7	12.0
RH (%)	42	52	71	43	78	92	33	58	80

[a]Percentiles are calculated for water content only with the other chemical species linked to it. Only cases where a convergent SCAPE water calculation was obtained have been taken into account in the statistics. Units are in $\mu g/m^3$ for species.

[b]Number in the parentheses is the number of available cases used in the statistics.

[c]Total carbon is constructed as EC+1.4[OC], where [OC] is measured as carbon.

[d]Crustal mass is constructed as 1.67[Mg]+1.89[Al]+2.14[Si]+1.2[K]+1.4[Ca]+1.43[Fe]+trace elements. No weighting factors are applied to the trace elements, which have less mass concentrations than those given above.

[e]Gravimetric mass measured at 45% RH.

[f]Difference between the total mass and summation of the measured constituent mass excluding water.

[g]Calculated by SCAPE at ambient RH.

Table 3.4. The 10th, 50th and 90th percentile values of the calculated water content and concentrations of each measured chemical species for PM_{10} aerosols in the summer periods of 1987 SCAQS[a]

	Burbank (41)[b]			Long Beach (47)			Riverside (50)			San Nicolas Isl. (15)		
Observable	10th	50th	90th	10th	50th	90th	10th	50th	90th	10th	50th	90th
Na^+	0.71	2.59	1.18	2.92	0.53	2.80	0.66	1.21	1.24	0.00	1.46	0.90
NH_4^+	0.90	4.74	5.96	4.16	2.20	3.44	2.89	9.78	17.1	0.22	0.88	0.85
SO_4^{2-}	4.15	9.87	9.60	11.2	7.30	8.55	5.09	11.1	13.1	2.43	3.84	3.26
NO_3^-	3.76	14.9	13.8	11.5	1.44	7.15	11.1	27.5	57.5	0.70	2.28	1.32
Cl^-	0.05	0.47	1.19	0.30	0.02	1.73	0.62	0.73	1.11	1.79	1.37	0.47
Tot. carbon[c]	18.5	33.3	24.1	40.3	5.18	3.07	13.7	19.8	29.8	2.49	2.15	3.65
Crustal[d]	9.63	17.4	9.44	26.3	1.84	3.93	18.3	26.6	37.3	0.37	3.53	1.14
Tot. mass[e]	50.7	97.7	67.0	121.	22.4	44.2	76.5	115.	180.	5.87	18.9	16.1
Other[f]	13.0	14.4	1.76	24.9	3.92	13.5	24.1	18.7	22.9	-2.13	3.36	4.55
Water[g]	0.00	10.2	51.0	0.02	16.8	41.6	0.00	0.03	71.6	7.52	28.0	431.
T (°C)	40.0	20.6	16.7	29.5	17.8	19.8	31.2	30.0	18.4	15.3	18.5	16.2
RH (%)	16	59	83	42	82	83	34	37	70	64	90	99

[a]Percentiles are calculated for water content only with the other chemical species linked to it. Only cases where a convergent SCAPE water calculation was obtained have been taken into account in the statistics. Units are in $\mu g/m^3$ for species.

[b]Number in the parentheses is the number of available cases used in the statistics.

[c]Total carbon is constructed as EC+1.4[OC], where [OC] is measured as carbon.

[d]Crustal mass is constructed as 1.67[Mg]+1.89[Al]+2.14[Si]+1.2[K]+1.4[Ca]+1.43[Fe]+trace elements. No weighting factors are applied to the trace elements, which have less mass concentrations than those given above.

[e]Gravimetric mass measured at 45% RH.

[f]Difference between the total mass and summation of the measured constituent mass excluding water.

[g]Calculated by SCAPE at ambient RH.

Table 3.5. The 10th, 50th and 90th percentile values of the calculated water content and concentrations of each measured chemical species for PM_{10} aerosols in the winter periods of 1987 SCAQS[a]

	Burbank (25)[b]			Long Beach (27)			Riverside (26)		
Observable	10th	50th	90th	10th	50th	90th	10th	50th	90th
Na^+	0.50	0.03	0.64	0.47	0.62	1.01	0.07	0.62	0.38
NH_4^+	17.4	0.30	19.5	8.47	7.36	11.3	0.00	9.58	6.04
SO_4^{2-}	8.67	0.78	7.65	5.28	5.21	4.57	0.56	4.41	4.78
NO_3^-	69.5	4.82	65.1	30.	23.3	37.3	0.00	39.1	38.1
Cl^-	0.27	0.08	1.28	0.02	0.14	5.49	0.00	0.65	1.21
Tot. carbon[c]	47.9	35.1	71.5	31.5	32.6	77.6	9.13	37.2	36.7
Crustal[d]	12.7	6.40	15.5	7.15	9.33	14.7	5.11	23.3	41.1
Tot. mass[e]	175.1	51.5	195.	83.9	79.1	156.	16.5	122.	145.
Other[f]	18.1	3.96	14.0	1.04	0.49	4.00	1.63	7.64	17.0
Water[g]	0.00	3.67	76.1	0.00	8.91	143.	0.00	9.29	71.7
T (°C)	13.4	11.4	8.4	26.2	22.8	12.3	25.3	16.7	12.0
RH (%)	34	65	70	31	57	86	33	58	80

[a]Percentiles are calculated for water content only with the other chemical species linked to it. Only cases where a convergent SCAPE water calculation was obtained have been taken into account in the statistics. Units are in $\mu g/m^3$ for species.

[b]Number in the parentheses is the number of available cases used in the statistics.

[c]Total carbon is constructed as EC+1.4[OC], where [OC] is measured as carbon.

[d]Crustal mass is constructed as 1.67[Mg]+1.89[Al]+2.14[Si]+1.2[K]+1.4[Ca]+1.43[Fe]+trace elements. No weighting factors are applied to the trace elements, which have less mass concentrations than those given above.

[e]Gravimetric mass measured at 45% RH.

[f]Difference between the total mass and summation of the measured constituent mass excluding water.

[g]Calculated by SCAPE at ambient RH.

Table 3.6. Average total extractable $PM_{2.5}$ aerosol acidity (units of nmol m^{-3})

	Burbank	Long Beach	Riverside	San Nicolas Isl.
Summer	18.2	0.52	13.4	25.6
Winter	80.3	26.1	134.1	

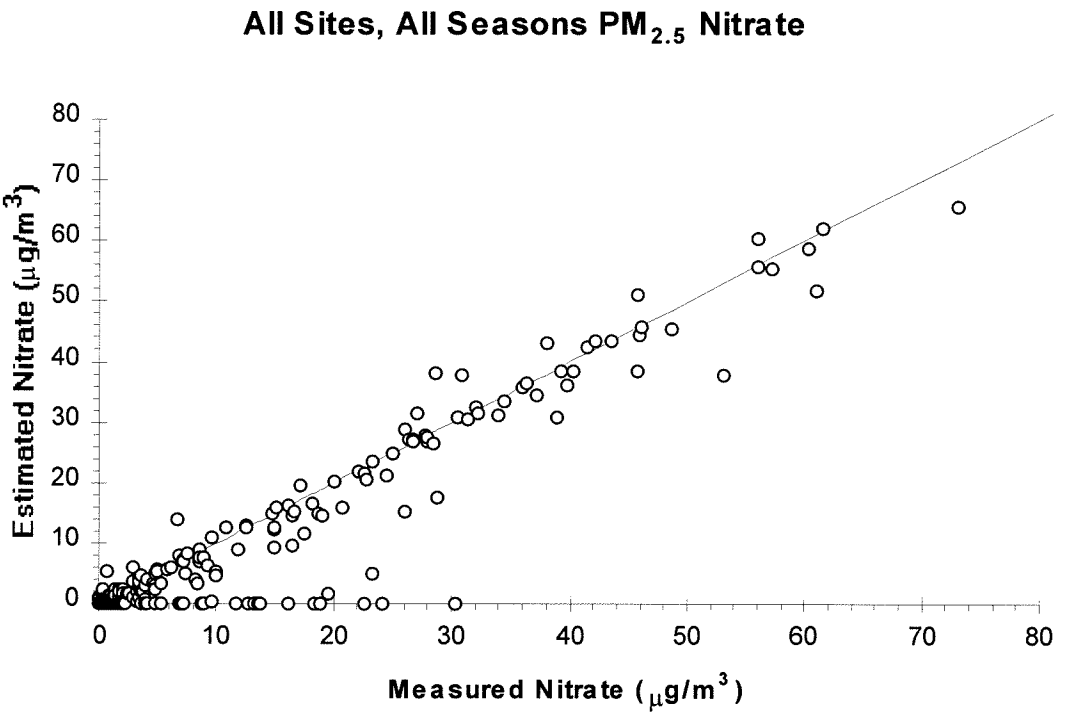

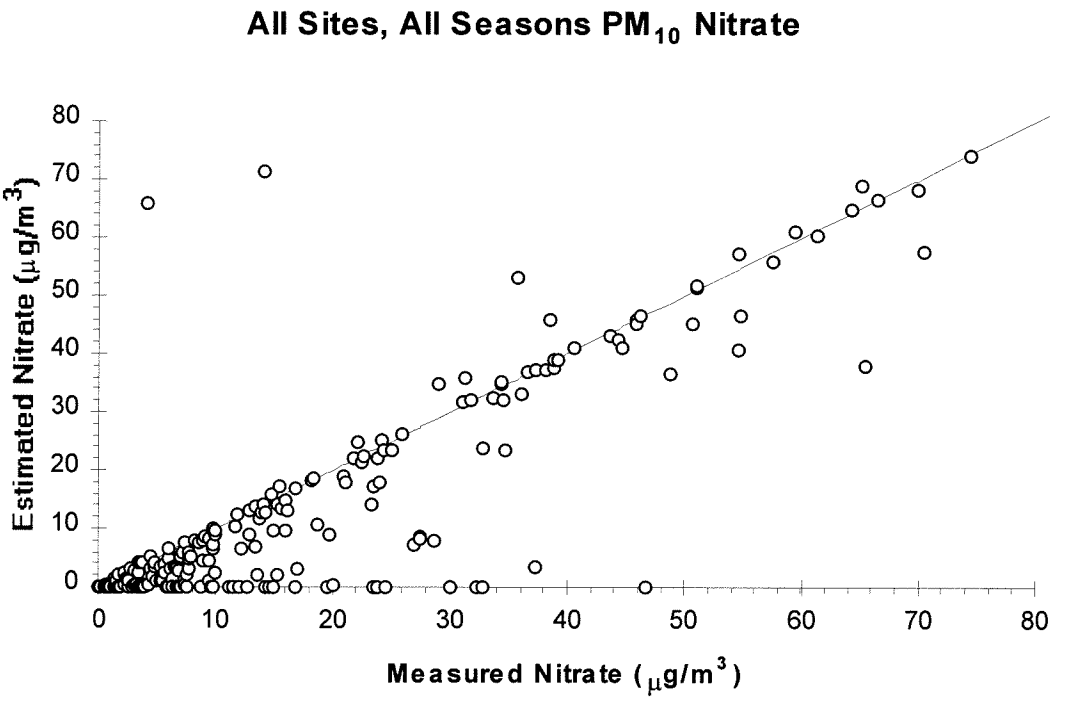

Fig. 3.1 Estimated and measured $PM_{2.5}$ and PM_{10} nitrate at Burbank, Long Beach, Riverside, and San Nicolas Island during the 1987 SCAQS. The straight line indicates where the estimated concentrations are equal to those of the measured.

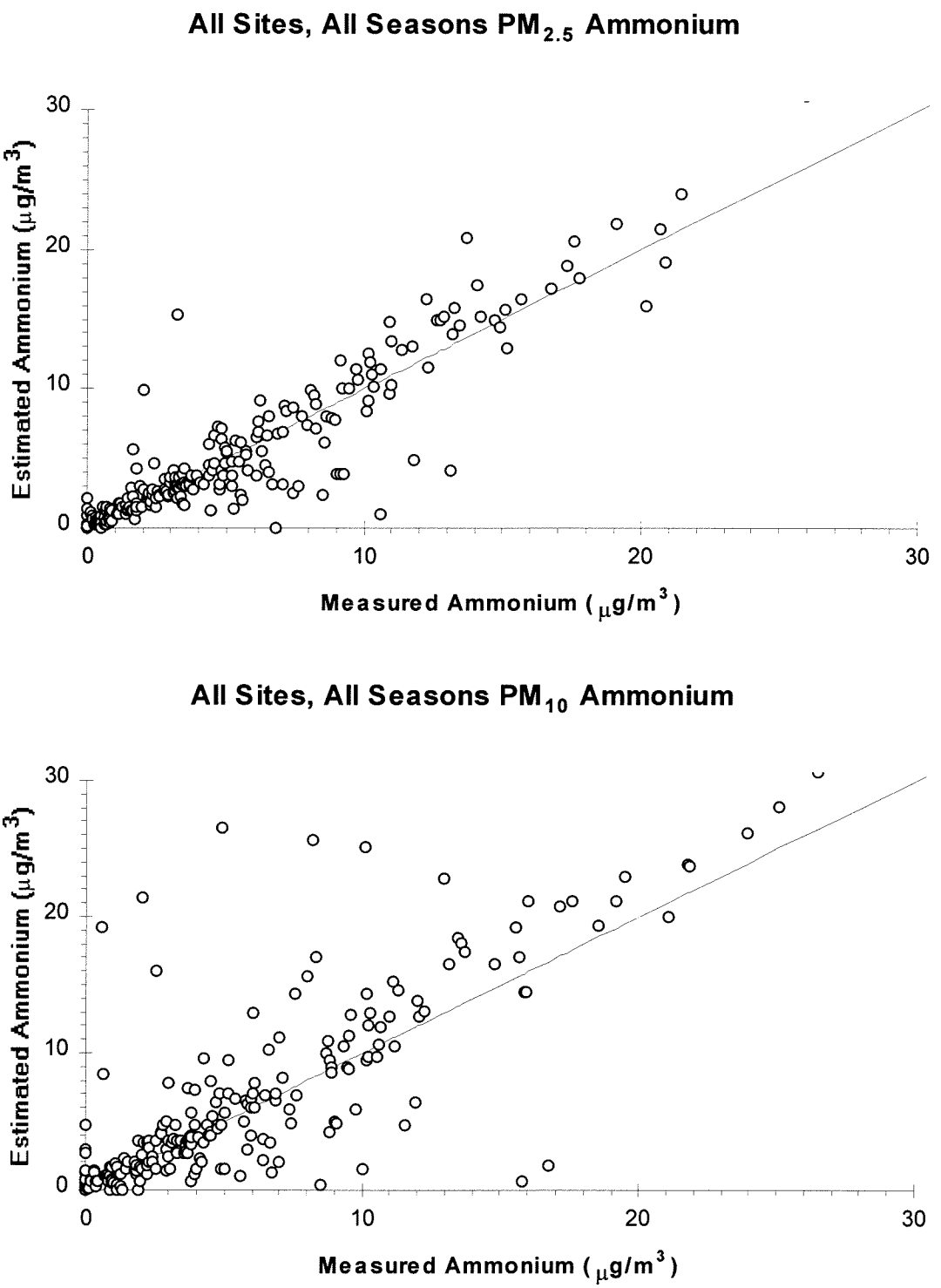

Fig. 3.2 Estimated and measured $PM_{2.5}$ and PM_{10} ammonium at Burbank, Long Beach, Riverside, and San Nicolas Island during the 1987 SCAQS. The straight line indicates where the estimated concentrations are equal to those of the measured.

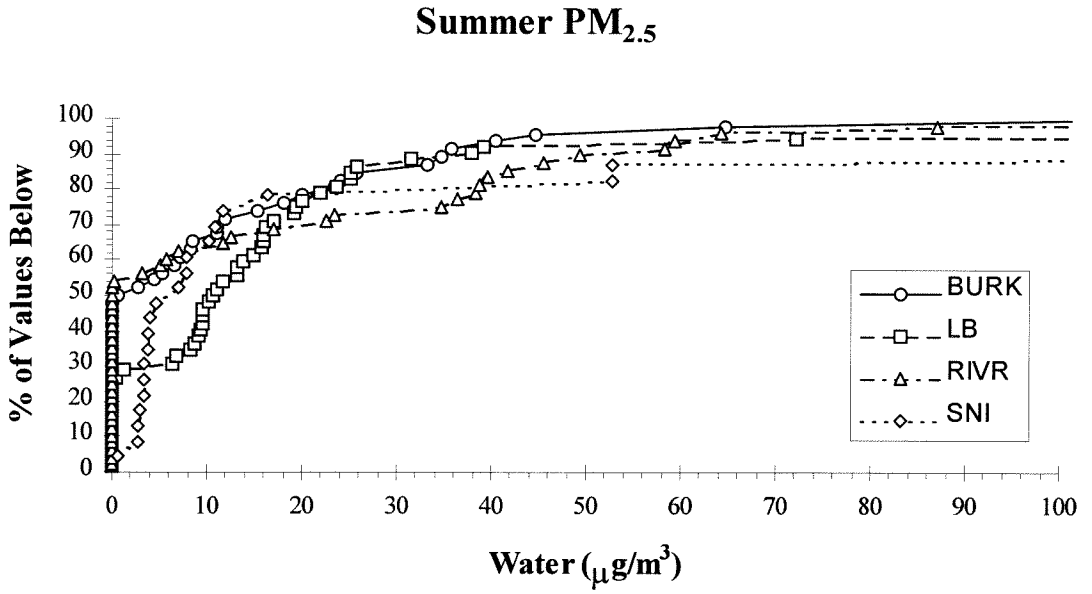

Fig. 3.3 Cumulative frequency distribution for the calculated water content for the $PM_{2.5}$ aerosols in the summer at Burbank, Long Beach, Riverside, and San Nicolas Island during the 1987 SCAQS.

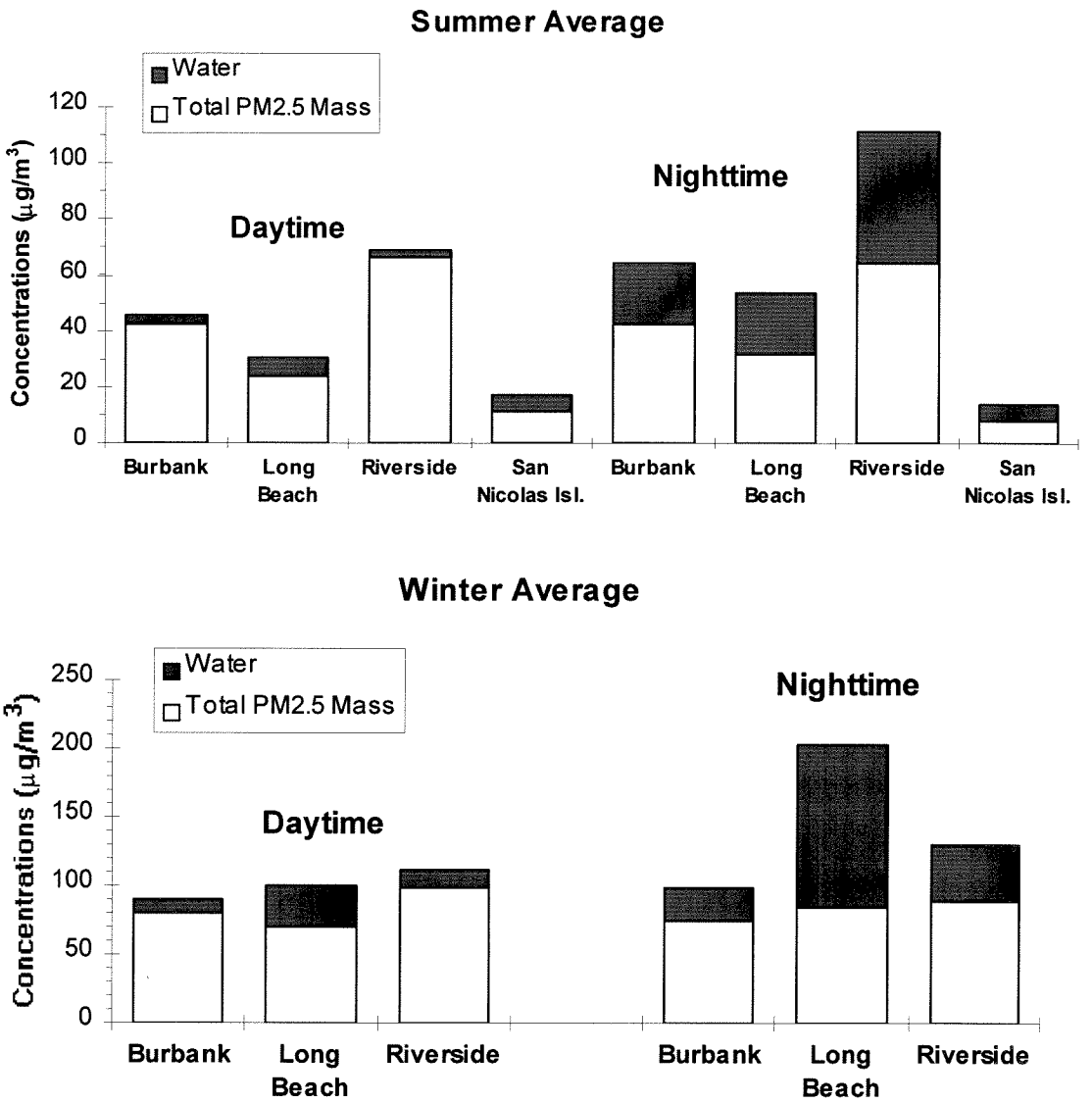

Fig. 3.4 Average calculated water content (ambient RH) and observed total $PM_{2.5}$ mass (RH=45%) over the summer (top) and winter (bottom) SCAQS sampling periods at Burbank, Long Beach, Riverside, and San Nicolas Island. Daytime and nighttime averages are carried out separately.

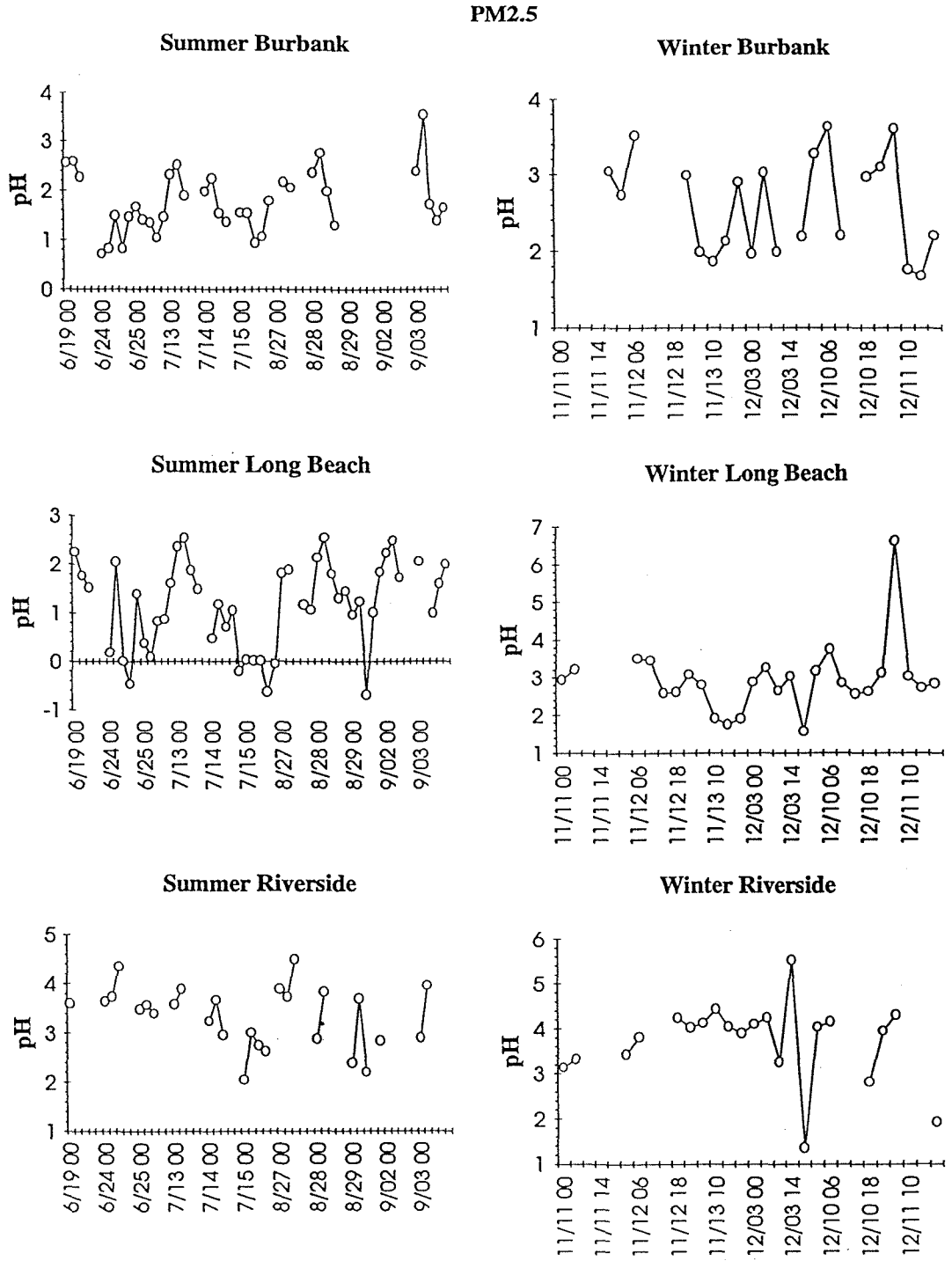

Fig. 3.5 Estimated pH associated with $PM_{2.5}$ aerosol for the SCAQS sampling periods at Burbank, Long Beach, and Riverside, California (X-Axis: month, day and start hour).

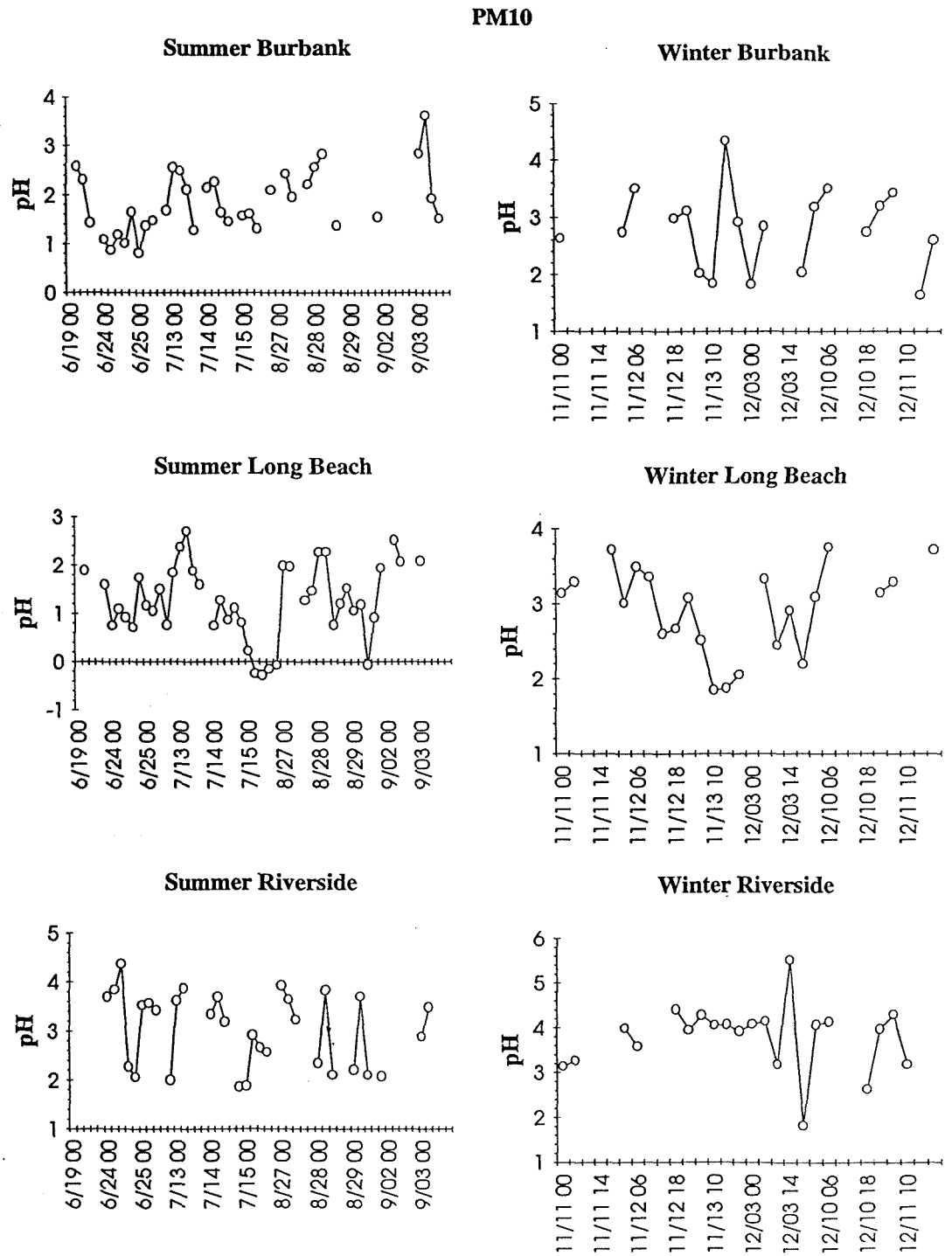

Fig. 3.6 Estimated pH associated with PM_{10} aerosol for the SCAQS sampling periods at Burbank, Long Beach, and Riverside, California (X-Axis: month, day and start hour).

Chapter 4

Atmospheric Gas-Aerosol Equilibrium:

IV.

Thermodynamics of Carbonates

[The text of this chapter appears in: Meng Z., Seinfeld J. H., Saxena P., and Kim Y. P. (1995) *Aerosol Science and Technology* **23**, 131-154.]

ABSTRACT

Data and correlations for incorporating carbonate and bicarbonate salts into a gas/aerosol equilibrium model are developed. The species considered include $CO_2(g)$, $CO_2(aq)$, HCO_3^-, CO_3^{2-}, $NH_2CO_2^-$, $Na_2CO_3(s)$, $NaHCO_3(s)$, $K_2CO_3(s)$, $KHCO_3(s)$, $CaCO_3(s)$, $MgCO_3(s)$, $NH_4HCO_3(s)$, and $NH_2COONH_4(s)$. Three activity coefficient estimation methods (Bromley, K-M, and Pitzer) are examined. Necessary parameters for these three methods are obtained. It is found that, in general, the Pitzer method performs better than the other two, and is selected as the multicomponent activity coefficient estimation method of choice. Water activity correlations for binary carbonate solutions are obtained by polynomial fitting of available data. Deliquescence points for the important atmospheric carbonate salts and their temperature dependence are given.

1. Introduction

An atmospheric gas/aerosol equilibrium model (SCAPE) has been recently developed (Kim et al., 1993a, 1993b; Kim and Seinfeld, 1994). This newest equilibrium model differs from previous ones (i.e., EQUIL(Bassett and Seinfeld, 1983), KEQUIL (Bassett and Seinfeld, 1984), MARS (Saxena et al., 1986; Binkowski, 1991), SEQUILIB (Pilinis and Seinfeld, 1987), and AIM (Wexler and Seinfeld, 1991)) in both computational and thermodynamic approaches. SCAPE has been applied to investigations of aerosol water content and particle acidity (Saxena et al., 1993a, 1993b; Meng et al., 1994). The original SCAPE accounted only for substances such as sodium, ammonium and ammonia, sulfate, nitrate, and chloride. In subsequent work Kim and Seinfeld (1994) expanded the thermodynamic data base to include the crustal species, K^+, Ca^{2+}, and Mg^{2+}.

Dust from arid and semi-arid regions of continents can be a significant source of tropospheric aerosol particles (Junge, 1979; Schütz, 1980; Pye, 1987; Andronova et al., 1993; Gomes and Gillette, 1993). The Asian deserts (Chinese, Arabian, Persian), the North American arid and semi-arid areas at about 40°±10°N, and the Sahara Desert constitute large sources for mineral dust in the Northern Hemisphere (Gomes and Gillette, 1993). In the deserts of southwestern United States, dust accounts for about 20 to 30% of the total fine mass and contributes about one-third to one-half of the total light scattering by particles (Vasconcelos et al., 1994; White et al., 1994). Generally, the soil or mineral dust is rich in alkaline elements such as Ca, K, and Mg. The northern part of

the Sahara Desert is known to be a region enriched in carbonates (Gomes and Gillette, 1993). Gillette et al. (1992) reported emissions of alkaline elements (Ca, Mg, K, and Na) from soils in the southwestern United States, primarily in the form of carbonates. In the U.S.S.R.-U.S. dust experiment conducted during dust storms in Tadzhikistan (Soviet Central Asia) during September 1989, samples of soil-derived aerosol exhibited alkaline elements such as Ca and K (Andronova et al., 1993). Ca was found mainly as $CaCO_3$ (calcite).

In urban areas dust containing alkaline carbonates can also originate from local sources, such as construction materials, road salt, and etc. Sturges et al. (1989) collected aerosol samples in suburban Toronto, Canada, between January and July 1986, and observed carbonate concentrations to be 1-2 $\mu g/m^3$ (about 6% of the total mass), with summer concentrations slightly higher due to the greater degree of construction activity. Clarke and Karani (1992) found that in the atmosphere of the city of Leeds, U.K., carbonate comprised 2-3% of the coarse particulate mass. They also found that more carbonate was measured than could be attributed to calcite and inferred that the fine particles contained apparently volatile carbonate for which the most likely source is the surface of soot particles.

Since a considerable fraction of the crustal species (i.e., Ca, K, and Mg) is in the form of carbonate, inclusion of these species in an equilibrium aerosol model is desirable. Such inclusion will enable estimation of pH, water content and CCN potential of dust

particles by themselves or in mixtures with other inorganic compounds. In this work we evaluate the currently available thermodynamic data related to the carbonate salts and develop that data into a form for inclusion in a gas/aerosol equilibrium model such as SCAPE. In some cases necessary data are not available in the literature and we acquire them from the related experimental data, such as solubility.

2. Chemical Reactions Involving Carbonate Salts

The chemical reactions of carbonates considered in this work are given in Table 4.1. There are 12 chemical reactions, of which 8 involve solids. The equilibrium constant is expressed as by Kim et al. (1993a),

$$K(T) = K(T_0)\exp\left\{-\frac{\Delta H_f^0}{RT_0}\left(\frac{T_0}{T}-1\right)-\frac{\Delta C_p^0}{R}\left(1+\ln\left(\frac{T_0}{T}\right)-\frac{T_0}{T}\right)\right\} \quad (1)$$

where $K(T)$ and $K(T_0)$ are the equilibrium constants at temperature T and T_0 (298.15 K), respectively. ΔG_f^0, ΔH_f^0, and ΔC_p^0 are change of the standard molar Gibbs free energy of formation, molar enthalpy of formation, and molar heat capacity at constant pressure, respectively. ΔH_f^0, and ΔC_p^0 are assumed to be constant over the temperature range T to T_0. These thermodynamic data are listed in Table 4.2. Most of the values cited are from the NBS Thermodynamic Tables (Wagman et al., 1982) so as to maintain internal

consistency. The heat capacity data of aqueous carbon dioxide, bicarbonate ion, and carbonate ion are not available in the NBS Thermodynamic Tables, and we obtained these values by the best fit of Maurer's (1980) equilibrium constants as a function of temperature for the related equilibria over the temperature range 0-50 °C. The overall average relative deviations of the equilibrium constants in these fits from those of Maurer are smaller than 3%. Data for carbamate ion ($NH_2CO_2^-$) are also deduced from the equilibrium constant relation of reaction between aqueous ammonia and bicarbonate ion in Maurer's work.

Values of the equilibrium constants at 298.15 K and their dependence on temperature are also given in Table 4.1. Equilibria involving Ca^{2+} and Mg^{2+} ions are assumed to be temperature independent due to absence of heat capacity data. The temperature dependence of the last two reactions in Table 4.1, which involve solid ammonium bicarbonate and ammonium carbamate, is also not available and is not included.

3. Estimation of Activity Coefficients

The equilibrium constant can be expressed as (Denbigh, 1981; Kim et al., 1993a),

$$K_j = \prod_i a_i^{\nu_{ij}} \tag{2}$$

where ν_{ij} is the stoichiometric coefficient of the ith species in the jth reaction, and the activity of aqueous-phase species i is defined as

$$a_i = \gamma_i m_i \tag{3}$$

where m_i is the species concentration in molality (mol kg^{-1}) and γ_i is its activity coefficient. Combining Eqs. (2) and (3) gives

$$K_j = \prod_i (\gamma_i m_i)^{\nu_{ij}} \tag{4}$$

Eq. (4) is the basis of the equilibrium constant expressions given in Table 4.1. The accuracy of the calculated equilibrium species concentrations depends critically on estimation of the activity coefficients. In SCAPE (Kim et al., 1993a, 1993b; Kim and Seinfeld, 1994) the three widely used multicomponent activity coefficient estimation methods, namely Bromley (1973), Kusik and Meissner (K-M, 1978), and Pitzer (Pitzer and Kim, 1974; Pitzer, 1991), have all been evaluated in detail for the species considered in those works: H^+, NH_4^+, Na^+, NO_3^-, Cl^-, HSO_4^-, SO_4^{2-}, Ca^{2+}, K^+, and Mg^{2+}. The first two methods are actually based on individual binary activity coefficients, while the Pitzer method is based on estimation of the individual ion (or neutral molecular) activity coefficients, though, in reality, only ion-pair activity coefficients can be measured. In

this work we do not consider the temperature dependence of the activity coefficients but use the values at 25°C, at which most of the experimental results have been obtained. Including the temperature effect on the activity coefficient is desirable. When the results given here are used at temperatures much different from 25°C, special caution should be taken. Formulation of the temperature dependency of the activity coefficient can be found in the paper of Bassett and Seinfeld (1983).

Binary Activity Coefficients

The formulae and parameter values for the Bromley, Kusik and Meissner, and Pitzer methods for estimation of the binary activity coefficients are given in Tables 4.3-4.5, respectively, for substances of interest here. Note that the Bromley and K-M methods were originally developed only for strong electrolytes; they were not intended for weak electrolytes such as H-HCO_3 and H_2CO_3 pairs. It is therefore not surprising that the B or q parameter values of the two methods are generally lacking for the weak electrolytes. Also, they are not expected to perform well when strong ion association occurs unless additional terms are added to the original expressions (Bromley, 1973). Of relevance here, calcium carbonate and magnesium carbonate are believed to exhibit strong association. Most of the necessary parameter values for the Bromley and K-M methods are generally not available or must be obtained from fitting the models to data at low ionic strength. We obtained or re-calculated these necessary parameters by best fitting the activity coefficient data available in the literature.

Figure 4.1 shows the activity coefficient as a function of ionic strength for $NaHCO_3$ predicted by the three methods together with the experimental data acquired by Sarbar et al. (1982a). Values of the parameters B and q for the Bromley and K-M methods have been obtained by the least-square fitting of $\ln\gamma$ to Sarbar et al.'s experimental data for ionic strength up to 1 m. All three methods, as expected, perform equally well at low ionic strength, but may lead to potentially large errors at high ionic strength where no experimental data are available. At high ionic strength the Bromley and K-M methods behave similarly for $NaHCO_3$, whereas the Pitzer method predicts a considerably higher value of the activity coefficient.

Figures 4.2-4.5 show similar results to those in Figure 4.1 for Na_2CO_3, $KHCO_3$, K_2CO_3, and NH_4HCO_3, respectively. For Na_2CO_3 and K_2CO_3, Bromley (1973) obtained B values from early work (Robinson and Stokes, 1965). We have refitted the newer data of Goldberg (1981) and Sarbar et al. (1982b) and obtained new values of B. Relatively high ionic strengths can be reached in these two electrolyte solutions, and we see that generally all three methods perform well in the tested ranges. For K_2CO_3, the Bromley and Pitzer methods accurately predict the experimental data whereas the K-M method does not. Nevertheless, the K-M method still predicts the activity coefficient within acceptable errors over the range for which data are available. For all the bicarbonate salts only limited data are available even at low ionic strengths, and it is impossible to judge the behavior of the three methods at high ionic strength. The Pitzer

method does seem to predict unreasonably low activity coefficient values for potassium bicarbonate at high ionic strengths, although, again, no data are available against which to evaluate the theories.

The K-M method has been chosen as the binary activity coefficient estimation method for multicomponent activity coefficient calculation in the previous SCAPE work (Kim et al., 1993a; Kim and Seinfeld, 1994). Without strong evidence to the contrary, for consistency we will use the K-M method here for the extension to carbonate salts. From Figures 4.1-4.5 we see that the K-M method performs well in binary activity coefficient estimation, and, particularly, gives reasonable predictions for the bicarbonate salts at high ionic strength.

Multicomponent Activity Coefficients

Formulae for multicomponent activity coefficient estimation by the three methods are given by Kim et al. (1993a). The binary activity coefficients of all the possible ion pairs in the solution are needed in the estimation of multicomponent activity coefficient for the Bromley and K-M methods. As noted earlier, SCAPE uses the K-M method to estimate the binary activity coefficient for both the multicomponent Bromley and K-M methods. The multicomponent Pitzer method requires additional ion interaction parameters besides those specific parameters for the binary salts listed in Table 4.5. Most of the binary parameters in Table 4.5 have been obtained from Harvie et al. (1984). New and

presumably more accurate parameter values appeared after Harvie et al.'s work (Harvie et al. only used the literature data up to 1980 and fitted some Pitzer parameters from the solubility data) for $NaHCO_3$ and Na_2CO_3 (Peiper and Pitzer, 1982), $KHCO_3$ (Roy et al., 1983), K_2CO_3 (Sabar et al., 1982b), $Mg(HCO_3)_2$ and $Ca(HCO_3)_2$ (Pitzer et al., 1985), and NH_4HCO_3 (Roy et al., 1988). However, we shall only use the values given by Harvie et al. (1984), if available, for estimation of the multicomponent activity coefficients because all the parameters are interrelated. Clegg and Whitfield (1991), for example, pointed out that substitution of revised parameters, even from more accurate data, can lead to dramatic worsening of predicted activity coefficients. Plummer et al. (1988) have shown that, for the solubility of $NaHCO_3$ in aqueous Na_2CO_3 at 25 °C, substitution of parameters $\beta^{(0)}$, $\beta^{(1)}$ and C^{ϕ} obtained from recent data for the system $NaHCO_3$-CO_3-CO_2-H_2O for those of Harvie et al. leads to large inaccuracies in predicted $NaHCO_3$ solubility in Na_2CO_3 solutions.

The second and third virial coefficients, i.e., θ and ψ, for the Pitzer method for a mixed electrolyte solution are given in Table 4.6. θ is the interaction parameter for two ions of like charge, and ψ is the mixed electrolyte parameter. These two parameters are generally lacking for systems involving nitrate and bicarbonate or nitrate and carbonate. Some parameters involving ammonium ion are also not available in the literature. Since nitrate and ammonium are important species in atmospheric aerosols, these parameters have to be acquired for a robust atmospheric gas/aerosol equilibrium calculation.

In Figures 4.6a, 4.6b, and 4.6c, predictions of the Bromley method, the K-M method, and the Pitzer method are compared with measurements of the solubility of NH_4HCO_3 in NH_4HCO_3-NH_4NO_3, in NH_4HCO_3-NH_4Cl, and in NH_4HCO_3-$(NH_4)_2SO_4$ solutions, respectively. The solubility is predicted based on the equilibrium constant (solubility product), which is obtained from the measured saturation molality and the calculated activity coefficients of a pure solution of that electrolyte at saturation. We do not use the Gibbs free energy data in the table of Wagman et al. (1982) for the solubility calculations because discrepancies exist between the measured solubilities in the binary solutions and those calculated from Wagman et al.'s data and this would complicate our comparisons. Note that the binary activity coefficient estimation methods for the Bromley and the K-M methods are used correspondingly for full comparison (In SCAPE only K-M method is used for estimation of the binary activity coefficients). As noted earlier, some of the Pitzer ion-interaction parameters for these systems, i.e., θ_{NO_3,HCO_3}, ψ_{NO_3,HCO_3,NH_4}, ψ_{Cl,HCO_3,NH_4} and ψ_{SO_4,HCO_3,NH_4} are not available. We first fitted the solubility data for the NH_4^+/NO_3^-/HCO_3^- ternary system and obtained the values of θ_{NO_3,HCO_3} (0.0414) and ψ_{NO_3,HCO_3,NH_4} (0.000559). The procedure to obtain θ and ψ values from solubility data in a ternary system was described by Harvie and Weare (1980). As can be seen in Figure 4.6a for the Pitzer curve, the predicted solubility of ammonium bicarbonate in an aqueous ammonium nitrate solution by the Pitzer method with the above two parameter values agrees well with the experimental data at a temperature of 15 °C (Seidell and Linke, 1965). We also obtained ψ_{Cl,HCO_3,NH_4} = -

0.001168 and ψ_{SO_4,HCO_3,NH_4} = 0.005424, based on the corresponding θ values given by Harvie et al. (1984) (see Table 4.6). Evidently, the Pitzer method performs much better than the other two, with the Bromley method giving the worst predictions for these systems. For the NH_4HCO_3-$(NH_4)_2SO_4$ solution, a convergent result could not be obtained for the Bromley method so no result is shown for this case. The K-M method performs well for the NH_4HCO_3-NH_4Cl system, but gives large errors for the other two systems. The poorer performance of the Bromley method and occasionally for the K-M method are very likely a result of the fact that the binary parameters for these two methods, particularly for NH_4HCO_3, have been fitted only to low ionic strength data.

The solubilities of $NaHCO_3$ in $NaHCO_3$-$NaNO_3$, in $NaHCO_3$-NaCl, and in $NaHCO_3$-Na_2SO_4 solutions, are shown in Figures 4.7a, 4.7b, and 4.7c, respectively. For these ternary systems, only data for $\psi_{NO_3,HCO_3,Na}$ are not available; θ_{NO_3,HCO_3} was already obtained and fixed from the NH_4HCO_3-NH_4NO_3 system. Now with this value of θ_{NO_3,HCO_3} we obtained $\psi_{NO_3,HCO_3,Na}$ = -0.007438. The good performance of Pitzer method in Figure 4.7a implies that the θ_{NO_3,HCO_3} value we have obtained is not specific to just one ternary system. For the above three systems all three methods give correct predictions. The performance of the K-M method in the $NaHCO_3$-Na_2SO_4 solution is slightly better than the other two, but the Pitzer method is sufficiently accurate for estimation of the solubility in this system.

The solubilities of $KHCO_3$ in $KHCO_3$-KNO_3, in $KHCO_3$-KCl, and in $KHCO_3$-K_2SO_4 solutions, are presented in Figures 4.8a, 4.8b, and 4.8c, respectively. The parameter $\psi_{NO_3,HCO_3,K}$ obtained is -0.000894 for the nitrate system. In the $KHCO_3$-KCl solution, all three methods follow the trend of the solubility curve, but the Pitzer method is superior to the other two methods. For the $KHCO_3$-KNO_3 and $KHCO_3$-K_2SO_4 systems, the Bromley method gives completely incorrect predictions. Predictions of the K-M method exhibit the correct behavior but with large deviations from the available data. Only the Pitzer method accurately predicts the solubility data.

In Figures 4.9a and 4.9b, we present the solubilities of $NaNO_3$ in Na_2CO_3-$NaNO_3$ and NaCl in Na_2CO_3-NaCl solutions. No Na_2CO_3 solubility is compared because Na_2CO_3 generally crystallizes in hydrated forms. Therefore, predictions of water activity in the solution are also necessary; this will complicate our comparison of solubilities predicted by the three methods. The θ and ψ values for nitrate and carbonate systems are: θ_{NO_3,CO_3}=-0.081, $\psi_{NO_3,CO_3,Na}$= 0.0103. Note that the θ value given here was obtained directly without considering the unsymmetrical effect, which arises when the interacting ions with like charge carry different number of charges (Pitzer, 1979). It was originally thought that this unsymmetrical effect can be neglected for 2-1 mixing salts (Pitzer, 1975). However, Harvie and Weare (1980) showed that it may be important in some cases. For the Na_2CO_3-$NaNO_3$ system, the Pitzer method agrees well with the data while the Bromley and K-M methods significantly overpredict the $NaNO_3$ solubility. For

the Na_2CO_3-NaCl system, the Pitzer method and the Bromley method perform equally well, and the K-M method overpredicts the NaCl solubility.

In Figures 4.10a, 4.10b, and 4.10c, we show the solubilities of KNO_3 in K_2CO_3-KNO_3, KCl in K_2CO_3-KCl, and K_2SO_4 in K_2CO_3-K_2SO_4 solutions, respectively. For the K_2CO_3-KNO_3 system, we obtained $\psi_{NO_3,CO_3,K} = 0.012$ for the Pitzer method. For the K_2CO_3-KNO_3 system the Bromley method is unable to follow the data, whereas the Pitzer method performs the best and the K-M method slightly underestimates the KNO_3 solubility over most of the range of K_2CO_3 concentrations. For the K_2CO_3-KCl system, the Bromley and the Pitzer methods perform well while the K-M method overpredicts the KCl solubility. For K_2CO_3-K_2SO_4 system, all the three methods perform well but the Pitzer method is still deemed best.

Based on predictions of the solubility data, we see that the overall performance of Pitzer method is evidently superior to the Bromley and K-M methods. The Pitzer method can always predict reasonable solubility values within the available data range whereas the Bromley and K-M methods may lead to considerable over- or under-estimations. Kim and Seinfeld (1994) showed that the Pitzer method is generally in better agreement with measurement than the Bromley and K-M methods for the crustal cations. This conclusion agrees with our findings here. Since the Pitzer method is ideally capable of predicting the activity coefficients of neutral species (presented below) in

multicomponent solutions, it is deemed to be the multicomponent activity coefficient estimation method of choice.

Activity Coefficient of Aqueous Carbon Dioxide

Harvie et al. (1984) found that in the carbonate system, the inclusion of neutral species, e.g., CO_2(aq), is required to describe observed solution behavior. The activity coefficients of aqueous molecular species can be calculated by the salting-out equations (Setschénow, 1889; Pawlikowski and Prausnitz, 1983) and the Pitzer method. It appears that the Pitzer method is superior in estimating the activity coefficients of the weak or neutral species (Zemaitis et al., 1986). The activity coefficient of the neutral species N in the Pitzer method (for which self-interactions are negligible) is given by (Harvie et al., 1984; Clegg and Whitfeld, 1991)

$$\ln \gamma_N = \sum_c (2\lambda_{Nc}) m_c + \sum_a (2\lambda_{Na}) m_a \qquad (5)$$

where λ is the Pitzer molecule-ion interaction parameter, "c" and "a" denote cations and anions, respectively, and the summations are over all the present cations or anions in the solution. The higher-order interaction parameters are generally not required for the neutral species.

Most of the λ values for CO_2(aq) of interest here have been obtained by Harvie et al. (1984). Those lacking are for CO_2-NO_3^- and CO_2-NH_4^+, and we obtained them by fitting the CO_2 solubilities in $NaNO_3$ and $(NH_4)_2SO_4$ solutions measured by Yasuniski and Yoshida (1979). All these values that are important in modeling the carbonate system in atmospheric aerosols are given in Table 4.7. Note that in reality the interaction parameter between neutral species and the individual ion cannot be directly determined because no single ion solution could exist alone. Only the combined effect of ion pairs can be measured; therefore, it is necessary to set an arbitrary value to λ for some ion i. Harvie et al. (1984) chose λ_{CO_2,H^+} to be zero. All the values given in Table 4.7 are based on this convention.

The activity coefficient of CO_2(aq) in $NaNO_3$ solution is shown in Figure 4.11. The experimental activity coefficient has been converted from the original solubility data (Ostwald coefficient) of Yasuniski and Yoshida (1979). Predictions by the Pitzer method agree well with the experimental data. Note that the activity coefficient of CO_2(aq) in $NaNO_3$ solution changes from 1 to about 3 when the ionic strength increases to 10 m. In Figure 4.12 we show the activity coefficient of CO_2(aq) in the KNO_3 solution to examine if the previously obtained λ_{CO_2,NO_3^-} value in $NaNO_3$ solution can also be applied to the KNO_3 solution. There is a slight underestimation by the Pitzer method, but the relative errors are small. This suggests that the λ_{CO_2,NO_3^-} value that we have obtained is not merely specific to one single system.

Figures 4.13 and 4.14 show the activity coefficient of CO_2(aq) in $(NH_4)_2SO_4$ and NH_4Cl solutions, respectively. The agreement between the estimation and the data is good for the $(NH_4)_2SO_4$ solutions, but systematic underprediction has occurred for the NH_4Cl solution. The relative deviations of the Pitzer method from the data for the NH_4Cl solution are still smaller than 10%.

4. Estimation of Water Activity

There are several methods, e.g., the Bromley (1973), Kusik and Meissner (1978), Pitzer (Pitzer and Kim, 1974), and ZSR (Stokes and Robinson, 1966; Chen et al., 1973) methods, to predict the water activity of a multicomponent solution; all of these estimation methods are, at best, semi-empirical. Since we have recommended the Pitzer method as the multicomponent activity coefficient estimation method, to maintain thermodynamic consistency, it would be best to use the Pitzer method as the water activity estimation method also. However, in the Pitzer method the dissolved species concentrations for a given chemical composition in the solution can only be implicitly determined in the equation; therefore, numerical iterations are required for a solution if given the water activity. In atmospheric aerosol modeling, the water activity is usually fixed as the ambient relative humidity. Noting that the water activity is frequently "called" in solving the full gas/aerosol equilibrium problem, a more efficient water activity estimation method than the Pitzer method is desirable for an efficient numerical

model. In the ZSR method the dissolved species concentrations, and thus the aerosol water content, can be readily obtained for a given relative humidity; therefore, we choose the ZSR method to estimate atmospheric water content. The ZSR method has already been used in predicting atmospheric aerosol water content in the previous aerosol models and SCAPE (Pilinis and Seinfeld, 1987; Wexler and Seinfeld, 1991; Kim et al., 1993a), and detailed comparisons between the ZSR and the Pitzer and/or other methods have been made by Saxena and Peterson (1981), Cohen et al. (1987), and Chan et al. (1992). They have found that generally there are no major differences in accuracy between the ZSR and the Pitzer methods. Nevertheless, we compare here the predictions of the ZSR and the Pitzer methods for the carbonate and bicarbonate systems again because thermodynamic consistency is an important issue. The aerosol water content W in the ZSR method is given by (Kim et al., 1993a)

$$W = \sum_i \frac{M_i}{m_{i0}(a_w)} \tag{6}$$

where M_i is the molar concentration of substance i in the atmosphere (mole/m^3 air) and $m_{i0}(a_w)$ is the molality of the binary solution at the equilibrium water activity, a_w of the multicomponent solution.

Parameters of the polynomial fits for the available water activity data for the carbonate and bicarbonate substances of interest here are given in Table 4.8. For

magnesium and calcium bicarbonates no direct measurement of water activity is available; instead, we have used the predicted water activities by the Pitzer method for molalities up to 10 m with the parameters given by Pitzer et al. (1985). Most of the carbonates (except K_2CO_3) deliquesce at high RH (≥90%) and therefore water activity data are only available for the high RH range; extrapolating these data down to the low RH range may produce large errors.

The comparison between the predictions of the ZSR method and the Pitzer method for the Na_2CO_3-$NaHCO_3$ and K_2CO_3-$NaHCO_3$ ternary systems is presented in Table 4.9. In the calculations we have assumed no chemical reactions in the solutions and the molar ratio of the two compounds to be 1.0, and neglected the cooperated interactions between ions, e.g., between HCO_3^- and CO_3^{2-} and between Na^+ and K^+, in the Pitzer method. Cohen et al. (1987) and Chan et al. (1992) showed that the higher-order terms in the Pitzer method are not necessary in predicting the water activity. It can be seen in Table 4.9 that in the experimental ionic-strength range, the predictions of the two methods agree within 6%. Even at high ionic strengths much beyond the experimentally tested range, the differences between the two methods' predictions are in all cases smaller than 30%. Note when the ionic strength is very high (~30 m, found by Kim et al., 1993b) the Pitzer method with the present parameters may not be applicable.

5. Deliquescence Relative Humidity

A solid substance absorbs water and becomes a saturated solution when the ambient relative humidity (RH) reaches its deliquescence point. The single salt relative humidity of deliquescence (RHD) is generally larger than its RHD in a multicomponent mixed system (Wexler and Seinfeld, 1991). Knowing the exact RHD of the atmospheric aerosol particle is important in aerosol modeling, but unfortunately, few data are available for solutions with more than two electrolytes.

Wexler and Seinfeld (1991) obtained a relationship between the single-salt RHD and temperature,

$$\begin{aligned} \ln \mathrm{RHD}(T) &= \ln \mathrm{RHD}(T_0) - \frac{M_w}{1000} m_s \frac{L_s}{R}\left(\frac{1}{T} - \frac{1}{T_0}\right) \\ &= \ln \mathrm{RHD}(T_0) + \alpha\left(\frac{1}{T} - \frac{1}{T_0}\right) \end{aligned} \tag{7}$$

where M_w is the molecular weight of water, m_s is the molality of the solute at saturation, $L_s = \Delta H^0_{f,s} - \Delta H^0_{f,aq}$ is the latent heat of fusion of the salt from a saturated solution at molality m_s, and $\Delta H^0_{f,s}$ and $\Delta H^0_{f,aq}$ are the standard heat of formation of the crystalline solid phase and of the substance in aqueous saturated solution at m_s, respectively.

Data at 298.15 K for calculating temperature dependence of RHDs of interest here and the calculated α values are given in Table 4.10. Note that only data for unhydrated solids are given. $CaCO_3$ (calcite) and $MgCO_3$ (magnesite) have very low solubilities so

we assume them to remain solids at ambient relative humidities. They can dissolve into the solution by reaction with some other species (e.g., H^+).

It is interesting to note that the RHDs of carbonate salts in Table 4.10 increase with increasing temperature whereas those of bicarbonate salts decrease with increasing temperature. Also, the RHDs of Na_2CO_3 and K_2CO_3 are highly dependent on temperature, while those of the bicarbonate salts are only slightly or moderately dependent on temperature.

6. Conclusions

Thermodynamic data for carbonate and bicarbonate salts that exist as components of atmospheric particles have been developed for gas/aerosol equilibrium models. The important carbonate species considered include $CO_2(g)$, $CO_2(aq)$, HCO_3^-, CO_3^{2-}, $NH_2CO_2^-$, $Na_2CO_3(s)$, $NaHCO_3(s)$, $K_2CO_3(s)$, $KHCO_3(s)$, $CaCO_3(s)$, $MgCO_3(s)$, $NH_4HCO_3(s)$, and $NH_2COONH_4(s)$. Three activity coefficient estimation methods, the Bromley, K-M, and Pitzer methods, have been critically examined for carbonate salts. Necessary parameters for these three methods are obtained or refitted to new available thermodynamic data. In general, the Pitzer method has been found to be superior to the other two methods for estimation of the multicomponent activity coefficient (The Pitzer method has been found to perform better in systems including crustal cations (Kim and Seinfeld, 1994)). Also with its capability of treating neutral species and weak

electrolytes, the Pitzer method is believed to be the best choice of the multicomponent activity coefficient estimation method for the gas/aerosol system.

To calculate aerosol water content, water activity data on binary carbonate solutions have been fitted by polynomial regression for the ZSR method. The relative humidities of deliquescence for the important carbonate salts and their temperature dependence have been described. Only the carbonates of potassium and sodium are expected to be in aqueous phase at ambient humidities.

Acknowledgment

This work was supported by the Electric Power Research Institute under agreement RP3189-03.

REFERENCES

Andronova, A.V., Gomes, L., Smirnov, V.V., Ivanov, A.V. and Shukurova, L.M. (1993). *Atmos. Environ.* 27A:2487-2493.

Babenko, A.M. and Andrianov, A.M. (1981). *Zh. Neorg. Khim.* 26:483-486.

Bassett, M. and Seinfeld, J.H. (1983). *Atmos. Environ.* 17:2237-2252.

Bassett, M. and Seinfeld, J.H. (1984). *Atmos. Environ.* 18:1163-1170.

Binkowski, F.S. (1991). *MARS-8 source Code*. U.S. EPA, Research Triangle Park, NC.

Bogoyavlenskii, P.S. and Gashpar, E.D. (1973). *Zh. Neorg. Khim.* 18:3125-3128.

Bromley, L.A. (1973). *AIChE J.* 19:313-320.

Chan, C.K., Flagan, R.C. and Seinfeld, J.H. (1992). *Atmos. Environ.* 26:1661-1673.

Chen, H., Sangster, J., Teng, T.T. and Lenzi, F. (1973). *Can. J. Chem. Eng.* 51:234-241.

Clarke, A.G. and Karani, G.N. (1992). *J. Atmos. Chem.* 14:119-128.

Clegg, S.L. and Whitfeld, M. (1991). In *Activity Coefficients in Electrolyte Solutions.* 2nd ed. (Pitzer, K.S., ed.) CRC Press, Boca Raton, Florida. pp. 279-434.

Cohen, M.D., Flagan, R.C. and Seinfeld, J.H. (1987). *J. Phys. Chem.* 91:4575-4582.

Denbigh, K. (1981). *The Principles of Chemical Equilibrium*, 4th ed. Cambridge University Press, Cambridge.

Gillette, D.A., Stensland, G.J., Williams, A.L., Barnard, W., Gatz, D., Sinclair, P.C. and Johnson, T.C. (1992). *Biogeochem. Cycles.* 6:437-457.

Goldberg, R.N. (1981). *J. Phys. Chem. Ref. Data.* 10:671-764.

Gomes, L. and Gillette, D.A. (1993). *Atmos. Environ.* 27A:2539-2544.

Harvie, C.E. and Weare, J.H. (1980). *Geochim. Cosmochim. Acta* 44:981-997.

Harvie, C.E., Møller, N. and Weare, J.H. (1984). *Geochim. Cosmochim. Acta* 48:723-751.

Junge, C. (1979). In *Saharan dust* (Morales, ed.). John Wiley, New York. pp. 49-60.

Kim, Y.P., Seinfeld, J.H. and Saxena, P. (1993a). *Aerosol Sci. Technol.* 19:157-181.

Kim, Y.P., Seinfeld, J.H. and Saxena, P. (1993b). *Aerosol Sci. Technol.* 19:182-198.

Kim, Y.P. and Seinfeld, J.H. (1994). "Atmospheric gas-aerosol equilibrium: III. Thermodynamics of crustal elements Ca^{2+}, K^{+}, and Mg^{2+}. *Aerosol Sci. Technol.* In press.

Kremann, R. and Zitak, A. (1909). *Monatsh.* 30:311-340.

Kusik, C.L. and Meissner, H.P. (1978). *AIChE Symp. Series.* 173:14-20.

Maurer, G. (1980). In *Thermodynamics of Aqueous Systems with Industrial Applications* (Newman, S.A. ed.). ACS Symposium Series 133, Washington D.C. pp. 139-172.

Meng, Z., Seinfeld, J.H., Saxena, P. and Kim, Y.P. (1994). "Contribution of water to particulate mass in the South Coast Air Basin." *Aerosol Sci. Technol.* In press.

Pawlikowski, E.M. and Prausnitz, J.M. (1983). *Ind. Eng. Chem. Fundam.* 22:86-90. "Correction" (1984). 23:270.

Peiper, J.C. and Pitzer, K.S. (1982). *J. Chem. Thermodyn.* 14:613-638.

Pilinis, C. and Seinfeld, J.H. (1987). *Atmos. Environ.* 21:2453-2466.

Pitzer, K.S. (1975). *J. Solution Chem.* 4:249-265.

Pitzer, K.S. (1991). In *Activity Coefficients in Electrolyte Solutions.* 2nd ed. (Pitzer, K.S., ed.) CRC Press, Boca Raton, FL. pp.75-153.

Pitzer, K.S. and Kim, J. (1974). *J. Ame. Chem. Soc.* 96:5701-5707.

Pitzer, K.S., Olsen, J., Simonson, J.M., Roy, R.N., Gibbons, J.J. and Rowe, L.-A. (1985). *J. Chem. Eng. Data.* 30:14-17.

Plummer, L.N., Parkhurst, D.L., Fleming, G.W. and Dunkle, S.A. (1988). *A Computer Program Incorporating Pitzer's Equations for Calculation of Geochemical Reactions In Brines,* Water-Resources Investigations Report 88-4153, U.S. Geological Survey, Reston, VA.

Pye, K. (1987). *Aeolian Dust and Dust Deposits.* Academic Press, London.

Robinson, R.A. and Stokes, R.J. (1965). *Electrolyte Solutions.* 2nd ed. Butterworth, London.

Roy, R.N., Gibbons, J.J., Wood, M.D. and Williams, R.W. (1983). *J. Chem. Thermodyn.* 15:37-47.

Roy, R.N., Hufford, K., Lord, P.J., Mrad, D.R., Roy, L.N. and Johnson, D.A. (1988). *J. Chem. Thermodyn.* 20:63-77.

Sarbar, M., Covington, A.K., Nuttall, R.L. and Goldberg, R.N. (1982a). *J. Chem. Thermodyn.* 14:967-976.

Sarbar, M., Covington, A.K., Nuttall, R.L. and Goldberg, R.N. (1982b). *J. Chem. Thermodyn.* 14:695-702.

Saxena, P., Hudischewskyj, A.B., Seigneur, C. and Seinfeld, J.H. (1986). *Atmos. Environ.* 20:1471-1483.

Saxena, P., Meng, Z. and Seinfeld, J.H. (1993a). In Twelfth Annual Meeting, AAAR, Oak Brook, IL, USA.

Saxena, P., Muller, P. K., Kim, Y. P., Seinfeld, J. H. and Koutrakis, P. (1993b). *Aerosol Sci. Technol*, 19:279-293.

Saxena, P. and Peterson, T.W. (1981). *J. Colloid Interface Sci.* 79:496-510.

Schütz, L. (1980). *Ann. N.Y. Acad. Sci.* 338:515-532.

Seidell, A. and Linke, W.F. (1965). *Solutilities of Inorganic and Metal-Organic Compounds*. Am. Chem. Soc., Washington D.C., Vol. II.

Setschénow, J. (1889). *Z. Physik. Chem.* 4:117.

Slivko, T.A., Shakhno, I.V., Plyushchev, V.E. and Malyshko, L.F. (1968). *Russian J. Inorganic Chem.* 13:1047-1049.

Stokes, R.H. and Robinson, R.A. (1966). *J. Phys. Chem.* 70:2126-2130.

Sturges, W.T., Harrison, R.M. and Barrie, L.A. (1989). *Atmos. Environ.* 23:1083-1098.

Vasconcelos, L.A., Macias, E.S. and White, W.H. (1994). Aerosol composition as a function of haze and humidity levels in the southwestern U.S. Submitted to *Atmos. Environ.*

Wagman, D.D., Evans, W.H., Parker, V.B., Schumm, R.H., Harlow, I., Bailey, S.M., Churney, K.L. and Nuttall, R.L. (1982). *The NBS Tables of Chemical Thermodynamic Properties, J. Phys. Chem. Ref. Data*, Vol. 11 suppl. 2.

Wexler, A.S. and Seinfeld, J.H. (1991). *Atmos. Environ.* 25A:2731-2748.

White, W.H., Macias, E.S., Nininger, R.C. and Schorran, D. (1994). Size-resolved measurements of light scattering by ambient particles. *Atmos. Environ.* (in press).

Yasunishi, A. and Yoshida, F. (1979). *J. Chem. Eng. Data.* 24:11-14.

Zemaitis, J.F., JR., Clark, D.M., Rafal, M. and Scrivner, N.C. (1986). *Handbook of Aqueous Electrolyte Thermodynamics*. AIChE, New York.

Table 4.1. Equilibrium relations and constants for carbonates

Equilibrium Relation	Equilibrium Constant Expression	Equilibrium Constant[a] K(298.15 K)	a	b	Units
$CO_2(g) = CO_2(aq)$	$\frac{[CO_2(a)]\gamma_{CO_2}}{p_{CO_2}}$	3.404×10^{-2}	8.1858	-28.9307	mole/kg /atm
$CO_2(aq) + H_2O = HCO_3^- + H^+$	$\frac{[HCO_3^-][H^+]\gamma_{HCO_3^-}\gamma_{H^+}}{[CO_2(a)]\gamma_{CO_2}a_w}$	4.299×10^{-7}	-3.0821	31.8139	mole/kg
$HCO_3^- = H^+ + CO_3^{2-}$	$\frac{[CO_3^{2-}][H^+]\gamma_{CO_3^{2-}}\gamma_{H^+}}{[HCO_3^-]\gamma_{HCO_3^-}}$	4.678×10^{-11}	-5.9908	38.8440	mole/kg
$NH_3(aq) + HCO_3^- = NH_2CO_2^- + H_2O$	$\frac{[NH_2CO_2^-]a_w\gamma_{NH_2CO_2^-}}{[NH_3(a)][HCO_3^-]\gamma_{HCO_3^-}\gamma_{NH_3}}$	3.0424	9.7119	0	kg/mole
$Na_2CO_3(s) = 2Na^+ + CO_3^{2-}$	$[Na^+]^2[CO_3^{2-}]\gamma^2_{Na^+}\gamma_{CO_3^{2-}}$	18.11	10.7713	30.5533	$mole^3/kg^3$
$NaHCO_3(s) = Na^+ + HCO_3^-$	$[Na^+][HCO_3^-]\gamma_{Na^+}\gamma_{HCO_3^-}$	0.3914	-7.5439	-5.6796	$mole^2/kg^2$
$K_2CO_3(s) = 2K^+ + CO_3^{2-}$	$[K^+]^2[CO_3^{2-}]\gamma^2_{K^+}\gamma_{CO_3^{2-}}$	2.541×10^5	12.4575	36.7272	$mole^3/kg^3$
$KHCO_3(s) = K^+ + HCO_3^-$	$[K^+][HCO_3^-]\gamma_{K^+}\gamma_{HCO_3^-}$	13.99	-7.5964	-2.5210	$mole^2/kg^2$
$CaCO_3(calcite, s) = Ca^{2+} + CO_3^{2-}$	$[Ca^{2+}][CO_3^{2-}]\gamma_{Ca^{2+}}\gamma_{CO_3^{2-}}$	4.959×10^{-9}	-	-	$mole^2/kg^2$
$MgCO_3(s) = Mg^{2+} + CO_3^{2-}$	$[Mg^{2+}][CO_3^{2-}]\gamma_{Mg^{2+}}\gamma_{CO_3^{2-}}$	6.812×10^{-6}	-	-	$mole^2/kg^2$
$NH_4HCO_3(s) = NH_4^+ + HCO_3^-$	$[NH_4^+][HCO_3^-]\gamma_{NH_4^+}\gamma_{HCO_3^-}$	-849.4	-	-	$mole^2/kg^2$
$NH_2COONH_4(s) = NH_2CO_2^- + NH_4^+$	$[NH_2CO_2^-][NH_4^+]\gamma_{NH_2CO_2^-}\gamma_{NH_4^+}$	64.023	-	-	$mole^2/kg^2$

[a] Constants a and b are in

$$K(T) = K(T_0)\exp\left\{a\left(\frac{T_0}{T}-1\right)+b\left(1+\ln\left(\frac{T_0}{T}\right)-\frac{T_0}{T}\right)\right\}, \text{ where } T_0 = 298 \text{ K}.$$

Table 4.2. Thermodynamic parameters for atmospheric aerosol carbonates[a]

Species	ΔG_f^0 kJ/mol	ΔH_f^0 kJ/mol	C_p^0 J/mol/K
CO_2 (g)	-394.359	-393.509	37.11
CO_2 (aq)	-385.98	-413.80	277.64[b]
Na_2CO_3 (s)	-1044.44	-1130.68	112.30
$NaHCO_3$ (s)	-851.0	-950.81	87.61
K_2CO_3 (s)	-1063.5	-1151.02	114.43
$KHCO_3$ (s)	-863.5	-963.2	89.27[c]
$CaCO_3$ (calcite, s)	-1128.79	-1206.92	81.88
$MgCO_3$ (s)	-1012.1	-1095.8	75.52
NH_4HCO_3 (s)	-665.9	-849.4	-
NH_2COONH_4(s)	-447.90	-645.05	-
HCO_3^-	-586.77	-691.99	88.43[b]
CO_3^{2-}	-527.81	-677.14	-234.52[b]
$NH_2CO_2^-$	-378.90[b]	-24.07[b]	93.039[b]

[a] All values are from Wagman et al. (1982) except noted.

[b] Obtained in this work by best fit of Maurer's (1980) equilibrium relations as a function of temperature.

[c] $C_p^0(NaHCO_3)C_p^0(K_2CO_3) / C_p^0(Na_2CO_3)$

Table 4.3. Parameter values for the Bromley method used for binary activity coefficient calculation[a]

Species	B (kg/mole)	upper limit of tested ionic strength (m)
$H\text{-}HCO_3$	-	-
H_2CO_3	-	-
NH_4HCO_3	-0.09092[c]	1
$(NH_4)_2CO_3$	-[d]	-
$NaHCO_3$	0.0065496[c]	1.3
Na_2CO_3	0.0089[b], -0.0038784[c]	3, 9.345
$KHCO_3$	-0.06174[c]	1
K_2CO_3	0.0372[b], 0.034872[c]	3, 24.306
$CaCO_3$	-	-
$MgCO_3$	-	-
$Ca(HCO_3)_2$	-	-
$Mg(HCO_3)_2$	-	-

[a]Formula:

$$\log \gamma_{12}^{0} = -\frac{0.511 z_1 z_2 I^{1/2}}{1 + I^{1/2}} + \frac{(0.06 + 0.6B) z_1 z_2 I}{\left(1 + \frac{1.5}{z_1 z_2} I\right)^2} + BI$$

[b]Values are from Bromley (1973).

[c]This work.

[d]$$\gamma_{(NH_4)_2CO_3}^{0} = \left(\frac{\gamma_{NH_4HCO_3}^{0}}{\gamma_{NaHCO_3}^{0}} \right)^{4/3} \gamma_{Na_2CO_3}^{0}$$

Table 4.4. Parameter values for the Kusic and Meissner method used for binary activity coefficient calculation[a]

Species	q [b]	upper limit of tested ionic strength (m)
H-HCO_3	-	-
H_2CO_3	-	-
NH_4HCO_3	-1.9974	1
$(NH_4)_2CO_3$	-[c]	-
$NaHCO_3$	0.4771	1.3
Na_2CO_3	0.00177	9.345
$KHCO_3$	-1.3162	1
K_2CO_3	0.9216	24.306
$CaCO_3$	-	-
$MgCO_3$	-	-
$Ca(HCO_3)_2$	-	-
$Mg(HCO_3)_2$	-	-

[a]Formula:

$$\Gamma^0 = [1 + B(1+0.1I)^q - B]\Gamma^*$$

$$B = 0.75 - 0.065q$$

$$\log\Gamma^* = \frac{-0.5107I^{1/2}}{1+CI^{1/2}}$$

$$C = 1 + 0.055q\exp(-0.023I^3)$$

$$\Gamma^0 = \left(\gamma_{12}^0\right)^{1/z_1z_2}$$

[b]*All of the data given here are obtained in this work; none of them were* available in the original Kusik and Meissner's work (1978).

[c]$$\gamma^0_{(NH_4)_2CO_3} = \left(\frac{\gamma^0_{NH_4HCO_3}}{\gamma^0_{NaHCO_3}}\right)^{4/3}\gamma^0_{Na_2CO_3}$$

Table 4.5. Parameter values for the Pitzer method used for binary activity coefficient calculation[a]

Species	$\beta^{(0)}$	$\beta^{(1)}$	$\beta^{(2)}$	C^{ϕ}
H-HCO_3	0	0	0	0
H_2CO_3	0	0	0	0
Na_2CO_3	0.0399	1.389	0	0.0044
$NaHCO_3$	0.0277	0.0411	0	0
K_2CO_3	0.1488	1.43	0	-.0015
$KHCO_3$	0.0296	-.013	0	-.008
$CaCO_3$	0	0	0	0
$Ca(HCO_3)_2$	0.4	2.977	0	0
$MgCO_3$	0	0	0	0
$Mg(HCO_3)_2$	0.329	0.6072	0	0
NH_4HCO_3[b]	-0.038	0.070	0	0
$(NH_4)_2CO_3$[c]	0.1488	1.43	0	-.0015

[a] All data are from Harvey et al. (1984) unless noted. Formula:

$$\ln \gamma_{12}^{0} = z_1 z_2 f^{\gamma} + m\left(\frac{2\upsilon_1\upsilon_2}{\upsilon}\right)B_{12}^{\gamma} + m^2\frac{2(\upsilon_1\upsilon_2)^{1/2}}{\upsilon}C_{12}^{\gamma}$$

$$f^{\gamma} = -0.392\left[\frac{I^{1/2}}{1+bI^{1/2}} + \frac{2}{b}\ln(1+bI^{1/2})\right]$$

$$b = 1.2$$

$$B_{12}^{\gamma} = 2\beta_{12}^{(0)} + \frac{2\beta_{12}^{(1)}}{\alpha^2 I}\left[1 - e^{-\alpha I^{1/2}}\left(1+\alpha I^{1/2} - \frac{\alpha^2}{2}I\right)\right]$$

$$C_{12}^{\gamma} = \frac{3}{2}C_{12}^{\phi}$$

$$\alpha = 2.0$$

[b] Roy et al., 1988.

[c] Data for K_2CO_3.

Table 4.6. Common-ion two electrolyte parameter values for the Pitzer method[a]

c	c'	$\theta_{cc'}$	$\Psi_{cc'HCO_3}$	$\Psi_{cc'CO_3}$
Na^+	K^+	-.012	-.003	.003
Na^+	Ca^{2+}	.07	0	0
Na^+	Mg^{2+}	.07	0	0
Na^+	NH_4^+	-	-	-
Na^+	H^+	.036	0	0
K^+	Ca^{2+}	.032	0	0
K^+	Mg^{2+}	0.	0	0
K^+	NH_4^+	-	-	-
K^+	H^+	.005	0	0
Ca^{2+}	Mg^{2+}	.007	0	0
Ca^{2+}	NH_4^+	-	-	-
Ca^{2+}	H^+	.092	0	0
Mg^{2+}	NH_4^+	-	-	-
Mg^{2+}	H^+	.10	0	0
NH_4^+	H^+	-.019[b]	-	-

Table 4.6. (Continued)

a	a'	$\theta_{aa'}$	$\Psi_{aa'Na}$	$\Psi_{aa'K}$	$\Psi_{aa'Ca}$	$\Psi_{aa'Mg}$	$\Psi_{aa'NH4}$	$\Psi_{aa'H}$
HCO_3^-	SO_4^{2-}	.01	-.005	0	0	-.161	0.005424[c]	0
HCO_3^-	HSO_4^-	0	0	0	0	0	-	0
HCO_3^-	NO_3^-	0.0414[c]	-0.007438[c]	0.001373[c]	-	-	0.000559[c]	-
HCO_3^-	Cl^-	.03	-.015	0	0	-.096	-0.001168[c]	0
HCO_3^-	CO_3^{2-}	-.04	.002	.012	0	0	-	0
CO_3^{2-}	SO_4^{2-}	.02	-.005	-.009	0	0	-	0
CO_3^{2-}	HSO_4^-	0	0	0	0	0	-	0
CO_3^{2-}	NO_3^-	-0.081[c]	0.0103[c]	0.012[c]	-	-	-	-
CO_3^{2-}	Cl^-	-.02	.0085	.004	0	0	-	0

[a] All data are from Harvey et al. (1984) unless noted.

[b] From Pitzer (1979).

[c] This work.

Table 4.7. Neutral-ion parameter values for the Pitzer method[a]

i	$\lambda_{CO_2,i}$
H^+	0
NH_4^+	0.01[b]
Na^+	0.100
K^+	0.051
Ca^{2+}	0.183
Mg^{2+}	0.183
Cl^-	-0.005
NO_3^-	-0.0457[b]
HSO_4^-	-0.003
SO_4^{2-}	0.097
HCO_3^-	0
CO_3^{2-}	0

[a] All data are from Harvey et al. (1984) unless noted.

[b]This work.

Table 4.8. Coefficients of $m(a_w)$ for the polynomial fit of water activity data[a]

Species	a_0	a_1	a_2	a_3	a_4	a_5	Maximum tested molality (m) and data references
H-HCO_3	-	-	-	-	-	-	
H_2CO_3	-	-	-	-	-	-	
Na_2CO_3[b]	8.4770	4.5415	-0.95135	-9.1968	-10.374	7.4862	3.1, Goldberg, 1981
$NaHCO_3$	34.563	-10.302	-8.7146	-41.714	8.4842	17.685	1.3, Sarbar et al., 1982a
K_2CO_3	12.520	-2.8762	-26.332	20.214	13.551	-17.087	8.1, Sarbar et al., 1982b
$KHCO_3$[c]	2.0051	17.786	-8.1065	-1.7529	-18.033	8.0898	1.0, Roy et al., 1983
$CaCO_3$	-	-	-	-	-	-	
$Ca(HCO_3)_2$[d]	13.343	-42.201	124.57	-234.02	218.83	-80.501	1.0, Pitzer et al., 1985
$MgCO_3$	-	-	-	-	-	-	
$Mg(HCO_3)_2$[d]	22.444	-15.847	-11.481	8.8506	2.2333	-6.3022	1.6, Pitzer et al., 1985
NH_4HCO_3	15.204	3.6435	-13.439	5.8801	-26.206	14.905	1.0, Roy et al., 1988
$(NH_4)_2CO_3$	-	-	-	-	-	-	

[a] $m(a_w) = a_0 + a_1 a_w + a_2 a_w^2 + a_3 a_w^3 + a_4 a_w^4 + a_5 a_w^5$

[b]Valid down to RH=30%.

[c]Valid down to RH=60%.

[d]Water activities are predicted by the Pitzer method for the molality up to 10 m with the parameters given by Pitzer et al. (1985).

Table 4.9. Comparison of the ZSR and Pitzer methods for estimation of water activity†

Na_2CO_3-$NaHCO_3$				K_2CO_3-$NaHCO_3$			
a_W	*m*-Pitzer	*m*-ZSR	δ(%)	a_W	*m*-Pitzer	*m*-ZSR	δ(%)
0.986	0.200	0.212	6.2	0.985	0.200	0.202	0.9
0.934	1.000	1.026	2.6	0.932	1.000	0.949	5.1
0.864	2.000	2.177	8.8	0.859	2.000	1.892	5.4
0.778	3.000	3.488	16.3	0.778	3.000	2.816	6.1
0.679	4.000	4.806	20.1	0.693	4.000	3.691	7.7
0.571	5.000	5.921	18.4	0.609	5.000	4.519	9.6
0.459	6.000	6.686	11.4	0.528	6.000	5.303	11.6
0.350	7.000	7.079	1.1	0.452	7.000	6.028	13.9
0.253	8.000	7.190	10.1	0.384	8.000	6.673	16.6
0.171	9.000	7.146	20.6	0.323	9.000	7.222	19.8
0.108	10.000	7.051	29.5	0.271	10.000	7.670	23.3

†In the calculation we have assumed that the molar ratio of the two compounds is 1.0 and neglected the cooperated interactions between ions in the Pitzer method. The solutions are hypothetical only; chemical reactions in the solutions are ignored. a_W is water activity, "*m*" is molality in units of M, and δ is the relative difference between predictions of the two methods.

Table 4.10. Data for calculating temperature dependence of deliquescence relative humidity (RHD)

Species	RHD[a]	$\Delta H^0_{f,s}$ [b] (kJ/mol)	$\Delta H^0_{f,aq}$ [c] (kJ/mol)	m_s (mol/kg)	α
Na_2CO_3	0.897697[d]	-1130.68	-1163.68	2.767[d]	-198
$NaHCO_3$	0.96400[e]	-950.81	-932.90	1.223[e]	47.4
K_2CO_3	0.444778[f]	-1151.02	-1182.8	8.102[f]	-557
$KHCO_3$	-	-963.2	-942.2	3.6758[g]	167
NH_4HCO_3	-	-849.4	-821.7[h]	3.0594[i]	183

[a]At 298.15 K.

[b]Wagman et al. (1982).

[c]Extrapolated from Wagman et al. (1982).

[d]Goldberg (1981).

[e]Sarbar et al. (1982a).

[f]Sarbar et al. (1982b).

[g]Babenko and Andrianov (1981).

[h]In unspecified dilution. -824.50, if at infinite dilution.

[i]Interpolated from Seidell and Linke (1965).

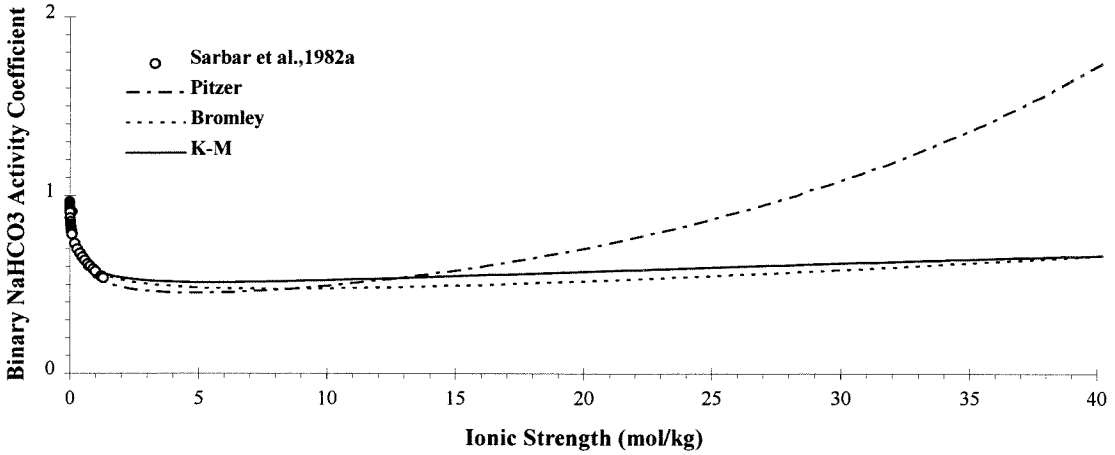

Fig. 4.1 Comparison of mean binary activity coefficient estimation methods for $NaHCO_3$. Data are from Sarbar et al. (1982a).

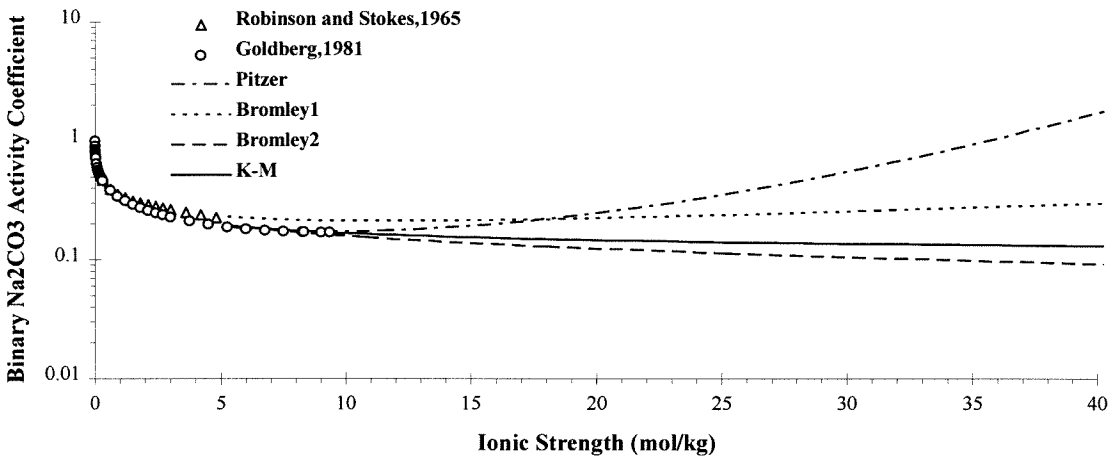

Fig. 4.2 Comparison of mean binary activity coefficient estimation methods for Na_2CO_3. Data are from Robinson and Stokes (1965) and Goldberg (1981).

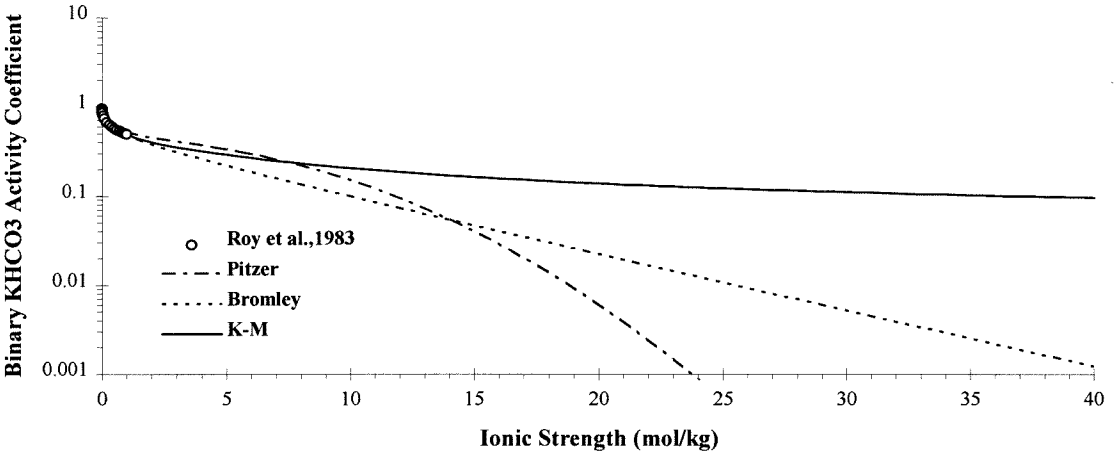

Fig. 4.3 Comparison of mean binary activity coefficient estimation methods for $KHCO_3$. Data are from Roy et al. (1983).

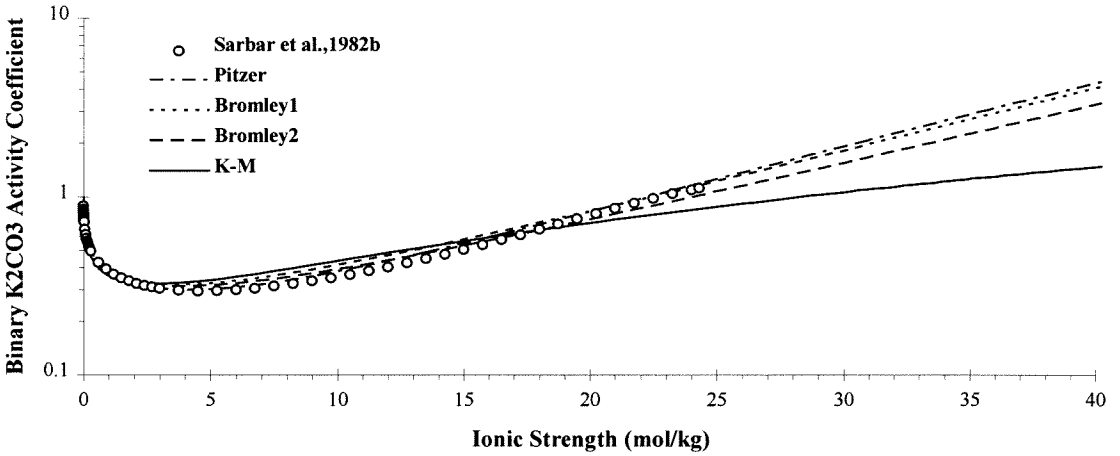

Fig. 4.4 Comparison of mean binary activity coefficient estimation methods for K_2CO_3. Data are from Sarbar et al. (1982b). "Bromley1" and "Bromley2" correspond to the "B" values from Bromley (1973) and this work.

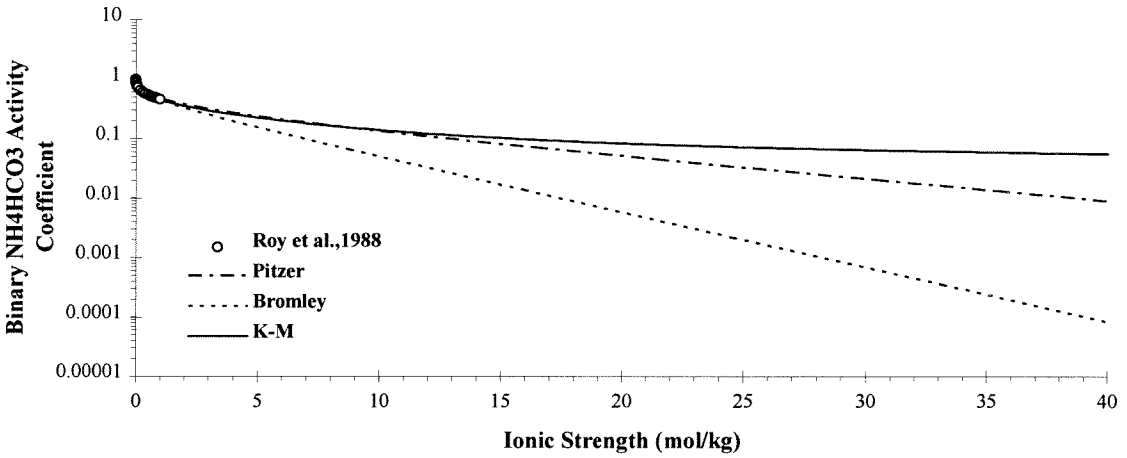

Fig. 4.5 Comparison of mean binary activity coefficient estimation methods for NH_4HCO_3. Data are from Roy et al. (1988).

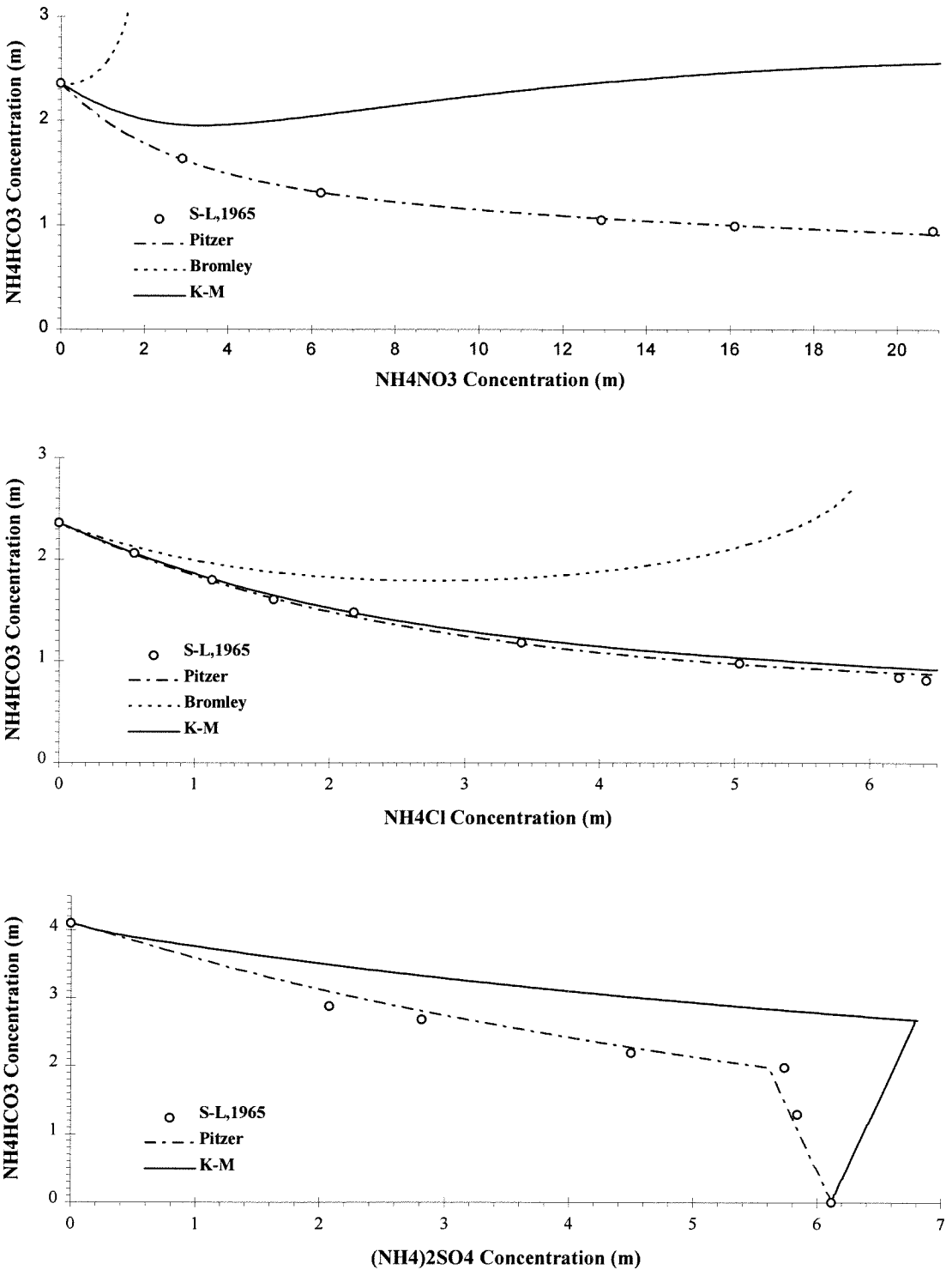

Fig. 4.6 Comparison of the estimated solubility of NH_4HCO_3 by the Bromley, the K-M and the Pitzer methods. S-L: Seidell and Linke, 1965. (a) in NH_4HCO_3-NH_4NO_3 solution, data measured at T=15 °C; (b) in NH_4HCO_3-NH_4Cl solution, data measured at T=15 °C; (c) in NH_4HCO_3-$(NH_4)_2SO_4$ solution, data measured at T=35 °C.

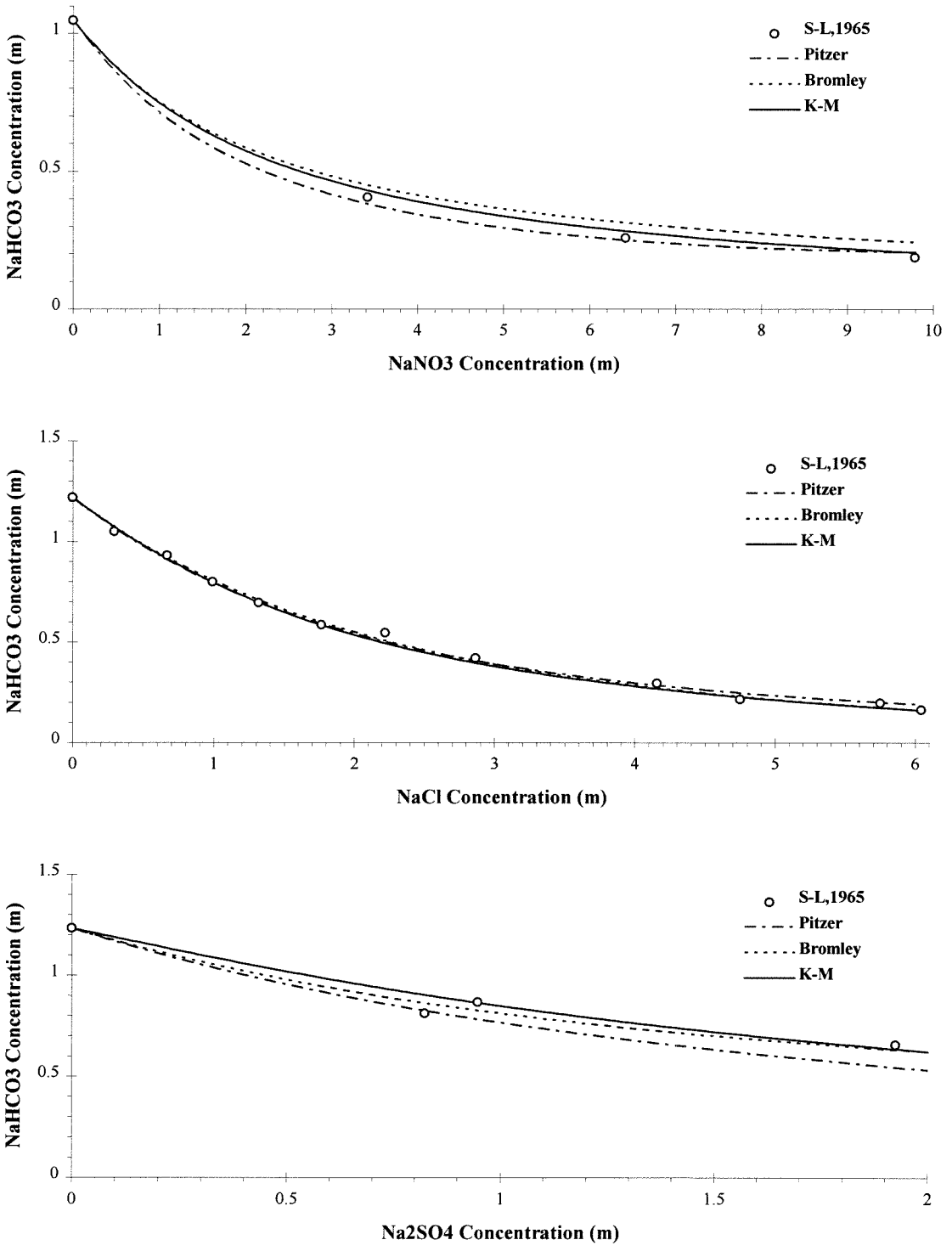

Fig. 4.7 Comparison of the estimated solubility of $NaHCO_3$ by the Bromley, the K-M and the Pitzer methods. S-L: Seidell and Linke, 1965. (a) in $NaHCO_3$-$NaNO_3$ solution, data measured at T=15 °C; (b) in $NaHCO_3$-NaCl solution, data measured at T=25 °C; (c) in $NaHCO_3$-Na_2SO_4 solution, data measured at T=25 °C.

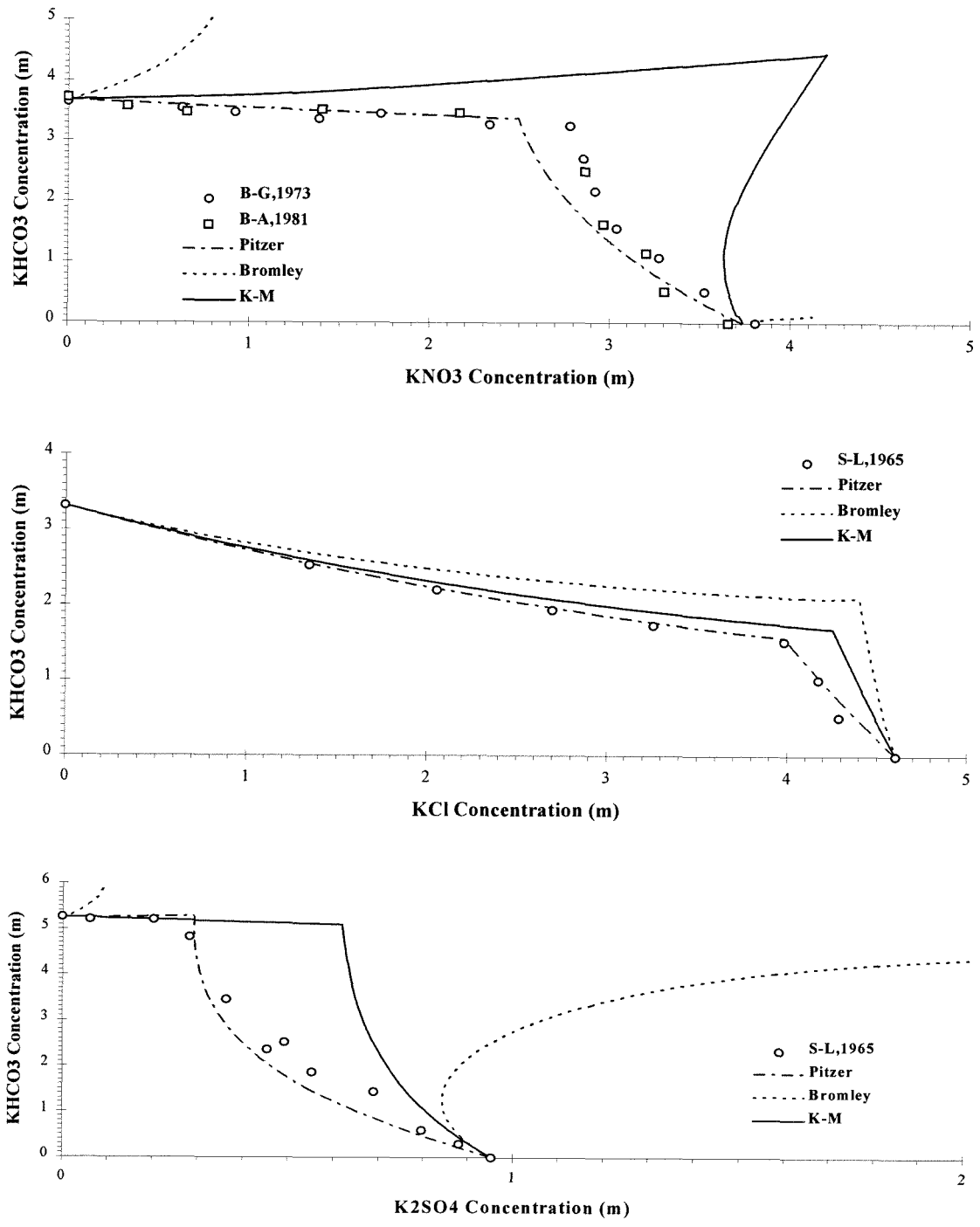

Fig. 4.8 Comparison of the estimated solubility of $KHCO_3$ by the Bromley, the K-M and the Pitzer methods. S-L: Seidell and Linke, 1965; B-G: Bogoyavlenskii and Gashpar (1973); B-A: Babenko and Andrianov (1981). (a) in $KHCO_3$-KNO_3 solution, data measured at T=25 °C; (b) in $KHCO_3$-KCl solution, data measured at T=20 °C; (c) in $KHCO_3$-K_2SO_4 solution, data measured at T=50 °C.

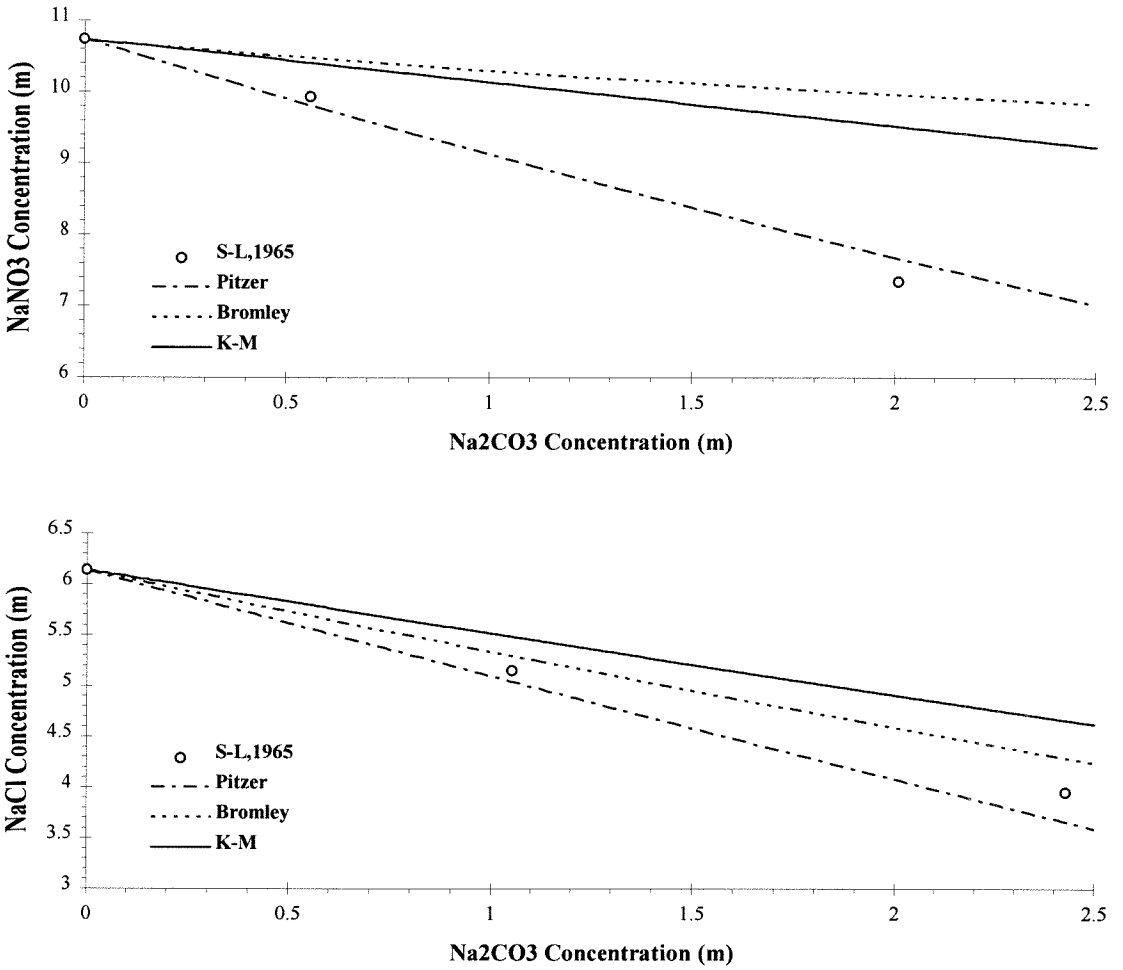

Fig. 4.9 Comparison of the estimated solubility by the Bromley, the K-M and the Pitzer methods. S-L: Seidell and Linke, 1965. (a) $NaNO_3$ in $NaNO_3$-Na_2CO_3 solution, data measured at T=24.2 °C; (b) NaCl in NaCl-Na_2CO_3 solution, data measured at T=25 °C.

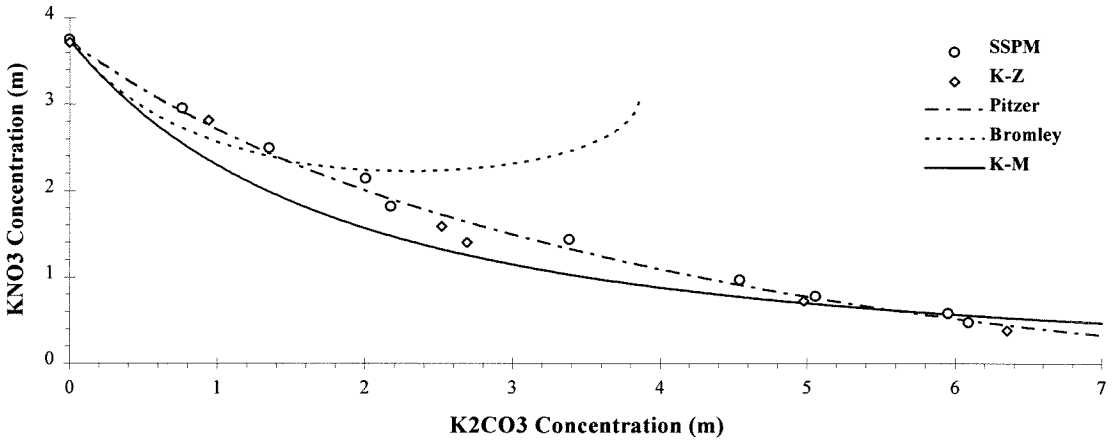

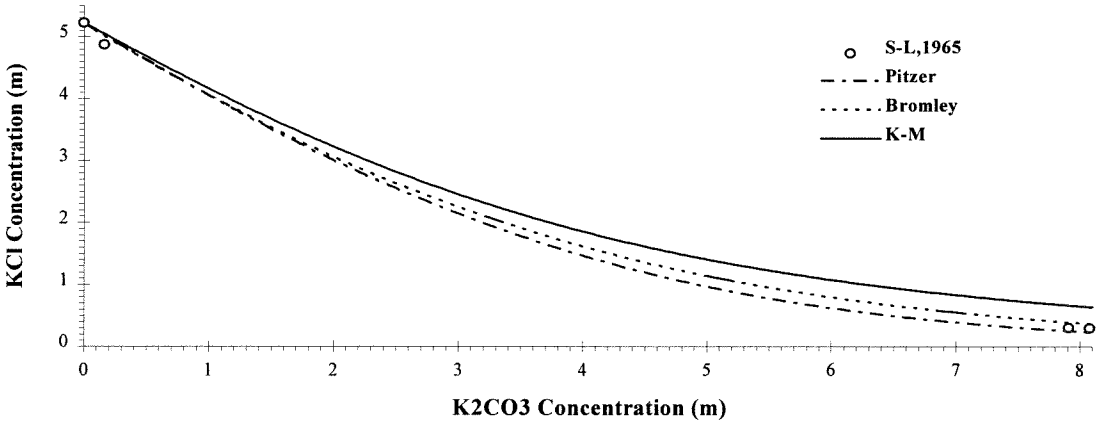

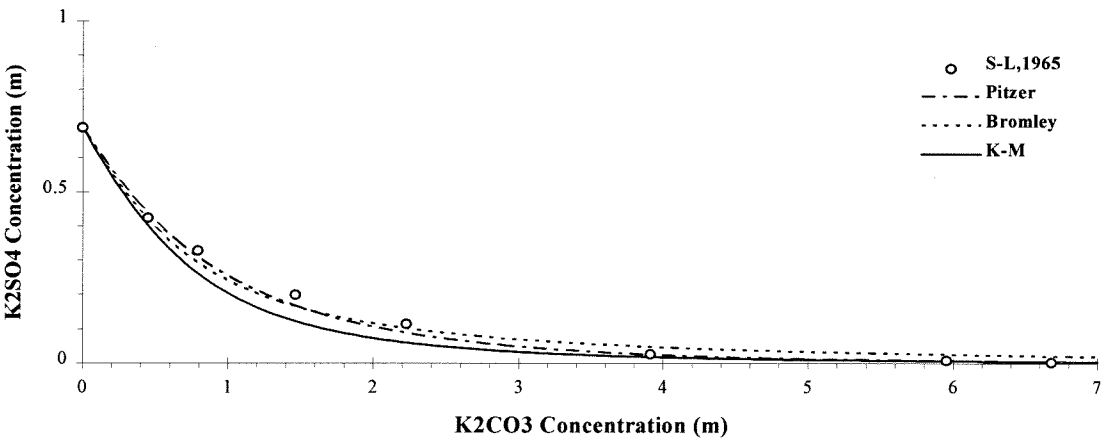

Fig. 4.10 Comparison of the estimated solubility by the Bromley, the K-M and the Pitzer methods. S-L: Seidell and Linke, 1965; SSPM: Slivko et al. (1968); K-Z: Kremann and Zitak (1909). (a) KNO_3 in KNO_3-K_2CO_3 solution, data measured at T=25 °C (SSPM) and T=24.2 °C (K-Z); (b) KCl in KCl-K_2CO_3 solution, data measured at T=30 °C; (c) K_2SO_4 in K_2SO_4-K_2CO_3 solution, data measured at T=25 °C.

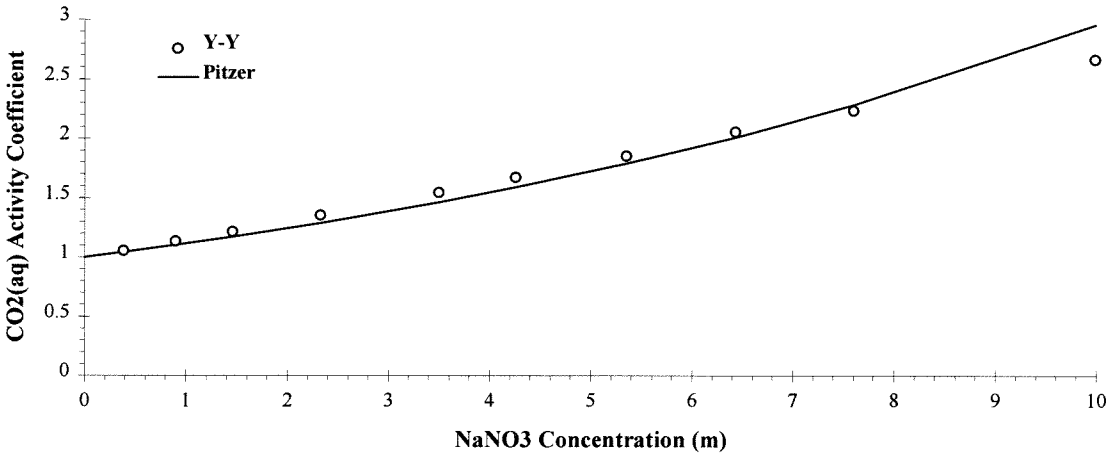

Fig. 4.11 Activity coefficient of aqueous CO_2 in $NaNO_3$ solution predicted by the Pitzer method. Data are converted from Yasunishi and Yoshida (1979)'s solubility data measured at T=25 °C.

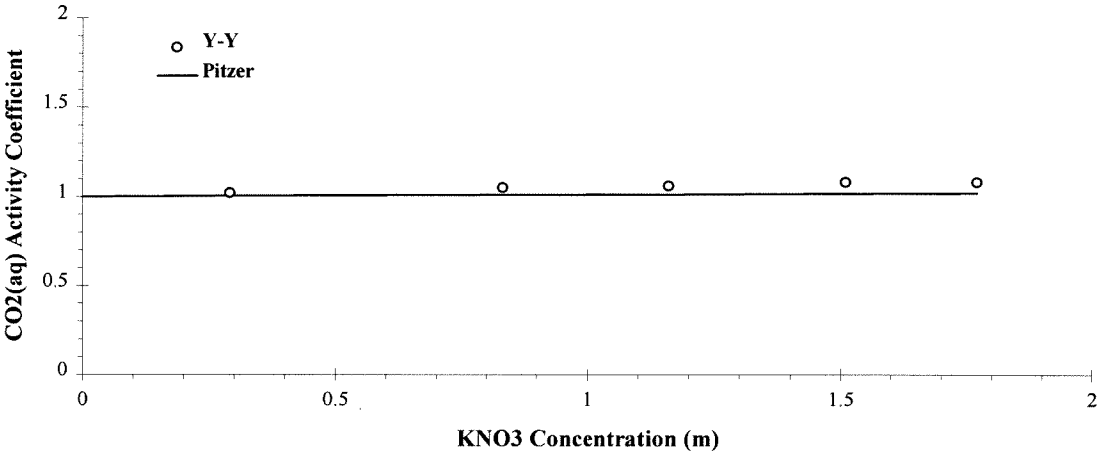

Fig. 4.12 Activity coefficient of aqueous CO_2 in KNO_3 solution predicted by the Pitzer method. Data are converted from Yasunishi and Yoshida (1979)'s solubility data measured at T=25 °C.

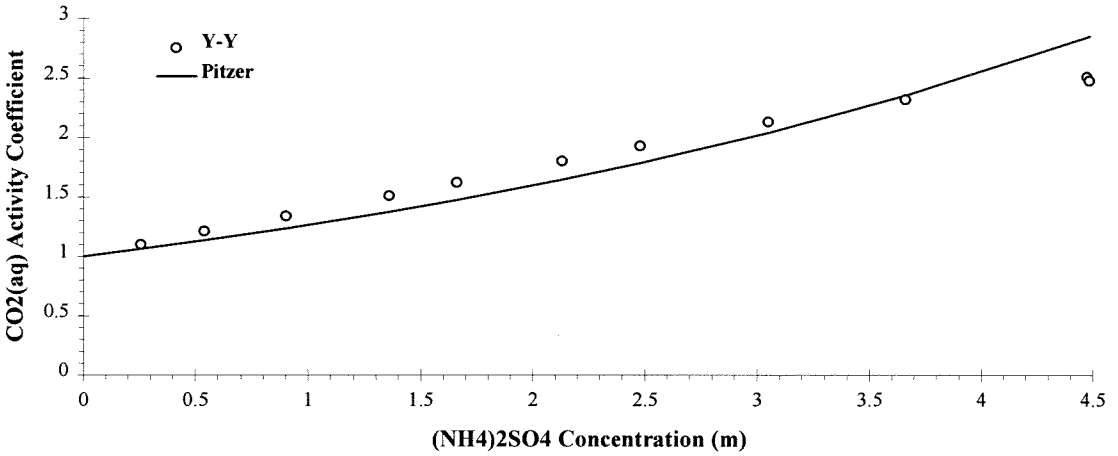

Fig. 4.13 Activity coefficient of aqueous CO_2 in $(NH_4)_2SO_4$ solution predicted by the Pitzer method. Data are converted from Yasunishi and Yoshida (1979)'s solubility data measured at T=25 °C.

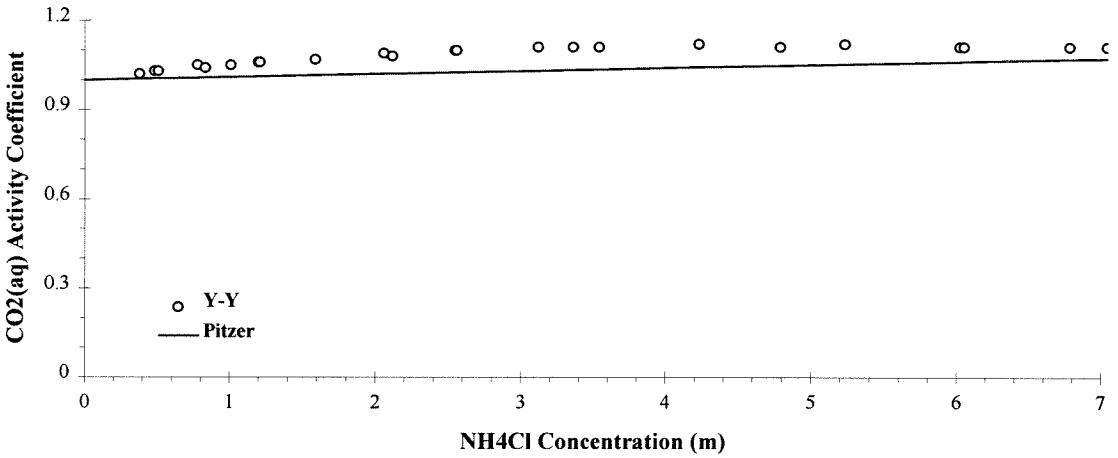

Fig. 4.14 Activity coefficient of aqueous CO_2 in NH_4Cl solution predicted by the Pitzer method. Data are converted from Yasunishi and Yoshida (1979)'s solubility data measured at T=25 °C.

Chapter 5

Gas/Aerosol Distribution of Formic and Acetic Acids

[The text of this chapter appears in: Meng Z., Seinfeld J. H., and Saxena P. (1995) *Aerosol Science and Technology* **23**, 561-578.]

ABSTRACT

Data and correlations for evaluating the gas/aerosol equilibrium of formic and acetic acids are developed. The species considered include HCOOH(g), CH_3COOH(g), HCOOH(aq), CH_3COOH(aq), $HCOO^-$, CH_3COO^-, HCOONa(s), CH_3COONa(s), HCOOK(s), $(HCOO)_2Ca$(s), and $(CH_3COO)_2Ca$(s). Based on available thermodynamic data, we show that the gas/aerosol distribution of formic and acetic acids is strongly on the gas-phase side for typical sulfate/nitrate/ammonium/sodium/chloride/water aerosols and that dissolved formate and acetate have negligible effect on the gas/aerosol equilibrium of the other components.

1. Introduction

Organic acids are apparently ubiquitous in the atmosphere (Table 5.1). Formic (HCOOH) and acetic (CH_3COOH) are the most abundant organic acids measured in the atmosphere. It is also seen from Table 5.1 that the concentrations of organic acids are generally elevated in the urban as compared to the non-urban atmosphere.

Organic acids are also important chemical constituents of rain water (Noller et al., 1990; Avery et al., 1991; Sanhueza et al., 1992; Kumar et al., 1993) and of fog and cloud water (Keene and Galloway, 1986; Murano et al., 1988; Collett et al., 1990). Avery et al. (1991) reported that HCOOH and CH_3COOH contributed 23% of the acidity in rain water received in Wilmington, NC, between October 1, 1987, and September 30, 1990. In the Venezuelan savanna region, Sanhueza et al. (1992) found that over 50% of the free acidity in the rain water may be attributable to HCOOH and CH_3COOH. Pierson et al. (1988) have found evidence that organic acids can affect the acidity of dew. Kotronarou and Sigg (1993) reported that, as a result of the presence of formate and acetate, S(IV) oxidation rates in fog water were significantly lower than those expected in their absence.

Observations of organic acids in the aerosol phase, as opposed to the droplet, are relatively scarce. From aerosol samples taken in Charlottesville, Virginia, Andreae et al. (1987) reported mixing ratios of formic and pyruvic acids of 1.82 and 0.086 ppb in the gas phase, and 0.025 and 0.015 ppb in the aerosol phase. This implies that both acids

were present predominantly as gas; only about 1-2% of the total atmospheric formate and 10-20% of the total pyruvate were in the particulate phase.

Quantitative information on the gas/aerosol equilibrium of organic species is generally not available. Organic acids are, as noted above, ubiquitous in the atmosphere. Of fundamental interest to atmospheric chemistry is the gas/particle distribution of organic acids. In this work we assemble and organize existing thermodynamic data relevant to the atmospheric gas/aerosol distribution of formic and acetic acids. Second, we evaluate, based on these data, the gas/aerosol distribution of formic and acetic acids in typical sulfate, nitrate, ammonium, sodium, chloride, water systems.

2. Chemical Equilibria Involving Formate and Acetate Salts

Chemical equilibria involving atmospherically important formates and acetates are given in Table 5.2. The equilibrium constant is expressed as (Kim et al., 1993a)

$$K(T) = K(T_0)\exp\left\{-\frac{\Delta H_f^0}{RT_0}\left(\frac{T_0}{T}-1\right)-\frac{\Delta C_p^0}{R}\left(1+\ln\left(\frac{T_0}{T}\right)-\frac{T_0}{T}\right)\right\} \quad (1)$$

where $K(T)$ and $K(T_0)$ are the equilibrium constants at temperatures T and T_0 (298 K). ΔH_f^0 and ΔC_p^0 are changes of the standard molar enthalpy of formation and the molar heat capacity in the reaction at temperature T_0. In deriving Equation (1) the specific heat

is assumed to be constant and thus the enthalpy varies linearly with temperature over the range T to T_0. These thermodynamic data are listed in Table 5.3. Most of the values cited are from the NBS Thermodynamic Tables (Wagman et al., 1982) so as to maintain internal consistency.

Values of the equilibrium constants at 298 K and parameters that determine their dependence on temperature are also given in Table 5.2. However, since some necessary thermodynamic data required to calculate the temperature dependence of the equilibrium constants are lacking, data from other sources are required. The Henry's law constants for formic acid and acetic acid and their dissociation constants in solution, for example, are available from Clegg and Brimblecombe (1988). While there is virtually no difference between the Henry's law constants of formic acid at 298 K as given by Clegg and Brimblecombe (1988) and calculated from Wagman et al.'s (1982) data, the difference for acetic acid is as large as 40%. The equilibrium constants for dissolution of solid $HCOONH_4$, CH_3COONH_4, CH_3COOK, $(HCOO)_2Mg$, and $(CH_3COO)_2Mg$ are not available in the literature; therefore, their effects on aerosol chemistry cannot be predicted. The ammonium salts are most likely to be important and their formation in the atmosphere has been discussed by Grosjean et al. (1988) but remains speculative.

3. Estimation of Activity Coefficients

The equilibrium constant can be expressed as (Denbigh, 1981; Kim et al., 1993a)

$$K_j = \prod_i (\gamma_i m_i)^{\nu_{ij}} \tag{2}$$

where ν_{ij} is the stoichiometric coefficient of the ith species in the jth reaction, m_i is the species molality (mol kg^{-1}), and γ_i is its activity coefficient. The accuracy of the calculated equilibrium species concentrations depends critically on estimation of the activity coefficients. In the recently developed gas/aerosol equilibrium code SCAPE (Kim et al., 1993ab; Kim and Seinfeld, 1995), the three widely used multicomponent activity coefficient estimation methods, namely Bromley (1973), Kusik and Meissner (1978), and Pitzer (Pitzer and Kim, 1974; Pitzer, 1991), have been evaluated in detail for the species: H^+, NH_4^+, Na^+, NO_3^-, Cl^-, HSO_4^-, SO_4^{2-}, Ca^{2+}, K^+, and Mg^{2+}.

Formulae and parameter values for the Bromley, Kusik and Meissner (K-M), and Pitzer methods for estimation of the binary activity coefficients for the formate and acetate system are given in Tables 5.4-5.6, respectively. Measurements of osmotic and activity coefficients are only available for HCOONa, CH_3COONa, CH_3COOK, and $(CH_3COO)_2Mg$; therefore the original parameter values are only available for these compounds. The B values for other compounds for the Bromley method are estimated based on a formula given by Bromley (1973), which uses information on the individual ions of the compound. These estimated B values are generally less accurate than those

derived from measurements and are only intended as an approximation when the direct fitting B values are not available.

Figure 5.1 shows the HCOONa binary activity coefficient as a function of ionic strength predicted by the three methods, together with the experimental data acquired by Bonner (1988). Values of the parameters B and q for the Bromley and K-M methods have been refitted to both Hamer and Wu's and Bonner's experimental data for ionic strength up to 14.7 m. In spite of using new fitting parameters (i.e., B and q) for the Bromley and K-M methods, there is some disagreement between predicted and measured values of the activity coefficient. The Pitzer method, whose parameters were obtained by fitting Hamer and Wu's (1972) experimental data for ionic strength only up to 3.5 m, starts to depart from the measured activity coefficients at an ionic strength of about 7 m. At high ionic strength the Bromley and K-M methods behave similarly for HCOONa, whereas the Pitzer method predicts a considerably lower value of the activity coefficient.

Figures 5.2-5.4 show results similar to those in Figure 5.1 for CH_3COONa, CH_3COOK, and $(CH_3COO)_2Mg$, respectively. For CH_3COONa, the behavior of the three methods is similar to that for HCOONa. The Pitzer method agrees well with the new data, although its parameters were obtained from the old data (Hamer and Wu, 1972) that were measured for ionic strength up to only 3.5 m. For CH_3COOK, the experimental data are only available at low ionic strengths, and all the three methods perform well. At high ionic strengths, however, the Pitzer method behaves quite differently from the

Bromley and K-M methods. For $(CH_3COO)_2Mg$, the Bromley and K-M methods accurately predict the measured data while the Pitzer method, with parameters given by Kim and Frederick (1988), greatly overestimated the binary activity coefficients. This systematic overestimate of the Pitzer method is not likely a result of the Pitzer theory itself but the choice of its fitting parameters.

The multicomponent Pitzer method requires additional ion interaction parameters besides those specific parameters for the binary salts listed in Table 5.6. Because many important parameter values for this system are not available for the Pitzer method, we do not adopt the multicomponent Pitzer method at this time. Limited by the available data and keeping consistency with previous work, it appears that we can use the Bromley method to estimate the binary activity coefficients and employ the K-M method as the multicomponent activity coefficient estimation method. The K-M method has been chosen as the binary activity coefficient estimation method for multicomponent activity coefficient calculation in previous work related to the development of the gas/aerosol equilibrium code SCAPE (Kim et al., 1993a; Kim and Seinfeld, 1995). For the four formate and acetate salts considered here, the behavior of the Bromley and K-M methods is similar. Considering that all the necessary parameter (B) values for the Bromley method are available for the aerosol system of interest here, we will employ the Bromley method as the binary activity coefficient estimation method.

Because of a lack of data it is not possible to evaluate the activity coefficients of aqueous molecular HCOOH and CH_3COOH, and consequently these are assumed to be unity. Such approximations have been used by Clegg and Brimblecombe (1988) in less concentrated solutions than expected in aerosols. The activity coefficients of the aqueous molecules in a concentrated solution are generally larger than 1.0 as a result of the salting effect that tends to reduce the gas solubilities in the solution (e.g., Khan et al., 1994). However, it should be noted that an increase of gas solubilities in the presence of salts has also been observed (Ohe, 1991).

4. Estimation of Water Activity

The ZSR method (Stokes and Robinson, 1966; Chen et al., 1973) has been used to estimate atmospheric aerosol water content in SCAPE (Kim et al., 1993a; Kim and Seinfeld, 1995). Aerosol water content W is given by (Kim et al., 1993a)

$$1 = \sum_i \frac{m_i}{m_{i0}(a_w)}, \tag{3}$$

$$W = \sum_i \frac{M_i}{m_{i0}(a_w)} \tag{4}$$

where M_i and m_i are the molar concentrations of substance i in the atmosphere (mole/m^3 air) and in the aerosol water (mole/kg water), and $m_{i0}(a_w)$ is the molality of the binary solution at the equilibrium water activity, a_w, of the multicomponent solution.

The influence on aerosol water content resulting from dissolved formic and acetic acids is actually small at ambient conditions. This can be seen by examining Eq. (3). By assuming $p_{HCOOH} = p_{CH3COOH} = 10$ ppb, $T = 298$ K, and pH = 5, the calculated aqueous-phase concentrations are: [HCOOH(aq)] $\approx 5.5\times10^{-5}$ M, [$HCOO^-$] $\approx 1.0\times10^{-3}$ M, [$CH_3COOH(aq)$] $\approx 5.5\times10^{-5}$ M, and [CH_3COO^-] $\approx 9.6\times10^{-5}$ M. However, the values of m_{i0} generally range from 1 to 10 M for RH between 65% and 95%. Therefore, the contributions to the summation in Eq. (3) from formate and acetate are negligibly small, and aerosol water content change due to dissolved formic and acetic acids from the gas phase can be neglected at normal ambient conditions.

5. Gas/Aerosol Distribution of Formic and Acetic Acids

The few existing measurements available suggest that, of the total atmospheric amounts, a small percentage of formate and acetate resides in the aerosol phase (Table 5.1). Based on the above formulation, we can estimate theoretically the gas/aerosol distribution of formic and acetic acids in the typical sulfate, nitrate, ammonium, sodium, chloride, water aerosol system. We have selected three cases to study that span the range of expected behavior in the inorganic aerosol system (Table 5.7). The first is a sulfate-rich case, that

is, insufficient ammonium and sodium to completely neutralize the divalent sulfate ion, and therefore, the aerosol will be expected to be quite acidic. The second is a sulfate-poor case in which there is sufficient ammonium and sodium to neutralize the sulfate (i.e., the bisulfate ion is a minor constituent). Additional ammonium and sodium may combine with the nitrate and chloride depending on their atmospheric abundance. The third is an extreme case in which we assume that most of the sulfate and chloride are in combination with sodium (i.e., of the sea-salt origin) and only about 3-4% of the sulfate is available to combine with ammonium. No nitrate is assumed to be present. These assumptions lead to a much less acidic aerosol system than the first two cases. In the gas/aerosol equilibrium calculation, mixing ratios of the formic and acetic acids are varied from 1 to 20 ppb, which covers their typical ranges under ambient conditions (see Table 5.1).

In Figures 5.5 and 5.6 aerosol formate and acetate equilibrium concentrations are shown as a function of the partial pressure of the gaseous formic and acetic acids for the three cases, at 80% RH. In any of the three cases, formate and acetate are predicted to be only minor constituents of the particles. This is consistent with the findings of Khan et al. (1995). It is also found that the influence of formic and acetic acids on aerosol chemistry is small. For the first two cases, the aerosol is quite acidic (pH<3.71); this results in essentially no change of the pH values, and the major aerosol species concentrations remain unaltered. For the last case, when the relative humidity increases beyond 90%, the aerosol becomes slightly more acidic as gas-phase formic acid increases

in mixing ratio from 1 to 20 ppb. The minimum influence of formic and acetic acids on the aerosol pH is a result of the fact that they are weak acids. The aerosol system has sufficient buffer capacity to maintain the same acidity. The only detectable change of the aerosol species concentrations occurs with ammonium. The change of ammonium concentration becomes most pronounced in the third case and at high-RH conditions. Most of the dissolved formate and acetate ions are neutralized by the dissolved ammonia so that the aerosol acidities virtually do not change.

The aerosol fraction of the total atmospheric formate is shown as a function of the relative humidity in Figure 5.7. Also shown are the pH values for the different cases and RHs. Less than 0.1% of the total atmospheric formate is predicted to be present in the aerosol phase; this is a smaller value than some of the measurements (i.e., Andreae et al., 1987; Grosjean, 1989) showed. It should be noted that we have not taken into account the reaction of the organic acids with ammonia because of a lack of data. The importance of this reaction has been discussed by Grosjean et al. (1988) and remains uncertain pending appropriate data. Nevertheless, at high humidities there is no need to consider this reaction directly. We shall now address the possible formation of formate and acetate in the associated form.

A detailed discussion of modeling of multicomponent solutions with ion association is given by Johnson and Pytkowicz (1979). In essence, the associated acetate (or formate) with sodium or ammonium can be formed in aerosols; the equilibria are

$$CH_3COO^- + Na^+ = CH_3COONa \quad (5)$$

$$CH_3COO^- + NH_4^+ = CH_3COONH_4 \quad (6)$$

CH_3COO-Na and CH_3COO-NH_4 may be in the molecular form or, more likely, in the form of ion pairs. If K_1 and K_2 are the stability constants for equilibria (5) and (6), the extent of acetate association can be estimated from

$$[CH_3COONa] = K_1[CH_3COO^-][Na^+]\frac{\gamma_{CH_3COO^-}\gamma_{Na^+}}{\gamma_{CH_3COONa}} \quad (7)$$

$$[CH_3COONH_4] = K_2[CH_3COO^-][NH_4^+]\frac{\gamma_{CH_3COO^-}\gamma_{NH_4^+}}{\gamma_{CH_3COONH_4^+}} \quad (8)$$

Calculations for the three test cases for various RHs are given in Table 5.8. It is seen that, except for the sulfate-rich case, most of the aerosol acetate exists in the associated form with cations. The possible association of formate and acetate with cations will not alter the concentrations of free sodium and ammonium ions because of their relative abundance. Aerosol acetate concentrations in the presence of association can exceed those in its absence by two orders of magnitude.

6. Conclusions

We have shown that the gas/aerosol distribution of formic and acetic acids is overwhelmingly on the gas-phase side. As a result, dissolved formate and acetate have negligible effect on the gas-aerosol equilibrium of other components.

The framework presented here can be used to analyze the gas/aerosol distribution of other organic species. In general, the longer chain monocarboxylic acids are less soluble and less acidic than formic and acetic acids; therefore, the full family of the monocarboxylic acids are not expected to be important in the aerosol phase. The low-molecular-weight dicarboxylic acids are more soluble and acidic than formic and acetic acids. Because they are generally not abundant in the atmosphere, their influence on aerosol phase chemistry is likely limited. Organic acids with high molecular weights generally have low vapor pressures, and thus are expected to be present primarily in the particulate phase; they are not believed to have large impacts on aerosol phase chemistry.

Acknowledgment

This work was supported by the Electric Power Research Institute under agreement RP3189-03.

REFERENCES

Andreae, M.O., Talbot, R.W., Andreae, T.W. and Harriss, R.C. (1988). *J. Geophys. Res.* 93:1616-1624.

Andreae, M.O., Talbot, R.W. and Li, S.M. (1987). *J. Geophys. Res.* 92:6635-6641.

Avery, G.B., Jr., Willey, J.D. and Wilson, C.A. (1991). *Environ. Sci. Technol.* 25:1875-1880.

Bonner, O.D. (1988). *J. Solution. Chem.* 17:999-1002.

Brewer, R.L., Gordon, R.J., Ip, W.M., Kaplan, I.R., Lee, C.C. and Pau, S.T. (1983). Characterization of organic aerosols from the Southern California Air Basin. Global Geochemistry Corp., Canoga Park, California, June 1983.

Brimblecombe, P., Clegg, S.L. and Khan, I. (1992). *J. Aerosol Sci.* 23:S901-S904.

Bromley, L.A. (1973). *AIChE J.* 19:313-320.

Chen, H., Sangster, J., Teng, T.T. and Lenzi, F. (1973). *Can. J. Chem. Eng.* 51:234-241.

Clegg, S.L. and Brimblecombe, P. (1988). In *Chemical Modeling of Aqueous Systems II* (Melchior, D.C. and Bassett, R.L., eds.), *ACS Symp. Ser.* 416:58-73.

Collett, J.L., Daube, B.C., Jr., Gunz, D. and Hoffmann, M.R. (1990). *Atmos. Environ.* 24A:1741-1757.

Denbigh, K. (1981). *The Principles of Chemical Equilibrium*, 4th ed. Cambridge University Press, Cambridge.

Gorzelska, K. and Galloway, J. N. (1990). *Global Biogeoche. Cycles.* 4:309-333.

Grosjean, D. (1988). *Atmos. Environ.* 22:1637-1648.

Grosjean, D. (1989). *Environ. Sci. Technol.* 23:1506-1514.

Grosjean, D. (1990). *Atmos. Environ.* 24A:2699-2702.

Grosjean, D., Williams, E. and Neste, A.V. (1988). *Measurements of Organic Acids in the South Coast Air Basin.* Final report, California Air Resources Board, Sacramento, California.

Hamer, W.J. and Wu, Y.-C. (1972). *J. Phys. Chem. Ref. Data* 1:1047-1099.

Högteldt, E. (1979). *Stability constants of metal-ion complexes, part A: inorganic ligands.* IUPAC chemical data series, No. 21. Pergamon press, New York.

Hoshika, Y. (1982). *Anal. Chem.* 54:2433-2437.

Jacob, D.J., Munger, J.W., Waldman, J.M. and Hoffmann, M.R. (1986). *J. Geophys. Res.* D91:1073-1088.

Jaffrezo, J.L., Davidson, C.I., Legrand, M. and Dibb, J.E. (1994). J. Geophys. Res. 99D:1241-1253.

Johnson, K.S. and Pytkowicz, R. M. (1979). In *Activity Coefficients in Electrolyte Solutions* (Pitzer, K.S., ed.), vol. 2. CRC Press, Boca Raton, FL. pp.1-62.

Karapetyants, M.Kh. and Karapetyants, M.L. (1970). Thermodynamic constants of inorganic and organic compounds. Humphrey Sci., Ann Arbor.

Kawamura, K. and Kaplan, I.R. (1984). *Anal. Chem.* 56:1616-1620.

Kawamura, K., Ng, L.L. and Kaplan, I.R. (1985). *Environ. Sci. Technol.* 19:1082-1086.

Keene, W.C. and Galloway, J.N. (1986). *J. Geophys. Res.* 91:14466-14474.

Khan, I. and Brimblecombe, P. (1992). *J. Aerosol Sci.* 23:S897-S900.

Khan, I. Brimblecombe, P. and Clegg, S.L. (1994). "Solubilities of pyruvic acid and the lower (C1-C6) carboxylic acids. Experimental determination of equilibrium vapour pressures above pure aqueous and salt solutions." *J. Atmos. Chem.* In press.

Kim, H.T. and Frederick, W.J., Jr. (1988). *J. Chem. Eng. Data.* 33:177-184.

Kim, Y.P. and Seinfeld, J.H. (1995). *Aerosol Sci. Technol. 22*: 93-110.

Kim, Y.P., Seinfeld, J.H. and Saxena, P. (1993a). *Aerosol Sci. Technol.* 19:157-181.

Kim, Y.P., Seinfeld, J.H. and Saxena, P. (1993b). *Aerosol Sci. Technol.* 19:182-198.

Kotronarou, A. and Sigg, L. (1993). *Environ. Sci. Technol.* 27:2725-2735.

Kumar, N., Kulshrestha, U.C., Saxena, A., Kumari, K.M. and Srivastava, S.S. (1993). *J. Geophys. Res.* 98:5135-5137.

Kusik, C.L. and Meissner, H.P. (1978). *AIChE Symp. Series.* 173:14-20.

Li, S.M., Barrie, L.A., Talbot, R.W., Harriss, R.C., Davidson, C.I. and Jaffrezo, J.-L. (1993). *Atmos. Environ.* 27A:3011-3024.

Li, S.M. and Winchester, J.W. (1993). *Geophys. Res. Lett.* 20:45-48.

Martell, A.E. and Smith, R.M. (1977). *Critical stability constants, vol. 3: other organic ligands.* Plenum press, New York.

Murano, K., Sekiguchi, K., Matsumoto, M., Salazar, S., Izumi, K. and Fukuyama, T. (1988). *Kokuritsu Kogai Kenkyusho Kenkyu Hokoku* 112:63-86 (Japan).

Noller, B.N., Currey, N.A., Ayers, G.P. and Gillett, R.W. (1990). *Total Environ.* 91:23-48.

Norton, R.B., Roberts, J.M. and Huebert, B.J. (1983). *Geophys. Res. Lett.* 10:517-520.

Ohe, S. (1991). *Vapor-liquid equilibrium data-salt effect.* Kodansha, Tokyo and Elsevier, New York.

Pierson, W.R. and Brachaczek, W.W. (1990). *Aerosol Sci. Technol.* 12:8-27.

Pierson, W.R., Brachaczek, W.W., Japar, S.M., Cass, G.R. and Solomon, P.A. (1988). *Atmos. Environ.* 22:1657-1663.

Pitzer, K.S. (1991). In *Activity Coefficients in Electrolyte Solutions* (Pitzer, K.S., ed.), 2nd ed. CRC Press, Boca Raton, FL. pp.75-153.

Pitzer, K.S. and Kim, J. (1974). *J. Ame. Chem. Soc.* 96:5701-5707.

Ridley, B.A. and Robinson, E. (1992). *J. Geophys. Res.* 97:10285-10290.

Rogge, W.F., Mazurek, M.A., Hildemann, L.M. and Cass, G.R. (1993). *Atmos Environ.* 27A:1309-1330.

Sanhueza, E., Arias, M.C., Donoso, L., Graterol, N., Hermoso, M., Marti, I., Romero, J., Rondon, A. and Santana, M. (1992). *Tellus*, 44B:54-62.

Schuetzle, D., Cronn, D., Crittenden, A.L. and Charlson, R.J. (1975). *Environ. Sci. Technol.* 9:838-845.

Serjeant, E.P. and Dempsey, B. (1979). *Ionisation constants of organic acids in aqueous solution*, IUPAC. Pergamon Press, Elmsford, N.Y.

Steinberg, S.K., Kawamura, K. and Kaplan, I.R. (1985). *Int. J. Environ. Anal. Chem.* 19:251-260.

Stokes, R.H. and Robinson, R.A. (1966). *J. Phys. chem.* 70:2126-2130.

Wagman, D.D., Evans, W.H., Parker, V.B., Schumm, R.H., Harlow, I., Bailey, S.M., Churney, K.L. and Nuttall, R.L. (1982). *The NBS Tables of Chemical Thermodynamic Properties, J. Phys. Chem. Ref. Data*, Vol. 11, suppl. 2.

Winiwarter W. and Puxbaum, H. (1988). *Tellus*. 40B:348-357.

Table 5.1. Organic acids in the atmosphere

Compounds	Gas-phase mixing ratio (ppb)		Particulate-phase concentration (μM†)		Henry's law constant ($\times 10^4$ M atm^{-1})	ΔH_{298} (kJ mol^{-1})	pK_1 (298 K)	pK_2 (298 K)
	Urban	Non-urban	Urban	Non-urban				
Aliphatic monocarboxylic acids								
Formic (HCOOH)	0.07-3.0[a], 1.9-10.5[b], 1.3-13[c], 0.1-3.5[d]	1.6[h], 0.58[i], 0.36[j]	11-175[d], 91.5[m], 118[n]	0.02 ppb[h], 22‡,[t]	0.553[x]	-46.84[x]	3.752[aa]	
Acetic (CH_3COOH)	0.3-3.9[a], 2.5-9.5[b], 1.9-16[c], 0.1-3.5[d], 1.69[e]	2.2[h], 0.62[i], 0.30[j]	10-269[d], 42.8[m], 52[n]	0.02 ppb[h], 44‡,[t]	0.550[x]	-69.19[x]	4.755[aa]	
Propionic (C_2H_5COOH)	0.02-0.3[a], 0.102[e]		2.94[m], 2.3[n]	6‡,[t]	0.564[x]		4.870[z]	
n-Butyric (C_3H_7COOH)	0.006-0.083[a], 0.025[e]		0.51[m]		0.455[x]		4.820[z]	
i-Butyric (C_3H_7COOH)	0.003-0.031[a], 0.009[e]		0.25[m]		0.113[x]		4.619[bb]	
n-Valeric (C_4H_9COOH)	0.004-0.033[a], 0.014[e]		0.21[m]		0.212[x]	-57.19[x]	4.8[bb]	
i-Valeric (C_4H_9COOH)	0.003[e]				0.120[x]		4.77[z]	

Table 5.1. (Continued)

Compounds	Gas-phase mixing ratio (ppb)		Particulate-phase concentration (μM†)		Henry's law constant ($\times 10^4$ M atm^{-1})	ΔH_{298} (kJ mol^{-1})	pK_1 (298 K)	pK_2 (298 K)
	Urban	Non-urban	Urban	Non-urban				
neo-Valeric (C_4H_9COOH)					0.036[x]		5.04[bb]	
n-Caproic ($C_5H_{11}COOH$)	0.006-0.044[a]		0.27[m]		0.132[x]	-49.12[x]	4.88[z]	
C_7-C_{10}	0.001-0.021[a]				<0.1[y]			
C_9-C_{30}			256-294‡,[o]					
C_{11}-C_{24}			16-39‡,[p]					
Aliphatic dicarboxylic acids								
Oxalic ($(COOH)_2$)	<0.08[b]		0-940‡,[b], 4-30[q], 2.1[n]	27‡,[t], <0.05 ppb[u]	320[y]	-60.57[y]	1.23[z]	4.19[z]
Malonic ($C_3H_4O_4$)			28-51‡,[o]				2.83[z]	5.69[z]
Succinic ($C_4H_6O_4$)			51-84‡,[o]				4.16[z]	5.61[z]
Methylsuccinic ($C_5H_8O_4$)			12-20‡,[o]				4.13[z]	5.64[z]

Table 5.1. (Continued)

Compounds	Gas-phase mixing ratio (ppb)		Particulate-phase concentration (μM†)		Henry's law constant ($\times 10^4$ M atm^{-1})	ΔH_{298} (kJ mol^{-1})	pK_1 (298 K)	pK_2 (298 K)
	Urban	Non-urban	Urban	Non-urban				
Hydroxysuccinic ($C_4H_6O_5$)			7.8-22‡,o				3.459bb	5.097bb
Glutaric ($C_5H_8O_4$)			28-39‡,o				4.31z	5.41z
Methylglutaric ($C_6H_{10}O_4$)			16-24‡,o				4.33bb	5.49bb
Adipic ($C_6H_{10}O_4$)			14-24‡,o		0.107z		4.43z	5.41z
Pimelic ($C_7H_{12}O_4$)							4.49bb	5.55bb
Suberic ($C_8H_{14}O_4$)			2.5-4.1‡,o				4.517bb	5.403bb
Azelaic ($C_9H_{16}O_4$)			23-45‡,o				4.525bb	5.395bb
Other aliphatic carboxylic acids								
Glyoxylic ($C_2H_2O_3$)			4-30q				2.98bb	

Table 5.1. (Continued)

Compounds	Gas-phase mixing ratio (ppb)		Particulate-phase concentration (μM†)		Henry's law constant ($\times 10^4$ M atm^{-1})	ΔH_{298} (kJ mol^{-1})	pK_1 (298 K)	pK_2 (298 K)
	Urban	Non-urban	Urban	Non-urban				
Pyruvic ($C_3H_4O_3$)	0.086[f], 0.054[g]	0.01-0.4[k], 0.039[l]	0.015 ppb[f], 0.009 ppb[g]	0.004 ppb[k], 0.003 ppb[l], 4‡,[t]	31[y]	-43.43[y]	2.39[bb]	
Lactic ($C_3H_6O_3$)			2-15[r]	4‡,[t]			3.86[z]	
Aromatic acids			< 1.5 μg m^{-3}[s]					
Benzoic ($C_7H_6O_2$)	0.001-0.026[a]		0.4[n]	23‡,[t]	1.427[z]		4.19[z]	
Amino acids								
Glycine ($C_2H_5NO_2$)				0-0.16¶,[v]	1.2×10^9[y]	-132.6[y]	2.34[z]	
Alanine ($C_3H_7NO_2$)				0-0.12¶,[v]	3.6×10^8[y]	-136.9[y]	2.34[z]	
Serine ($C_3H_7NO_3$)				0-0.18¶,[v]			2.21[z]	
Methane sulfonic acid (CH_4O_3S)		0.00008-0.0061[cc]		5[t], 0-23‡,[w]			-1.53[bb]	

[†]Units in μM unless noted.

[‡]ng m^{-3}.

[¶]nmol N m^{-3}.

[a]Los Angeles, California, 1984 (Kawamura et al., 1985).

[b]Claremont, California, 1985 (Grosjean, 1988).

[c]Glendora, California, 1986 (Grosjean 1989).

[d]Gas phase and fog in Po Valley, Italy, in 1985 and 1986 (Winiwarter and Puxbaum, 1988).

[e]Nagoya, Japan, 1981 (Hoshika, 1982).

[fgkl]Gas and aerosol phase (< 1.0-μm diameter) in Charlottesville, Virginia, 1986; in Tallahassee, Florida, 1986; in Amazon forest, Brazil, 1985; and in Western North Atlantic, 1986, respectively (Andreae et al., 1987).

[h]Gas and aerosol phase in Amazon forest, Brazil, during the 1985 dry season (Andreae et al., 1988).

[i]San Nicholas Island, California, August, 1987 (Grosjean, 1990).

[j]Mauna Loa, Hawaii, 1988 (Ridley and Robinson, 1992).

[m]Fog samples in Los Angeles, California, 6/11/83 (Kawamura and Kaplan, 1984).

[n]Dew samples in Glendora, California, 1986 (Pierson and Brachaczek, 1990).

[o]South Coast Air Basin, California, 1982 (Rogge et al., 1993).

[p]Duarte, California (Brewer et al., 1983).

[q]Fog and cloud in Los Angeles (Henninger Flats), California (Steinberg et al., 1985).

[r]Fog samples in San Joaquin Valley, California, 1984 (Jacob et al., 1986).

[s]South Coast Air Basin, California, 1972 (Schuetzle et al., 1975).

[t]Barrow, Alaska, in March-April, 1989 (Li and Winchester, 1993).

[u]Remote Colorado mountain, 1981 (Norton et al., 1983).

[v]North Atlantic Ocean, 1988 (Gorzelska and Galloway, 1990).

[w]Greenland Ice Sheet in the summer of 1990 and 1991 (Jaffrezo et al., 1994).

[x]Khan and Brimblecombe (1992).

[y]Brimblecombe et al. (1992).

[z]CRC Handbook of Chemistry and Physics (1994). Estimated by assuming the activity coefficient of the saturated solution to be one.

[aa]Clegg and Briblecombe (1988).

[bb]Serjeant and Dempsey (1979).

[cc]Arctic troposphere (Li et al., 1993).

Table 5.2. Equilibrium parameters for formates and acetates

Equilibrium Relation	Equilibrium Constant Expression	Equilibrium Constant[a] K (298.15 K)	a	b	Units
$HCOOH(g) = HCOOH(aq)$	$\frac{[HCOOH(aq)]\gamma_{HCOOH}}{p_{HCOOH}}$	[b]5.2×10^{3}	b-	b-	mole/kg /atm
$CH_3COOH(g) = CH_3COOH(aq)$	$\frac{[CH_3COOH(aq)]\gamma_{CH_3COOH}}{p_{CH_3COOH}}$	[c]5.24×10^{3}	c-	c-	mole/kg /atm
$HCOOH(aq) = HCOO^- + H^+$	$\frac{[HCOO^-][H^+]\gamma_{HCOO^-}\gamma_{H^+}}{[HCOOH(aq)]\gamma_{HCOOH}}$	[d]1.772×10^{-4}	d-	d-	mole/kg
$CH_3COOH(aq) = CH_3COO^- + H^+$	$\frac{[CH_3COO^-][H^+]\gamma_{CH_3COO^-}\gamma_{H^+}}{[CH_3COOH(aq)]\gamma_{CH_3COOH}}$	[e]1.758×10^{-5}	e-	e-	mole/kg
$HCOONH_4(s) = HCOO^- + NH_4^+$	$[NH_4^+][HCOO^-]\gamma_{NH_4^+}\gamma_{HCOO^-}$	-	-3.8002	-	$mole^2/kg^2$
$CH_3COONH_4(s) = CH_3COO^- + NH_4^+$	$[NH_4^+][CH_3COO^-]\gamma_{NH_4^+}\gamma_{CH_3COO^-}$	-	3.0902	-	$mole^2/kg^2$
$HCOONa(s) = HCOO^- + Na^+$	$[Na^+][HCOO^-]\gamma_{Na^+}\gamma_{HCOO^-}$	189.89	-0.3348	14.94	$mole^2/kg^2$
$CH_3COONa(s) = CH_3COO^- + Na^+$	$[Na^+][CH_3COO^-]\gamma_{Na^+}\gamma_{CH_3COO^-}$	1.6255×10^{4}	6.9872	4.787	$mole^2/kg^2$
$HCOOK(s) = HCOO^- + K^+$	$[K^+][HCOO^-]\gamma_{K^+}\gamma_{HCOO^-}$	3.5153×10^{7}	-0.7262	-	$mole^2/kg^2$
$CH_3COOK(s) = CH_3COO^- + K^+$	$[K^+][CH_3COO^-]\gamma_{K^+}\gamma_{CH_3COO^-}$	-	6.2086	-	$mole^2/kg^2$
$Ca(HCOO)_2(s) = 2HCOO^- + Ca^{2+}$	$[Ca^{2+}][HCOO^-]^2\gamma_{Ca^{2+}}\gamma^2_{HCOO^-}$	0.3079	2.9571	-	$mole^3/kg^3$
$Ca(CH_3COO)_2(s) = 2CH_3COO^- + Ca^{2+}$	$[Ca^{2+}][CH_3COO^-]^2\gamma_{Ca^{2+}}\gamma^2_{CH_3COO^-}$	0.2340	14.261	-	$mole^3/kg^3$
$Mg(HCOO)_2(s) = 2HCOO^- + Mg^{2+}$	$[Mg^{2+}][HCOO^-]^2\gamma_{Mg^{2+}}\gamma^2_{HCOO^-}$	-	25.314	-	$mole^3/kg^3$
$Mg(CH_3COO)_2(s) = 2CH_3COO^- + Mg^{2+}$	$[Mg^{2+}][CH_3COO^-]^2\gamma_{Mg^{2+}}\gamma^2_{CH_3COO^-}$	-	13.341	-	$mole^3/kg^3$

[a] Constants a and b are in

$$K(T) = K(T_0)\exp\left\{a\left(\frac{T_0}{T}-1\right)+b\left(1+\ln\left(\frac{T_0}{T}\right)-\frac{T_0}{T}\right)\right\}, \text{ where } T_0 = 298 \text{ K}.$$

[bcde]From Clegg and Brimblecombe (1988). Temperature dependence is given by $\ln K = a + b/T + cT$. (b): a = -10.3069, b = 5634.802, and c = 0.0; (c): a = -25.6721, b = 8322.372, and c = 0.02121; (d): a = 13.2948, b = -3258.651, and c = -0.03691; (e): a = 7.4850, b = -2724.347, and c = -0.03118.

Table 5.3. Thermodynamic parameters for formates and acetates[a]

Species	ΔG_f^0 kJ/mol	ΔH_f^0 kJ/mol	C_p^0 J/mol/K
HCOOH (g)	-351.00	-378.57	45.23[b]
CH_3COOH (g)	-374.0	-432.25	66.5
HCOOH (aq)	-372.3	-425.43	-
CH_3COOH (aq)	-396.46	-485.76	-
$HCOONH_4$ (s)	-	-567.48	-
CH_3COONH_4 (s)	-	-610.86[b]	-
HCOONa (s)	-599.9	-666.5	82.68
CH_3COONa (s)	-607.18	-708.81	79.9
HCOOK (s)	-591.20[b]	-679.73	-
CH_3COOK (s)	-	-723.0	-
$Ca(HCOO)_2$ (s)	-1258.5[b]	-1386.6	-
$Ca(CH_3COO)_2$ (s)	-1295.8[b]	-1479.5	-
$Mg(HCOO)_2$ (s)	-	-1255.2[b]	128.28
$Mg(CH_3COO)_2$ (s)	-646.43[b]	-1405.8[b]	-
$HCOO^-$	-351.0	-425.55	-87.9
CH_3COO^-	-369.31	-486.01	-6.3

[a] All values are from Wagman et al. (1982) except noted.

[b] From Karapetyants and Karapetyants (1970).

Table 5.4. Parameter values for the Bromley method used for binary activity coefficient calculation[a]

Species	B (kg/mole)	upper limit of tested ionic strength (m)
HCOOH	0.0874[c]	-
CH_3COOH	0.1163[c]	-
$HCOONH_4$	0.044[c]	-
CH_3COONH_4	0.0766[c]	-
HCOONa	0.0519[b], 0.02976[d]	3-4[b], 14.7[d]
CH_3COONa	0.1048[b], 0.06894[d]	3-4[b], 15.2[d]
HCOOK	0.0821[c]	-
CH_3COOK	0.1188[b]	3-4[b]
$Ca(HCOO)_2$	0.0261[c]	-
$Ca(CH_3COO)_2$	0.0545[c]	-
$Mg(HCOO)_2$	0.0191[c]	-
$Mg(CH_3COO)_2$	0.0339[b], 0.0353[d]	12[bd]

[a]Formula:

$$\log \gamma_{12}^{0} = -\frac{0.511 z_1 z_2 I^{1/2}}{1 + I^{1/2}} + \frac{(0.06 + 0.6B) z_1 z_2 I}{\left(1 + \frac{1.5}{z_1 z_2} I\right)^2} + BI$$

[b]Values are directly from Bromley (1973).

[c]Values are constructed according to $B = B_+ + B_- + \delta_+ \delta_-$, given by Bromley (1973).

[d]This work.

Table 5.5. Parameter values for the Kusik and Meissner method used for binary activity coefficient calculation[a]

Species	q	upper limit of tested ionic strength (m)
HCOOH	-	-
CH_3COOH	-	-
$HCOONH_4$	-	-
CH_3COONH_4	-	-
HCOONa	1.83[b], 1.36[c]	3-4[b], 14.7[c]
CH_3COONa	4.20[b], 3.10[c]	3-4[b], 15.2[c]
HCOOK	-	-
CH_3COOK	5.05[b], 5.22[c]	3-4[bc]
$Ca(HCOO)_2$	-	-
$Ca(CH_3COO)_2$	-	-
$Mg(HCOO)_2$	-	-
$Mg(CH_3COO)_2$	0.83[b],	12[b]

[a]Formula:

$$\Gamma^0 = [1 + B(1 + 0.1I)^q - B]\Gamma^*$$

$$B = 0.75 - 0.065q$$

$$\log\Gamma^* = \frac{-0.5107I^{1/2}}{1 + CI^{1/2}}$$

$$C = 1 + 0.055q\exp(-0.023I^3)$$

$$\Gamma^0 = \left(\gamma_{12}^0\right)^{1/z_1z_2}$$

[b]Data are from Kusik and Meissner (1978).

[c]This work.

Table 5.6. Parameter values for the Pitzer method used for binary activity coefficient calculation[a]

Species	$\beta^{(0)}$	$\beta^{(1)}$	$\beta^{(2)}$	C^{ϕ}	upper limit of tested ionic strength (m)
HCOOH	-	-	-	-	-
CH_3COOH	-	-	-	-	-
$HCOONH_4$	-	-	-	-	-
CH_3COONH_4	-	-	-	-	-
HCOONa	0.0820	0.2872	0	-0.00523	3.5
CH_3COONa	0.1426	0.3237	0	-0.00629	3.5
HCOOK	-	-	-	-	-
CH_3COOK	0.1587	0.3251	0	-0.00660	3.5
$Ca(HCOO)_2$	-	-	-	-	-
$Ca(CH_3COO)_2$	-	-	-	-	-
$Mg(HCOO)_2$	-	-	-	-	-
$Mg(CH_3COO)_2$[b]	0.22930	2.04167	0	-0.01460	4.0

[a] All data are from Pitzer (1991). Formula:

$$\ln\gamma_{12}^{0} = z_1 z_2 f^{\gamma} + m\left(\frac{2\upsilon_1\upsilon_2}{\upsilon}\right)B_{12}^{\gamma} + m^2\frac{2(\upsilon_1\upsilon_2)^{3/2}}{\upsilon}C_{12}^{\gamma}$$

$$f^{\gamma} = -0.392\left[\frac{I^{1/2}}{1+bI^{1/2}} + \frac{2}{b}\ln(1+bI^{1/2})\right]$$

$$b = 1.2$$

$$B_{12}^{\gamma} = 2\beta_{12}^{(0)} + \frac{2\beta_{12}^{(1)}}{\alpha^2 I}\left[1 - e^{-\alpha I^{1/2}}\left(1+\alpha I^{1/2} - \frac{\alpha^2}{2}I\right)\right]$$

$$C_{12}^{\gamma} = \frac{3}{2}C_{12}^{\phi}$$

$$\alpha = 2.0$$

[b] From Kim and Frederick (1988).

Table 5.7. Model cases of gas/aerosol chemistry[†]

	Total sulfate	Total nitrate	Total chloride	Total ammonium	Total sodium	R_S[‡]
Case 1	50	30	9.36	10	5.9	1.66
Case 2	5	5	9.36	20	5.9	28.09
Case 3	8	0	1.7	40	4.7	32.21

[†]All species concentrations are in units of μg/m^3.

[‡]$R_s = ([NH_4^+]_T + [Na^+]_T) / [SO_4^{2-}]_T$.

Table 5.8. Concentration of the ionic species and possible associated acetate ion-pairs in aerosol[†]

	H^+	NH_4^+	Na^+	Water	CH_3COO^-	CH_3COOH	CH_3COONH_4[¶]	CH_3COONa[‖]	Ratio[‡]
RH=0.6									
Case 1	79.8	587	257	55.9	3.34×10^{-8}	2.93×10^{-3}	6.75×10^{-4}	7.00×10^{-8}	0.23
Case 2	3.84×10^{-3}	83.5	84.3	9.66	5.22×10^{-6}	5.06×10^{-4}	0.0851	2.67×10^{-5}	166
Case 3	7.59×10^{-6}	0.167	2.84	0.224	3.50×10^{-6}	1.17×10^{-5}	4.58×10^{-3}	2.14×10^{-5}	302
RH=0.7									
Case 1	71.3	586	257	76.4	9.39×10^{-8}	4.00×10^{-3}	1.09×10^{-3}	1.1×10^{-7}	0.27
Case 2	7.77×10^{-3}	128	257	40.0	5.92×10^{-5}	2.10×10^{-3}	0.337	2.11×10^{-4}	156
Case 3	5.92×10^{-5}	1.96	44.2	5.90	1.67×10^{-4}	3.09×10^{-4}	0.110	7.82×10^{-4}	233
RH=0.8									
Case 1	62.3	586	257	110	2.78×10^{-7}	5.76×10^{-3}	1.88×10^{-3}	1.88×10^{-7}	0.33
Case 2	0.0154	154	257	60.7	1.28×10^{-4}	3.18×10^{-3}	0.499	2.33×10^{-4}	151
Case 3	2.99×10^{-4}	4.38	100	15.0	7.09×10^{-4}	7.86×10^{-4}	0.279	1.61×10^{-3}	188
RH=0.9									
Case 1	69.4	586	257	218	1.24×10^{-6}	0.0114	3.80×10^{-3}	3.68×10^{-7}	0.33
Case 2	0.0331	173	257	120	4.90×10^{-4}	6.27×10^{-3}	0.956	3.43×10^{-4}	141
Case 3	6.25×10^{-4}	5.38	204	43.8	6.36×10^{-3}	2.30×10^{-3}	0.821	6.79×10^{-3}	95.7
RH=0.95									
Case 1	123	587	257	503	4.08×10^{-6}	0.0264	5.73×10^{-3}	5.33×10^{-7}	0.22
Case 2	0.0488	179	257	245	1.95×10^{-3}	0.0128	1.94	6.15×10^{-3}	131
Case 3	7.61×10^{-4}	5.48	204	85.9	0.0239	4.50×10^{-3}	1.60	0.0124	56.8

[†]In units of nmol m^{-3} except for water, which is in unit of μg m^{-3}.

[¶]The stability constant is 3.388×10^{3} M^{-1}, estimated from $K_{CH_3COONa}K_{NH_4Cl}/K_{NaCl}$, where $K_{NH_4Cl} = 10^{2.94}$ and $K_{NaCl} = 10^{-0.77}$ are from Högteldt (1979).

[¡]The stability constant is 0.661 M^{-1} (Martell and Smith, 1977).

[‡]$\{[CH_3COONH_4] + [CH_3COONa]\} / \{[CH_3COOH] + [CH_3COO^-]\}$.

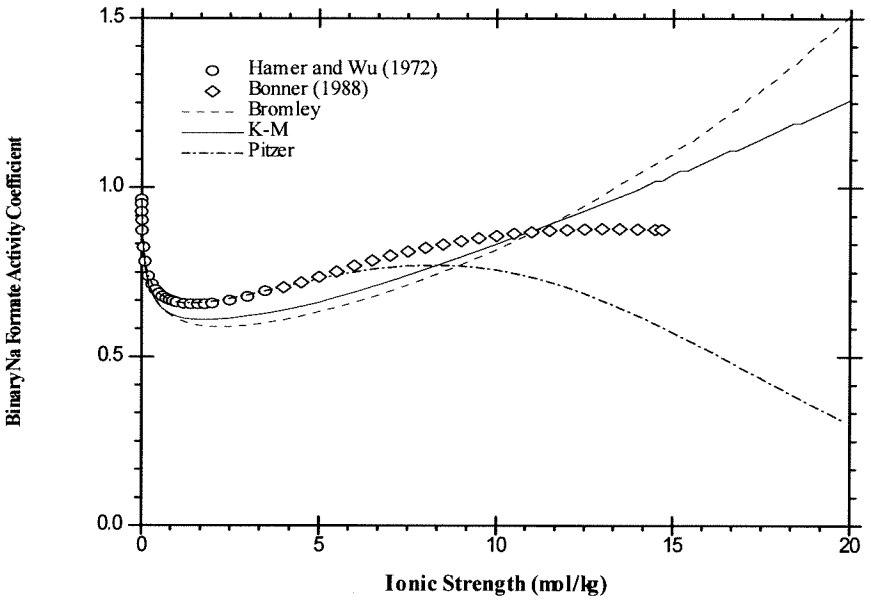

Fig. 5.1 Comparison of mean binary activity coefficient estimation methods for HCOONa. Data are from Hamer and Wu (1972) and Bonner (1988).

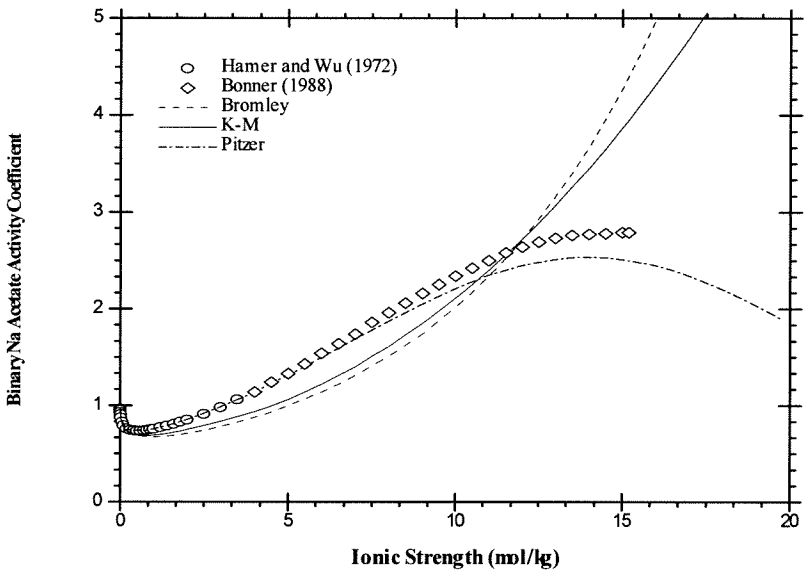

Fig. 5.2 Comparison of mean binary activity coefficient estimation methods for CH_3COONa. Data are from Hamer and Wu (1972) and Bonner (1988).

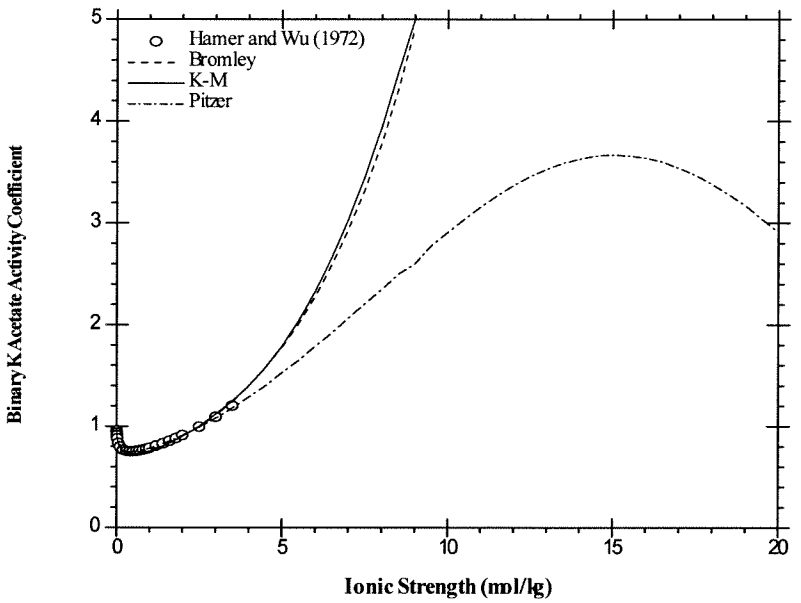

Fig. 5.3 Comparison of mean binary activity coefficient estimation methods for CH_3COOK. Data are from Hamer and Wu (1972).

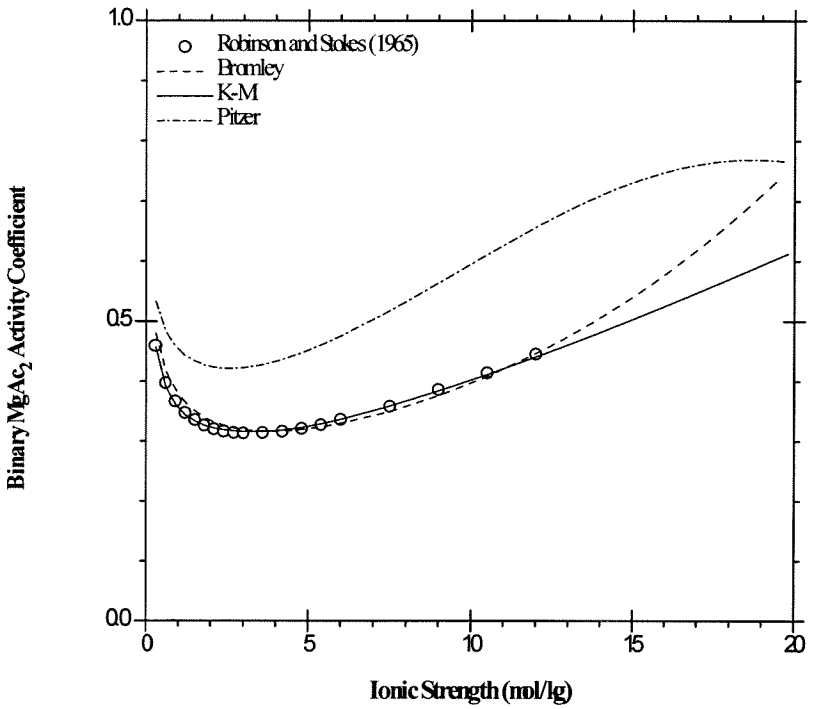

Fig. 5.4 Comparison of mean binary activity coefficient estimation methods for $Mg(CH_3COO)_2$. Data are from Robinson and Stokes (1965).

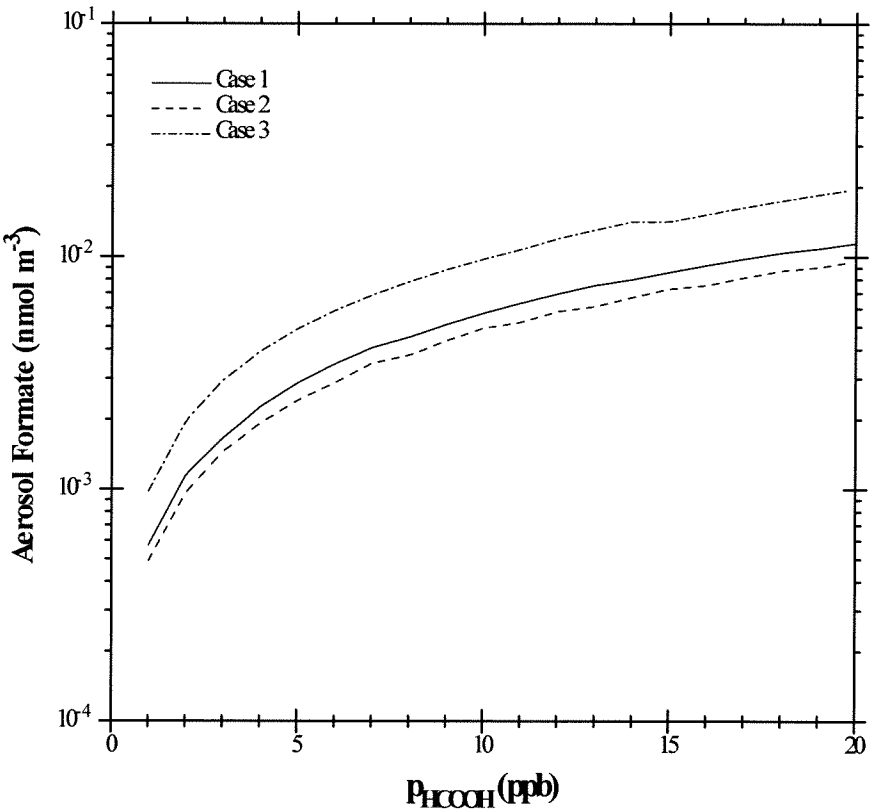

Fig. 5.5 Aerosol formate concentrations as a function of partial pressure of gas-phase formic acid for the three studied cases at RH = 80%.

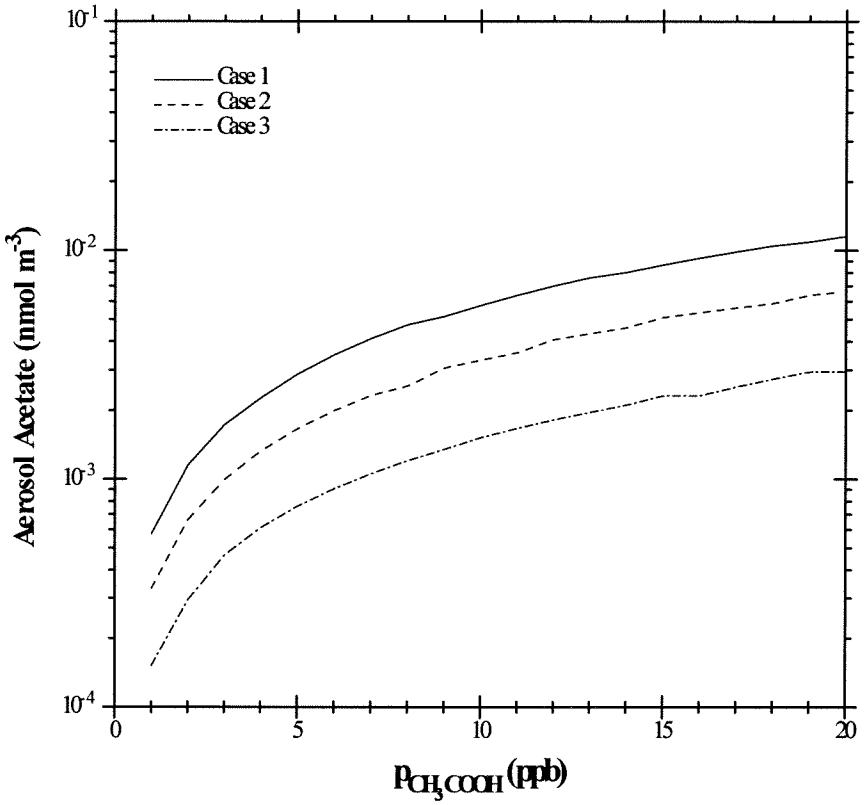

Fig. 5.6 Aerosol acetate concentrations as a function of partial pressure of gas-phase acetic acid for the three studied cases at RH = 80%.

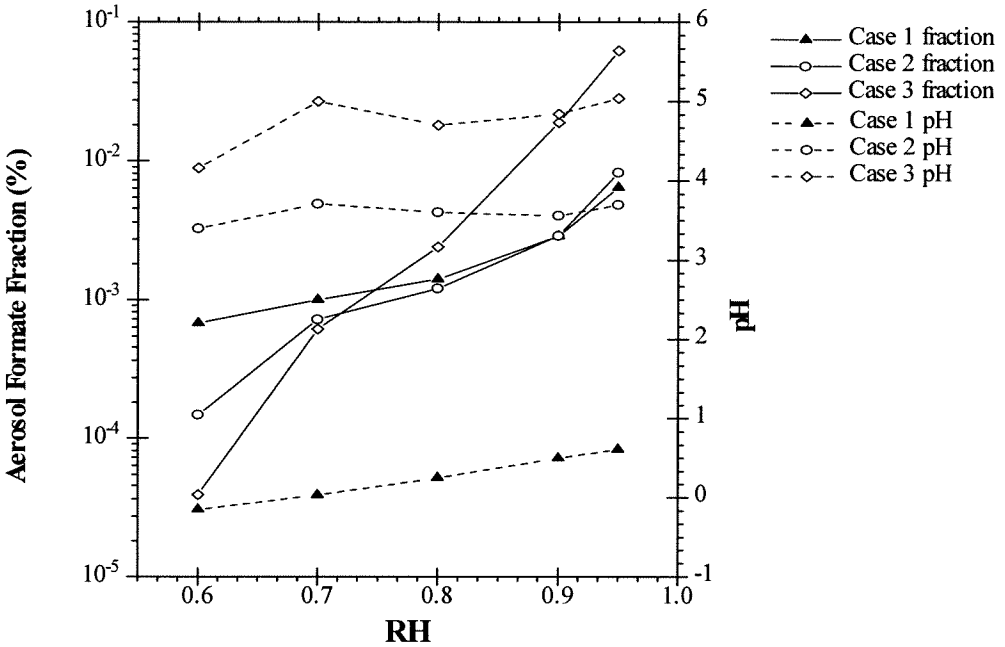

Fig. 5.7 Aerosol-phase fraction of the total atmospheric formate and aerosol pH as a function of relative humidity for the three modeling cases.

Chapter 6

Time Scales to Achieve Atmospheric Gas-Aerosol Equilibrium for Volatile Species

[The text of this chapter appears in: Meng Z. and Seinfeld J. H. (1996) *Atmospheric Environment* **30**, 2889-2900.]

ABSTRACT

Time scales to achieve gas-aerosol equilibrium for volatile atmospheric species are systematically studied. It is found that equilibration between submicron aerosol and the gas phase is attainable on a time scale comparable to that of typical ambient gas and aerosol dynamics. However, the time required for the coarse aerosol to reach equilibrium is predicted to be sufficiently long that volatile species in atmospheric coarse aerosol particles may generally exist in non-equilibrium transition states. Variation of the gas-phase concentrations of volatile compounds is generally controlled by equilibration with the fine-mode particles. Volatile compounds in the gas phase can approach the equilibrium state on a much shorter time than that of the gas-aerosol system. Sensitivity analysis is performed to study how the equilibration times depend on relative humidity, initial gas-phase concentrations, aerosol mass concentration, aerosol size, temperature, accommodation coefficient, and different chemical compositions. The equilibration time increases with increasing particle size, or decreasing accommodation coefficient or temperature. Transport calculations performed for typical ambient aerosols confirm the results obtained from hypothetical cases. Equilibrium for ammonia between the gas phase and submicron marine aerosol is also examined.

1. Introduction

Chemical components of atmospheric aerosols include elemental and organic carbon and a variety of inorganic compounds. The inorganic substances, typically comprising 25-50% of the total aerosol mass (Gray et al., 1986; Heintzenberg, 1989), include sulfate, nitrate, chloride, ammonium, sodium, and crustal species such as aluminum, silicon, calcium, and iron. Sulfates have sufficiently low vapor pressures that, when present, tend to reside overwhelmingly in the aerosol phase. Inorganic volatile compounds of atmospheric importance include ammonia, nitric acid, hydrochloric acid, and/or their products (i.e., ammonium nitrate and ammonium chloride). Some organic acids, aldehydes, and organic compounds, such as polycyclic aromatic hydrocarbons (PAHs), also are distributed between gas and aerosol phases.

Modeling of the dynamics of atmospheric aerosols requires that one be able to predict transfer of volatile species to and from aerosol particles. It has frequently been assumed that a local equilibrium exists for volatile species between the gas and aerosol phases. Thermodynamic relations that allow one to predict the gas-aerosol partitioning of volatile inorganic species have been developed in a series of papers dating back to 1979 (Stelson et al., 1979; Stelson and Seinfeld, 1982abc; Russell et al., 1983; Saxena et al., 1983, 1986; Bassett and Seinfeld, 1983, 1984; Pilinis and Seinfeld, 1987; Brimblecombe and Clegg, 1990; Brimblecombe et al., 1992; Clegg and Brimblecombe, 1986, 1988ab, 1989, 1990, 1992; Khan and Brimblecombe, 1992; Wexler and Seinfeld, 1991; Kim et

al., 1993ab, 1995; Meng et al., 1995ab). There also exist a number of studies in which ambient gas and aerosol data have been evaluated with respect to gas-aerosol equilibrium (Doyle et al., 1979; Cadle et al., 1982; Tanner, 1982; Grosjean, 1982; Hildemann et al., 1984; Allen et al., 1989; Pio et al., 1992; Quinn et al., 1992). Knowledge of whether or not an air mass exhibits local gas-aerosol equilibrium is useful in evaluating ambient measurements and in guiding computational implementation of atmospheric aerosol models (Pilinis and Seinfeld, 1987, 1988; Wexler et al., 1994).

Establishment of local gas-aerosol equilibrium in an air mass requires that the time scale to establish equilibrium is short when compared to that over which the volatile species and aerosol concentrations are changing in the air mass. The most ubiquitous volatile species in atmospheric aerosols is water. Because of the relatively large amount of water in the atmosphere, the time scale to establish gas-aerosol equilibrium for it is extremely short. Thus, local gas-aerosol equilibrium can always be assumed to hold for water. Wexler and Seinfeld (1990) formulated expressions for the characteristic times associated with gas-to-particle conversion processes. The time scale to establish gas-aerosol equilibrium depends on the vapor pressure of the species (which depends on temperature), its partial pressure in the gas phase, the quantity of aerosol and its size distribution, the species diffusivity, and the species accommodation coefficient of the particle surface. Wexler and Seinfeld (1990) evaluated the magnitudes of these time scales for equilibration of the vapor-phase species with a population of aerosol particles and found that ammonium salts in the gas and aerosol phases are not always in

equilibrium, especially under low aerosol loading and cooler conditions. Furthermore, they showed that thermodynamic equilibrium often does not uniquely determine the size distribution of ammonium salts; both transport and thermodynamic properties of the aerosol are important.

In this paper we reexamine the equilibrium conditions for gas-aerosol systems. Since the characteristic time is different from the actual equilibration time for the gas-aerosol system, especially considering that the aerosol phase state is a strong function of the transport process, we will perform detailed transport calculations for various ambient conditions to investigate the equilibration process. We investigate not only how long the equilibration process takes but also how the equilibration actually proceeds. It is also important that we know how the intermediate states differ from the final equilibrium state. Finally, we seek to apply our results to draw implications about gas-aerosol equilibrium for different categories of ambient aerosols (i.e., marine and continental aerosols).

2. Existence of a Size-Composition Equilibrium State

Even if a thermodynamic equilibrium state exists for a particular species between the gas phase and the bulk (i.e., over all particles) aerosol phase, a unique thermodynamic equilibrium state may not exist between the vapor phase and the size-distributed aerosol (as shown below). Technically, this means that there may exist more than one aerosol

size-composition distribution corresponding to the same minimum Gibbs free energy of the system at the given conditions (Wexler and Seinfeld, 1990). For example:

1. Particles in more than one size range exist as pure solids.

In this case the particle surface vapor pressure of the volatile compound over the solid particles is, neglecting the Kelvin effect, independent of particle size. Thermodynamics alone will then not be able to govern this substance's distribution as a function of particle size because any distribution of the substance among the solid particles is automatically in equilibrium with the gas phase. Mass transport will be the only factor to control this substance's distribution among the solid particles as a function of size.

2. Particles in more than one size range are dominated by volatile species.

In this case if the aerosol is aqueous and the volatile species dissolved in the solution are the only species or are osmotically dominant to the nonvolatile species (i.e., the nonvolatile species concentrations in the solution are negligibly small), thermodynamic equilibrium will also not be able to predict the aerosol size-composition distribution. Consider a simple example: two aqueous aerosol particles of different sizes composed only of NH_4NO_3 and water. When gaseous NH_4NO_3 (or its gas-phase

precursors, NH_3 and HNO_3) transfers to the aerosol phase, each particle will simultaneously absorb water in accordance with

$$W_j = \frac{M_j}{m_0(a_w)} \tag{1}$$

where W_j (kg (m^3 air)$^{-1}$) and M_j (mole (m^3 air)$^{-1}$) are aerosol water content and molar concentration of NH_4NO_3 in the jth size particle, respectively, and $m_0(a_w)$ (mol (kg water)$^{-1}$) is the molality of the binary solution at the equilibrium water activity, a_w, equal to the relative humidity, RH. Eq. (1) is equivalent to

$$m_j = \frac{M_j}{W_j} = m_0(a_w) \tag{2}$$

where m_j is the molality of NH_4NO_3 in the jth size particle. m_j is the same for the two differently sized particles because the water activity must equal the same value, i.e., RH, for every size particle. Thermodynamics dictates therefore only that the aerosol-phase NH_4NO_3-to-water molar ratio must be equal for these two particles but cannot determine how the amount of total NH_4NO_3 that is required to be in the aerosol phase at equilibrium is to be distributed between these two particles. This can only be determined by mass transfer considerations. Although thermodynamics cannot uniquely determine the

equilibrium size-composition distribution of the volatile species in the above two cases, the overall gas-aerosol partitioning is still governed by thermodynamic equilibrium.

If there exists a unique equilibrium state, the equilibrium aerosol size-composition distribution can be determined as follows. It is convenient to discretize the aerosol size composition into size sections. The total amount of volatile compounds are then distributed among the gas phase and the different size sections so that the surface vapor pressures of the volatile compounds over all the particles are equal to the gas-phase partial pressures. For instance, one can use the algorithm proposed by Pilinis and Seinfeld (1987) to perform this calculation. If a mass transfer calculation has to be performed (e.g., the above two cases), an aerosol phase thermodynamic model such as that of Kim et al. (1993ab) is needed to predict the particle surface vapor pressure.

3. Characteristic Time to Reach Equilibrium

The mass flux of a volatile species i to a single aerosol particle of diameter D_p (Wexler and Seinfeld, 1990) is

$$J_i = 2\pi D_p D_i \frac{C_{\infty,i} - C_{s,i}}{\frac{2\lambda}{\alpha_i D_p} + 1} \tag{3}$$

where D_i is the diffusivity of species i, $C_{\infty,i}$ and $C_{s,i}$ are the concentrations of i in the bulk gas phase and in the gas phase at the particle surface, respectively, λ is the air mean free path, and α_i is the accommodation coefficient of species i on the particle. Variation of the gas-phase concentration of species i with time as a result of gas-to-particle conversion is governed by

$$\frac{dC_{\infty,i}}{dt} = -\int_0^{\infty} n(D_p,t)J_i(D_p,t)dD_p \tag{4}$$

where $n(D_p,t)dD_p$ is the number concentration of particles between diameter D_p and $D_p + dD_p$. It is convenient to break the aerosol size distribution into a number of discrete size sections and represent Eq. (4) as

$$\frac{dC_{\infty,i}}{dt} = -\sum_j N_j J_{ij} \tag{5}$$

where N_j is the number concentration of particles in size section j and J_{ij} is the mass flux of species i to the jth section. The characteristic time scale for species i in the size section j to reach the final equilibrium level as a result of transport is

$$\tau_{j,i} = \left| \frac{C_{e,i} - C_{s,i}}{N_j J_{ij}} \right| \tag{6}$$

where $C_{e,i}$ is the final equilibrium gas-phase concentration of species *i*. The characteristic time scale for species *i* in the bulk gas phase to reach the final equilibrium level is

$$\tau_{\infty,i} = \left| \frac{C_{\infty,i} - C_{e,i}}{dC_{\infty,i}/dt} \right| \tag{7}$$

Substituting Eqs. (6) and (7) into (5), we obtain

$$\frac{1}{\tau_{\infty,i}} = \sum_j \frac{1}{\tau_{j,i}} \left| \frac{C_{s,i} - C_{e,i}}{C_{\infty,i} - C_{e,i}} \right| \tag{8}$$

It can be seen from Eq. (8) that $\tau_{\infty,i}$ is controlled by the smaller values of $\tau_{j,i}$, multiplied by a weight factor. The physical meaning of Eq. (8) is that the characteristic time to achieve the overall equilibrium level in the gas phase is controlled by those particles for which the individual transport times are shortest.

There is an additional time scale, $\tau_{j,i}^{p}$, the characteristic time for change of the particle surface vapor pressure or for equilibrium at the gas-liquid interface to be established. $\tau_{j,i}^{p}$ differs from $\tau_{j,i}$ in that while $\tau_{j,i}$ is the characteristic time needed to transport the volatile species *i* between the gas phase and the size section *j*, $\tau_{j,i}^{p}$ is the

time scale needed for Henry's law to be established across the gas-liquid interface. $\tau_{j,i}^{p}$ can be approximated by (Wexler and Seinfeld, 1990),

$$\tau_{j,i}^{p} \approx H_i RTW_j \tau_{j,i} \tag{9}$$

where H_i is the ith species effective Henry's law constant (M atm^{-1}), R is the ideal gas constant (8.2×10^{-5} atm m^3 mol^{-1} K^{-1}), and T is temperature (K). Comparison of $\tau_{j,i}^{p}$ and $\tau_{j,i}$ for the volatile gases of interest here is given in Table 6.1. Because $\tau_{j,i}^{p}$ is generally comparable with or smaller than $\tau_{j,i}$ for the volatile species of atmospheric interest, we can assume that interfacial equilibrium is generally established more rapidly than gas-aerosol equilibrium except in some extreme cases (e.g., large pH values or an extremely soluble compound).

In summary, we can define the equilibration time scale for the gas-aerosol system as the larger of $\tau_{\infty,i}$ and $\tau_{j,i}$,

$$\tau_{e,i} = \max(\tau_{\infty,i}, \tau_{j,i}) \text{ for any } j. \tag{10}$$

4. Gas-Aerosol Transport Processes

The above time-scale analysis allows one to estimate the length of time needed to establish the equilibrium state. A detailed transport calculation allows one to investigate how the equilibrium state is approached.

The mass change of species i in aerosol size section j is

$$\frac{dm_{ij}}{dt} = J_{ij} \tag{11}$$

Equations (3), (5), and (11) can be solved to yield the distribution of volatile compounds among the gas phase and differently sized aerosol particles as a function of time. If the aerosol particles are liquid, the surface equilibrium concentration, $C_{s,i}$ in Eq. (3), can be evaluated based on the aqueous phase concentrations and the Henry's law relation. However, if the aerosol particles are solid, the equilibrium concentrations over a solid particle surface then cannot be determined based on the aerosol phase information only; the gas-phase concentrations are also required. Therefore, for transport to pure solid particles, a relationship replacing Eq. (3) has to be derived to give the correct flux. By solving the steady-state diffusion equation in the gas phase with an appropriate boundary condition for pure solid particles, Wexler and Seinfeld (1990) derived the following expression for transport of HNO_3 or HCl and NH_3 to form NH_4NO_3 or NH_4Cl on solid-phase particles,

$$J_{ij} = \pi D_{pj}\sqrt{D_{NH_3} D_{HX}}\,\overline{C}(1+\beta_{ij})\left[1-\sqrt{1-4\frac{C_{\infty,NH_3}C_{\infty,HX}-K_{NH_4X(s)}}{\overline{C}^2(1+\beta_{ij})^2}}\right] \qquad (12)$$

where $\overline{C} = (D_{NH_3}C_{\infty,NH_3} + D_{HX}C_{\infty,HX})/\sqrt{D_{NH_3}D_{HX}}$, $\beta_{ij} = 2\lambda/\alpha_i D_{pj}$ is the surface accommodation factor, and $K_{NH_4X(s)}$ is the equilibrium constant of the corresponding reaction.

Equation (12) applies to mass transfer in a system in which any reactions of the following type occur,

$$A(g) + B(g) \leftrightarrow AB(s).$$

Another type of reaction,

$$HA(g) + MB(s) \leftrightarrow HB(g) + MA(s),$$

for example,

$$HNO_3(g) + NaCl(s) \leftrightarrow HCl(g) + NaNO_3(s)$$

can also be treated. Using the appropriate boundary conditions, the mass flux of HNO_3 or HCl corresponding to this type of reaction is

$$J_{\mathrm{HNO}_3,j} = -J_{\mathrm{HCl},j} = 2\pi D_{pj} D_{\mathrm{HNO}_3} \frac{KC_{\infty,\mathrm{HNO}_3} - C_{\infty,\mathrm{HCl}}}{(\gamma_j + K)(1+\beta_{\mathrm{HNO}_3,j})} \tag{13}$$

where K is the equilibrium constant, and $\gamma_j = D_{\mathrm{HNO}_3}(1+\beta_{\mathrm{HCl,j}})/D_{\mathrm{HCl}}(1+\beta_{\mathrm{HNO}_3,j})$. Eqs. (12) and (13) will be used for those cases to be presented shortly in which the particles are predicted to be solids.

5. Case Studies on the Approach to Gas-Aerosol Equilibrium

We have devised a hypothetical case to study the equilibration process (Case 1 in Table 6.2). The aerosol initially consists of two groups of particles; one group has dry diameter of 0.2 μm and the other, 3 μm. These two size sections correspond to the accumulation mode and coarse mode of atmospheric aerosols typically observed in the ambient environment. The small particles are assumed to be composed of pure $(NH_4)_2SO_4$, while the large particles are pure NaCl. Though strictly hypothetical, this test case exhibits several of the characteristics of typical tropospheric aerosol populations. Ambient measurements have shown that NaCl is present at substantial concentrations in coastal regions (Russell and Cass, 1984; John et al., 1988), and it is well known that $(NH_4)_2SO_4$ is an important component of the secondary submicrometer aerosol. To investigate the approach to equilibrium we devise a transient "experiment" consisting of a step-change of gas-phase concentrations. At t = 0, we assume that the gas-phase ammonia and nitric

acid instantaneously acquire concentrations of 10 μg m^{-3} (14.4 ppb) and 30 μg m^{-3} (11.7 ppb), respectively. Since the given initial gas-phase concentrations of ammonia and nitric acid are larger than the surface equilibrium concentrations of these species over the two groups of particles, the volatile species will transport to the aerosol phase. Because there is more than one condensational species involved, the surface equilibrium concentrations have to be calculated by a thermodynamic aerosol model (e.g., Kim et al., 1993 ab). The moving sectional technique (Gelbard, 1990) was used to represent the condensation processes. The ambient temperature was assumed to be 298 K for the base case. Following Wexler et al. (1994), we have also assumed the diffusivity and accommodation coefficient to be 0.1 cm^2 s^{-1} and 0.01, respectively, for the species of interest here.

The gas-aerosol equilibrium model SCAPE (Kim et al., 1993 ab, 1995; Meng et al., 1995ab) was developed for partitioning the volatile species between the gas and aerosol phases and determining the phase state of the aerosol particles. It requires input data of the total concentrations of sulfate, nitrate, chloride, ammonium, sodium, potassium, calcium, and magnesium, as well as temperature and relative humidity. Sulfate, sodium, and crustal components are treated as nonvolatile species and are assumed to reside in the aerosol phase only, while nitrate, chloride, and ammonium are distributed between the gas and aerosol phases based on equilibrium calculations. The surface equilibrium concentrations of volatile compounds, as noted earlier, are required to solve the transport equations (i.e., Eqs. (5), (11), and (3), (12), or (13)).

Figure 6.1 shows the computed distributions of the aerosol species at $t = 0$ and $t \rightarrow \infty$ for RH values ranging from 40% to 90%. For the two lowest relative humidities, i.e., RH = 40% and RH = 50%, the initially dry particles do not contain any water at equilibrium. The small particles experience little change of their composition while $NaNO_3$ forms in the large particles in replacing the initial NaCl. Finally, all the chloride in the large particles is released as gaseous HCl, and a small amount of NH_4Cl is formed on the small particles (the amount is too little to be seen in the figure). Solid NH_4NO_3 is not formed. For RH = 60%, the initially dry small particles are aqueous at equilibrium, and NH_4NO_3 is formed finally because the aqueous solution lowers the equilibrium concentration product of HNO_3 and NH_3. The large particles remain solid experiencing only a composition change from NaCl to $NaNO_3$. At RH = 70%, $(NH_4)_2SO_4$ particles become aqueous while NaCl coarse particles remain solid. It is worth mentioning that $(NH_4)_2SO_4$ has a deliquescent point at RH = 80%; the predicted lower deliquescent point for $(NH_4)_2SO_4$ is a result of using the Kusik and Meissner method to predict the activity coefficients and of the thermodynamic data used to construct the equilibrium constants. By doing so, we sacrifice some local accuracy to acquire overall accuracy and consistency of model results. Water content associated with $(NH_4)_2SO_4$ here can be viewed as metastable water content, which is frequently observed in the atmosphere. At equilibrium, the small particles consist of sulfate, nitrate, and ammonium, while the large particles are a mixture of a solution of $NaNO_3$ and NH_4Cl. When the RH exceeds 80%,

both types of initial particles deliquesce and grow to larger sizes by absorbing nitric acid and ammonia at equilibrium.

Figure 6.2 shows the detailed transport processes for the different RHs. The equilibration times are routinely order of 10 hours or more, and they are not very sensitive to changes of RH. Although transport for the pure solid case (RH=40%) requires the shortest time, it is not significantly different from those for higher RHs. It is interesting to note that for all RHs the nitrate and ammonium concentrations of the small particles reached peak values at about 0.5 to 1.0 hour. This can be explained from the different characteristic time scales of the two groups of particles, as shown in Table 6.3.

Large particles generally require much longer times than small particles for transfer of volatile compounds between them and the gas phase. Initially, before the large particles have time to influence the gas-aerosol system, most of the mass transfer occurs between the gas phase and the small particles, and equilibrium between the gas phase and the small particles is actually established. This stage is characterized by the increase of NH_4NO_3 in the small particles. Because the gas-phase concentrations of NH_3 and HNO_3 at this stage are still larger than the NH_3 and HNO_3 surface vapor concentrations over the large particles, the volatile compounds eventually transfer, although slowly, to the large particles. The mass transfer to the large particles decreases the gas-phase concentrations of the volatile compounds and this actually drives these compounds in the small particles to transfer *back* to the gas phase; note the decrease of NH_4NO_3 concentration in the small

particles. The time period of the first stage is controlled by the characteristic time scale for the small particles, while the time span of the second stage is determined by that for the large particles.

We have calculated the transport when only the small particles are present or only the large particles are present for RH = 90% (not shown). The equilibration time in the case for small particles only agrees well with the timing of the peaks for RH = 90% in Figure 6.2 as well as the characteristic time (0.12 hr.) in Table 6.3 (here the characteristic time for HCl is no longer relevant). The equilibration time in Figure 6.2 is longer than that in the case for large particles only, but much shorter than the characteristic time for the large particles in Table 6.3. This implies that, although the characteristic time analysis is useful in qualitatively determining the equilibration time, the characteristic time can differ by two or three orders of magnitude from the real equilibration time. The reason for this discrepancy is that the characteristic time is estimated based on the initial conditions, but these conditions for the aerosol system can change substantially as mass transfer proceeds.

Figure 6.3 shows aerosol water content as a function of time for the two groups of particles and different RHs. For RH=40%, all the aerosol particles remain solid throughout the transport process. For RH=50%, the initially dry small particles first become aqueous at about 1.5 min. with the transport of NH_4NO_3 to them, then start to evaporate at about 1 hour later. Evaporation of water from the small particles is a result

of the loss of NH_4NO_3 to the gas phase, which then transports to the large particles. For RH = 60%, the small particles begin to accumulate water at the first half minute and remain aqueous throughout the transport process. The large particles become aqueous at t = 6 minutes at 70% relative humidity and the water content associated with them levels off about 6 hours later. The small particles are always aqueous for RH ≥ 70% and for large particles this is true for RH ≥ 80%.

To test the sensitivities of the results to initial conditions, we repeated the calculations for a different set of conditions. We choose RH = 80% for the sensitivity study. Figure 6.4a shows results similar to those in Figure 6.2 except that we now reduce the gas-phase concentrations to 10 μg m^{-3} (3.88 ppb) HNO_3 and 5 μg m^{-3} NH_3 (7.20 ppb) while the aerosol phase conditions remain the same. It is seen that the equilibration time is reduced to about half of that for the base case but is still longer than one day. In Figure 6.4b we reduce the concentrations of all the aerosol-phase components to one-half of those in the base case. It then takes a longer time for the equilibrium to be established, because fewer particles are available to accept the volatile materials. Next we decrease the large particle size by half (the dry large particle diameter is 1.5 μm) and maintain the total aerosol mass unchanged. This implies that the large-particle number concentration increases to maintain the same total mass concentration. The result is shown in Figure 6.4c. The equilibration time becomes considerably shorter than that in the base case; now it takes about 15 hours for the equilibrium state to be reached. When the temperature is decreased from 298 K to 288 K (not shown), the equilibration time becomes dramatically

longer for the cool environment. This is in qualitative agreement with the findings of Wexler and Seinfeld (1990) based on a characteristic time scale analysis. The major reason for this is that most of the volatile species favor the particulate phase when temperature is lower; it takes longer time to transport extra volatile species from the gas phase to aerosol phase. Since we have used $(NH_4)_2SO_4$ to represent the submicron particles and NaCl to represent the coarse particles, it is interesting to investigate whether chemistry plays a role in affecting the transport. We have: (a) replaced NaCl in the large particles by $(NH_4)_2SO_4$; (b) assumed both NaCl and $(NH_4)_2SO_4$ particles are present at a diameter of 0.2 μm; and (c) assumed both NaCl and $(NH_4)_2SO_4$ particles are present at a diameter of 3.0 μm. Species concentrations as a function of transport time are presented in Figure 6.5. When NaCl is replaced by $(NH_4)_2SO_4$ in the large particles, the transport proceeds faster than in the original case, primarily because less NH_4NO_3 transports to the large particles as a result of the fact that $(NH_4)_2SO_4$ is more acidic than NaCl. Nevertheless, the overall equilibration time is still about one day as a result of the presence of the large particles. The equilibration time is substantially reduced if only submicron particles exist in an external mixture of $(NH_4)_2SO_4$ and NaCl, while Figure 6.5c shows that the equilibration time is quite long if only large particles are present. The results shown in Figure 6.5 demonstrate that particle size, rather than chemistry, determinines the overall equilibration time of the gas-aerosol system.

Since the equilibration time is very sensitive to change of accommodation coefficient, we have varied the accommodation coefficient from 0.001 to 1.0 and show

corresponding variation of the equilibration times in Figure 6.6. The equilibration time for large particles is defined as that when all the volatile species concentrations have reached within 5% of the equilibrium values, while for small particles, it is defined as the time when the NH_4NO_3 concentration in small particles peaks. It is seen in Figure 6.6 that the equilibration time for small particles ranges from 1.5 mins to several hours when accommodation coefficient varies from 1.0 to 0.001, whereas the equilibration time for large particles remains longer than 10 hours.

The transport calculations show that coarse particles are generally not in equilibrium with either the fine particles or gas phase if they require much longer mass transport times than the time scale over which the air mass is changing. The submicron particles in the test case generally require 1.5 mins to several hours as the equilibration time, a time scale more conducive to establish equilibrium under ambient conditions than that for larger particles. It is noteworthy that the intermediate states obtained on the path to equilibrium exhibit quite different features than either the initial state or the final equilibrium state.

6. Implications for Ambient Aerosols

To apply the foregoing results to ambient aerosols we first consider typical urban aerosol compositions for the fine and coarse particles (Table 6.2) from the 1987 Southern California Air Quality Study (SCAQS) (Chow et al., 1994). During the SCAQS in fall

1987, Chow et al. (1994) reported average concentrations of sulfate (3.13-4.93 μg m^{-3}), nitrate (16.57-30.56 μg m^{-3}), ammonium (5.53-9.93 μg m^{-3}), chloride (0.54-1.14 μg m^{-3}), and sodium (0.14-0.47 μg m^{-3}) of $PM_{2.5}$ aerosols. Average gas-phase concentrations ranged from 0.86-21.56 μg m^{-3} for nitric acid and 4.10-21.89 μg m^{-3} for ammonia. In the calculations we assume that the total aerosol-phase concentrations were those typically measured in SCAQS, except that we assume initially all ammonium nitrate exists in the gas phase as ammonia and nitric acid. The assumed gas-phase concentrations of nitric acid and ammonia are within the measured range in SCAQS. We then calculate the transport of ammonia, nitric acid, and hydrochloric acid between the gas and aerosol phases. An accommodation coefficient of 0.01 is assumed again in the calculation. We show the concentrations of the volatile species as a function of time in Figure 6.7, and the result is similar to what we have found in Case 1. The coarse particles are predicted to require several days to reach the final equilibrium state. An interesting feature for this urban aerosol is that HNO_3 and NH_3 vapor concentrations approach the equilibrium levels much more rapidly than the corresponding aerosol species. The reason is that the time scales for the gas phase to reach equilibrium are controlled by the small particles (see Eq. (8)). HCl is an exception, because all HCl in the gas phase originates from the coarse particles. Note that after the gas phase approaches equilibrium, a substantial amount of the volatile compounds still transfer from the small particles to the large particles via the gas phase. The aerosol species concentrations of the large particles have barely gained any significant mass before the gas-phase concentrations reach equilibrium levels. This interesting case demonstrates that even though the gas-phase concentrations may have

already reached an overall equilibrium, it is still possible that different sized particles are not in mutual equilibrium. Therefore, the equilibration time of the gas-aerosol system $\tau_{e,i}$ (Eq. (10)) is different from the gas-phase equilibration time $\tau_{\infty,i}$ (Eq. (7)).

Air flows in South Coast Air Basin (SoCAB) are affected by the land/sea breeze. The residence times for airflows in SoCAB are generally less than 12 hours during the summer time while recirculation and stagnation occur more frequently in the winter (Douglas et al., 1991). In particular, we can estimate the time scale for change of ammonia concentration in an air parcel flowing from Claremont to Riverside, two sampling sites in the 1987 SCAQS. The average ammonia concentrations during the summer SCAQS at these two locations are 2.06 μg m^{-3} and 18.67 μg m^{-3} (Chow et al., 1994). This leads to the time scale estimate for change of ammonia concentration at Riverside,

$$\tau = \frac{C_{\text{rivr}}}{dC/dt} \approx \frac{C_{\text{rivr}}}{V\,\Delta C/\Delta x}$$

The distance between these two locations is about 35 km, and the wind speed can be estimated as 4 m s^{-1}. This gives $\tau \approx 3$ hr. Therefore, the time scales for change of the gas-phase compounds are probably less than several hours. This implies that coarse particles in SoCAB may not have sufficient time to establish equilibrium with gas-phase volatile compounds. It should be noted that assuming all NH_4NO_3 initially in the gas phase does

not have a major effect on our results. It can be seen in Figure 6.7 that it takes less than half an hour for half of the total NH_4NO_3 to transport to the aerosol phase. It should be noted that the longer equilibration times are not a result of the magnitude of the step-change of initial gas-phase concentrations, since the equilibration time does not change significantly when the difference between initial gas-phase concentrations and the final equilibrium concentrations is reduced (Figure 6.4a). This is because when the difference of the concentrations is reduced, although the amount of mass to transfer is decreased, the mass transfer rate (Eq. (3)) is also reduced.

Marine aerosol is an important class of atmospheric particles. The major component of marine fine particles is non-sea-salt sulfate (nss-sulfate), at a mass concentration ranging from 0.2 to 1.5 $\mu g\ m^{-3}$ (Fitzgerald, 1991). Aerosols in the marine free troposphere contain an appreciable amount of sulfuric acid, which makes the particles more acidic than NH_4HSO_4 (Yamato and Tanaka, 1994). In contrast, for marine air parcels that have passed over the continent within several days, sulfate aerosols neutralized fully by ammonia are predominant. Coarse mode marine aerosols primarily consist of sea salt, at a mass concentration ranging from 2 $\mu g\ m^{-3}$ to 50 $\mu g\ m^{-3}$ (Fitzgerald, 1991). Nitrates in clean marine aerosols occur only about 0.1-0.2 $\mu g\ m^{-3}$ (Fitzgerald, 1991). During measurements at Mauna Loa Observatory, Hawaii, between May 1 and June 5, 1988, Norton et al. (1992) reported 30 pptv (0.08 $\mu g\ m^{-3}$) nitrate aerosol and 103 pptv (0.27 $\mu g\ m^{-3}$) nitric acid at night (representative of the free troposphere) but 60 pptv

(0.15 μg m^{-3}) aerosol nitrate and 130 pptv (0.33 μg m^{-3}) nitric acid during daytime (representative of anthropogenically influenced marine boundary layer).

The ammonium-sulfate-bisulfate-water system is thought to be the most representative of marine submicron aerosol. Quinn et al. (1992) reported discrepancies between ammonia concentrations from measurements and from calculations based on an equilibrium model for ammonium to non-seasalt sulfate molar ratio, R_{as}, larger than 1.8. However, they observed equilibrium between ammonia and acidic particles and explained their results through analysis of the relevant time scales.

It is meaningful to study the time scale for gas-aerosol transport in a marine environment. We have assumed typical marine aerosol composition and gas-phase concentrations (Table 6.2). We assume only monodisperse submicron aerosol particles of dry diameter 0.1 μm, the main component of which is sulfate with various amounts of ammonium as defined by the ammonium to sulfate molar ratio, R_{as}. At $t = 0$ the particles were exposed to a given gas-phase NH_3 concentration. We have calculated the ammonia concentration change in an initial ammonia content of 0.07 μg m^{-3} (0.1 ppb) and 0.007 μg m^{-3} (0.01 ppb). The times needed for ammonia to reach the equilibrium values vary from 1 hour to several hours for R_{as} decreasing from 2 to 0.25. These equilibration times agree with the time scale analysis of Quinn et al. (1992).

7. Conclusions

We have systematically studied the conditions for gas-aerosol equilibrium of the volatile components of both fine- and coarse-mode atmospheric aerosols through detailed transport calculations for hypothetical cases. It is found that the times required for the coarse-mode aerosol particles to reach the equilibrium state are generally sufficiently long that most of the atmospheric coarse aerosol particles are likely in non-equilibrium transition states. The equilibration time between the fine-mode particles and the gas phase is generally less than several hours, and whether submicron aerosol is in equilibrium with the gas phase or not depends on the comparison with other relevant ambient time scales. Sensitivity studies show that the gas-aerosol equilibration times are not sensitive to changes of RH, initial gas-phase concentrations, small variation of aerosol mass concentrations, and different chemical compositions, but are quite sensitive to changes of aerosol size distribution, temperature, and accommodation coefficient. At fixed total aerosol mass, equilibration time increases with increasing particle size, or decreasing accommodation coefficient or temperature. Increase of the accommodation coefficient towards unity does not substantially reduce the equilibration time for the corase-mode particles; it does, however, reduce the equilibration time by several orders of magnitude for the fine-mode particles.

Acknowledgment

This work was supported by the Electric Power Research Institute under agreement RP3189-03 and by National Science Foundation grant ATM-9307603.

REFERENCES

Allen A.G., Harrison R.M. and Erisman J. (1989) Field measurements of the dissociation of ammonium nitrate and ammonium chloride aerosols. *Atmos. Environ.* 23, 1591-1599.

Bassett M. and Seinfeld J. H. (1983) Atmospheric equilibrium model of sulfate and nitrate aerosols. *Atmos. Environ.* 17, 2237-2252.

Bassett M. and Seinfeld J. H. (1984) Atmospheric equilibrium model of sulfate and nitrate aerosols—II. Particle size analysis. *Atmos. Environ.* 18, 1163-1170.

Brimblecombe P. and Clegg S. L. (1990). Equilibrium partial pressures of strong acids over concentrated-solutions. 3. The temperature-variation of HNO_3 solubility. *Atmos. Environ.* 24A, 1945-1955.

Brimblecombe P., Clegg S. L. and Khan I. (1992) Thermodynamic properties of carboxylic acids relevant to their solubility in aqueous solutions. *J. Aerosol Sci.* 23, S901-S904.

Cadle S.H., Countess R. J. and Kelly N. A. (1982) Nitric acid and ammonia in urban and rural locations. *Atmos. Environ.* 16, 2501-2506.

Chow J.C., Watson J. G., Fujita E. M., Lu Z., Lawson D. R. and Ashbaugh L. L. (1994) Temporal and spatial variations of $PM_{2.5}$ and PM_{10} aerosol in the Southern California Air Quality Study. *Atmos Environ* 28, 2061-2080.

Clegg S. L. and Brimblecombe P. (1986) The dissociation-constant and Henry law constant of HCl in aqueous-solution. *Atmos. Environ.* 20, 2483-2485.

Clegg S. L. and Brimblecombe P. (1988a) Equilibrium partial pressures of strong acids over concentrated saline solutions. 1. HNO_3. *Atmos. Environ.* 22, 91-100.

Clegg S. L. and Brimblecombe P. (1988b) Equilibrium partial pressures of strong acids over concentrated saline solutions. 2. HCl. *Atmos. Environ.* 22, 117-129.

Clegg S. L. and Brimblecombe P. (1989) Solubility of ammonia in pure aqueous and multicomponent solutions. *J. Phys. Chem.* 93, 7237-7248.

Clegg S. L. and Brimblecombe P. (1990) Equilibrium partial pressures and mean activity and osmotic coefficients of 0-100-percent nitric-acid as a function of temperature. *J. Phys. Chem.* 94, 5369-5380.

Clegg S. L. and Brimblecombe P. (1992) Chemical modeling of aqueous atmospheric aerosols. *J. Aerosol Sci.* 23, S893-S896.

Douglas S. G., Kessler R. C., Emery C. A. and Burtt J. L. (1991) "Diagnostic Analysis of Wind Observations Collected During the Southern California Air Quality Study, Final Report." Systems Applications International, San Rafael, California. Prepared under Contract #A832-133 for Research Division, California Resources Board, Sacramento, California.

Doyle G. J., Tuazon E. C., Graham R. A., Mischke T. M., Winer A. M. and Pitts J.N. (1979) Simultaneous concentrations of ammonia and nitric acid in a polluted atmosphere and their equilibrium relationship to particulate ammonium nitrate. *Envir. Sci. Technol.* 13, 1416-1419.

Fitzgerald J. W. (1991) Marine aerosols: a review. *Atmos Environ.* 25A, 533-545.

Gelbard F. (1990) Modeling multicomponent aerosol particle growth by vapor condensation. *Aerosol Sci. Technol.* 12, 399-412.

Gray H. A., Cass G. R., Huntzicker J. J., Heyerdahl E. K. and Rau J. A. (1986) Characteristics of atmospheric organic and elemental carbon particle concentrations in Los Angeles. *Envir. Sci. Technol.* 20, 580-589.

Grosjean D. (1982) The stability of particulate nitrate in the Los Angeles atmosphere. *Sci. Total Environ.* 25, 263-275.

Heintzenberg J. (1989) Fine particles in the global troposphere. A review. *Tellus* 41B, 149-160.

Hildemann L. M., Russell A. G. and Cass G. R. (1984) Ammonia and nitric acid concentrations in equilibrium with atmospheric aerosols: experiment vs theory. *Atmos. Environ.* 18, 1737-1750.

John W., Wall S. M. and Ondo J. L. (1988) A new method for nitric acid and nitrate aerosol measurement using the dichotomous sampler. *Atmos. Environ.* 22, 1627-1635.

Khan I. and Brimblecombe P. (1992) Henry's law constants of low molecular weight (<130) organic acids. *J. Aerosol Sci.* 23, S897-S900.

Kim Y. P. and Seinfeld J. H. (1995) Atmospheric gas-aerosol equilibrium III. Thermodynamics of crustal elements Ca^{2+}, K^{+}, and Mg^{2+}. *Aerosol Sci. Technol.* 22, 93-110.

Kim Y. P., Seinfeld J. H. and Saxena P. (1993a) Atmospheric gas-aerosol equilibrium I. Thermodynamic model. *Aerosol Sci. Technol.* 19, 157-181.

Kim Y. P., Seinfeld J. H. and Saxena P. (1993b) Atmospheric gas-aerosol equilibrium II. Analysis of common approximations and activity coefficient calculation methods. *Aerosol Sci. Technol.* 19, 182-198.

Meng Z., Seinfeld J. H., Saxena P. and Kim Y. P. (1995a) Atmospheric gas-aerosol equilibrium IV. Thermodynamics of carbonates. *Aerosol Sci. Technol.* 23, 131-154.

Meng Z., Seinfeld J. H., Saxena P. and Kim Y. P. (1995b) Gas/aerosol distribution of formic and acetic acids. *Aerosol Sci. Technol.* 23, 561-578.

Norton R. B., Carroll M. A., Montzka D. D., Hübler G., Huebert B. J., Lee G., Warren W. W., Ridley B. A. and Walega J. G. (1992) Measurements of nitric acid and aerosol nitrate at the Mauna Loa Observatory during the Mauna Loa Observatory photochemistry experiment 1988. *J. Geophys. Res.* 97D, 10,415-10,425.

Pilinis C. and Seinfeld J. H. (1987) Continued development of a general equilibrium model for inorganic multicomponent atmospheric aerosols. *Atmos. Environ.* 21, 2453-2466.

Pilinis C. and Seinfeld J. H. (1988) Development and evaluation of an Eulerian photochemical gas-aerosol model. *Atmos. Environ.* 22, 1985-2001.

Pio C.A., Nunes T. V. and Leal R. M. (1992) Kinetic and thermodynamic behaviour of volatile ammonium compounds in industrial and marine atmospheres. *Atmos. Environ.* 26A, 505-512.

Quinn P. K., Asher W. E. and Charlson R. J. (1992) Equilibria of the marine multiphase ammonia system. *J. Atmos Chem.* 14, 11-30.

Russell A. G and Cass G. R. (1984) Aquisition of regional air quality model validation data for nitrate, sulfate, ammonium ions and their precursors. *Atmos. Environ.* 18, 1815-1827.

Russell A. G., McRae G. J. and Cass G. R. (1983) Mathematical modeling of the formation and transport of ammonium nitrate aerosol. *Atmos. Environ.* 17, 949-964.

Saxena P., Hudischewskyj A. B., Seigneur C. and Seinfeld J. H. (1986) A comparative study of equilibrium approaches to the chemical characterization of secondary aerosols. *Atmos. Environ.* 20, 1471-1483.

Saxena P., Seigneur C. and Peterson T. W. (1983) Modeling of multiphase atmospheric aerosols. *Atmos. Environ.* 17, 1315-1329.

Stelson A. W., Friedlander S. K. and Seinfeld J. H. (1979) A note on the equilibrium relationship between ammonia and nitric acid and particulate ammonium nitrate. *Atmos. Environ.* 13, 369-371.

Stelson A. W. and Seinfeld J. H. (1982a) Relative humidity and temperature dependence of the ammonium nitrate dissociation constant. *Atmos. Environ.* 16, 983-992.

Stelson A. W. and Seinfeld J. H. (1982b) Relative humidity and pH dependence of the vapor pressure of ammonium nitrate-nitric acid solutions at 25 °C. *Atmos. Environ.* 16, 993-1000.

Stelson A. W. and Seinfeld J. H. (1982c) Thermodynamic prediction of the water activity, NH_4NO_3 dissociation constant, density and refractive index for the NH_4NO_3-$(NH_4)_2SO_4$-H_2O system at 25 °C. *Atmos. Environ.* 16, 2507-2514.

Tanner R. L. (1982) An ambient experimental study of phase equilibrium in the atmospheric system: aerosol H^+, NH_4^+, SO_2^{2-}, NO_3^--NH_3(g), HNO_3(g). *Atmos. Environ.* 16, 2935-2942.

Wexler A. S., Lurmann F. W. and Seinfeld J. H. (1994) Modelling urban and regional aerosols: I. Model development. *Atmos. Environ.* 28A, 531-546.

Wexler A. S. and Seinfeld J. H. (1990) The distribution of ammonium salts among a size and composition dispersed aerosol. *Atmos. Environ.* 24A, 1231-1246.

Wexler A. S. and Seinfeld J. H. (1991) Second-generation inorganic aerosol model. *Atmos. Environ.* 25A, 579-591.

Yamato M. and Tanaka H. (1994) Aircraft observations of aerosols in the free marine troposphere over the North Pacific Ocean: Particle chemistry in relation to air mass origin. *J. Geophys. Res.* 99D, 5353-5377.

Table 6.1. Ratio of the equilibration times, $\tau_{j,i}^{p}/\tau_{j,i}$, for some atmospheric species for 50 μg m^{-3} aerosol water content at 298 K

	$\tau_{j,i}^{p}/\tau_{j,i}$			
	pH = 0	pH = 1	pH = 2	pH = 3
NH_3	2.2	0.2	0.02	0.002
HCl	0.002	0.02	0.24	2.4
HNO_3	0.003	0.03	0.3	3.1
HCOOH	6.8×10^{-6}	6.8×10^{-6}	6.9×10^{-6}	8.0×10^{-6}
CH_3COOH	6.7×10^{-6}	6.7×10^{-6}	6.7×10^{-6}	6.8×10^{-6}
$(COOH)_2$	0.004	0.006	0.03	0.2
$C_3H_4O_3$ (Pyruvic acid)	3.8×10^{-4}	3.9×10^{-4}	5.3×10^{-4}	1.9×10^{-3}

Table 6.2. Initial concentrations ($\mu g\ m^{-3}$) for equilibration test cases

	Size[†]	NH_3 or NH_4^+	HNO_3 or NO_3^-	HCl or Cl^-	SO_4^{2-}	Na^+	K^+	Ca^{2+}	Mg^{2+}	Other insoluble
Case 1										
Gas phase	-	10	30	0	-	-	-	-	-	-
Size 1	0.2	7.718	0	0	22.246	0	0	0	0	0
Size 2	3.0	0	0	12.483	0	7.866	0	0	0	0
Urban Case										
Gas phase	-	15	15	0	-	-	-	-	-	-
Size 1	0.2	1.734	0	0	4.998	0	0	0	0	0
Size 2	3.0	0	6.97	0.51	1.47	1.495	0.30	1.00	0.39	4.0[*]
Marine Case										
Gas phase	-	0.007 or 0.07	0.27	0	-	-	-	-	-	-
Size 1	0.1	[‡]	0.10	0.00	0.98	0	0	0	0	0

[†]Dry diameter (μm).

[‡]Depends on R_{as}, the ammonium-to-sulfate molar ratio.

[*]Insoluble soil components such as Al, Si, Fe, etc.

Table 6.3. Characteristic time scales for volatile compounds to transport to particles

	τ_0 (hr)†		$C_{s,i}$ (μg/m^3)		$C_{e,i}$	$C_{\infty,i}$	$\tau_{j,i}$ (hr)		$\tau_{\infty,i}$ (hr)
	Section 1	Section 2	Section 1	Section 2	(μg/m^3)	(μg/m^3)	Section 1	Section 2	
RH=0.9									
NH_3	0.12	2.61	1275.3	0	2.6	10	0.12	0.68	0.0007
HNO_3	0.12	2.61	0	0	1.13	30	0.004	0.098	0.11
HCl	0.12	2.61	0	0.00017	0.67	0	460*	10288	440.1
RH=0.8									
NH_3	0.16	3.61	1444.5	0	3.71	10	0.16	1.34	0.0007
HNO_3	0.16	3.61	0	0	2.16	30	0.012	0.26	0.14
HCl	0.16	3.61	0	0.00013	2.55	0	3160*	70830	3025.3
RH=0.7									
NH_3	0.19	11.94	1522.1	8.61	4.65	10	0.19	34.03	0.0007
HNO_3	0.19	11.94	0	1.06	2.89	30	0.018	0.76	0.19
HCl	0.19	11.94	0	13.78	4.19	0	0.057*	8.31	0.057
RH=0.6									
NH_3	0.36	11.94	8.67	8.61	6.47	10	0.60	18.39	0.923
HNO_3	0.36	11.94	25.07	1.06	3.43	30	1.59	0.98	1.65
HCl	0.36	11.94	0	13.78	7.8	0	0.20*	5.18	0.20
RH≤0.5									
NH_3	0.36	11.94	8.67	8.61	9.59	10	0.25	8.42	0.11
HNO_3	0.36	11.94	25.07	1.06	8.2	30	1.24	2.95	1.34
HCl	0.36	11.94	0	13.78	11.75	0	0.31*	1.76	0.30

†$\tau_0 = \dfrac{2\lambda/\alpha_i D_{pj} + 1}{2\pi D_{pj} D_i N_j}$, where the symbols are defined in the text.

*Since $C_{\infty,i} = C_{s,i} = 0$ for these cases, the relevant background concentration scales become $C_{s,i}$'s of the large particles.

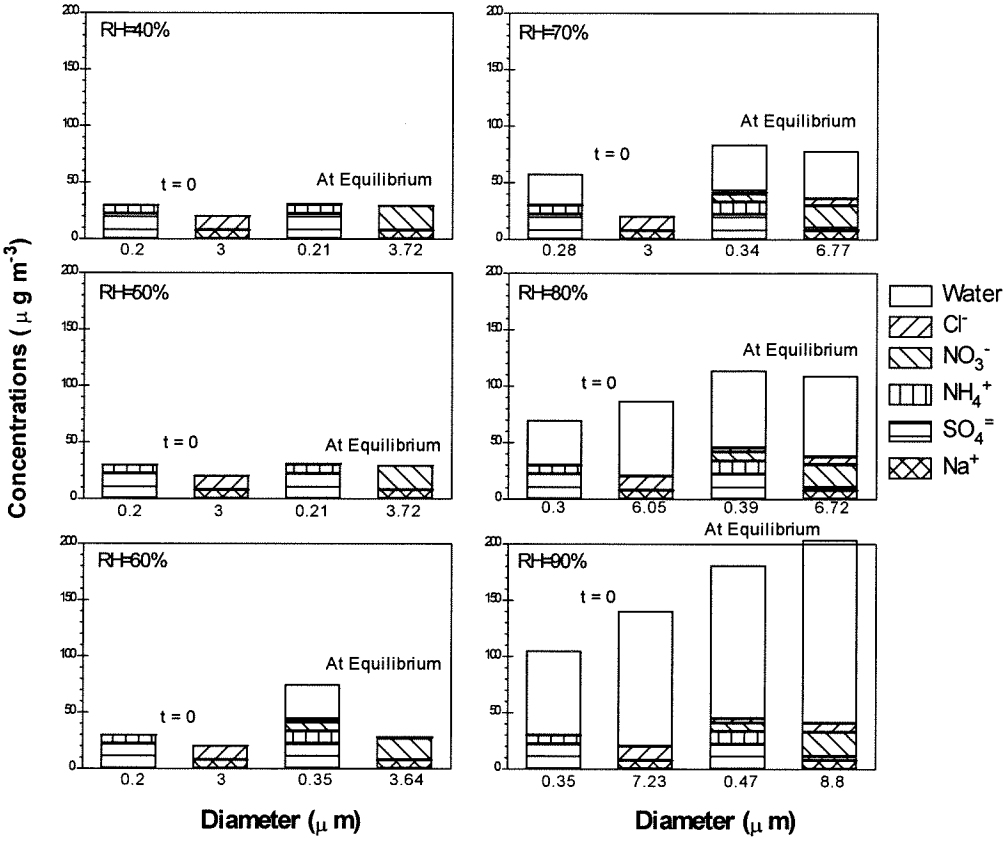

Fig. 6.1 Initial and equilibrium aerosol sizes and compositions.

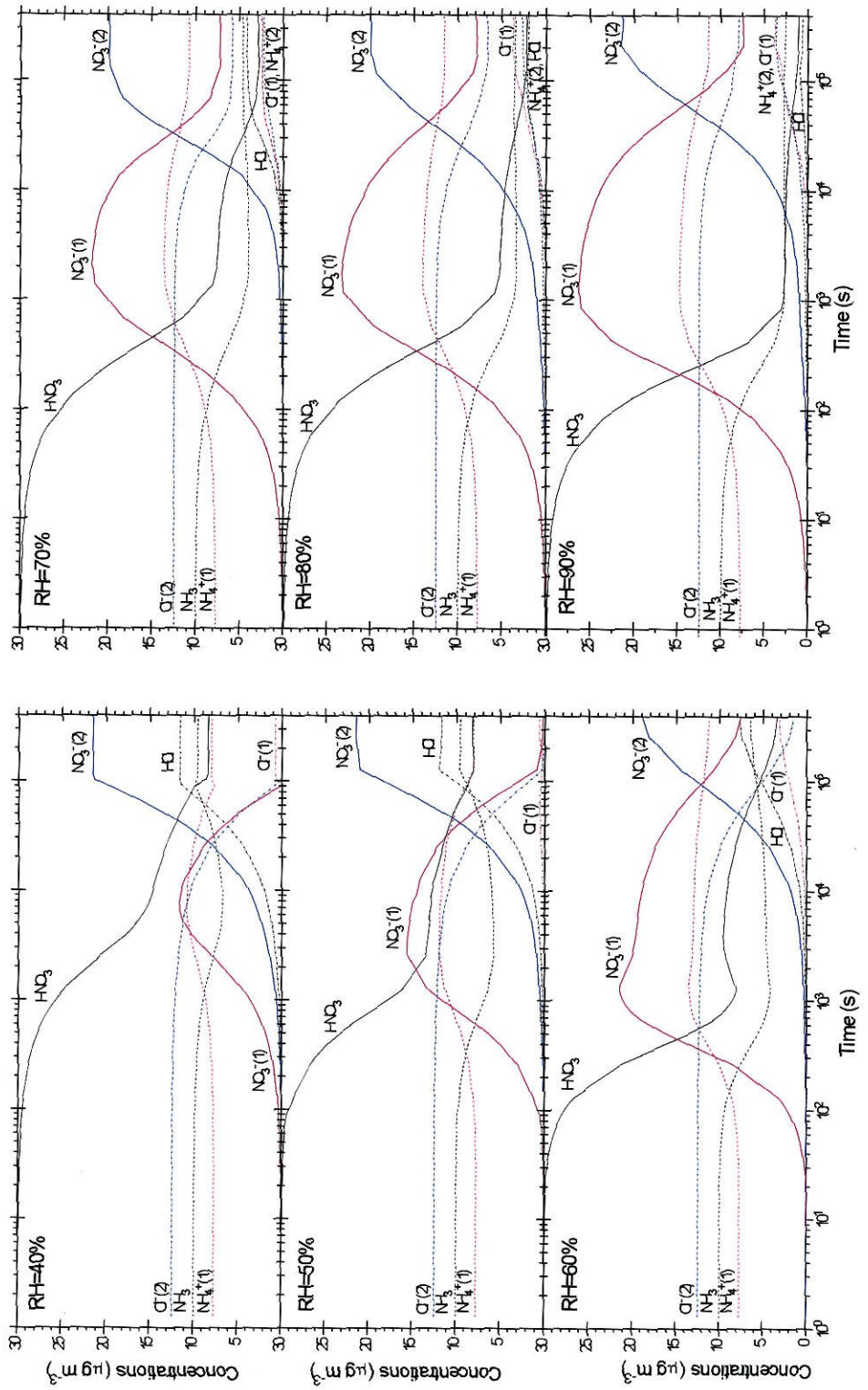

Fig. 6.2 Species concentrations in the gas and aerosol phases as a function of transport time for RH ranging from 40% to 90% in Case 1. Initial gas- and aerosol-phase data are given in Table 6.2.

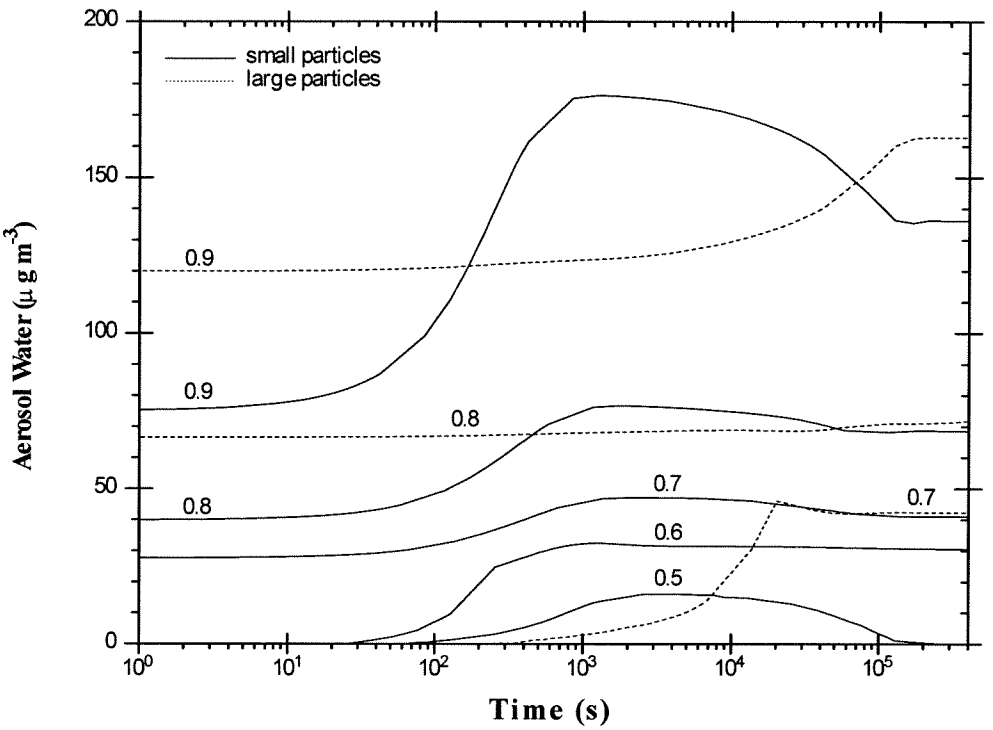

Fig. 6.3 Aerosol water content for the two size sections as a function of transport time for RH = 90%, 80%, 70%, 60%, 50%, and 40% (zero, invisible in the figure) in Case 1.

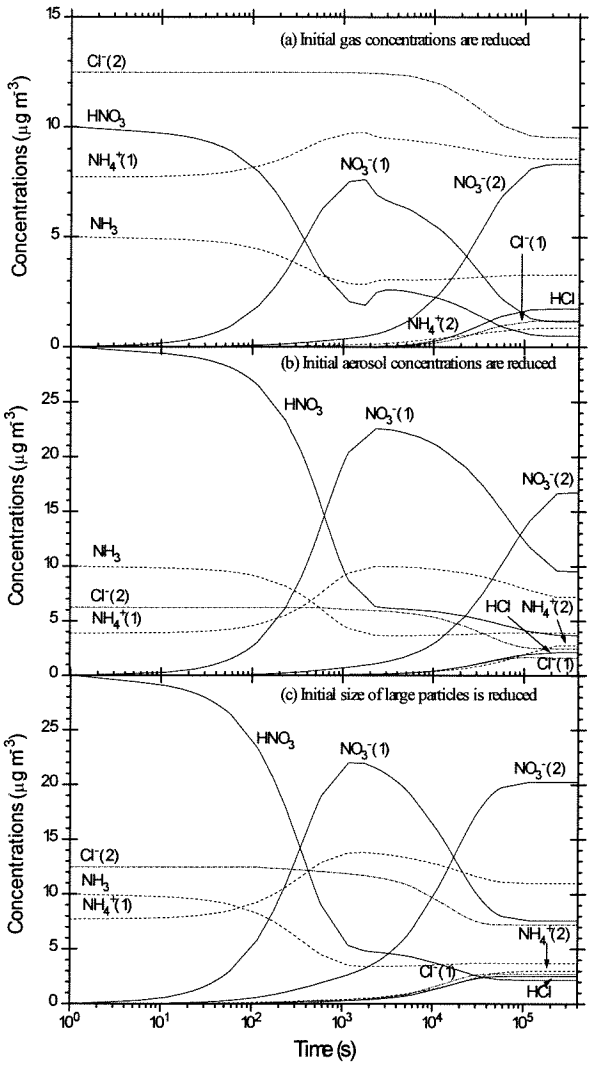

Fig. 6.4 Species concentrations in the gas and aerosol phases as a function of transport time for RH=80% in Case 1. Initial gas- and aerosol-phase data are given in Table 6.2, except that (a) HNO_3 = 10 μg m^{-3} and NH_3 = 5 μg m^{-3}; (b) all the species concentrations in the aerosol phase are reduced by one-half; (c) the size of the large particles is reduced by one-half.

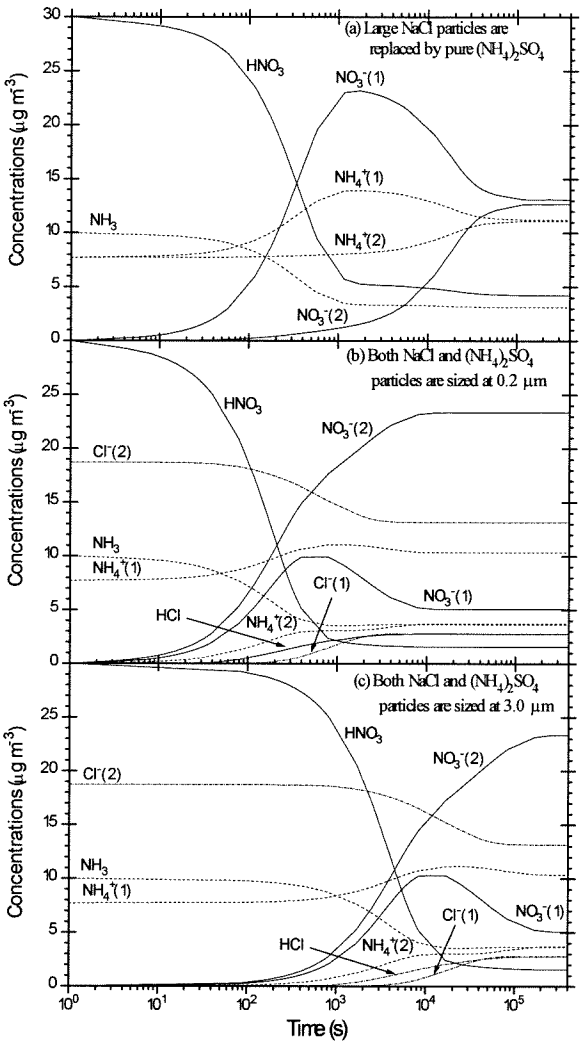

Fig. 6.5 Species concentrations in the gas and aerosol phases as a function of transport time for RH=80% in Case 1. Initial gas- and aerosol-phase data are given in Table 6.2, except that (a) NaCl in the large particles is replaced by $(NH_4)_2SO_4$; (b) both NaCl and $(NH_4)_2SO_4$ particles are assumed to be present at a diameter of 0.2 μm; (c) both NaCl and $(NH_4)_2SO_4$ particles are assumed to be present at a diameter of 3.0 μm.

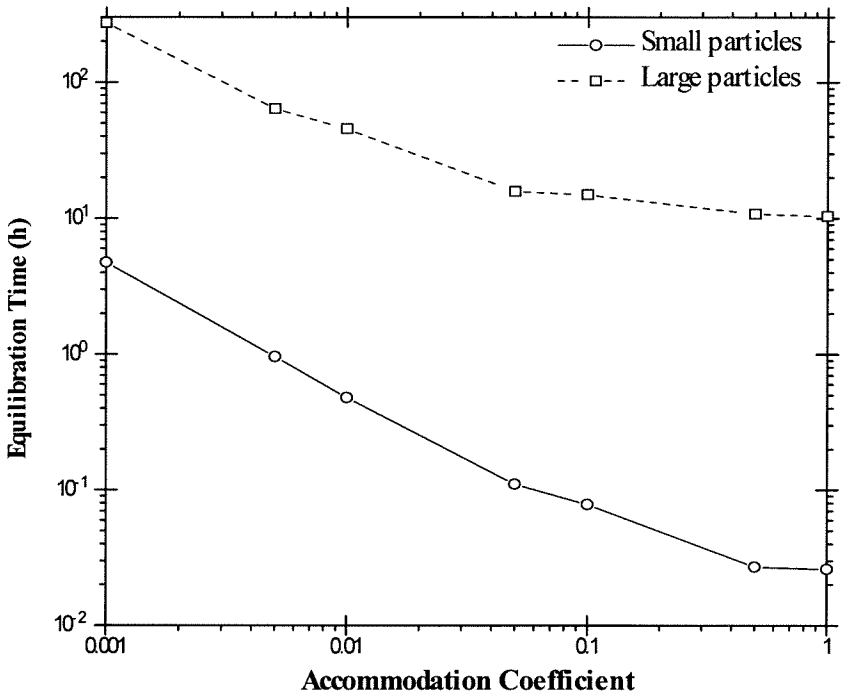

Fig. 6.6 Equilibration times as a function of accommodation coefficient for both small and large particles. Initial gas- and aerosol-phase data are given in Table 6.2. RH = 80%.

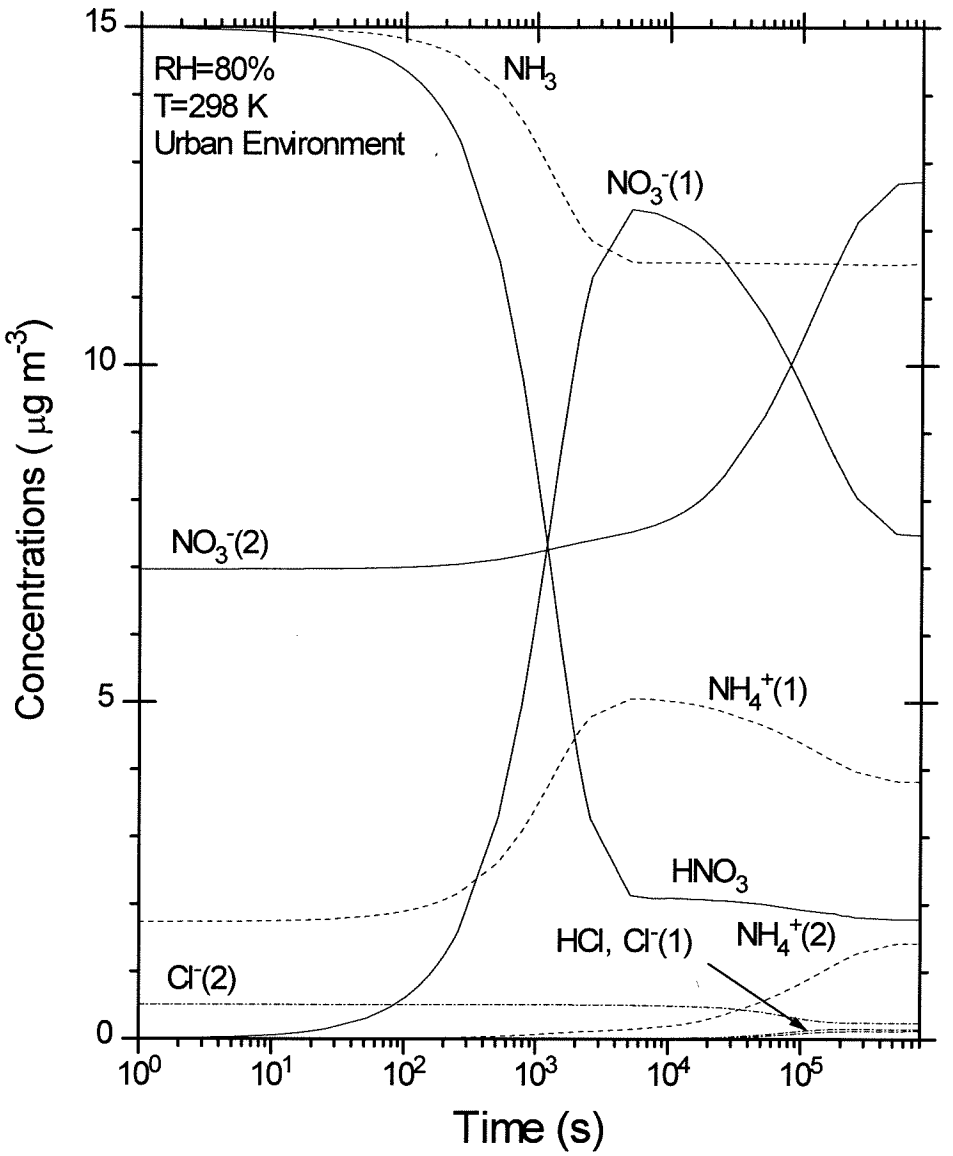

Fig. 6.7 Species concentrations in the gas and aerosol phases as a function of transport time for RH=80% in the urban case. Initial gas- and aerosol-phase data are given in Table 6.2.

Chapter 7

Size- and Chemically-Resolved Model of Atmospheric Aerosol Dynamics

[The text of this chapter will appear in: Meng Z., Dabdub D., and Seinfeld J. H. (1997) *J. Geophys. Res.*]

Abstract

A three-dimensional, size- and chemically-resolved aerosol model is developed. Gas-to-particle conversion is represented by dynamic mass transfer between the gas and aerosol phases. Particle-phase thermodynamics is computed by a new thermodynamic model, SCAPE2. The aerosol model is applied to simulate gas and aerosol behavior in the 27-29 August 1987 episode in the South Coast Air Basin of California. The assumption that volatile inorganic species such as NH_4NO_3 are at instantaneous, local equilibrium is examined and it is found that, in many instances, gas/aerosol mass transfer limits the rate of gas-to-particle conversion.

1. Introduction

Particles in the Earth's atmosphere play an important role in atmospheric chemistry, climate, and human health. Atmospheric formation and removal of particles are governed by a number of complex dynamic processes, including nucleation, condensation, coagulation, chemical transformation in the gas, aerosol, and aqueous (cloud and fog) phases, interphase exchange and equilibria, and wet and dry deposition. Atmospheric particle sizes range from a few nanometers (nm) in diameter to several micrometers (μm). This factor of 10^3 in diameter translates into a factor of 10^9 in particle mass between the two extremes of the size spectrum. Particle chemical composition can vary substantially depending on particle size; indeed this variation is, at once, one of the most important features from the point of view of atmospheric chemistry and human health effects and one of the most demanding aspects to model theoretically.

A gas-phase atmospheric chemical-transport model predicts the spatial and temporal distribution of gaseous species concentrations, $c_i(x, y, z, t), i = 1, 2, \ldots, N$. An atmospheric aerosol is characterized by both its size and composition distribution. The most general form of an atmospheric aerosol chemical-transport model predicts the size-composition distribution as a function of location and time. The starting point for an aerosol model is the equation of conservation of particle number (or mass). Within that equation are terms that account for transport and dispersion, gas-to-particle conversion, coagulation, and removal processes. *Pilinis and Seinfeld* [1988] constructed the first three-dimensional size- and chemically-resolved atmospheric aerosol model. The major features of the

model, as well as those of other existing aerosol models, are summarized in Tables 7.1-7.4. The two currently available three-dimensional aerosol models, the Regional Particulate Model [*Binkowski and Shankar*, 1995] and that of *Lurmann et al.* [1997], assume instantaneous gas-aerosol equilibrium for volatile inorganic compounds. It has been shown, however, that for some compounds under certain conditions equilibrium is slow to be established relative to the time scale over which other changes are occurring [*Wexler and Seinfeld*, 1990; *Meng and Seinfeld*, 1996]. Thus, it is desirable that the most general form of an aerosol model not rely on the assumption of instantaneous, local equilibrium of volatile species.

The models of *Pilinis and Seinfeld* [1988] and *Lurmann et al.* [1997] represent the aerosol size distribution by the sectional approximation [*Gelbard et al.*, 1980; *Gelbard and Seinfeld*, 1980], wherein the size domain is segmented into a series of sections, or bins, within which the aerosol has a uniform composition. The RPM [*Binkowski and Shankar*, 1995] assumes that the aerosol size distribution adheres to a bimodal log-normal distribution and then solves equations for the 0th, 3rd, and 6th moments of the distribution. In theory, the moment method requires solving equations for all three moments simultaneously. The RPM solves only the 0th moment completely; the 3rd and 6th moments are solved without the transport terms. Instead of solving mode-resolved equations for the chemical components, the RPM solves only the total (summed over the two modes) mass concentration for the individual species. The total mass concentration is then distributed over the two modes; as currently formulated, the RPM assumes that each of the two modes has the same chemical composition. The RPM also assumes that growth

processes are fast compared with the generation of condensable vapor. Whereas this is generally true for H_2SO_4, it is not the case for HNO_3, HCl, and NH_3, for which detailed mass transport needs to be calculated. Given the limitations of the modal approximation, a sectional approach is deemed to be more appropriate, as it allows for general specification of the aerosol size-composition distribution.

We present here the development and application of a three-dimensional size- and chemically-resolved atmospheric aerosol chemical-transport model. The model is applied to simulate gas and aerosol behavior in the South Coast Air Basin of California over a three-day episode (27-29 August) during the 1987 Southern California Air Quality Study (SCAQS).

2. Governing Equations for Aerosol Dynamics

Let *n(m, t)* be the number concentration of particles having total particle mass in the range *m* to *m* + *dm*. (We need not explicitly indicate the spatial dependence of *n* for the moment.) The total mass of a particle is the sum of the masses of its *N* individual components,

$$m = \sum_{i=1}^{N} m_i \tag{1}$$

Let *I(m, t)* be the rate of change of the total mass of a particle of mass *m* as a result of condensation/evaporation processes,

$$I(m,t) = \sum_{i=1}^{N} I_i(m,t) \tag{2}$$

where $I_i = dm_i/dt$. If the coagulation coefficient between particles of masses m and m' is $\beta(m, m')$, the equation of conservation governing $n(m, t)$ can be written as

$$\frac{\partial n(m,t)}{\partial t} = -\frac{\partial}{\partial m}\left[I(m,t)n(m,t)\right] + \frac{1}{2}\int_0^m \beta(m', m-m')n(m',t)n(m-m',t)dm' - n(m,t)\int_0^\infty \beta(m,m')n(m',t)dm' + S(m,t) - L(m,t)n(m,t) \tag{3}$$

where $S(m, t)$ is any external source of particles of mass m (e.g., nucleation), and $L(m, t)n(m, t)$ is the first-order rate of removal of particles of mass m (e.g., wet and dry deposition).

For applications to urban/regional situations, one is generally interested in the aerosol *mass* distribution, rather than the *number* distribution. We define

$$q_i(m,t) = m_i n(m,t) \tag{4}$$

as the mass concentration distribution for species i. The total aerosol mass concentration distribution function is

$$q(m,t) = mn(m,t) = \sum_{i=1}^{N} q_i(m,t) \tag{5}$$

The normalized growth/evaporation rate of species i in a particle of mass m is

$$H_i(m,t) = \frac{1}{m}\frac{dm_i}{dt} \tag{6}$$

and the total normalized growth rate of a particle of mass m is

$$H(m,t) = \frac{1}{m}\frac{dm}{dt} = \sum_{i=1}^{N} H_i(m,t) \tag{7}$$

Using the above definitions, (3) becomes [*Pilinis*, 1990]

$$\frac{\partial q_i(m,t)}{\partial t} = H_i(m,t)q(m,t) - \frac{\partial}{\partial m}[mq_i H] + \int_0^m \beta(m', m-m')q_i(m',t)\frac{q(m-m',t)}{m-m'}dm' - q_i(m,t)\int_0^\infty \beta(m,m')\frac{q(m',t)}{m'}dm' + m_i S(m,t) - L(m,t)q_i(m,t) \tag{8}$$

Equation (8) is the general equation governing the mass distribution of species *i* over the aerosol mass spectrum. It includes condensation/evaporation, coagulation, sources (such as nucleation), and removal processes. Under the most extreme particle concentrations in urban areas, Brownian coagulation can be shown to have a negligible effect on the evolution of the aerosol size distribution over the time scales of interest [*Wexler et al.*, 1994]. Thus, for urban/regional applications coagulation can be neglected in (8). The spatial dependence of q_i can now be accounted for and terms, identical to those for gaseous species, for advection and turbulent mixing can be added. Finally, for computational purposes, the independent variable, *m*, can be transformed to a normalized particle diameter, $\mu = ln(D_p/D_{p0})$, where D_{p0} is a reference particle diameter (e.g., the smallest diameter in the size domain). With $p_i(\mu, \mathbf{x}, t) = (dm/d\mu)q_i$, the result is

$$\frac{\partial p_i(\mu,\mathbf{x},t)}{\partial t} = -\left(\overline{\mathbf{V}}(\mathbf{x},t) - V_s(\mu)\mathbf{k}\right)\cdot\nabla p_i + \nabla\cdot\mathbf{K}(\mathbf{x},t)\nabla p_i$$
$$+ H_i(\mu,\mathbf{x},t)p(\mu,\mathbf{x},t) - \frac{1}{3}\frac{\partial}{\partial\mu}[Hp_i] \qquad (9)$$
$$+ S_i(\mu,\mathbf{x},t) - L(\mu,\mathbf{x},t)p_i$$

where $\boldsymbol{x}$ is the spatial coordinate vector, $\overline{\boldsymbol{V}}(\boldsymbol{x},t)$ is the mean wind velocity vector, V_S is the particle settling velocity, $\boldsymbol{k}$ is the unit vector in the upward vertical direction, and $\boldsymbol{K}(\boldsymbol{x},t)$ is the turbulent diffusivity tensor.

The condensation/evaporation rate of species i is [Wexler et al., 1994]

$$H_i = \frac{1}{m}\frac{dm_i}{dt} = \frac{2\pi D_p D_i}{m}\frac{C_{\infty,i} - C_{s,i}}{\frac{2\lambda}{\alpha_i D_p} + 1} \qquad (10)$$

where D_i is the molecular diffusivity of species i in air, $C_{\infty,i}$ and $C_{s,i}$ are the concentrations in the bulk gas phase and at the particle surface, λ is the air mean free path, and α_i is the accommodation coefficient for species i on the atmospheric aerosol. Particle surface vapor concentrations $C_{s,i}$ are estimated by a thermodynamic routine, SCAPE2, which will be described subsequently. Equation (10) is used to compute rates of gas/aerosol transfer for sulfate, ammonia, nitric acid, hydrochloric acid, and semi-volatile organic aerosols (SOA). Water and CO_2 (or carbonates) can be assumed to be in local, instantaneous equilibrium between the gas and aerosol phases. The condensation/ evaporation rate for water is [*Wexler et al.*, 1994]

$$H_w = \frac{1}{m}\frac{dm_w}{dt} = \sum_i \frac{1000 H_i}{M_i m_{0,i}(RH)} - \frac{1000}{p}\frac{\partial RH}{\partial t}\sum_i \frac{p_i}{M_i m_{0,i}^2(RH)}\frac{\partial m_{0,i}(RH)}{\partial RH} \qquad (11)$$

where M_i is the molecular weight of species i, and $m_{0,i}$ is the molality of species i in a binary aqueous solution with water activity equal to relative humidity RH.

In a three-dimensional model dry deposition of both gaseous and particulate species is included in the ground-level boundary condition to (9) in terms of a deposition velocity, $V_d = F/C(z_r)$,where F is the downward mass flux and $C(z_r)$ is the concentration at a reference height, z_r (typically z_r = 10 m) [*Russell et al.*, 1993]. The deposition flux is given by

$$F = \left[K_{zz}(z) + D\right]\frac{dC(z)}{dz} + V_s C(z) \tag{12}$$

where K_{zz} is eddy diffusivity, D is molecular diffusivity, and V_S is the settling velocity. Eq. (12) can be reduced to

$$\int_{C(z_d)}^{C(z_r)} \frac{dC(z)}{V_d C(z_r) - V_s C(z)} = \int_{z_d}^{z_r} \frac{dz}{\left[K_{zz}(z) + D\right]} \tag{13}$$

where z_d is the species sink height. Define

$$V_p = \frac{1}{\int_{z_d}^{z_r} \frac{dz}{\left[K_{zz}(z) + D\right]}} = \frac{\kappa^2 u(z_r)}{\left[\int_{z_0}^{z_r} \phi_m\left(\frac{z}{L}\right)\frac{dz}{z}\right]\left[\ln\left(\frac{z_0}{z_d}\right) + \int_{z_0}^{z_r} \phi_p\left(\frac{z}{L}\right)\frac{dz}{z}\right]} \tag{14}$$

where κ is von Karman's constant, $u(z_r)$ is the wind velocity at the reference elevation, z_0 is the surface roughness height, L is the Monin-Obukhov length, and ϕ_m and ϕ_p are experimentally derived functions that account for the influence of atmospheric stability on turbulent transport. Note that the definition of V_p for particles is the same as the

definition of the maximum deposition velocity, $V_{g\,max}$, for gases to deposit on a perfect-sink surface by *Russell et al.* [1993], except that the term, $\ln(z_0/z_d)$, in Eq. (14) is evaluated separately for particles and gases, namely, for gases,

$$\ln\left(\frac{z_0}{z_d}\right)=2\left(\frac{Sc}{\Pr}\right)^{2/3}, \tag{15}$$

where *Sc* and *Pr* are the Schmidt and Prandtl numbers [*Russell et al.*, 1993], while for particles,

$$\ln\left(\frac{z_0}{z_d}\right)=\kappa\left(Sc^{-2/3}+10^{-3/St}\right)^{-1}, \tag{16}$$

where the Stokes number $St=(V_s/g)(u_*^2/\upsilon)$, and g is the gravitational acceleration, u_* is the friction velocity, and υ is the viscosity of air [*Pleim et al.*, 1984]. Substituting (14) into (13) and noting $C(z_d)=0$ for particles, we obtain

$$V_d=\frac{V_s}{1-e^{-V_s/V_p}} \tag{17}$$

It is easy to see from (17) that V_d approaches the settling velocity if the particles are sufficiently large so that V_S is dominant over V_p; on the other hand, if $V_S << V_p$ (i.e., for small particles), $V_d \rightarrow V_p$, governed by the Brownian-diffusion controlled particle deposition.

3. Gas-to-Particle Conversion

3.1 Condensation/Evaporation and Nucleation

The condensation/evaporation driving force for species i is the difference between the concentration just above the particle surface $C_{s,i}$ and that in the bulk gas $C_{\infty,i}$. Most previous efforts in modeling condensation/evaporation of volatile species have assumed instantaneous gas/aerosol equilibrium. In this work condensation/evaporation processes are modeled dynamically. The thermodynamic model SCAPE2, which is described in Section 3.3, is used to calculate the particle surface vapor concentrations $C_{s,i}$ in (10) for all inorganic species. Later we will compare predictions based on the fully dynamic approach with those based on the equilibrium approach, which partitions the total concentration of volatile species between the gas and bulk aerosol phases and then allocates the aerosol species to different size sections based on aerosol surface area [*Pandis et al.*, 1993; *Lurmann et al.*, 1997].

Homogeneous nucleation is assumed to occur only with H_2SO_4/H_2O. A nucleation threshold H_2SO_4 concentration C_{crit,H_2SO_4} (in μg m^{-3}) can be calculated from [*Wexler et al.*, 1994]

$$C_{crit,H_2SO_4} = 0.16\exp(0.1T - 3.5RH - 27.7), \tag{18}$$

where T is in K and RH between 0 and 1. If the ambient H_2SO_4 vapor concentration exceeds C_{crit,H_2SO_4}, that amount exceeding the threshold is removed from the gas phase and placed in the smallest aerosol size section.

3.2 Secondary Organic Aerosol Formation

Secondary organic aerosol (SOA) results when a parent organic compound A reacts with OH, O_3, or NO_3 to yield products that have sufficiently low vapor pressures that they partition into the aerosol phase. For example,

$$A + OH \longrightarrow \cdots + \beta B + \cdots$$

where the semi-volatile product B formed with stoichiometric coefficient β partitions between the gas and particulate phases,

$$B(g) \rightleftharpoons B(p)$$

Once the semi-volatile condensable vapor B(g) is formed in the gas phase, mass transfer of B(g) to B(p) is governed by (10). Gas/particle partitioning of semi-volatile organic compounds to urban particulate matter containing a significant fraction of organic matter will be dominated by absorption of the compound into the particulate organic layer [*Odum et al.*, 1996]. Based on the absorption mechanism, the surface vapor concentrations of semi-volatile organic compounds are governed by

$$C_{s,i}^{eq} = \frac{F_i}{K_i^{OM} OM} \tag{19}$$

where F_i ($\mu g\ m^{-3}$) is the concentration of organic species i in the aerosol phase, K_i^{OM} ($m^3\ \mu g^{-1}$) is the absorption partitioning coefficient, and OM ($\mu g\ m^{-3}$) is the absorbing organic mass concentration.

Aromatic species can be presumed to be the major anthropogenic sources of SOA [*Odum et al.*, 1996]. Two condensable vapor products can be assumed to result from each of the reactions of toluene (TOLU) and higher aromatics (AROM) with OH, namely,

$$TOLU + OH \rightarrow ... + \beta_1 ATO1 + \beta_2 ATO2$$

$$AROM + OH \rightarrow ... + \beta_1 AAR1 + \beta_2 AAR2$$

where β_1 and β_2 are stoichiometric coefficients, and ATO1, ATO2, AAR1, and AAR2 are the generalized semi-volatile vapor products [*Odum et al.*, 1996].

3.3 Aerosol Thermodynamics

SCAPE (Simulating Composition of Atmospheric Particles at Equilibrium) is an aerosol thermodynamic model that was first introduced in 1993 [*Kim et al.* 1993ab] and has undergone continued development since that time. It has the most complete treatment of inorganic gas/aerosol equilibrium available, and provides the option of using three popular activity coefficient estimation methods (Bromley, K-M, and Pitzer); also, with respect to RH variations, one can choose to calculate either the metastable or full equilibrium state of the particles. The ZSR method [*Robinson and Stokes*, 1965] is used to estimate water activity because of its computational efficiency and comparable accuracy with other more complex methods. Temperature dependence of deliquescence points is also considered. The original version of SCAPE includes sodium, sulfate, ammonium, nitrate, and chloride. Subsequent work has added potassium, calcium, magnesium, and carbonates [*Kim and Seinfeld*, 1995; *Meng et al.*, 1995a].

In the original version of SCAPE the equilibrium relations, together with mass balance and electroneutrality conditions, are reduced to a single equation in the H^+ concentration. After gaseous and aqueous species concentrations are obtained, solid concentrations in the aerosol phase are calculated. The original version of SCAPE cannot

be used directly to calculate the particle surface vapor concentrations $C_{s,i}$. We have modified the original version and have developed an option to handle aerosol-phase-only thermodynamics. The new version is termed as SCAPE2. In determining the H^+ concentration, the original SCAPE uses the combined bisection-Newton method; in SCAPE2, only the bisectional method is applied to the logarithmic scale of the concentration domain.

Crustal compounds affect the general equilibria of volatile species. When the aerosol contains water, crustal species alter the ion balance and interactions. For pure solid particles, the following heterogeneous chemical reactions are relevant:

$$HNO_3 + NH_4Cl \rightleftharpoons NH_4NO_3 + HCl$$

$$HNO_3 + NaCl \rightleftharpoons NaNO_3 + HCl$$

$$HNO_3 + KCl \rightleftharpoons KNO_3 + HCl$$

$$HNO_3 + \tfrac{1}{2}CaCl_2 \rightleftharpoons \tfrac{1}{2}Ca(NO_3)_2 + HCl$$

$$HNO_3 + \tfrac{1}{2}MgCl_2 \rightleftharpoons \tfrac{1}{2}Mg(NO_3)_2 + HCl$$

where the equilibrium constants for the above five reactions, K_1, K_2, K_3, K_4, and K_5, are 1.8908, 4.0075, 12.694, 1461.7, and 2489.5, at 298 K, respectively. If surplus HNO_3 vapor is present, it reacts preferentially with $MgCl_2$ if available, then $CaCl_2$, KCl, NaCl, and NH_4Cl, based on the values of their equilibrium constants. For instance, if reaction of HNO_3 and NaCl is to proceed, nitric acid must have consumed the available KCl, $CaCl_2$, and $MgCl_2$ already. The reverse is true if excess HCl is available for reaction with

the nitrate salts, though this situation is less likely in the atmosphere. Similar considerations apply to reactions of the carbonate salts with HNO_3 and HCl.

4. Numerical Solution

Operator splitting [*McRae et al.*, 1982] is used to solve the different physical and chemical processes according to the following order, $T_x T_y T_{z,c} T_a T_y T_x$, where T_x, T_y, $T_{z,c}$, and T_a represent the operators of transport in x direction, transport in y direction, transport in z direction and gas-phase chemistry, and aerosol dynamics, respectively. Spatial advection and diffusion terms in the above equation are solved by the same methods as in the host gas-phase atmospheric chemical transport model.

The aerosol operator is activated after the gas-phase chemistry operator is finished; it calculates mass transport between the gas and aerosol phases while total mass concentrations are conserved. The numerical time step for the mass transport varies according to the characteristic mass transport time scale and Courant number at the beginning of each time step, and is determined by the smallest of these for all the aerosol size sections. Whether or not the particle surface vapor concentrations for a particular size section are updated at a given time step by "calling" the aerosol thermodynamic model (SCAPE2) is determined by the ratio of the time passed since the last update over the previous characteristic time scale for that section. The aerosol operator becomes inactive after the mass transport has proceeded for a time step of the gas-phase chemistry operator.

Representation of the size- and composition-resolved aerosol distribution function is based on a sectional approach. An internal mixture is assumed for the particles, that is, within each size section the chemical composition of the particles is unique, and furthermore, the mass concentration distribution of a given species is assumed to be constant in a given size section. The particle size domain is prescribed to be between $D_{p,min}$ and $D_{p,max}$, the values of which used in the application to be presented are 0.039 μm and 10 μm. The minimum value is chosen such that the division between the 6th and 7th sections occurs at a diameter of exactly 2.5 μm, thus facilitating comparison of the predictions with ambient $PM_{2.5}$ and PM_{10} observations. ($PM_{2.5}$ and PM_{10} denote the aerosol particles with diameter smaller than 2.5 μm and 10 μm.) If particles grow beyond $D_{p,max}$, their sizes are reduced and the number concentration is increased to maintain mass conservation; on the other hand, if the particles shrink below $D_{p,min}$, their sizes are increased and the number concentration is reduced. The above treatment of the upper and lower boundary conditions has a negligible influence on model predictions because, when the particle size spectrum is sufficiently broad, the mass fractions of particles outside the boundaries are small and small particles (sulfate dominant) are more likely to experience condensation than evaporation at the lower particle size boundary.

The condensation/evaporation term is solved by Bott's method [*Dhaniyala and Wexler*, 1996]. Numerical solution of the condensation/evaporation portion of (9),

$$\frac{\partial p_i(\mu,t)}{\partial t} = H_i(\mu,t)p(\mu,t) - \frac{1}{3}\frac{\partial H p_i(\mu,t)}{\partial \mu}, \tag{20}$$

is given by

$$[p_i]_j^{n+1} = [p_i]_j^n + \frac{[H_i]_j}{[H]_j}[p_i]_j^n[\exp(H\Delta t) - 1] - \frac{\Delta t}{\Delta \mu}\left(F_{j+1/2}^n - F_{j-1/2}^n\right) \quad (21)$$

where n denotes the discretized time (t), j, the discretized size domain (μ), Δt and $\Delta \mu$ are the time step and section width, and $F_{j+1/2}^n$ and $F_{j-1/2}^n$ are the p_i fluxes through the right and left boundaries of section j. Numerical values of the fluxes $F_{j+1/2}^n$ and $F_{j-1/2}^n$ are obtained by integration of the mass over the swept area by advection due to particle growth or shrinkage. These fluxes are then normalized by the actual available mass so that the numerical scheme is positive-definite. After comparing with other numerical methods for solving the condensation/evaporation process, *Dhaniyala and Wexler* [1996] found that Bott's method is accurate and numerically very efficient.

Before (20) or (21) can be solved, one needs to evaluate the growth rate H_i according to (10), which requires estimation of surface vapor concentrations, $C_{S,i}$. For sulfuric acid, we assume, because of its extremely low vapor pressure, the surface vapor concentration to be zero for all particles. Vapor concentrations for the volatile inorganic compounds, namely NH_3, HNO_3, and HCl, are estimated by the thermodynamic model SCAPE2, as described earlier. At the beginning of the aerosol time step, SCAPE2 is "called" to calculate the growth rates for all the inorganic aerosol components except water and carbonates. Growth rates for aerosol water and carbonates are calculated as follows:

$$H_{wat} = H_{w,adj} + H_w, \quad H_{car} = H_{c,adj} + fH_w \quad (22)$$

where H_w is defined in (11), f is the mass ratio of carbonate to water, and the adjusted growth rates $H_{w,adj}$ and $H_{c,adj}$ are calculated by

$$H_{w,adj} = \frac{1}{m}\frac{\Delta m_w}{\Delta t}, \qquad H_{c,adj} = \frac{1}{m}\frac{\Delta m_c}{\Delta t} \tag{23}$$

where Δm_w and Δm_c are the differences between the equilibrium-update water content and carbonates calculated at the beginning of the current aerosol time step and those from the previous time step. The mass change of carbonates is adjusted based on the change of aerosol water content.

Both sequential and parallel versions of the model have been implemented on IBM RISC 6000 computers. About 72 CPU hours are required for a typical one-day simulation of the South Coast Air Basin of California on a single IBM 390 computer, while the parallelized version requires about 14 hours running on 5 IBM 390 nodes. More than 95% of the CPU time associated with the aerosol model is consumed in calculating aerosol thermodynamics.

5. Dynamic vs. Hybrid Approaches

This work uses a dynamic approach to calculate detailed mass transfer of volatile species between the gas phase and size-resolved particles. The "hybrid" method has been used in previous aerosol studies [*Pandis et al.*, 1993; *Lurmann et al.*, 1997]. The hybrid method first calculates at any instant of time the equilibrium for volatile compounds between the gas and bulk aerosol phases, then distributes the aerosol mass increment over the size spectrum based on a particle surface area weighting.

The dynamic approach can simulate mass transfer between the gas phase and individual aerosol particles whereas the hybrid approach compute only overall gas-aerosol equilibrium. For example, Figure 7.1 shows a comparison between predictions by the dynamic and hybrid methods for a hypothetical single cell. The initial gas-phase concentrations are: 10 ppb NH_3 (6.95 μg m^{-3}), 20 ppb HNO_3 (51.52 μg m^{-3}), and 2 ppb HCl (2.98 μg m^{-3}). The initial size- and chemically-resolved aerosol concentrations are taken to be those at $t = 0$ in Figure 7.1. Temperature is assumed to be 298 K and relative humidity is 80%. Only condensation/evaporation is considered in this example; all other physical and chemical aspects, such as deposition and emissions, are ignored. Initially, particles in the 3rd and 5th size sections are more acidic than those in other size sections, and particles in these two size sections experience some evaporation of NH_4NO_3 even as NH_4NO_3 is condensing on particles of other sizes. At 2 hours, the concentrations in the 4th section have decreased because the original particles in this section have grown to larger particle sizes while those in the 3rd section have not grown fast enough to reach the 4th section. The condensation/evaporation rate is controlled by the difference between the concentration in the bulk gas phase and that at the particle surface, the single particle surface area, and the total number of particles in the size section. Changes in the aerosol size distribution after about 6 hours are negligible. That distribution, however, is quite different from that predicted by the hybrid method based solely on equilibrium between bulk gas and aerosol phases and the initial size distribution. The reason for this difference is that the hybrid method does not account for the chemistry of individual particles. The predicted partition of total nitrate and ammonium between the gas and bulk aerosol

phases by the two approaches is shown in Figure 7.2. In this case, the hybrid method just gives the equilibrium partitioning. After 6 hours, even though the size distributions are different, the overall gas-aerosol partitioning predicted by the dynamic model is close to the equilibrium value. In 3-dimensional aerosol modeling, this may not be the case since total nitrate and ammonium concentrations in a grid cell at a particular time will vary depending on the approach used. For instance, as a result of mass-transport limitation, the dynamic model may predict higher gaseous HNO_3 concentrations at a particular location and time than equilibrium would indicate. Because HNO_3 has a considerably larger dry deposition velocity than aerosol nitrate, the total nitrate concentration could, as a result, be substantially reduced from that predicted based on instantaneous local equilibrium as a result of the larger loss of HNO_3.

6. Simulation of an Episode in the South Coast Air Basin of California

We present the simulation of a three-day episode in the South Coast Air Basin of California (SoCAB), from 27-29 August, during the summer 1987 Southern California Air Quality Study (SCAQS). High ozone (>240 ppb) and PM_{10} (> 100 $\mu g\ m^{-3}$) levels were measured during this episode. The highest measured ozone concentration for this period was observed at Glendora on 28 August, with a peak 1-h average mixing ratio of 290 ppb.

Wind flow during the three-day period was generally characterized by sea breeze during the day and a weak land-mountain breeze at night. Weak onshore pressure gradient and warming temperatures aloft increased potential for photochemical ozone

formation on 27 August. Low clouds penetrated into the coastal valleys on 28 August, with pressures gradients still remaining weak onshore. The weak upper trough along the coast on 29 August lifted the inversion base and created a slight reversal of the pressure gradient, resulting in farther inland penetration of the morning low clouds and fog to coastal valleys. Over the three-day period there existed well-defined inversion layers atop neutral and unstable layers near the surface. Nocturnal ground-based inversions for 27-29 August were observed only at further inland locations. The nocturnal boundary layer was generally slightly stable or near neutral.

6.1 Gas-Phase CIT Model

The "host" gas-phase chemical-transport model is the CIT model [*McRae et al.*, 1982; *McRae and Seinfeld*, 1983; *Harley et al.*, 1993]. The CIT model is a three-dimensional urban-scale gas-phase photochemical model. Three-dimensional meteorological data are constructed through data interpolation with a diagnostic wind model [*Goodin et al.*, 1979, 1980]. The horizontal grid domain is 80×30, with a resolution of 5 km. Five vertical layers extend to a height of 1100 m above ground level. Gas-phase chemistry is based on the condensed version of the LCC chemical mechanism [*Lurmann et al.*, 1987] with extensions by *Harley et al.* [1993]. The species in the chemical mechanism are listed in Table 7.5. The original mechanism includes 35 chemical species, of which eight are lumped species representing organic compounds of similar reactivity. Hydrochloric acid (HCl) has been added to the original gas-phase chemical mechanism. A constant CH_4 mixing ratio of 2.2 ppm is assumed. Isoprene is used as a surrogate for all biogenic

hydrocarbon emissions. Since isoprene does not yield secondary organic aerosol [*Pandis et al.*, 1992a], the current simulation includes SOA only from anthropogenic aromatic compounds.

6.2 Emissions

Emission data for gaseous compounds are described by *Harly et al.* [1993]. In brief, day-specific pollutant emission inventories for the August 1987 episode were received from California Air Resources Board (CARB) [*Wagner and Allen*, 1990]. The inventories were based on EMFAC 7E mobile source emissions estimates [*Yotter and Wade*, 1989], adjusted to account for daily temperature variations. On-road vehicle hot exhaust emissions of CO and hydrocarbons were increased to three times the EMFAC 7E values to reflect realistic on-road vehicle emission rates [*Harley et al.*, 1993]. Stationary source emissions, which include day-specific power plant, aircraft, and refinery sources, were prepared by the South Coast Air Quality Management District (SCAQMD). The NH_3 emissions inventory used was developed by *Cass and Gharib* [1984]. SO_2 emissions and chemically- and size-resolved primary particle emissions used are those presented by *Lurmann et al.* [1997]. Particle emissions account for six chemical species: sulfate, elemental carbon (EC), organic material (OM), sodium, chloride, and "other" species. Ammonium and nitrate from primary emissions are small and can be neglected. A value of 75 metric tons per day is assumed for NaCl emissions following *Lurmann et al.* [1997]. The total amount of NaCl emissions is uniformly distributed over the computational domain, and the daily emissions are divided by 24 hours to obtain the

hourly emissions within each grid cell. The original CARB PM profiles have been distributed over the eight size sections for the current model based on an estimated continuous size distribution.

6.3 Initial and Boundary Conditions

Boundary and initial conditions for the episode are specified using routine surface-level air quality measurements and aircraft-based measurements acquired during SCAQS [*Harley et al.*, 1993]. PM10 data are based on monthly average [*Lurmann et al.*, 1997]. The initial size- and composition-resolved aerosol concentrations are provided by *Lurmann et al.* [1997], which were estimated based on the annual averages in SoCAB [*Solomon et al.*, 1988] and were distributed to the eight size sections used in the simulations. Since their estimated initial concentrations are close to the actual $PM_{2.5}$ measurements at midnight on 27 August 1987, it was not necessary to develop initial conditions based on the measured $PM_{2.5}$ concentrations at midnight on 27 August 1987. Boundary concentrations and initial concentrations above the mixing height are given in Table 7.5.

6.4 Simulation Results

Predicted 24-hour average $PM_{2.5}$ mass concentrations on 28 August are shown in Figure 7.3. A band of high concentrations extending from northwest to southeast in the region is predicted, with a maximum reached near Riverside. Although not shown, the maximum predicted PM_{10} mass concentration is about 45% higher than the $PM_{2.5}$ mass. Predicted

24-hour average $PM_{2.5}$ nitrate and ammonium mass concentrations on the same day are shown in Figures 7.4 and 7.5. Both exhibit spatial patterns similar to those of total PM mass concentrations.

Predicted size distributions of aerosol nitrate and ammonium are compared with available measurements [*John et al.*, 1989] on 28 August between 6 a.m. and 9:30 a.m. at three locations in Figures 7.6 and 7.7, respectively. The model predicts well the submicron-mode of the size distribution but does not predict the presence of the observed supermicron nitrate mode. In examining the sodium and chloride size distributions for the same period (not shown), we found that an observed single coarse mode was considerably underestimated. An underestimate of NaCl in the coarse mode will lead to an underestimate of nitrate in two ways. First, less NaCl will be available for reaction with gaseous HNO_3 to produce coarse-mode aerosol nitrate; second, an underestimate of NaCl also implies that less coarse mode surface area is available for condensation of NH_4NO_3. A more accurate estimate of size-resolved NaCl emissions would likely improve predictions of the coarse-mode aerosol distribution.

Figure 7.8 shows predicted nitrate size distributions at Rubidoux, the location of the maximum in both nitrate and ammonium, for various sampling periods on 28 August. In the early morning, two modes were observed for both species, nitrate being more pronounced. The submicron mode is centered at about 0.5 μm and the coarse mode is at about 4.0 μm. Between late morning and early afternoon, the aerosol size distribution narrows as a result of condensation and the submicron-mode diameter shifts toward larger

sizes. The coarse mode remains little changed. During late afternoon, two submicron modes become evident, with the larger submicron mode growing to a diameter of about 0.7 μm. During the evening, (observations not available) the model predicts continuous growth of the aerosol particles to a mode-diameter around 2 μm. Throughout the aging of the aerosol size distribution, predicted and measured NH_4NO_3 size distributions are in good agreement. The model underestimated peak values of the sulfate size distributions. This is almost certainly a result of the neglect of fog processing, which occurred in the coastal regions in the late night and early morning of 28-29 August [*Pandis et al.*, 1992b].

Figure 7.9 shows predicted one-hour-average aerosol concentrations as a function of size at various times during 28 August for Riverside. Sulfate, nitrate, ammonium, and EC primarily reside in fine ($PM_{2.5}$) particles while crustal (other) species are in coarse (PM_{10}) particles. Organic matter that is dominated by primary emissions is present in all size sections. Sodium and chloride are predicted to be minor constituents of the aerosol phase. Inland locations, such as Claremont and Riverside, are predicted to have higher NH_4NO_3 concentrations than coastal and central basin locations. Long Beach exhibits higher sulfate concentrations in smaller particles than other locations. During daytime, condensation of NH_4NO_3 causes smaller particles to grow faster than larger particles. For instance, at Riverside, the peak of the accumulation mode grows from the 4th section (0.31-0.62 μm) at 6 a.m. to the 5th section (0.62-1.25 μm) at 12 p.m. However, dry deposition of particles competes with particle growth. This can be seen from the decrease

of the total mass concentrations from 6 a.m. to 12 p.m., particularly for the larger particles, although condensation of NH_4NO_3 shifts the peak to the larger particle size. Since evaporation of volatile compounds would shift the submicron-mode peak to a smaller particle size and would have no effect on the overall concentration of crustal species ("other") in the bulk aerosol phase, the decrease in aerosol concentrations at noontime is a direct result of dry deposition. Note that, as expected, dry deposition has a larger effect on smaller and larger particles than those of intermediate size (~1 μm). At 4 p.m., a bimodal size distribution is formed for the submicron particles. At 8 p.m., continued growth causes the NH_4NO_3 concentration to peak at a supermicron particle size. Note that a large fraction of the small particles is also removed by dry deposition. By midnight the aerosol size distribution attains a shape similar to that at the previous midnight.

7. Model Performance

Predicted gaseous and $PM_{2.5}$ and PM_{10} species concentrations have been compared against available measurements. Both $PM_{2.5}$ and PM_{10} samples were collected on Teflon or prefired quartz fiber filters that were then analyzed to determine aerosol mass, trace element, ionic species, and organic and elemental carbon [*Countess*, 1989]. $PM_{2.5}$ NO_3^- samples were collected by both Teflon filter and denuder difference method. $PM_{2.5}$ NH_4^+ concentrations were measured by both Teflon filter and backup quartz filter impregnated with oxalic acid after NH_3 removal by denuder. However, some of the $PM_{2.5}$ ammonium

samples by the denuder method at Riverside were contaminated due to the high ammonia concentrations having overloaded the NH_3 denuder [*Hering et al.*, 1997]. Five samples were taken each day with sampling periods of 4 h during the daytime and 5-7 h during the nighttime.

Predicted $PM_{2.5}$ nitrate and ammonium concentrations are compared with measurements in Figures 7.10 and 7.11, respectively. Note that model predictions are 1-h averages while measurements are averages over 4-7 hours. Statistical analysis of performance by the model based on 24-h means is presented in Tables 7.6 and 7.7. Error analysis is carried out only for species with observed concentrations exceeding 1 $\mu g\ m^{-3}$.

7.1 Nitrate

The predicted time-series $PM_{2.5}$ nitrate is shown in Figure 7.10 and agrees well with observations. Overpredictions occur more frequently than underpredictions. Predicted 24-h means of $PM_{2.5}$ nitrate averaged over the eight SCAQS observation stations are 18.3, 23.9, and 22.9 $\mu g\ m^{-3}$, which were higher than the 14.6, 17.2, and 16.4 $\mu g\ m^{-3}$ measured on 27, 28, and 29 August, respectively. Predicted 24-h means averaged over the eight SCAQS observation stations of PM_{10} nitrate are 20.7, 26.5, and 25.4 $\mu g\ m^{-3}$ which were considerably higher than the 12.7, 13.4, and 14.8 $\mu g\ m^{-3}$ measured on the three days. Note that the Teflon-filter-sampled PM_{10} nitrate concentrations were even lower than the $PM_{2.5}$ nitrate from the denuder difference method, suggesting that losses occurred during PM_{10} nitrate sampling by Teflon filters.

The maximum 24-h means of nitrate occurred at Riverside for all three days. The predicted 48.0, 60.5, and 65.2 μg m^{-3} of $PM_{2.5}$ nitrate at Riverside were higher than the 39.1, 41.3, and 42.5 μg m^{-3} measured on 27, 28, and 29 August, respectively. The predicted maximum 24-h mean PM_{10} nitrate, at Riverside, 53.5, 68.5, and 71.2 μg m^{-3}, are to be compared with the measured 36.8, 40.1, and 42.9 μg m^{-3} by Teflon filters.

Overprediction of PM nitrate is a result of overprediction of total nitrate. Total nitrate predicted by the current model is very close to that given by *Harley et al.* [1993]. This behavior indicates that the gas-phase photochemistry may be producing too much HNO_3. There are two pathways for production of HNO_3: 1) NO_2 + OH; 2) N_2O_5 + H_2O. The second pathway contributes about a quarter of the total nitrate production.

7.2 Ammonium

Figure 7.11 shows patterns of predicted and observed $PM_{2.5}$ ammonium at 8 locations. Observations are based on Teflon-filter samples, plus the estimated volatilized ammonium. The volatilized ammonium is assumed to be in combination with nitrate and is determined by the difference between $PM_{2.5}$ nitrate sampled by the denuder difference method and Teflon-filter method. Although the $PM_{2.5}$ ammonium was also measured on an oxalic acid filter downstream of an oxalic acid coated glass tube denuder, the samples were contaminated when the denuder became overloaded at Riverside due to the high ammonia concentrations [*Hering et al.*, 1997]. At other locations, the ammonium ion concentrations inferred by this method agreed with those measured by the denuder difference method.

Predicted 24-h means of $PM_{2.5}$ ammonium averaged over the eight SCAQS observation stations are 6.4, 8.3, and 8.3 μg m^{-3} which agree well with the 6.5, 8.4, and 9.6 μg m^{-3} measured on 27, 28, and 29 August, respectively. The predicted 24-h means of PM_{10} ammonium averaged over the eight SCAQS observation stations are 7.3, 8.9, and 8.9 μg m^{-3} which were higher than the 4.3, 5.7, and 8.1 μg m^{-3} measured on the three days. Note that, similar to nitrate, the Teflon-filter-sampled PM_{10} ammonium concentrations were also lower than the $PM_{2.5}$ ammonium from the denuder method. Maximum 24-h means of ammonium occurred at Riverside for all three days. Predicted maximum $PM_{2.5}$ ammonium concentrations also agree very well with observations.

7.3 Nitric Acid

Predicted and observed time-series HNO_3 are shown in Figure 7.12. Predicted 24-h HNO_3 means averaged over the eight SCAQS observation stations are 6.3, 7.1, and 6.6 ppb, which exceeded the 3.2, 5.0, and 5.9 ppb measured on 27, 28, and 29 August, respectively. Overpredictions occurred at Azusa due to timing differences of the peak values. Maximum 24-h means of HNO_3 occurred at Claremont and Burbank. The predicted 9.4, 7.9, and 9.6 ppb of HNO_3 were comparable with the 7.4, 9.2, and 8.8 ppb measured on 27, 28, and 29 August, respectively.

7.4 Sulfate

Predicted 24-h means of $PM_{2.5}$ sulfate averaged over the 8 stations are 5.3, 6.4, and 6.3 μg m^{-3} which are much lower than the 6.5, 9.1, and 13.7 μg m^{-3} measured on 27, 28, and 29

August, respectively. Predicted 24-h means of PM_{10} sulfate are 6.6, 7.8, and 7.8 μg m^{-3}, which were also lower than the 7.9, 11.0, and 16.4 μg m^{-3} measured on the three days. Underprediction was most severe on the third day, when morning fogs and low clouds penetrated further into the coastal valleys, suggesting that most of the sulfate underprediction can be attributed to sulfate formed in the aqueous phase, a process that is not currently treated in the model.

7.5 PM Mass

The 24-h means of PM mass at the station where the maximum occurred are shown in Figure 7.13. PM mass is overpredicted when PM NH_4NO_3 is overpredicted. Maximum 24-h means of PM mass all occurred at Riverside. The predicted 92.9, 107, and 113 μg m^{-3} of $PM_{2.5}$ mass at Riverside agreed well with the 83.5, 96.8, and 90.6 μg m^{-3} measured on the three days. Predicted maximum PM_{10} mass is 140, 164, and 167 μg m^{-3}, in proximity to the measured 152, 167, and 147 μg m^{-3}.

8. Conclusions

We have developed a three-dimensional size- and chemically-resolved aerosol model that includes advection, turbulent diffusion, condensation/evaporation, nucleation, emissions, and dry deposition. For condensation/evaporation of volatile inorganic species, a new thermodynamic model, SCAPE2, which has a comprehensive treatment of gas/aerosol equilibrium is included. The aerosol model has been coupled with the three-dimensional

gas-phase photochemical CIT model, and has been applied to the 27-29 August 1987 episode in the South Coast Air Basin of California. Simulations have been compared systematically against available observations. Generally good agreement between predictions and measurements is observed. There is evidence that gas/aerosol mass transfer limits overall gas/particle conversion for volatile inorganic species.

Acknowledgment

This work was supported by the Electric Power Research Institute (EPRI) and the IBM Environmental Research Program. Any opioions, findings and conclusions or recommendations expressed in this material are those of the authors and do not necessarily reflect the views of EPRI and/or the IBM Corporation.

REFERENCES

Anthes, R. A., E. Y. Hsie, and Y. H. Kuo, *Description of the Penn State/NCAR Mesoscale Model Version 4 (MM4), NCAR Technical Note*, NCAR/TN-282+STR, National Center for Atmospheric Research, Boulder, CO., 1987.

Binkowski, F. S., and U. Shankar, The regional particulate matter model .1. Model description and preliminary-results, *J. Geophys. Res.*, *100*, 26191-26209, 1995.

Carter, W. P. L., A detailed mechanism for the gas-phase atmospheric reactions of organic compounds, *Atmos. Environ.*, *24A*, 481-518, 1990.

Cass, G. R., and S. Gharib, *Ammonia Emissions In The South Coast Air Basin 1982*, open file report 84-2, Environmental Quality Laboratory, California Institute of Technology, Pasadena, California, 1984.

Chang, J. S., P. B. Middleton, W. R. Stockwell, C. J. Walcek, J. E. Pleim, H. H. Lansford, S. Madronich, F. S. Binkowski., N. L. Seaman, D. R. Stauffer, D. Byun, J. N. McHenry, H. Hass, and P. J. Samson, *The Regional Acid Deposition Model and Engineering Model*, NAPAP Report 4, National Acid Precipitation Assessment Program, Washington, D.C., 1991.

Countess, R. J., *Southern California Air Quality Study sampler chemistry*, Final report under contract A5-186-32 to California Air Resources Board, Sacramento, California, 1989.

Dhaniyala, S., and A. S. Wexler, Numerical schemes to model condensation and evaporation of aerosols, *Atmos. Environ.*, *30*, 919-928, 1996.

Gelbard, F., and J. H. Seinfeld, Simulation of multicomponent aerosol dynamics, *J. Colloid Interface Sci.*, *78*, 541-556, 1980.

Gelbard, F., Y. Tambour, and J. H. Seinfeld, Sectional representation for simulating aerosol dynamics, *J. Colloid Interface Sci.*, *76*, 485-501, 1980.

Goodin, W. R., G. J. McRae, and J. H. Seinfeld, A comparison of interpolation methods for sparse data: application to wind and concentration fields, *J. appl. Met.*, *18*, 761-771, 1979.

Goodin, W. R., G. J. McRae, and J. H. Seinfeld, An objective analysis technique for constructing three-dimensional, urban-scale wind fields, *J. appl. Met.*, *19*, 98-108, 1980.

Harley, R. A., A. F. Russell, G. J. McRae, G. R. Cass, and J. H. Seinfeld, Photochemical modeling of the Southern California Air Quality Study, *Environ. Sci. Technol.*, *27*, 378-388, 1993.

Hering, S., A. Eldering, and J. H. Seinfeld, Bimodal character of accumulation mode aerosol mass distributions in southern California, *Atmos. Environ.*, *31*, 1-11, 1997.

John, W., S. M. Wall, J. L. Ondo, and W. Winklmayr, *Acidic aerosol size distributions during SCAQS, Compilation of data tables and graphs*, Prepared for California Air Resources Board, Sacramento, California, 1989.

Kim, Y. P., and J. H. Seinfeld, Atmospheric gas-aerosol equilibrium III. Thermodynamics of crustal elements Ca^{2+}, K^{+}, and Mg^{2+}, *Aerosol Sci. Technol.*, *22*, 93-110, 1995.

Kim, Y. P., J. H. Seinfeld, and P. Saxena, Atmospheric gas-aerosol equilibrium I. Thermodynamic model, *Aerosol Sci. Technol.*, *19*, 157-181, 1993a.

Kim, Y. P., J. H. Seinfeld, and P. Saxena, Atmospheric gas-aerosol equilibrium II. Analysis of common approximations and activity coefficient calculation methods, *Aerosol Sci. Technol.*, *19*, 182-198, 1993b.

Lurmann, F. W., W. P. L. Carter, and L. A. Coyner, *A surrogate species chemical reaction mechanism for urban-scale air quality simulation models, Vol. I and II.*, ERT Inc., Newbury Park, California, and Statewide Air Pollution Research Center,

University of California, Riverside, California., Report to the U.S. Environmental Protection Agency under contract 68-02-4104, 1987.

Lurmann, F. W., A. S. Wexler, S. N. Pandis, S. Musarra, N. Kumar, and J. H. Seinfeld, Modelling urban and regional aerosols: II. Application, Submitted to *Atmos. Environ.*, 1997.

McRae, G. J., W. R. Goodin, and J. H. Seinfeld, Development of a second-generation mathematical model for urban air pollution .1. Model formulation, *Atmos. Environ.*, *16*, 679-696, 1982.

McRae, G. J., and J. H. Seinfeld, Development of a second-generation mathematical model for urban air pollution .2. Evaluation of model performance, *Atmos. Environ.*, *17*, 501-522, 1983.

Meng, Z., and J. H. Seinfeld, Time scales to achieve atmospheric gas-aerosol equilibrium for volatile species, *Atmos. Environ.*, *30*, 2889-2900, 1996.

Meng, Z., J. H. Seinfeld, P. Saxena, and Y. P. Kim, Atmospheric gas-aerosol equilibrium IV. Thermodynamics of carbonates, *Aerosol Sci. Technol.*, *23*, 131-154, 1995a.

Meng, Z., J. H. Seinfeld, and P. Saxena, Gas/aerosol distribution of formic and acetic acids, *Aerosol Sci. Technol.*, *23*, 561-578, 1995b.

Odum, J. R., T. Hoffmann, F. Bowman, D. Collins, R. C. Flagan, and J. H. Seinfeld, Gas/particle partitioning and secondary organic aerosol yields, *Environ. Sci. Technol.*, *30*, 2580-2585, 1996.

Pandis, S. N., R. A. Harley, G. R. Cass, and J. H. Seinfeld, Secondary organic aerosol formation and transport, *Atmos. Environ.*, *26*, 2269-2282, 1992a.

Pandis, S. N., J. H. Seinfeld, and C. Pilinis, Heterogeneous sulfate production in an urban fog, *Atmos. Environ.*, *26A*, 2509-2522, 1992b.

Pandis, S. N., A. S. Wexler, and J. H. Seinfeld, Secondary organic aerosol formation and transport .2. Predicting the ambient secondary organic aerosol-size distribution, *Atmos. Environ.*, *27*, 2403-2416, 1993.

Pilinis, C., Derivation and numerical solution of the species mass distribution equations for multicomponent particulate systems, *Atmos. Environ.*, *24A*, 1923-1928, 1990.

Pilinis, C., and J. H. Seinfeld, Continued development of a general equilibrium model for inorganic multicomponent atmospheric aerosols, *Atmos. Environ.*, *21*, 2453-2466, 1987.

Pilinis, C., and J. H. Seinfeld, Development and evaluation of an Eulerian photochemical gas-aerosol model, *Atmos. Environ.*, *22*, 1985-2001, 1988.

Pleim, J., A. Venkatram, and R. J. Yamartino, *The dry deposition model. Vol. 4. ADOM/TADAP model development program*, Ontario Min. of the Environ., Rexdale, Ontario, Canada, 1984.

Robinson, R. A., and R. J. Stokes, *Electrolyte Solutions,* 2nd ed., Butterworth, London, 1965.

Russell, A. G., K. F. McCue, and G. R. Cass, Mathematical-modeling of the formation of nitrogen-containing air pollutants .1. Evaluation of an Eulerian photochemical model, *Environ. Sci. Technol.*, *22*, 263-270, 1988.

Russell, A. G., D. A. Winner, R. A. Harley, K. F. McCue, and G. R. Cass, Mathematical modeling and control of the dry deposition flux of nitrogen-containing air pollutants, *Environ. Sci. Technol.*, *27*, 2772-2782, 1993.

SAI, *User's guide for the urban airshed model, Vol. I*, Prepared by Systems Applications International, San Rafael, California, Report No. SYSAPP-90/018a, 1990a.

SAI, *User's guide for the urban airshed model, Vol. II: preprocessors and postprocessors for the UAM modeling system*, Prepared by Systems Applications International, San Rafael, California, Report No. SYSAPP-90/018b, 1990b.

SAI, *User's guide for the urban airshed model, Vol. III: the diagnostic wind model*, Prepared by Systems Applications International, San Rafael, California, Report No. SYSAPP-90/018c, 1990c.

SAI, *User's guide for the urban airshed model, Vol. IV: the emissions preprocessor system*, Prepared by Systems Applications International, San Rafael, California, Report No. SYSAPP-90/018d, 1990d.

SAI, *User's guide for the urban airshed model, Vol. V: description and operation of the ROM-UAM interface program system*, Prepared by Systems Applications International, San Rafael, California, Report No. SYSAPP-90/018e, 1990e.

Saxena, P., A. B. Hudischewskyj, C. Seigneur, and J. H. Seinfeld, A comparative study of equilibrium approaches to the chemical characterization of secondary aerosols, *Atmos. Environ.*, *20*, 1471-1483, 1986.

Solomon, P. A., T. Fall, S. M. Larson, P. Lin, F. Vasquez, and G. R. Cass, *Acquisition of acid and aerosol concentration data for use in dry deposition studies in the South*

Coast Air Basin, Vol. I, Report prepared under contract No. A4-144-32 for the California Air Resources Board, Sacramento, California, by Environmental Quality Lab, California Institute of Technology, California, Report No. 25, 1988.

Stockwell, W. R., D. Middleton, J. S. Chang, and X. Tang, The second-generation Regional Acid Deposition Model chemical mechanism for regional air quality modeling, *J. Geophys. Res.*, *95D*, 16343-16367, 1990.

Wagner, K. K., and P. D. Allen, *SCAQS emissions inventory for August 27-29, 1987 (Tape ARA714)*, Technical Support Division, California Air Resources Board, Sacramento, California, 1990.

Wexler, A. S., F. W. Lurmann, and J. H. Seinfeld, Modeling urban and regional aerosols .1. Model development, *Atmos. Environ.*, *28*, 531-546, 1994.

Wexler, A. S., and J. H. Seinfeld, The distribution of ammonium salts among a size and composition dispersed aerosol, *Atmos. Environ.*, *24A*, 1231-1246, 1990.

Wexler, A. S., and J. H. Seinfeld, Second-generation inorganic aerosol model, *Atmos. Environ.*, *25A*, 579-591, 1991.

Yotter, E. E., and D. L. Wade, Development of a gridded motor vehicle emission inventory for the Southern California Air Quality Study, Paper 89-137.2 presented at the 82nd annual meeting of the Air & Waste Management Association, Anaheim, California, 1989.

Table 7.1. Three-dimensional, size- and chemically-resolved aerosol models

	P&S (1988)	Lurmann et al. (1997)	RPM	This work
Overall Goal	Urban oxidant and aerosol model	Urban oxidant and aerosol model	Regional particulate model	Urban oxidant and aerosol dynamic model
Major Applications	Los Angeles Basin	Los Angeles Basin	Eastern U.S.	Los Angeles Basin
Host Air Quality Model	CIT [*McRae et al.*, 1982; *McRae and Seinfeld*, 1983]	UAM [*SAI*, 1990a,b,c,d,e]	RADM II [*Chang et al.*, 1991]	CIT [*Harley et al.*, 1993]
Meteorological Model	Constructed through data interpolation with diagnostic wind model	Constructed through data interpolation, or calculated with land-sea breeze or complex-terrain wind model	PSU/NCAR mesoscale model MM4 [*Anthes et al.*, 1987]	Constructed through data interpolation with diagnostic wind model
Gas-Phase Chemistry	*Russell et al.* [1988]	SAPRC90 [*Carter*, 1990]	*Stockwell et al.* [1990]	Extended LCC [*Harley et al.*, 1993]
Horizontal Resolution (km)	5	4-10	80	5
Vertical Resolution	Typically 5 layers to about 1.1 km	Typically 4 layers to about 1.5 km	15 layers to ~100 mb (~15 km)	Typically 5 layers to about 1.1 km
Major References	*Pilinis and Seinfeld* [1988]	*Wexler et al.* [1994], *Lurmann et al.* [1997]	*Binkowski and Shankar* [1995]	This paper

Table 7.2. Three-dimensional, size- and chemically-resolved aerosol models: aerosol characterization

	P&S (1988)	Lurmann et al. (1997)	RPM	This work
Number or Mass Concentration	Mass	Mass	3 moments	Mass
Size Resolution[a] (D_p in μm)	0.05-10 (3)	0.04-10 (8)	2 modes nuclei: 0.01 μm; accumulation: 0.07 μm	0.04-10 (8)
Multicomponent	Yes	Yes	Yes	Yes
Elemental Carbon	No	Yes	No	Yes
Organics	Yes	Yes	No	Yes
Inorganics	NH_3-H_2SO_4-HNO_3-HCl-Na-H_2O	NH_3-H_2SO_4-HNO_3-HCl-Na-H_2O	NH_3-H_2SO_4-HNO_3-H_2O	NH_3-H_2SO_4-HNO_3-HCl-Na-K-Ca-Mg-H_2O-CO_2

[a]The number in parentheses is the typical number of size sections used.

Table 7.3. Three-dimensional, size- and chemically-resolved aerosol models: aerosol processes

	P&S (1988)	Lurmann et al. (1997)	RPM	This work
Nucleation	H_2SO_4/H_2O	H_2SO_4/H_2O	H_2SO_4/H_2O	H_2SO_4/H_2O
Condensation/ Evaporation	Volatile Inorganics: Gas/particle equilib.; Sulfate+organics: transport	Volatile Inorganics: Gas/particle equilib.; Sulfate+organics: transport	Volatile Inorganics: Gas/particle equilib.; Sulfate: transport	H_2O and CO_2: equilib.; Other compounds: transport
Coagulation	Yes	No	Yes	No
Dry Deposition	Size independent resistance-transfer approach	Size dependent resistance-transfer approach + settling	Mode dependent resistance-transfer approach + settling	Size dependent resistance-transfer approach + settling
Wet Deposition	No	No	No	No
Chemical Reactions	No	No	No	No
Activation/ Interaction with Fog/Cloud	No	Yes	No	No

Table 7.4. Three-dimensional, size- and chemically-resolved aerosol models: treatment of aerosol thermodynamics[a]

	P&S (1988)	Lurmann et al. (1997)	RPM	This work
Thermodynamic Model	SEQUILIB [*Pilinis and Seinfeld*, 1987]	SEQUILIB [*Pilinis and Seinfeld*, 1987]	MARS [*Saxena et al.*, 1986]	SCAPE2 [*Kim et al.*, 1993a, b; *Kim and Seinfeld*, 1995; *Meng et al.*, 1995a, b]
Temperature Dependence[b]	*K*	*K*	*K*	*K*, RHD
Binary Activity Coefficient Estimation Method[c]	Pitzer	Pitzer	Pitzer	Kusik-Meissner
Multicomponent Activity Coefficient Estimation Method	Bromley	Bromley	Bromley	Option of Bromley, Kusik-Meissner, and Pitzer
Water Activity	ZSR	ZSR	ZSR	ZSR
Organics	No	No	No	Formate and acetate

[a]All the models assume chemical equilibrium within the aerosol phase.
[b]*K* and RHD are the equilibrium constant and relative humidity at deliquescence.
[c]Binary activity coefficients are not needed for the multicomponent Pitzer method.

Table 7.5 Boundary conditions for chemical species considered in the model

Species Name	Mixing Ratio (ppb)	Species Name	Concentration ($\mu g\ m^{-3}$)
NO	1	$PM_{2.5}\ NO_3^-$	1.7
NO2	1	$PM_{2.5\text{-}10}\ NO_3^-$	0.56
O3	60	$PM_{2.5}\ NH_4^+$	0.90
HONO	0	$PM_{2.5\text{-}10}\ NH_4^+$	0.27
HNO3	0.01	$PM_{2.5}\ SO_4^{2-}$	1.2
HNO4	0	$PM_{2.5\text{-}10}\ SO_4^{2-}$	0.30
N2O5	0	$PM_{2.5}\ Cl^-$	0.26
NO3	0	$PM_{2.5\text{-}10}\ Cl^-$	0.26
HO2	0	$PM_{2.5}\ Na^+$	0.22
CO	200	$PM_{2.5\text{-}10}\ Na^+$	0.18
HCHO	3	$PM_{10}\ K^+$	0
Acetaldehyde	5	$PM_{10}\ Ca^{2+}$	0
Methyl ethyl ketone	4	$PM_{10}\ Mg^{2+}$	0
Methyl glyoxal	0	$PM_{10}\ CO_3^{2-}$	0
PAN	0	$PM_{2.5}\ H_2O$	0.12
Total RO_2 radicals	0	$PM_{2.5\text{-}10}\ H_2O$	0.03
CH_3CO_3 radical	0	$PM_{2.5}$ EC	0.14
Alkyl nitrate	0	$PM_{2.5\text{-}10}$ EC	0.02
C_4^+ alkanes	9.5	$PM_{2.5}$ Primary OM	3.04
Ethene	1.7	$PM_{2.5\text{-}10}$ Primary OM	1.01
C_3^+ alkenes	1.8	PM_{10} SOA	0
Toluene	1.5	$PM_{2.5}$ Other	3.67
Higher aromatics	1.6	$PM_{2.5\text{-}10}$ Other	1.12
Unknown dicarbonyls	0		
Cresol	0		
Nitrophenols	0		
Hydrogen peroxide	0		
Methanol	0		
Ethanol	0		
Methyl tert-butyl ether	0		
Isoprene	0		
NH3	0.1		
SO2	1		
SO3	0		
CH4	2200		
HCl	0.01		
Vapors from toluene	0		
Vapors from higher aromatics	0		

Table 7.6 Model performance on 24-h mean concentrations averaged over the eight SCAQS observation stations on 28 August 1987 (units in $\mu g\ m^{-3}$) †

Species	Mean Observed	Mean Predicted	Mean Bias	Mean Normalized Bias (%)	Mean Error	Mean Normalized Error (%)
HNO_3	12.7	18.0	5.3	56	7.1	67
NH_3	3.3	1.5	-1.8	-33	2.3	79
$PM_{2.5}\ SO_4$	9.1	6.4	-2.7	-30	3.0	34
$PM_{2.5}\ NH_4$	8.4	8.3	-0.2	-1.0	2.3	29
$PM_{2.5}\ NO_3$	17.2	23.9	6.7	47	9.0	61
$PM_{2.5}$ EC	3.0	3.8	0.8	35	1.3	50
$PM_{2.5}$ OM	12.0	12.8	0.8	14	4.5	40
$PM_{2.5}$ Mass	49.6	70.4	20.7	46	20.7	46

†The 24-h mean of the measured concentrations is based on the five samples within each day. If some samples are missing, averages are performed only on the available samples, and the predicted concentrations are averaged for the same periods accordingly. Measured $PM_{2.5}$ NO_3^- and NH_4^+ concentrations used are from the denuder samples that recover evaporated NO_3^- and NH_4^+ during sampling while Teflon-filter measurements were only available for the PM_{10} samples. Thus, the reported measured $PM_{2.5}$ concentrations can be occasionally larger than the corresponding PM_{10} concentrations.

Table 7.7 Model performance at the monitoring station at which the maximum 24-h mean concentration was observed on 28 August 1987 (units in $\mu g\ m^{-3}$) †

Species	Location	Maximum Observed	Maximum Predicted	Maximum In Domain‡
HNO_3	Burbank	23.3	20.0	40.3
NH_3	Riverside	11.7	5.9	88.8
$PM_{2.5}\ SO_4$	Long Beach	11.4	12.9	19.1
$PM_{2.5}\ NH_4$	Riverside	15.5	17.5	21.0
$PM_{2.5}\ NO_3$	Riverside	41.3	60.5	72.9
$PM_{2.5}$ EC	Azusa	5.6	5.4	7.2
$PM_{2.5}$ OM	Azusa	17.9	16.3	24.5
$PM_{2.5}$ Mass	Riverside	96.8	106.5	126

†The 24-h mean of the measured concentrations is based on the five samples within each day. If some samples are missing, averages are performed only on the available samples, and the predicted concentrations are averaged for the same periods accordingly. Measured $PM_{2.5}$ NO_3^- and NH_4^+ concentrations used are from the denuder samples that recover evaporated NO_3^- and NH_4^+ during sampling while Teflon-filter measurements were only available for the PM_{10} samples. Thus, the reported measured $PM_{2.5}$ concentrations can be occasionally larger than the corresponding PM_{10} concentrations.

‡Maximum 24-h mean concentration predicted anywhere in entire domain.

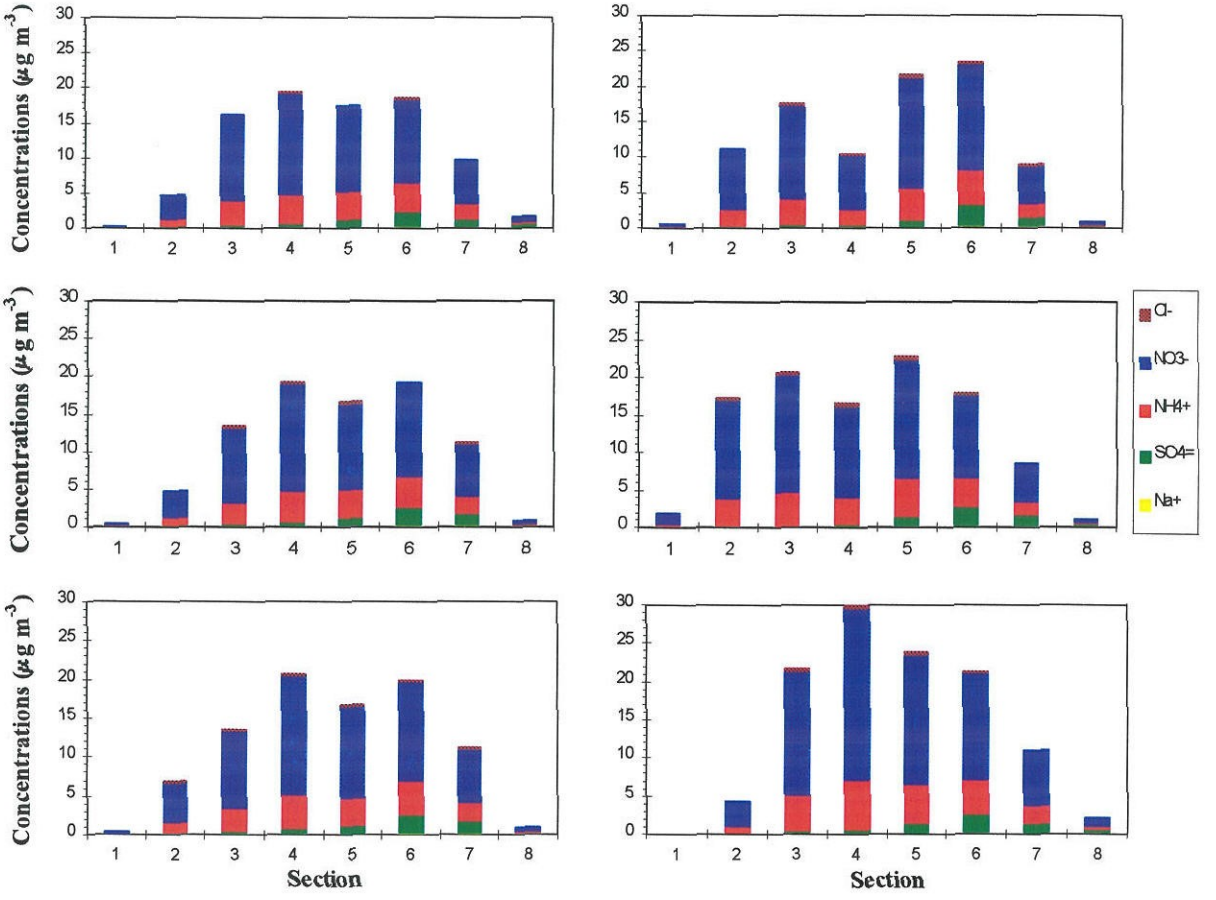

Fig. 7.1 Size- and composition-resolved aerosol distributions predicted by the dynamic model at various times and that predicted by the "hybrid" method for condensation/evaporation only in a single cell.

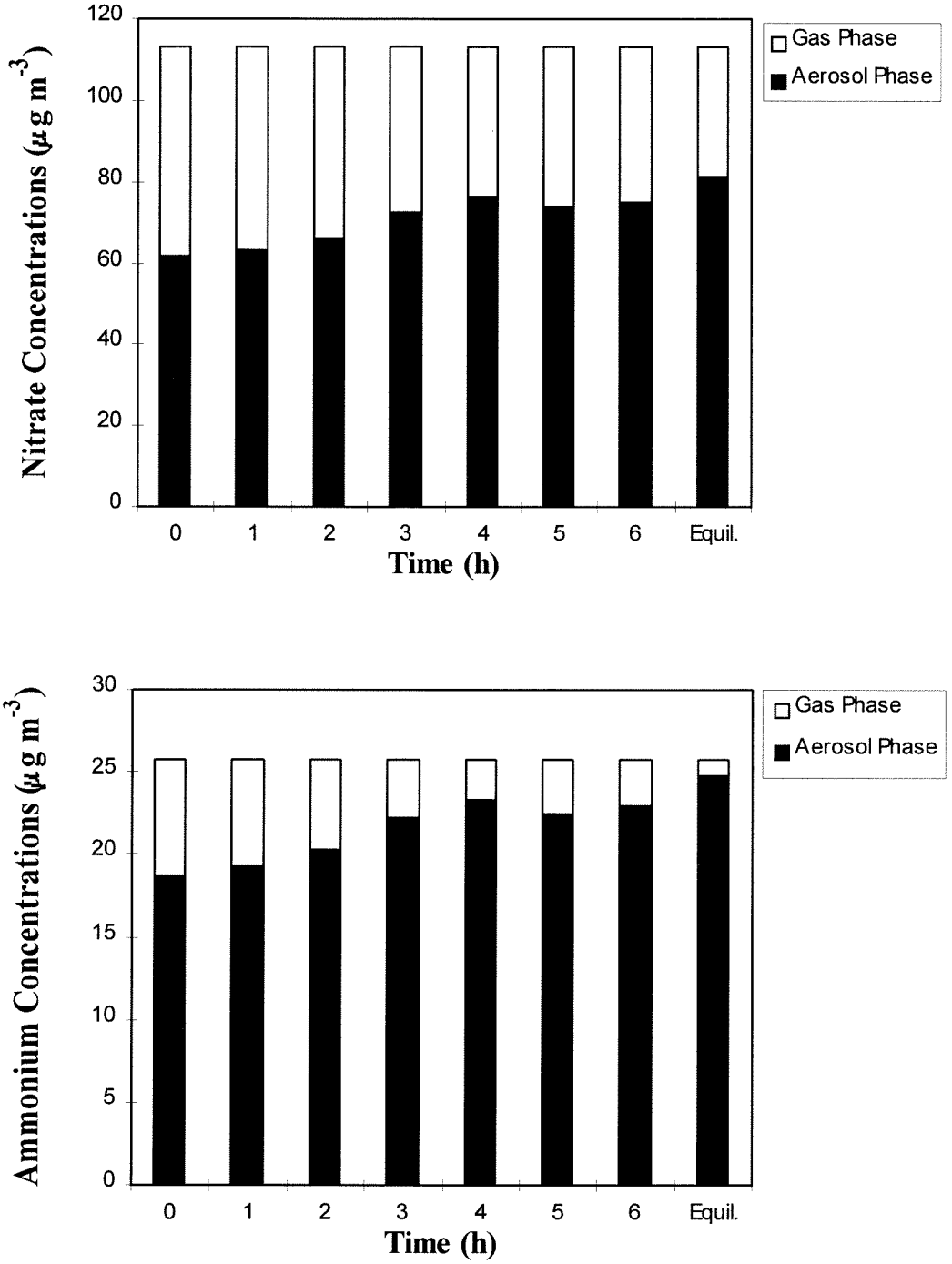

Fig. 7.2 Comparison between partitions of the total nitrate and ammonium predicted by the dynamic model at various times and those by the "hybrid" method for condensation/evaporation only in a single cell.

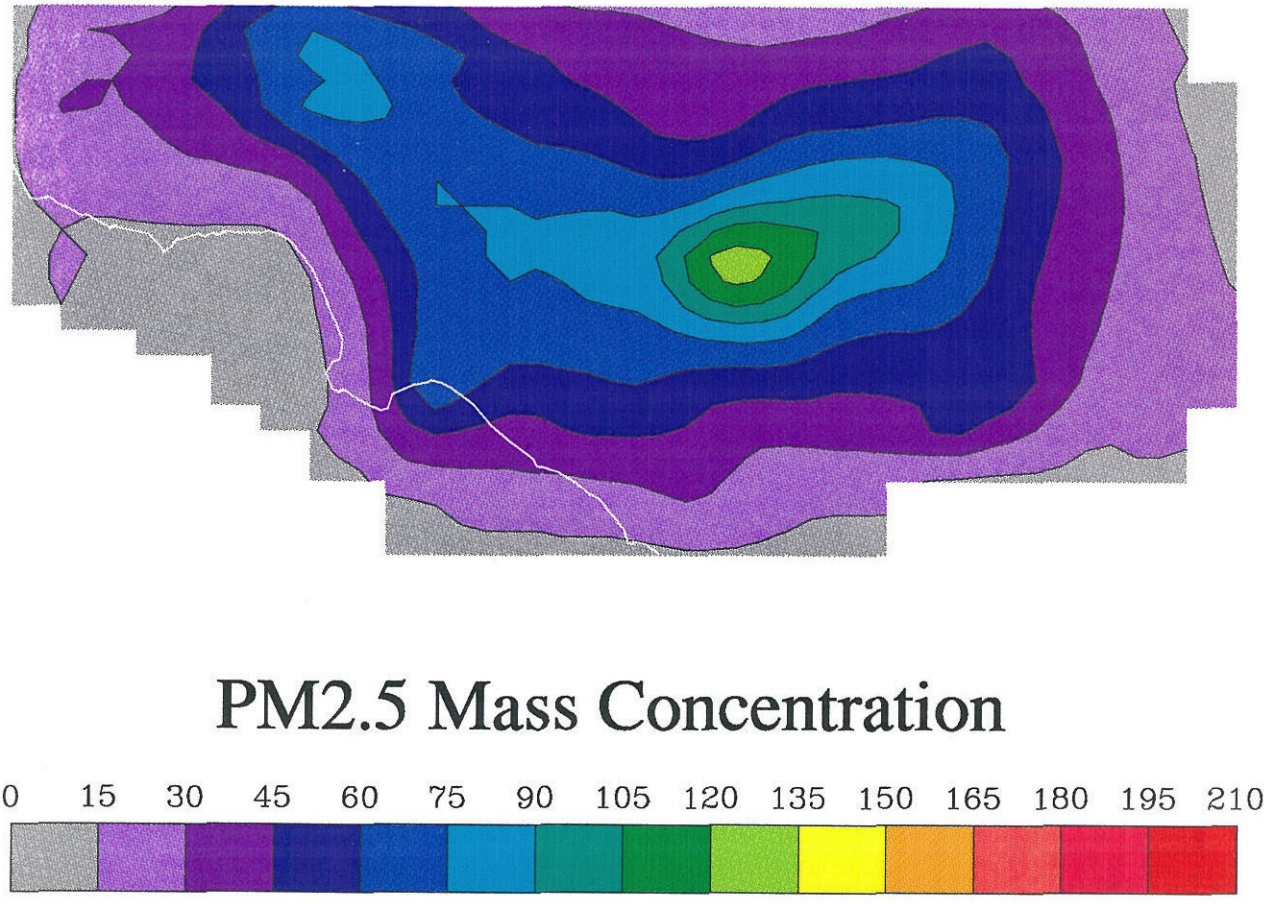

Fig. 7.3 Predicted 24-h average $PM_{2.5}$ mass concentrations on 28 August 1987 in South Coast Air Basin.

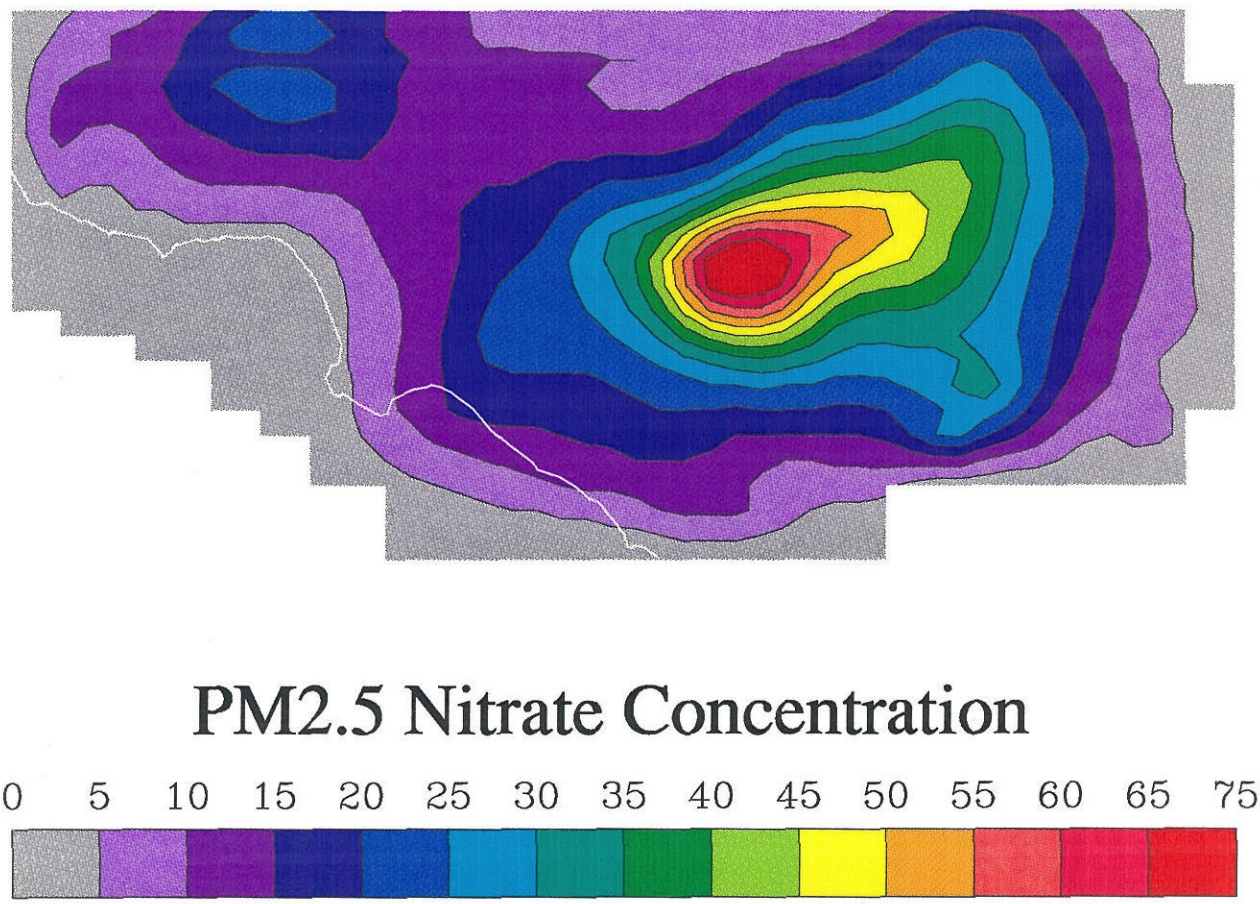

Fig. 7.4 Predicted 24-h average $PM_{2.5}$ nitrate concentrations on 28 August 1987 in South Coast Air Basin.

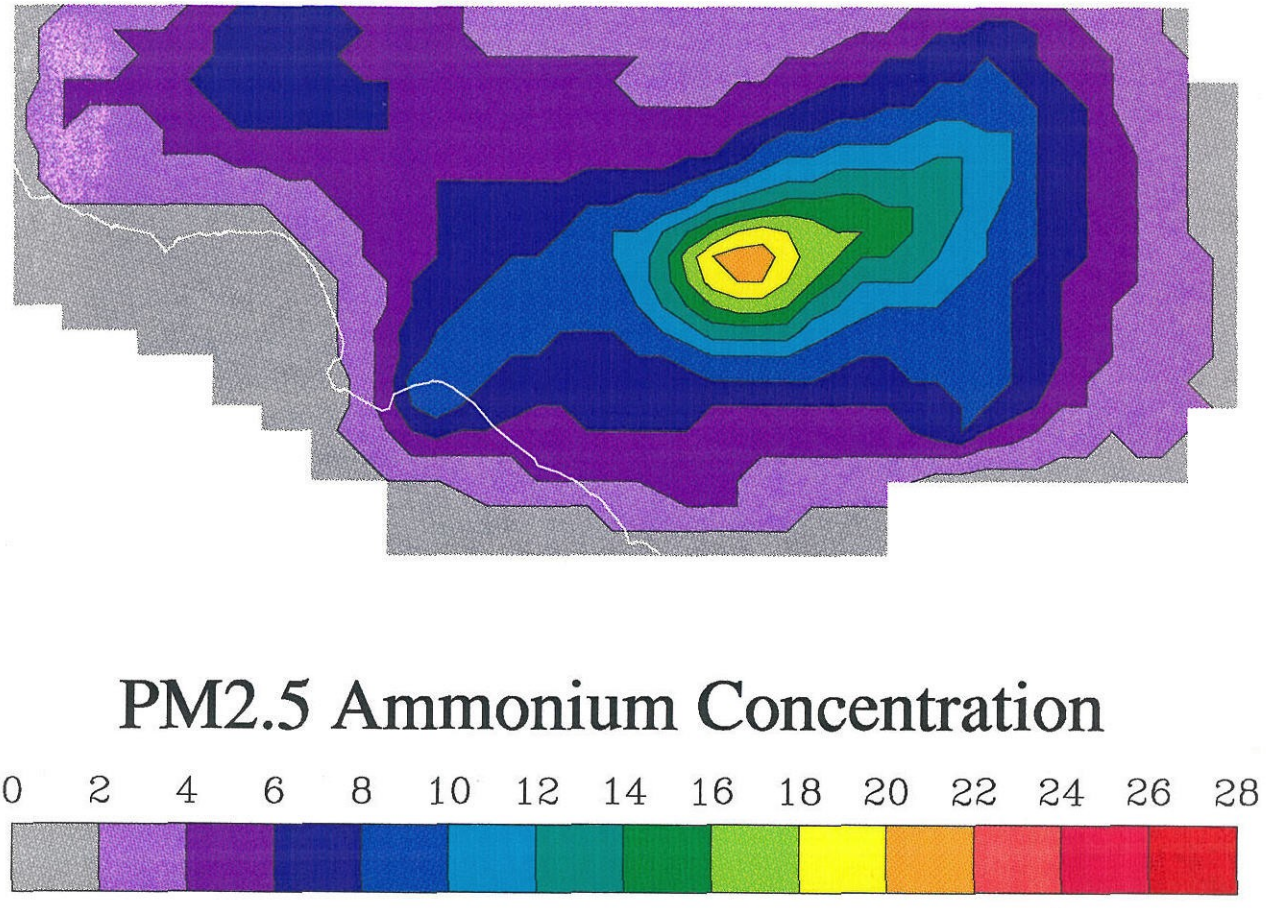

Fig. 7.5 Predicted 24-h average $PM_{2.5}$ ammonium concentrations on 28 August 1987 in South Coast Air Basin.

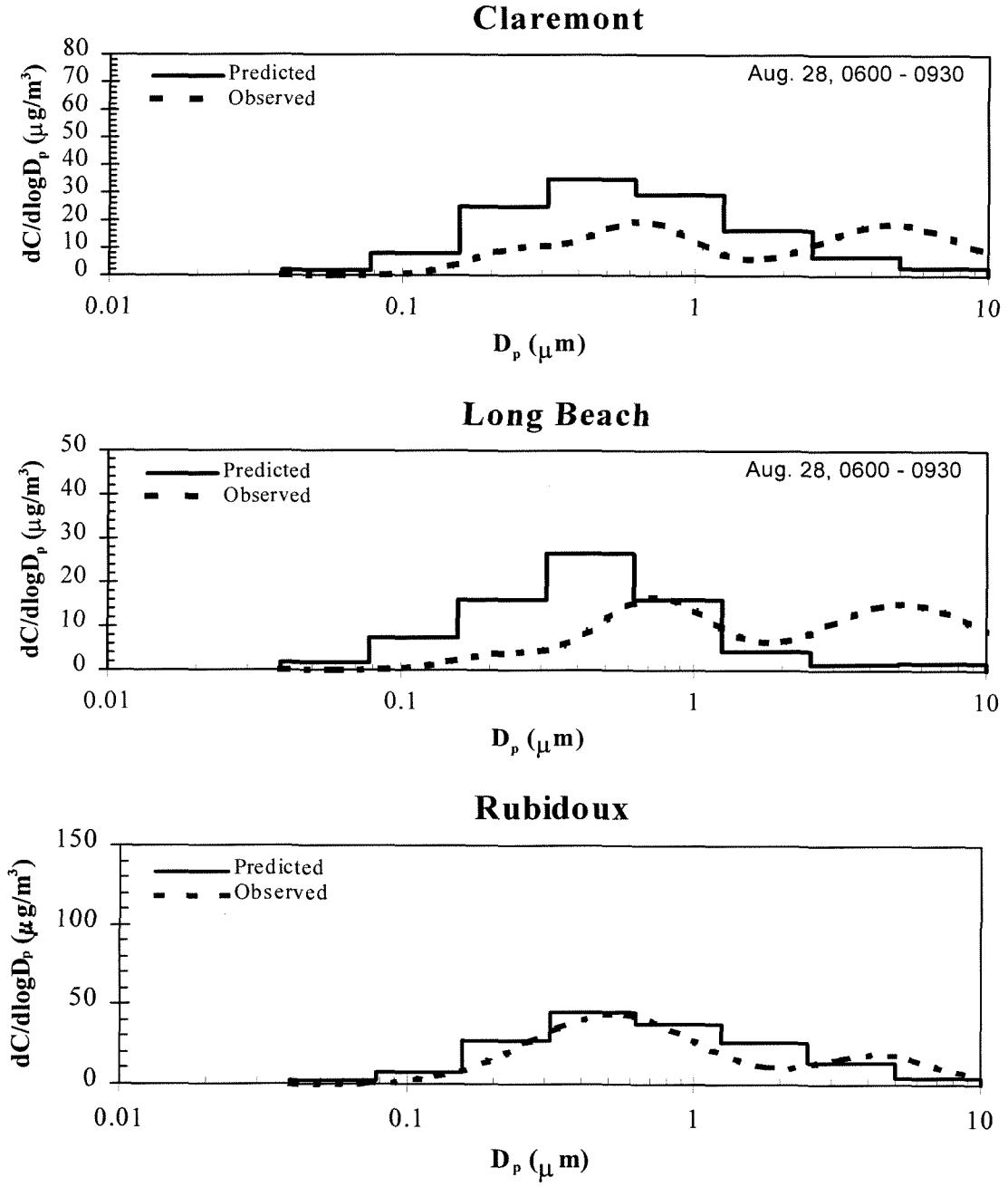

Fig. 7.6 Aerosol nitrate size distributions for three South Coast Air Basin locations between 6 a.m. and 9:30 a.m. on 28 August 1987. Air samples were taken with Berner Impactors at the intensive SCAQS sampling sites and analyzed for various inorganic ions. The impactor stage masses were transformed by a data reduction algorithm into mass size distributions and then fitted with log-normal functions. The measured aerosol size distributions presented are reconstructed from the fitted log-normal parameters.

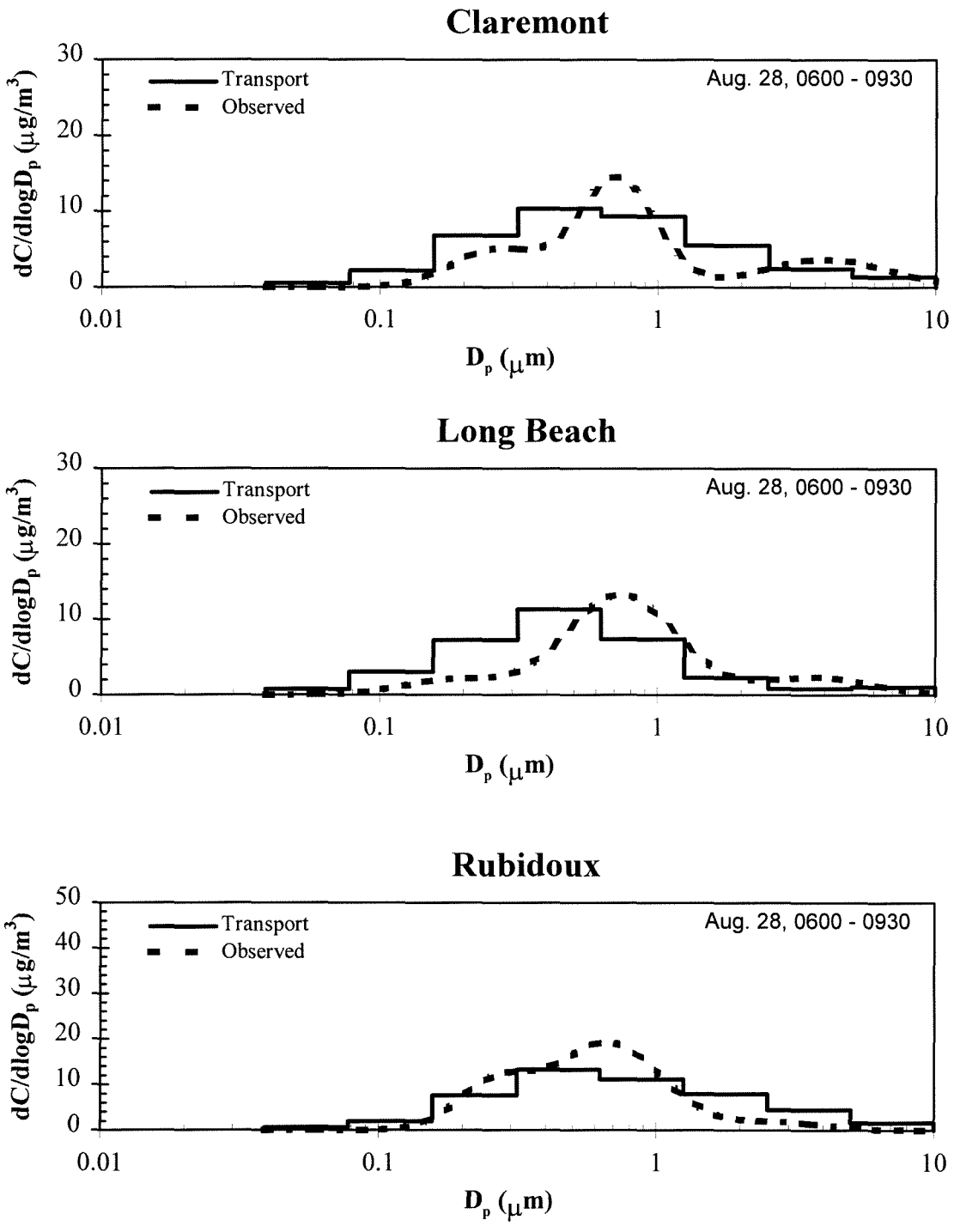

Fig. 7.7 Aerosol ammonium size distributions for three SCAQS locations between 6 a.m. and 9:30 a.m. on 28 August 1987.

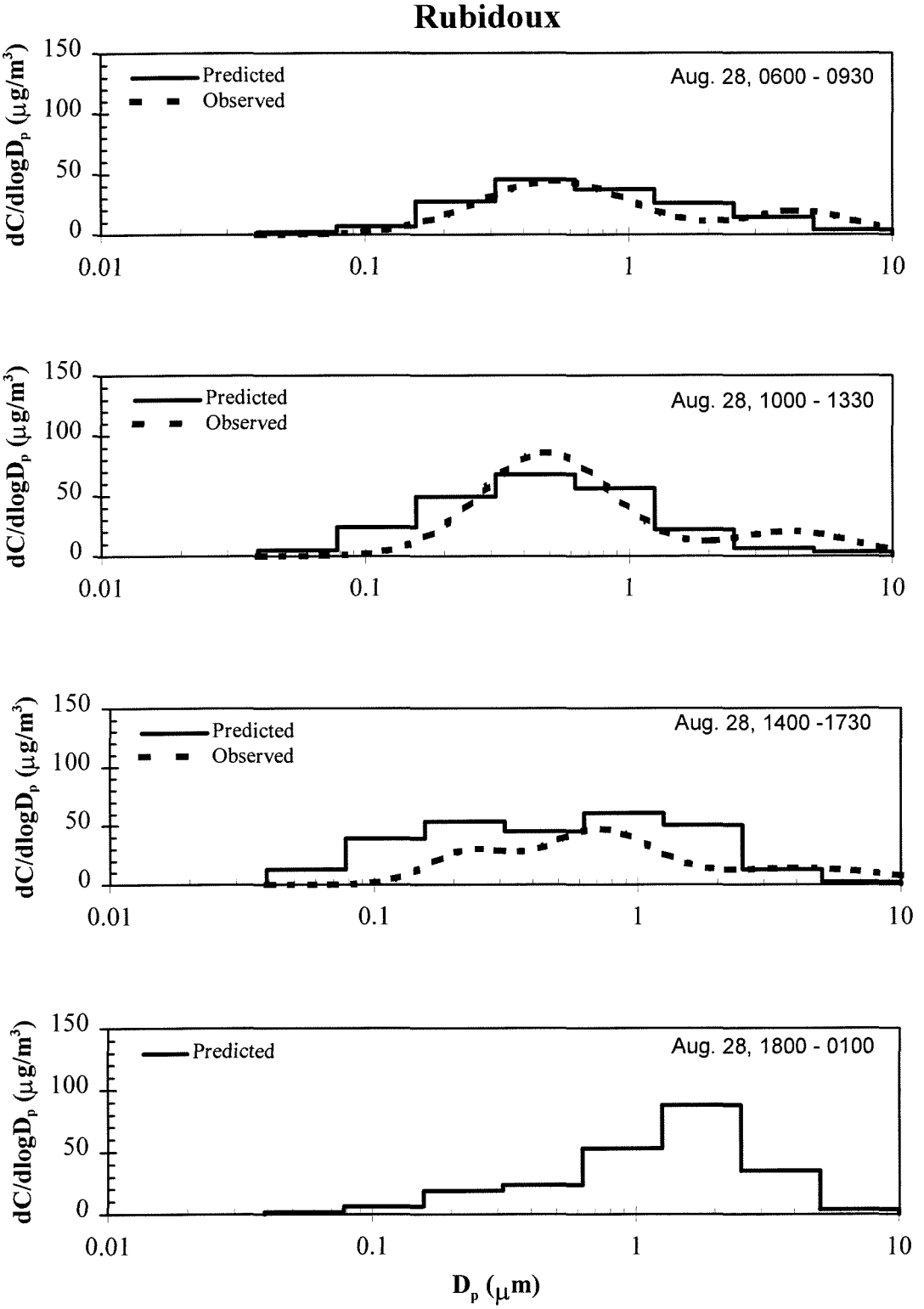

Fig. 7.8 Aerosol nitrate size distributions at Rubidoux (Riverside), California, for various sampling periods on 28 August 1987.

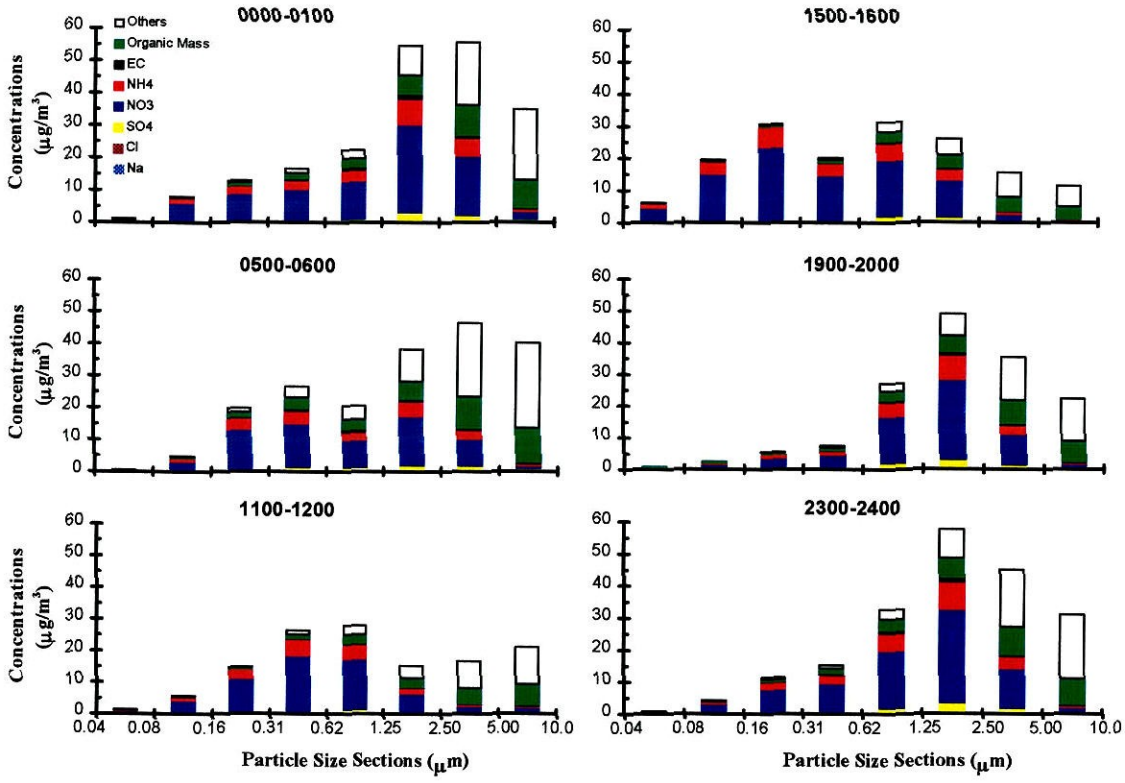

Fig. 7.9 Size- and composition-resolved aerosol distributions at Riverside, California, at various times on 28 August 1987. Water concentration is not shown.

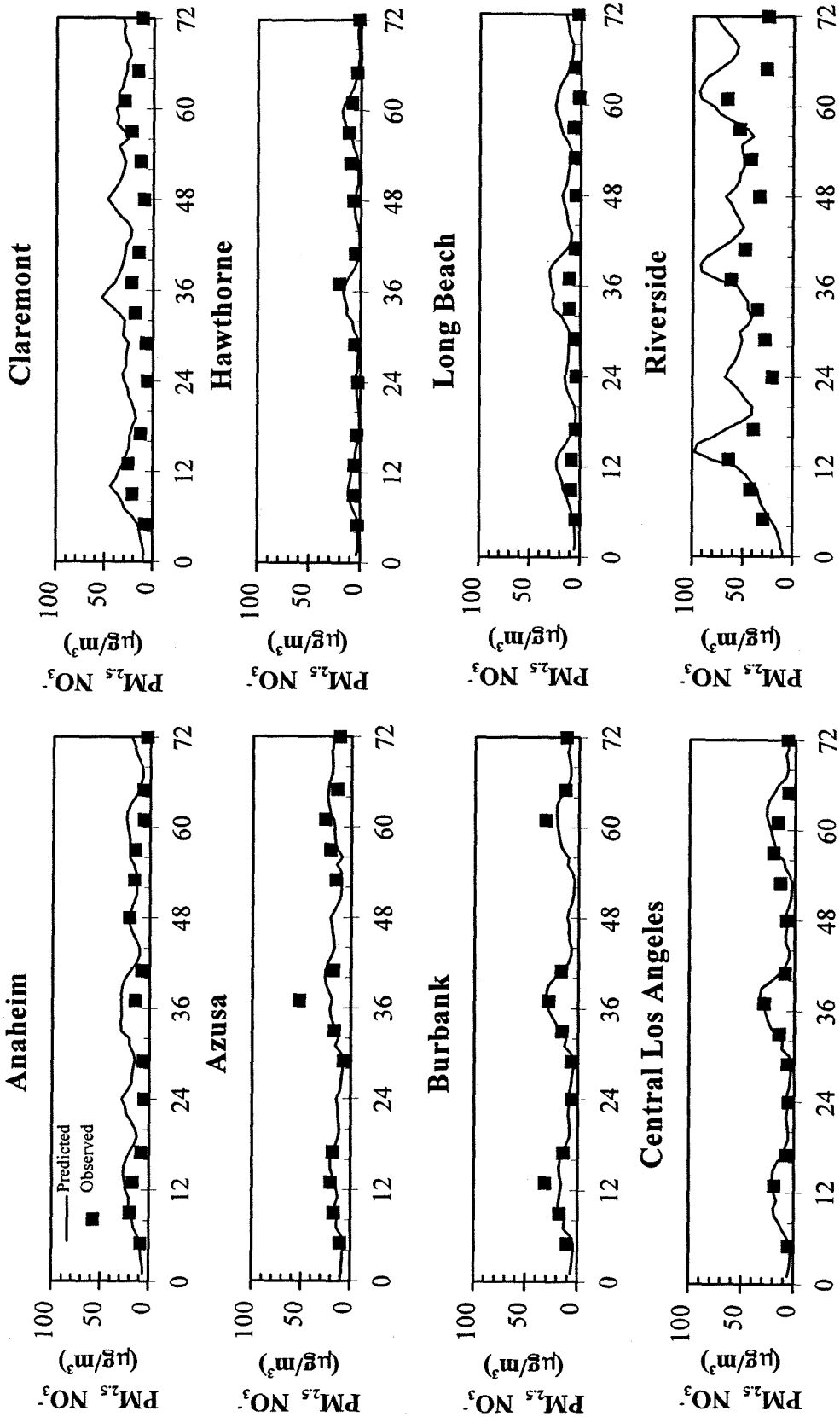

Fig. 7.10 Time-series of predicted and observed $PM_{2.5}$ nitrate concentrations at various locations during 27-29 August 1987.

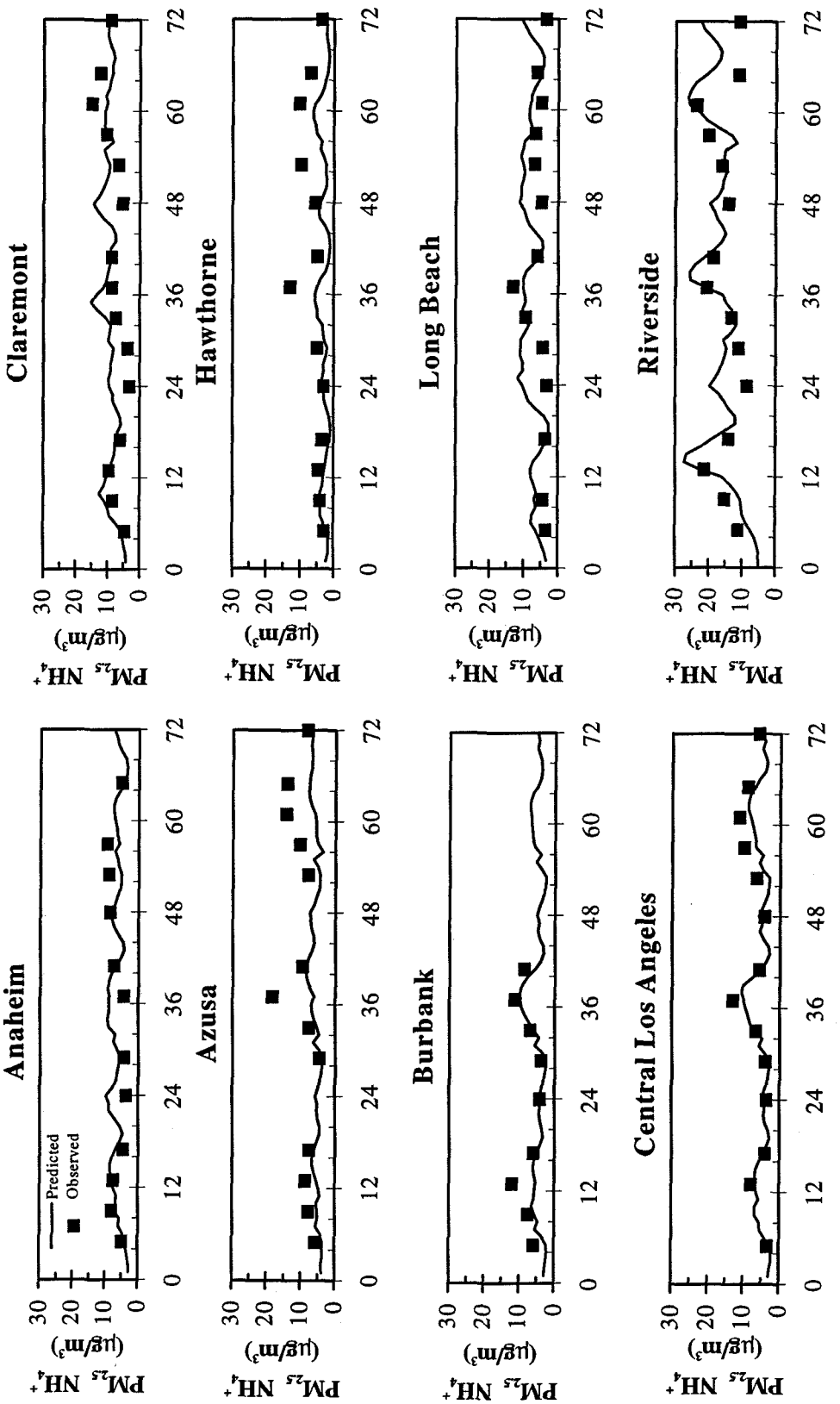

Fig. 7.11 Time-series of predicted and observed $PM_{2.5}$ ammonium concentrations at various locations during 27-29 August 1987.

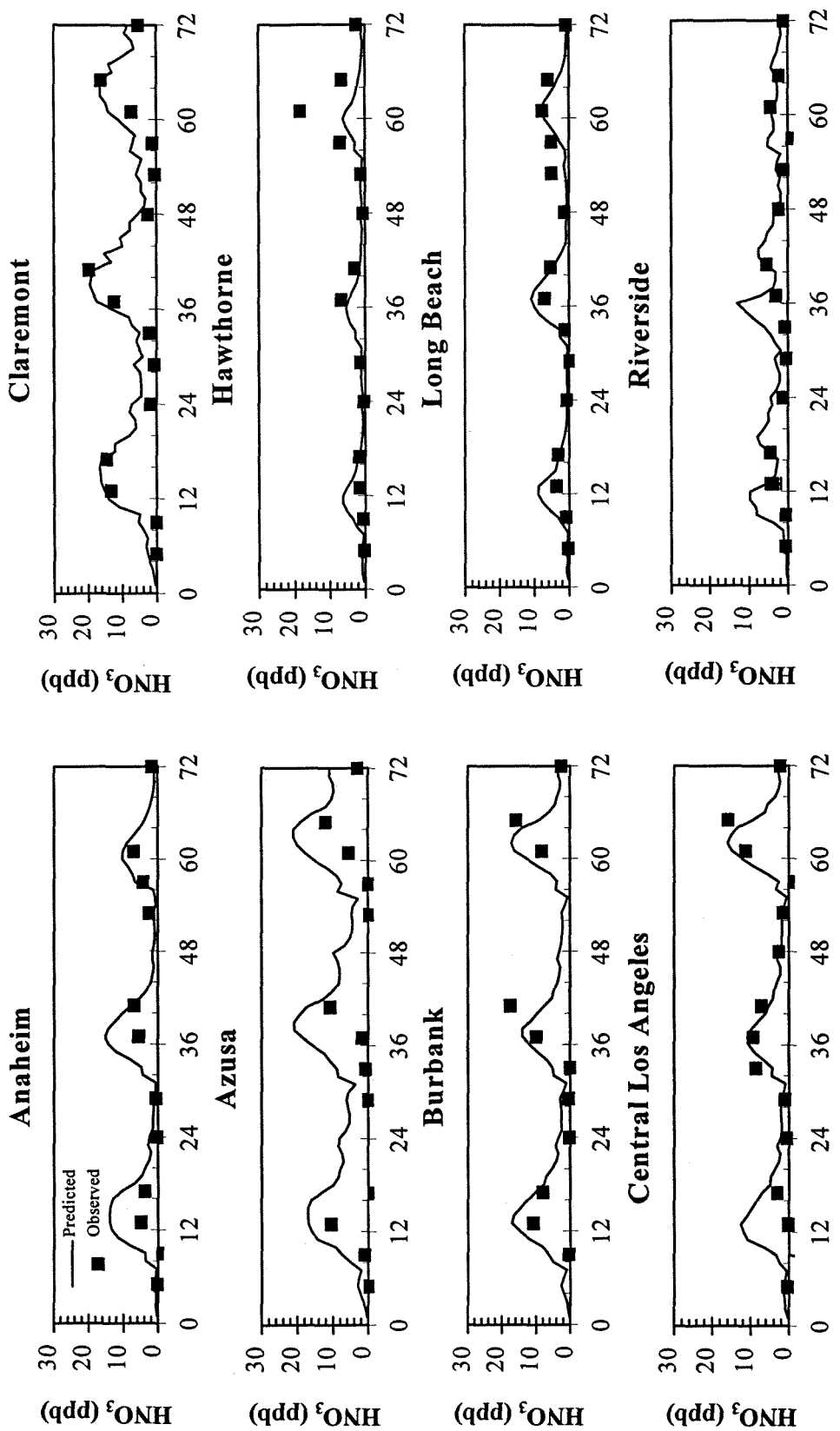

Fig. 7.12 Time-series of predicted and observed gaseous nitric acid concentrations at various locations during 27-29 August 1987.

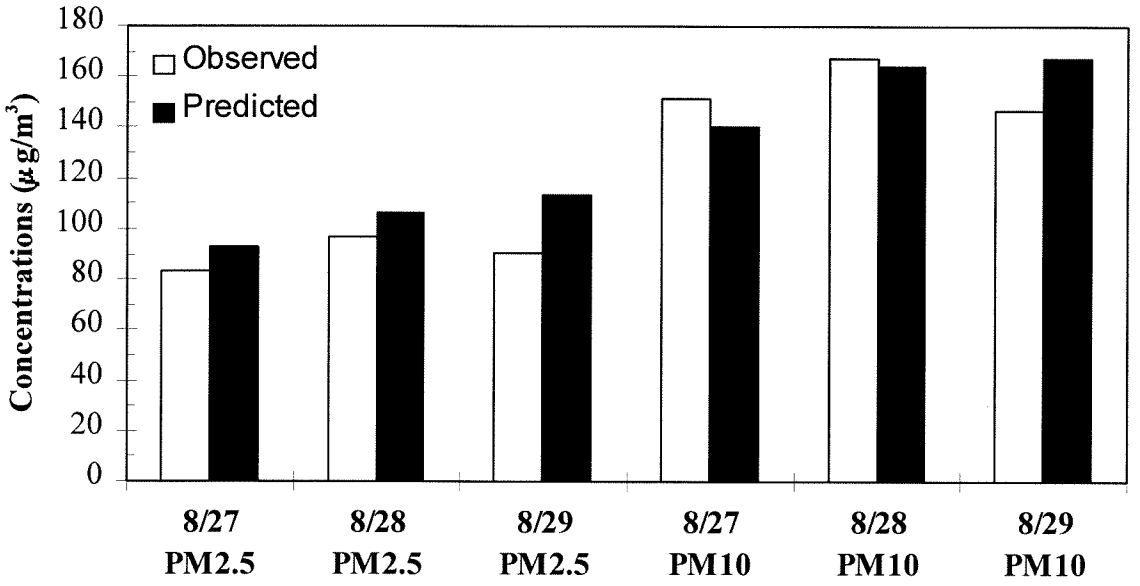

Fig. 7.13 Predicted and observed maximum 24-h-mean $PM_{2.5}$ and PM_{10} mass concentrations of the 8 SCAQS monitoring stations during 27-29 August 1987. The maxima all occurred at Riverside.

Chapter 8

Summary and Conclusions

This thesis is a composite of research works on urban aerosol thermodynamic and dynamic modeling. A new thermodynamic model, SCAPE2, which has the most complete treatment of gas/aerosol equilibrium has been developed. The new thermodynamic model is used in the development of a 3-D size- and chemically-resolved aerosol model that includes advection, turbulent diffusion, condensation/evaporation, nucleation, emissions, and dry deposition.

Chapter 1 is an introduction on the general background of aerosol thermodynamic and 3-D aerosol modeling. Chapter 2 studies the mechanisms of formation of the droplet mode in addition to the three typical modes (i.e., nucleation, accumulation, and coarse) of atmospheric aerosols. Water accretion alone is excluded for the growth of droplet-mode particles from the condensation mode. Aerosol-phase chemistry as currently understood and gas-phase sulfate formation do not also appear to be capable of explaining the existence of the droplet mode as resulting from growth of the condensation mode. The proposed most plausible explanation for formation of the droplet mode is activation of condensation mode particles to form fogs or clouds followed by aqueous-phase sulfate formation and fog evaporation.

Chapter 3 examines aerosol water content and acidity associated with the inorganic fraction of $PM_{2.5}$ and PM_{10} mass in South Coast Air Basin by using a thermodynamic gas/aerosol equilibrium model (SCAPE, the previous version of SCAPE2) and the measured aerosol composition data from the 1987 Southern California Air Quality Study (SCAQS). During nighttime when temperature is low and relative humidity is high, water is usually the predominant aerosol substance. Particulate water in

the winter is estimated to be considerably larger than in the summer at SCAQS observation sites. Aerosol acidity is estimated to be high for all the sampling sites, with the lowest pH values at Long Beach and San Nicolas Island (-0.8-3.3) and highest at Riverside (2-4.5) in the summer. Winter particles are less acidic than summer particles because of the smaller sulfate concentrations and larger water content.

Chapters 4 and 5 are devoted to develop the data and correlations for incorporating carbonates and formic and acetic acids into a gas/aerosol equilibrium model. The species of importance for atmospheric aerosols are considered. It is found in Chapter 5 that the gas/aerosol distribution of formic and acetic acids is strongly on the gas-phase side for typical sulfate/nitrate/ammonium/sodium/chloride/water aerosols and that dissolved formate and acetate have negligible effect on the gas/aerosol equilibrium of other components.

Chapter 6 investigates the time scales to achieve gas-aerosol equilibrium for volatile atmospheric species. It is found that equilibration between submicron aerosol and the gas phase is attainable on a time scale comparable to that of typical ambient gas and aerosol dynamics. However, the time required for the coarse aerosol to reach equilibrium is predicted to be sufficiently long that volatile species in atmospheric coarse aerosol particles may generally exist in non-equilibrium transition states. The equilibration time increases with increasing particle size, or decreasing accommodation coefficient or temperature. The research presented in this chapter demonstrates the general necessity of dynamic approach in calculating mass transport between the gas and aerosol phases.

In Chapter 7, the previous research results are used in developing a three-dimensional size- and chemically-resolved aerosol model that includes advection, turbulent diffusion, condensation/evaporation, nucleation, emissions, and dry deposition. For condensation/evaporation of volatile inorganic species, a new thermodynamic model, SCAPE2, which has the most complete treatment of gas/aerosol equilibrium is included. The model employs an absorption approach in dynamically modeling gas/particle partitioning of secondary organic aerosols. The aerosol model has been coupled with the three-dimensional gas-phase photochemical CIT model, and has been applied to the 27-29 August 1987 episode in South Coast Air Basin of California to evaluate model performance. Simulation results have been compared systematically against available observations. Generally good agreement between predictions and measurements is observed. There is evidence that gas/aerosol mass transfer limits overall gas/particle conversion for volatile inorganic species.

Several aspects in the current aerosol dynamic model can be improved in future research. The current model considers only aromatics, which is believed to be most important in producing secondary organic aerosols (SOA). The simulation results showed that SOA production based on the organic-absorption approach is considerably less than the primary organic materials, as well as that predicted by the previous models that assume very low saturation vapor pressures for the produced semi-volatile organic compounds. Although it is expected that our model should predict less SOA production as a result of the absorption approach that results in higher saturation vapor pressures for the condensable product vapors, more conclusive results can be obtained after inclusion

of gasoline and representative biogenic compounds into the current chemical mechanism with respect to SOA production. It is also desirable to see how the different chemical mechanisms may affect the model predictions. In this respect, the SAPRC90 chemical mechanism [*Carter*, 1990] can be employed instead of the currently used extended LCC chemical mechanism [*Lurmann et al.*, 1987; *Harley et al.*, 1993].

The current model formulation does not include fog/cloud module. Interaction between aerosol and fog/cloud particles is very important and should be considered in future model improvement. Inclusion of a sound fog/cloud module will undoubtedly improve the model predictions, in particular, the aerosol sulfate predictions. Future research in numerical improvement should focus on developing a more efficient integration method for the condensation/evaporation equation (i.e., Eq. (20) in Chapter 7) that requires minimal updates of the particle surface vapor concentrations calculated by SCAPE2.

REFERENCES

Carter, W. P. L. (1990). *Atmos. Environ. 24A*:481-518.

Harley, R. A., Russell, A. F., McRae, G. J., Cass, G. R. and Seinfeld, J. H. (1993). *Environ. Sci. Technol. 27*:378-388.

Lurmann, F. W., Carter, W. P. L. and Coyner, L. A. (1987). *A surrogate species chemical reaction mechanism for urban-scale air quality simulation models, Vol. I and II.*, ERT Inc., Newbury Park, California, and Statewide Air Pollution Research Center, University of California, Riverside, California. Report to the U.S. Environmental Protection Agency under contract 68-02-4104.

Appendix A

Comparison of SCAPE2 with SCAPE

Table A.1. Hypothetical cases for comparison of SCAPE2 with SCAPE[a]

Species	Case			
($\mu g\ m^{-3}$)	1	2	3	4
Total sulfate	40	10	50	10
Total nitrate	5	30	30	30
Total chloride	0	0	9.36	9.36
Total ammonium	10	10	10	10
Total sodium	0	0	5.90	5.90
R_S[b]	1.44	5.77	1.66	8.28

[a]The cases are the same as those in Table 1 of Kim et al. (1993b).

[b]R_S is the molar ratio of the total concentration of ammonium and sodium over the sulfate concentration.

Table A.2. Comparison of predicted aerosol concentrations for Case 3

	Relative Humidity					
Species	90	80	70	60	50	40
Acidity (pH)						
SCAPE (P) [a]	0.69	0.90	1.27	1.89	1.88	5.90
SCAPE (K) [a]	0.49	0.25	-0.01	-0.18	-0.19	-0.64
SCAPE (B) [a]	0.49	0.21	-0.03	-0.23	-0.22	-0.82
SCAPE2 (P)	0.69	0.92	1.28	1.92	-	3.34
SCAPE2 (K)	0.49	0.25	0.03	-0.21	-0.35	-0.77
SCAPE2 (B)	0.50	0.23	0.00	-0.25	-0.39	-0.77
NO_3^- ($\mu g\ m^{-3}$)						
SCAPE (P)	5.1	2.5	1.6	1.0	0.2	0.0
SCAPE (K)	4.8	1.9	0.9	0.4	0.1	0.2
SCAPE (B)	4.5	1.6	0.7	0.4	0.1	0.0
SCAPE2 (P)	4.9	2.4	1.5	1.0	0.0	0.0
SCAPE2 (K)	4.8	1.8	0.9	0.4	0.1	0.0
SCAPE2 (B)	4.5	1.6	0.8	0.4	0.1	0.0
NH_4^+ ($\mu g\ m^{-3}$)						
SCAPE (P)	10.5	10.5	10.5	10.5	10.4	10.3
SCAPE (K)	10.5	10.5	10.5	10.5	10.5	10.5
SCAPE (B)	10.5	10.5	10.5	10.5	10.5	10.5
SCAPE2 (P)	10.5	10.5	10.5	10.5	10.6	10.5
SCAPE2 (K)	10.6	10.6	10.6	10.6	10.6	10.6
SCAPE2(B)	10.6	10.6	10.6	10.6	10.6	10.6
Cl^- ($\mu g\ m^{-3}$)						
SCAPE (P)	0.9	0.4	0.2	0.1	0.0	0.0
SCAPE (K)	0.7	0.2	0.1	0.0	0.0	0.0
SCAPE (B)	0.7	0.2	0.1	0.0	0.0	0.0
SCAPE2 (P)	0.9	0.4	0.2	0.1	0.0	0.0
SCAPE2 (K)	0.7	0.2	0.1	0.0	0.0	0.0
SCAPE2 (B)	0.7	0.2	0.1	0.0	0.0	0.0
H_2O ($\mu g\ m^{-3}$)						
SCAPE (P)	222	114	78.7	57.4	5.50	9.99
SCAPE (K)	218	110	74.4	55.9	15.3	4.61
SCAPE (B)	218	109	76.0	55.8	15.7	3.91
SCAPE2 (P)	216	111	77.5	56.8	0.00	0.52
SCAPE2 (K)	216	110	76.5	55.9	7.36	2.79
SCAPE2 (B)	214	109	76.1	55.8	8.13	4.01

[a] P: Pitzer method; K: Kusik and Meissner method; B: Bromley method.

Table A.3. Comparison of predicted aerosol concentrations for Case 4

	Relative Humidity					
Species	90	80	70	60	50	40
Acidity (pH)						
SCAPE (P) [a]	2.18	2.52	2.68	2.27	3.03	2.14
SCAPE (K) [a]	2.02	2.21	2.37	2.51	2.69	2.71
SCAPE (B) [a]	2.03	2.22	2.38	2.52	2.70	2.82
SCAPE2 (P)	2.17	2.52	2.66	1.84	0.50	-1.90
SCAPE2 (K)	2.09	2.38	2.58	2.71	2.85	2.80
SCAPE2 (B)	2.10	2.40	2.59	2.73	2.91	2.75
NO_3^- ($\mu g\ m^{-3}$)						
SCAPE (P)	24.8	23.0	21.2	24.3	26.8	16.4
SCAPE (K)	24.7	23.3	22.3	21.0	18.8	16.5
SCAPE (B)	24.6	23.1	22.0	20.5	18.1	15.2
SCAPE2 (P)	24.8	22.9	21.1	21.1	23.3	29.5
SCAPE2 (K)	24.9	23.5	22.3	21.0	18.6	15.5
SCAPE2 (B)	24.8	23.3	22.1	20.8	17.6	15.2
NH_4^+ ($\mu g\ m^{-3}$)						
SCAPE (P)	9.4	7.9	6.5	7.2	8.7	5.1
SCAPE (K)	9.4	8.2	7.2	6.3	5.1	4.1
SCAPE (B)	9.3	8.1	7.1	6.2	4.8	3.5
SCAPE2 (P)	9.4	7.9	6.5	5.9	6.6	0.0
SCAPE2 (K)	9.5	8.3	7.3	6.3	5.0	3.8
SCAPE2 (B)	9.4	8.2	7.2	6.2	4.6	3.5
Cl^- ($\mu g\ m^{-3}$)						
SCAPE (P)	6.4	4.6	2.9	2.2	3.7	2.6
SCAPE (K)	6.4	4.7	3.4	2.3	1.1	0.6
SCAPE (B)	6.3	4.6	3.3	2.2	1.0	0.1
SCAPE2 (P)	6.4	4.5	2.8	1.8	2.1	9.1
SCAPE2 (K)	6.4	4.8	3.5	2.3	1.1	0.4
SCAPE2 (B)	6.4	4.7	3.4	2.2	0.9	0.1
H_2O ($\mu g\ m^{-3}$)						
SCAPE (P)	196	81.2	39.5	14.9	16.2	4.07
SCAPE (K)	189	81.8	48.4	31.2	17.3	9.73
SCAPE (B)	188	81.3	48.0	30.9	15.4	2.15
SCAPE2 (P)	189	80.8	38.7	19.8	15.8	34.0
SCAPE2 (K)	190	82.6	48.9	31.3	16.4	7.8
SCAPE2 (B)	190	81.9	48.5	31.2	14.2	1.42

[a] P: Pitzer method; K: Kusik and Meissner method; B: Bromley method.

Table A.4. Comparison of computing times (units in CPU second) [a]

	Case			
	1	2	3	4
SCAPE				
Pitzer	1.3	1.0	3.2	18
Kusik-Meissner	3.2	1.4	5.9	38
Bromley	3.5	1.6	6.3	42
SCAPE2				
Pitzer	0.4	0.8	0.6	1.0
Kusik-Meissner	1.3	0.3	0.9	0.4
Bromley	1.2	0.3	0.5	1.2

[a]Results of SCAPE were calculated on SUN SPARC station SLC, and SCAPE2 on SUN SPARC station 1+.

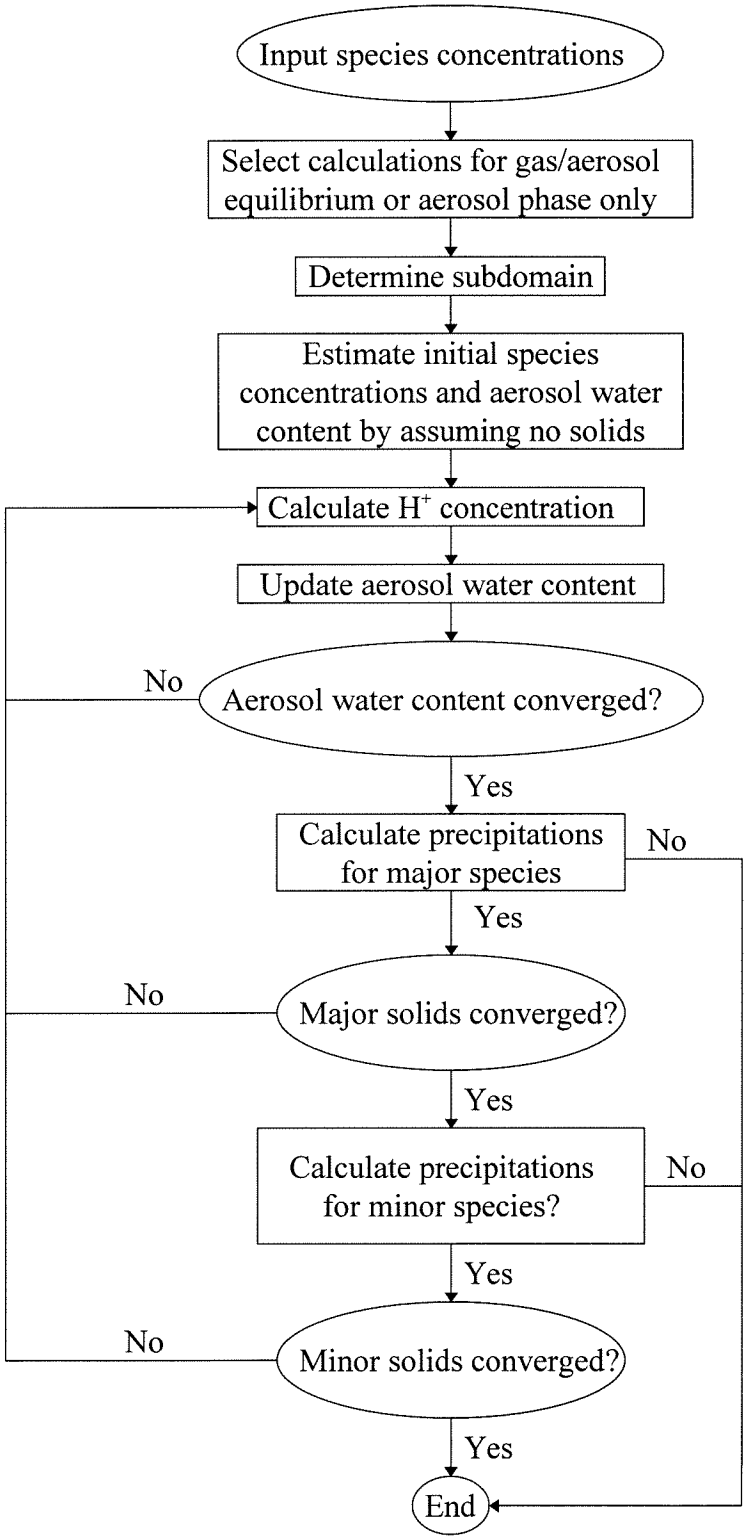

Fig. A.1 Schematic diagram of the computational approach used in SCAPE2

Appendix B

Time-Series of Predicted and Observed $PM_{2.5}$ Chemical Concentrations

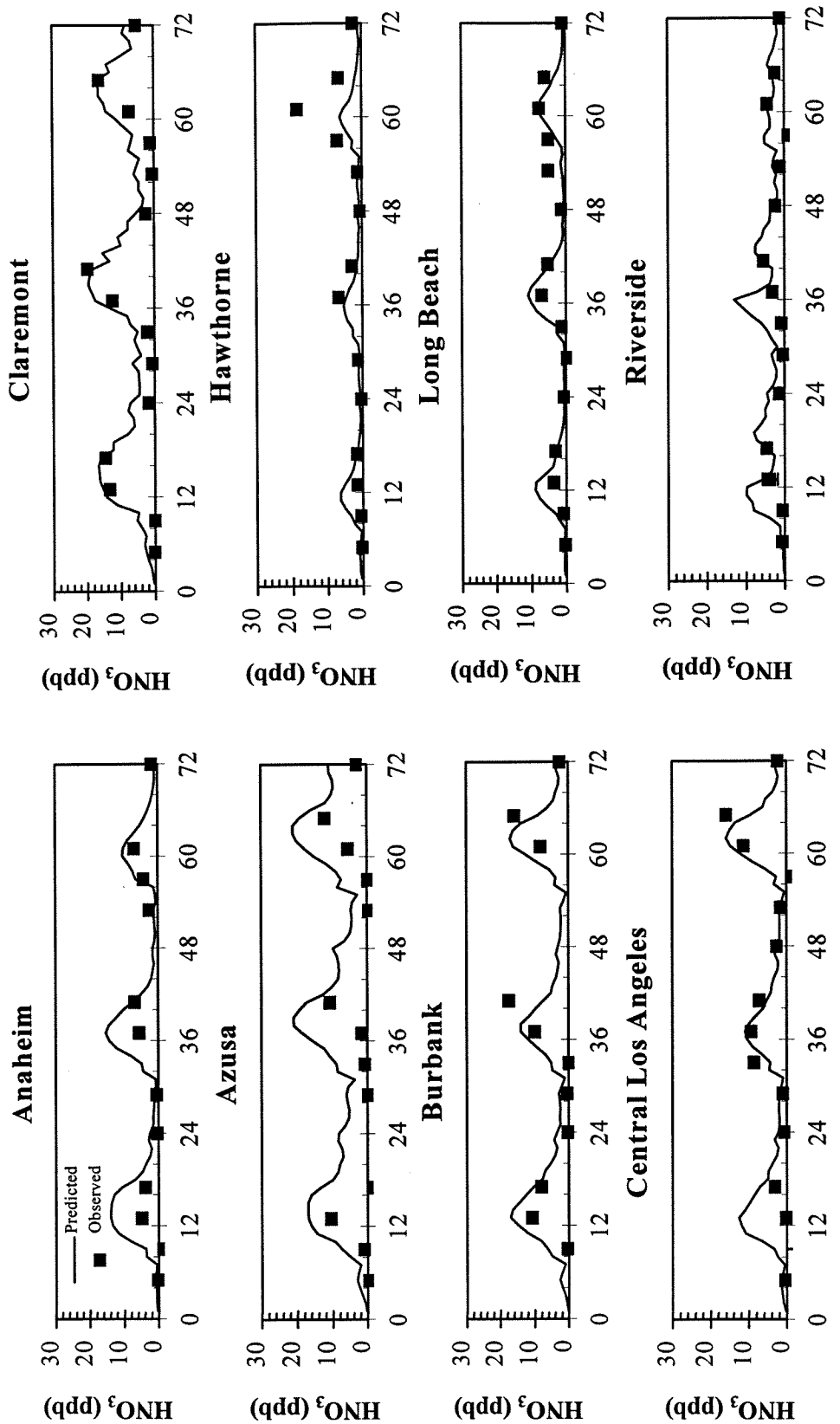

Fig. B.1 Time-series of predicted and observed gaseous nitric acid concentrations at various locations during 27-29 August 1987.

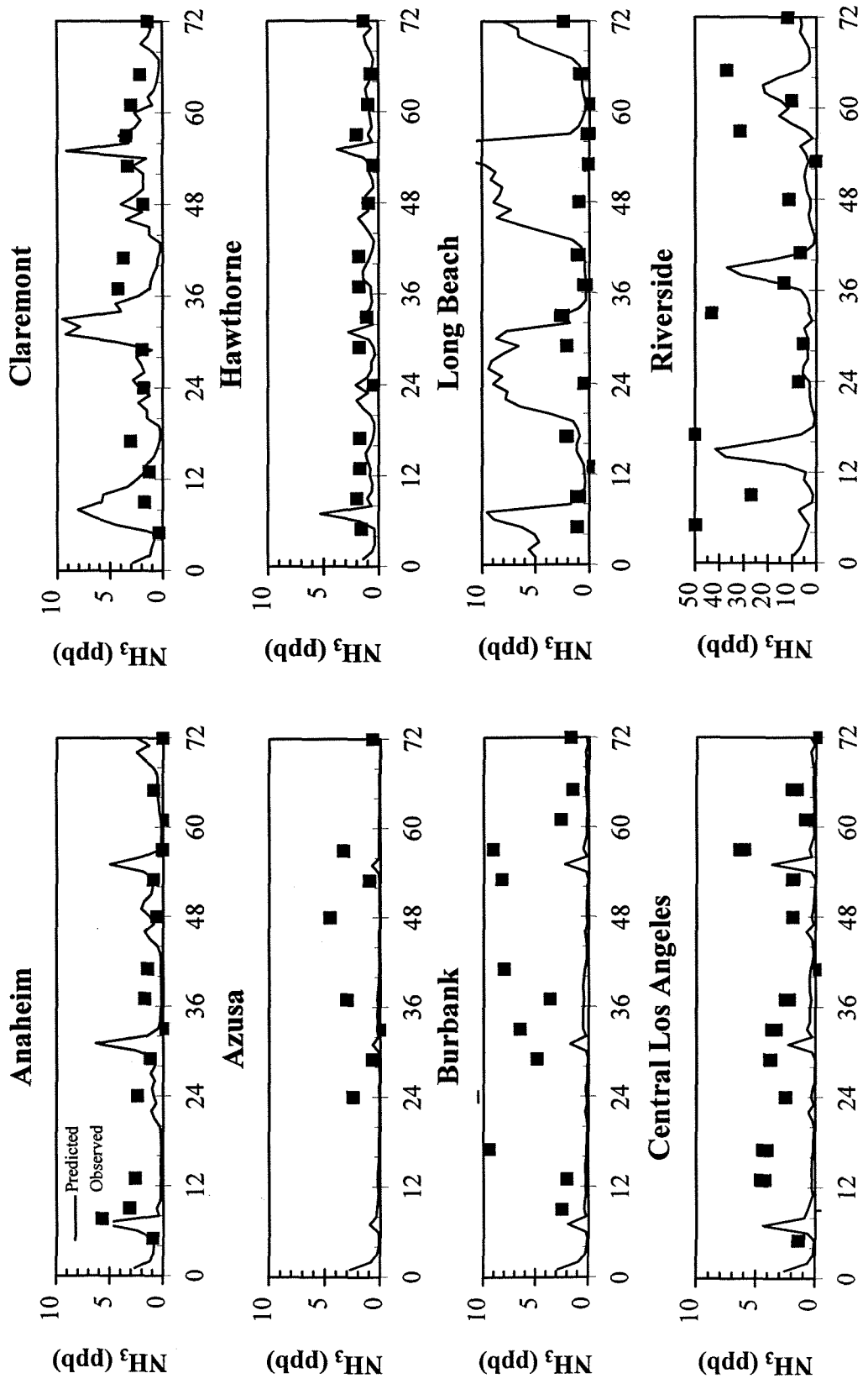

Fig. B.2 Time-series of predicted and observed gaseous ammonia concentrations at various locations during 27-29 August 1987.

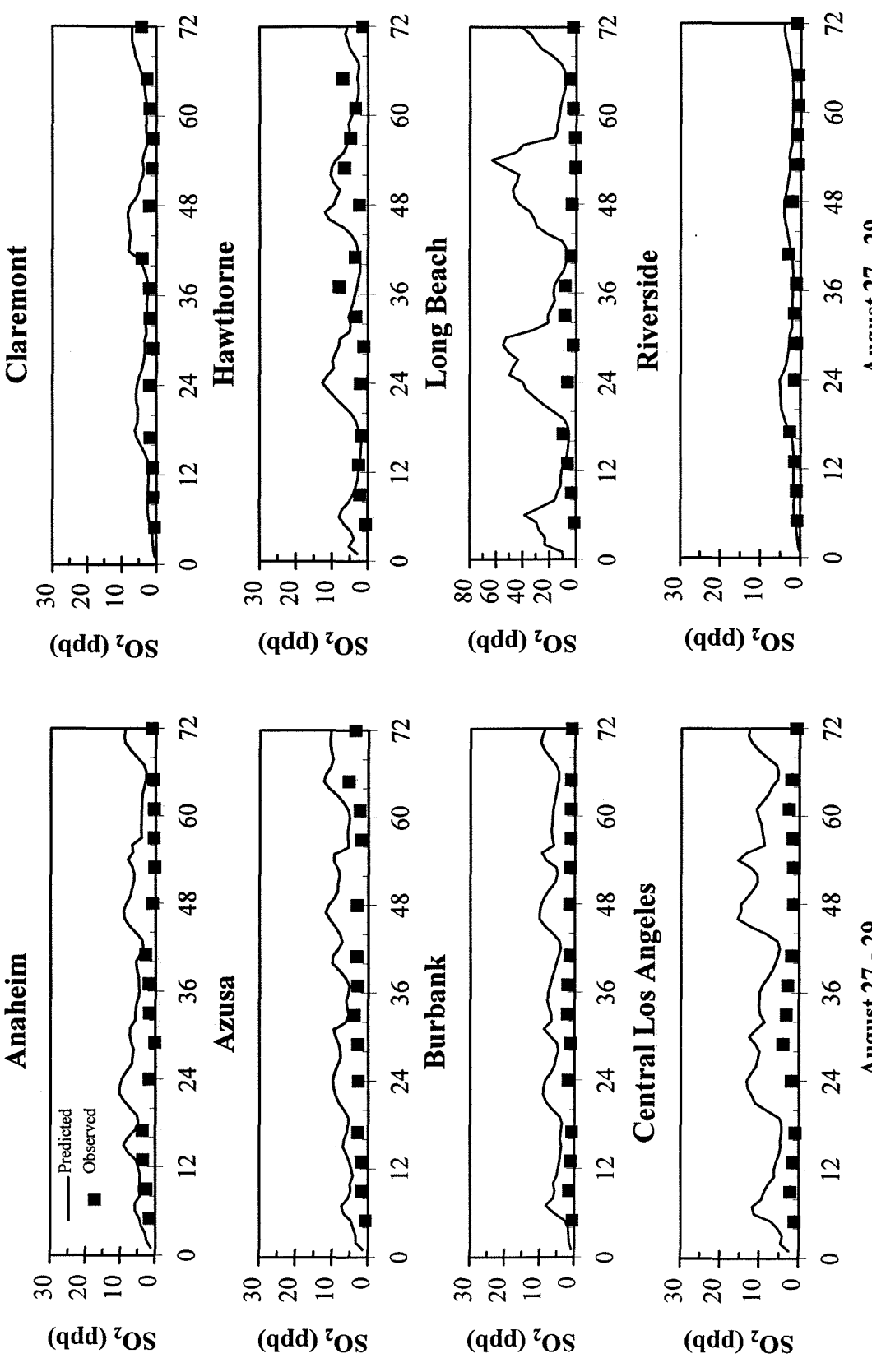

Fig. B.3 Time-series of predicted and observed gaseous sulfur dioxide concentrations at various locations during 27-29 August 1987.

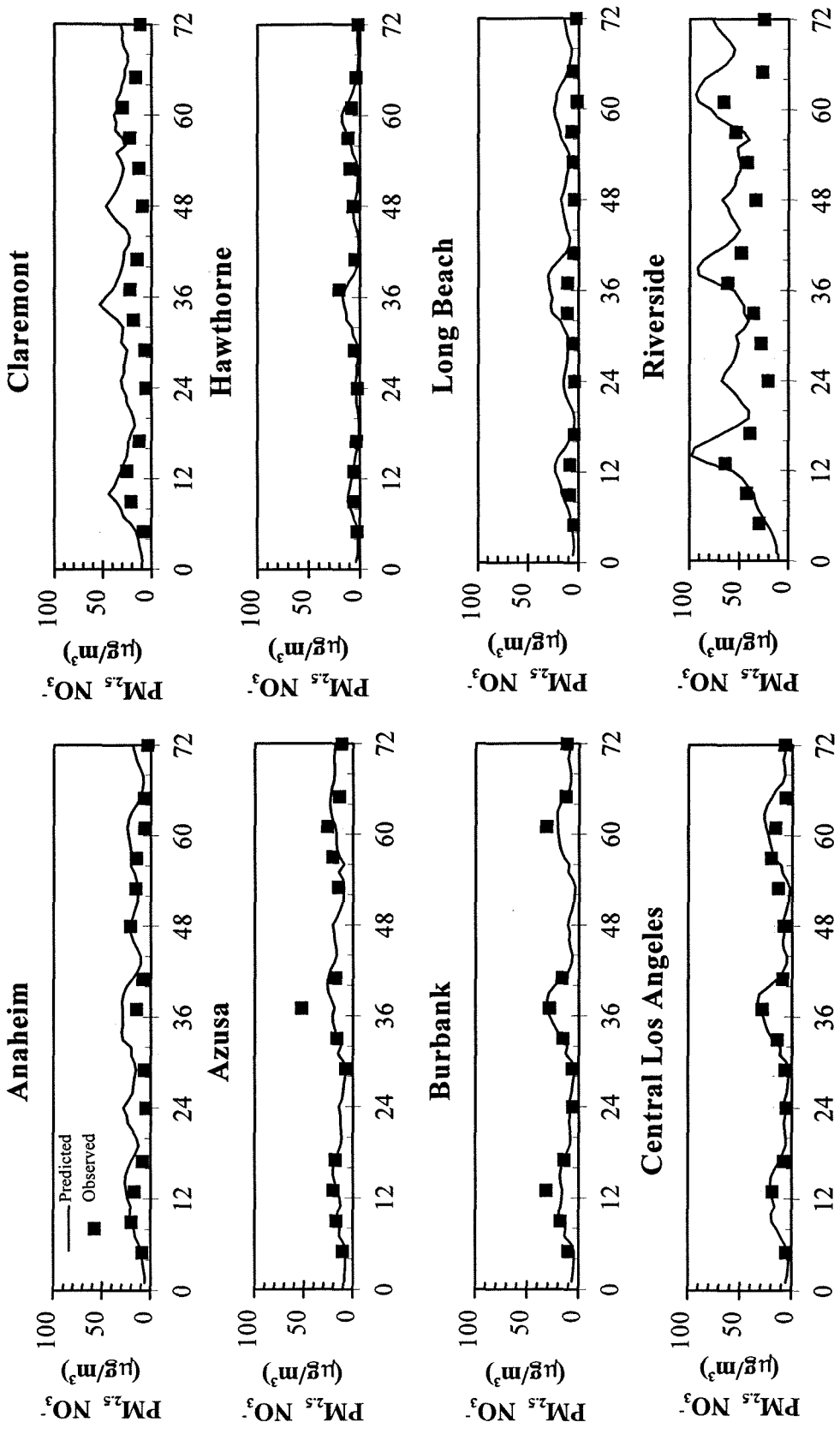

Fig. B.4 Time-series of predicted and observed $PM_{2.5}$ nitrate at various locations during 27-29 August 1987.

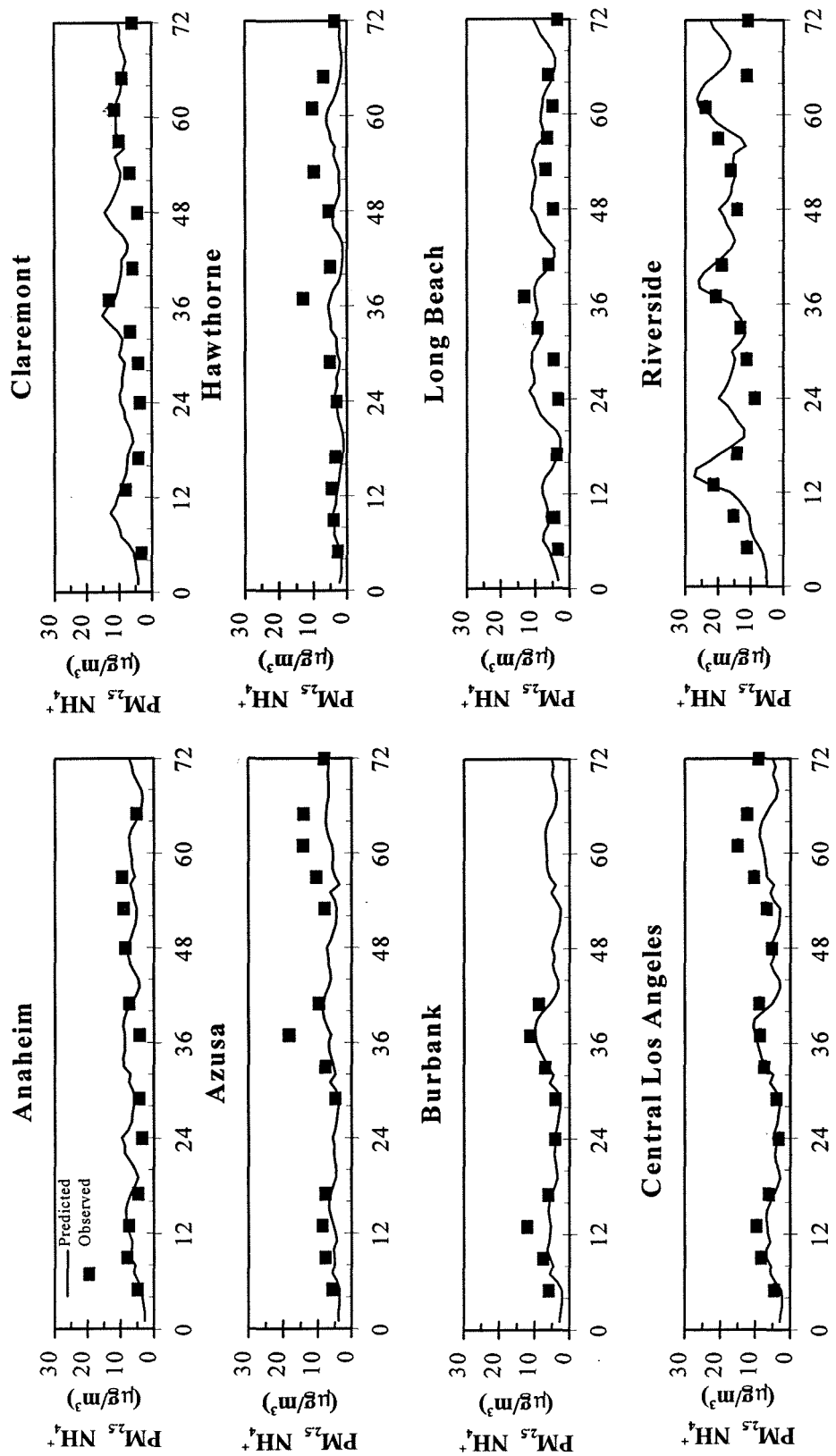

Fig. B.5 Time-series of predicted and observed $PM_{2.5}$ ammonium at various locations during 27-29 August 1987.

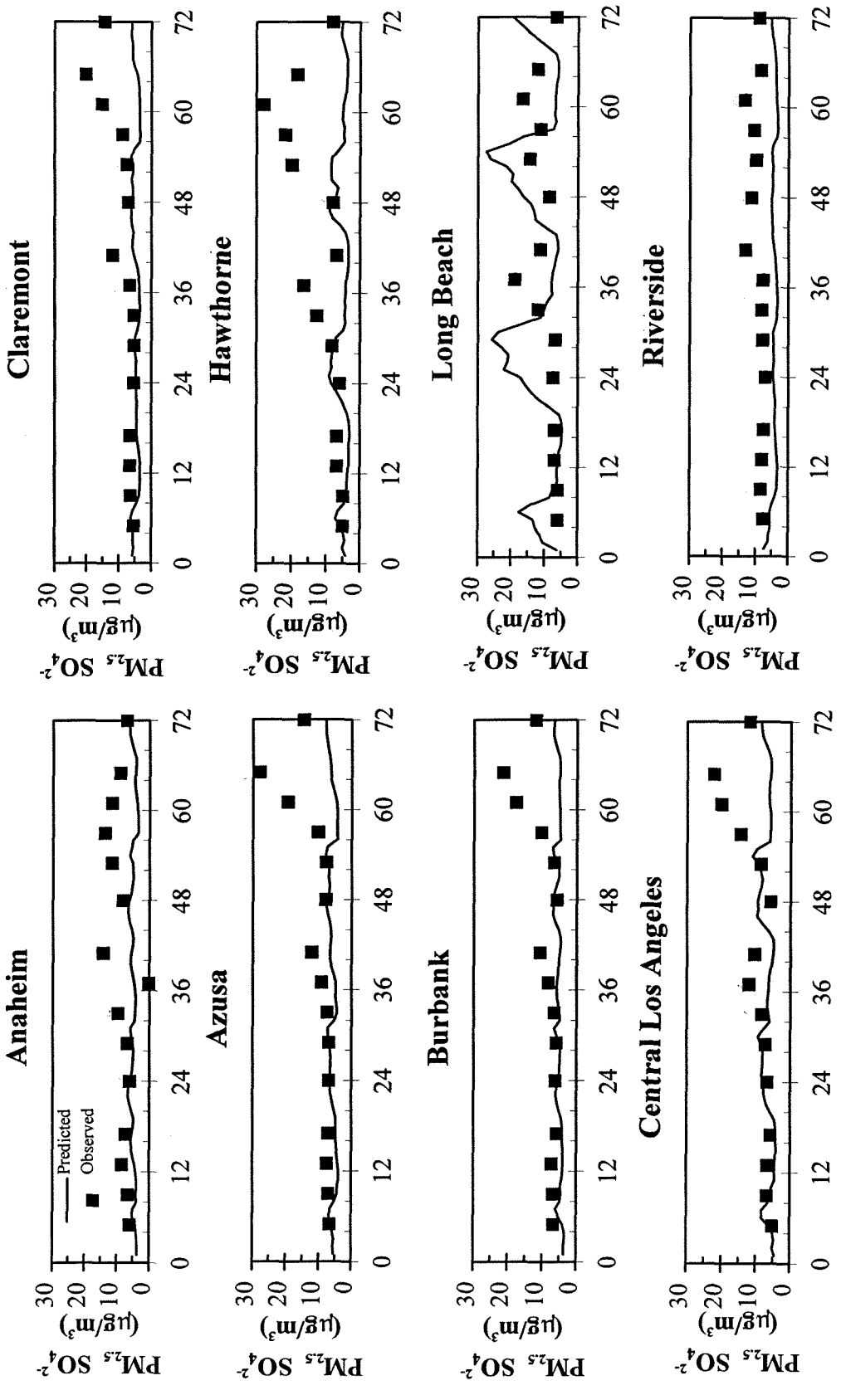

Fig. B.6 Time-series of predicted and observed $PM_{2.5}$ sulfate at various locations during 27-29 August 1987.

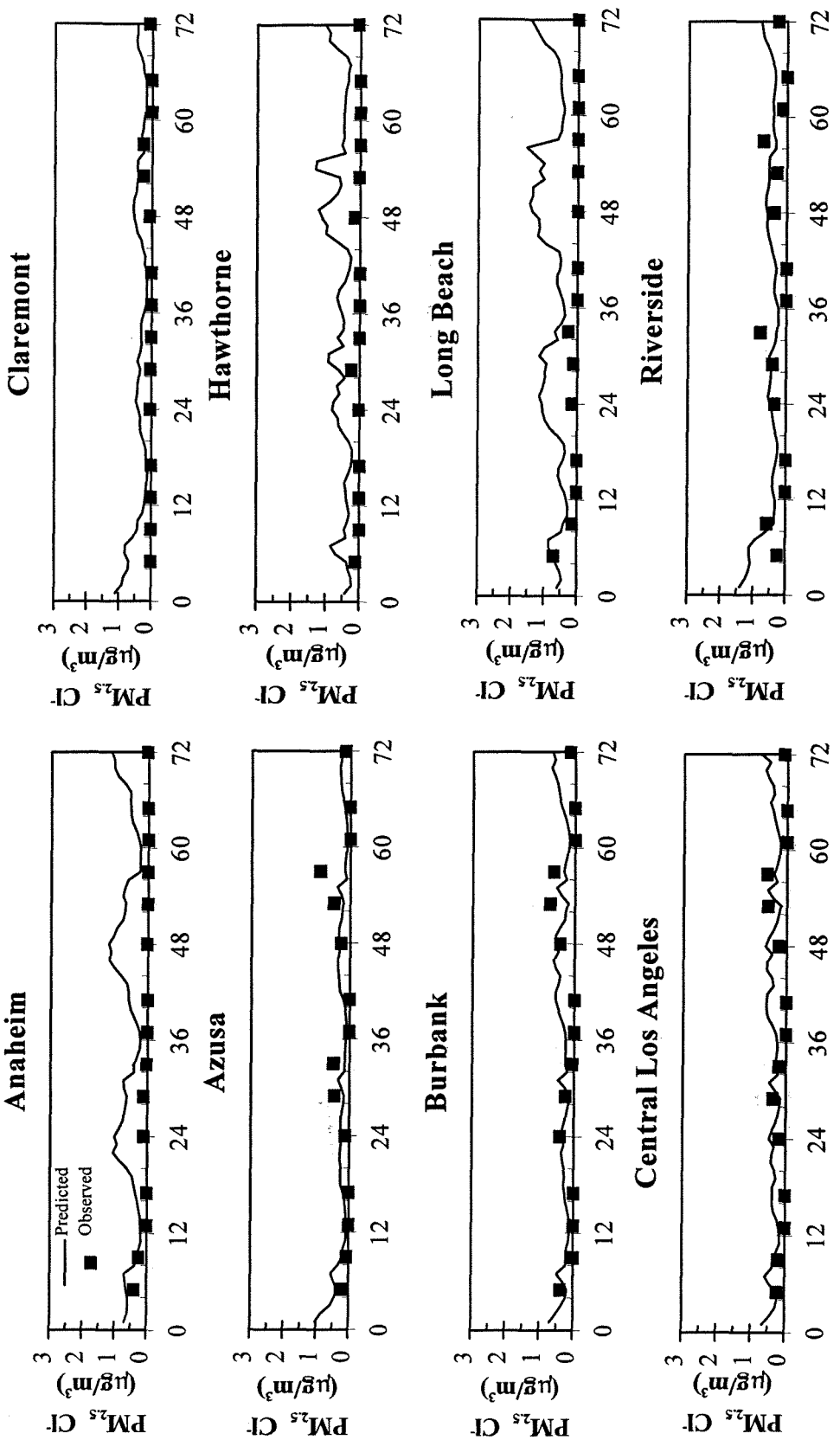

Fig. B.7 Time-series of predicted and observed $PM_{2.5}$ chloride at various locations during 27-29 August 1987.

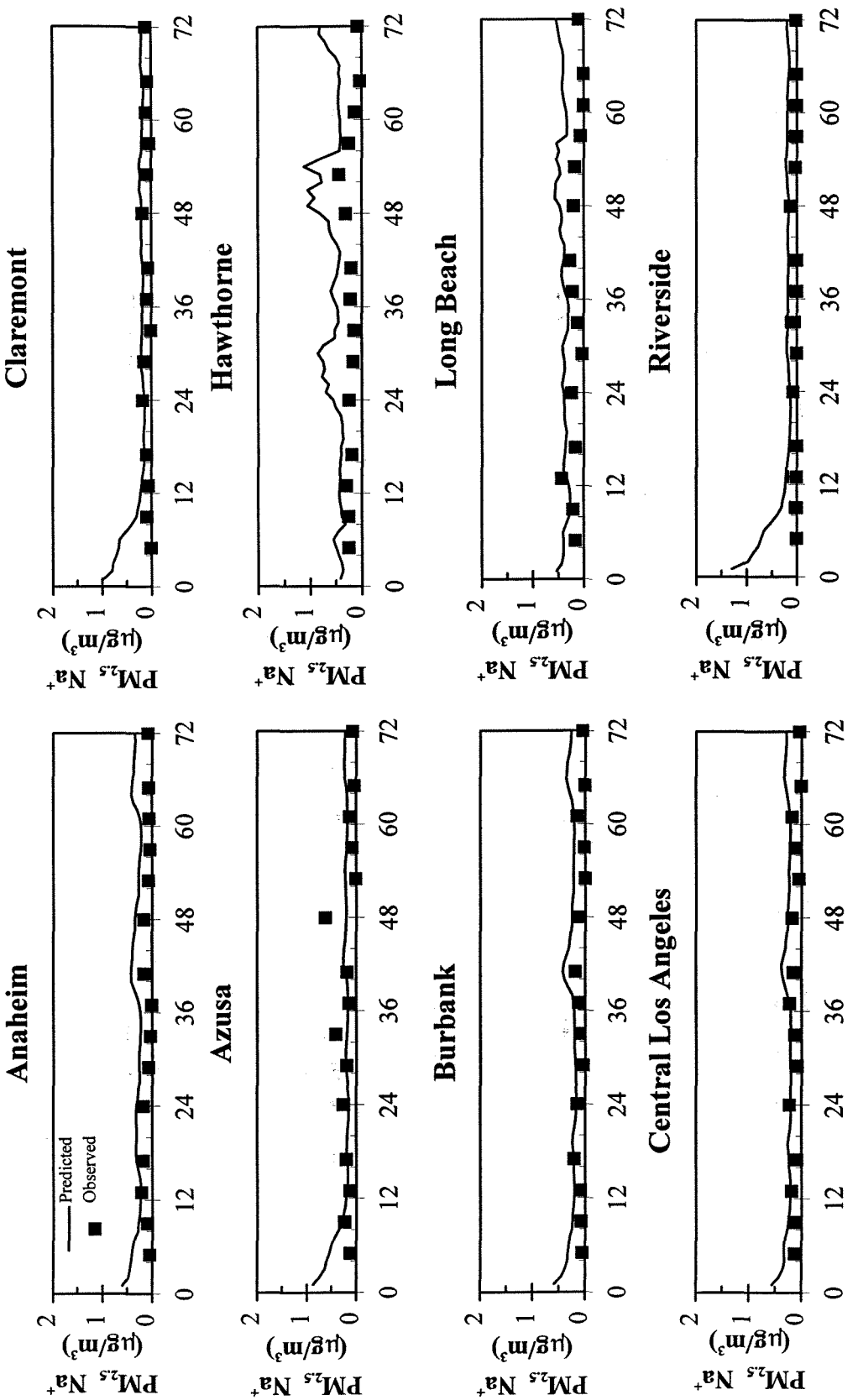

Fig. B.8 Time-series of predicted and observed $PM_{2.5}$ sodium at various locations during 27-29 August 1987.

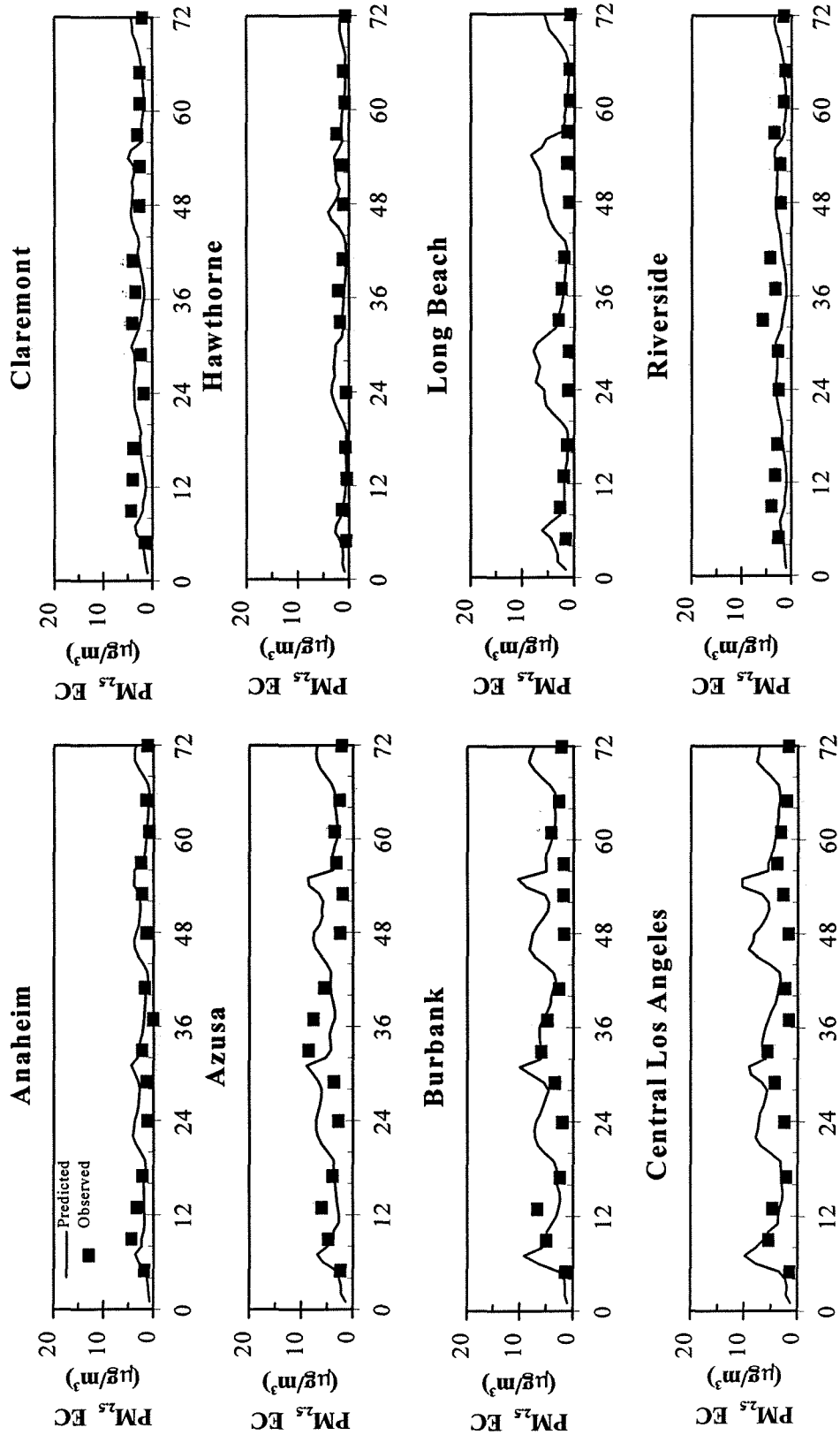

Fig. B.9 Time-series of predicted and observed $PM_{2.5}$ elemental carbon at various locations during 27-29 August 1987.

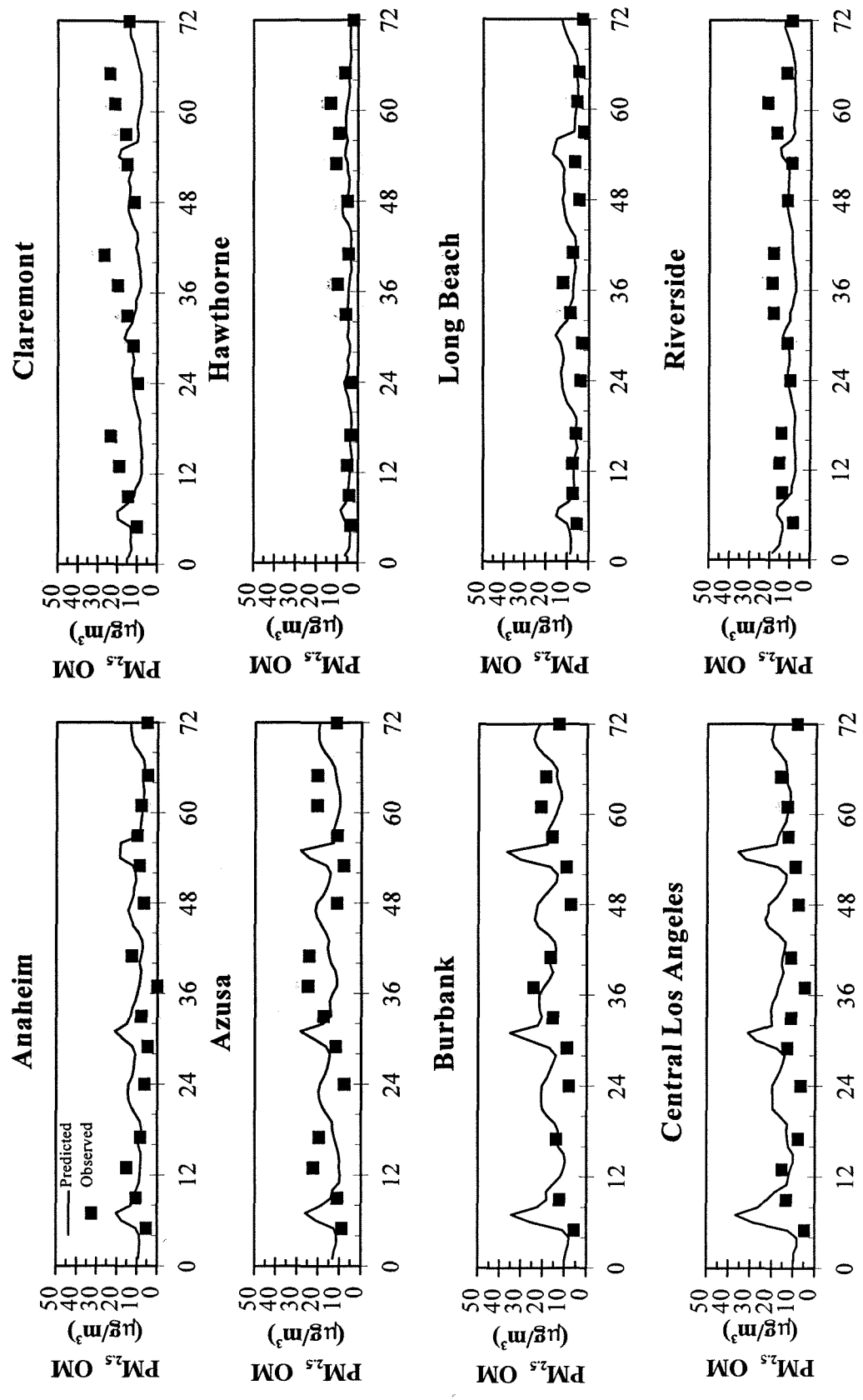

Fig. B.10 Time-series of predicted and observed $PM_{2.5}$ organic matter at various locations during 27-29 August 1987.

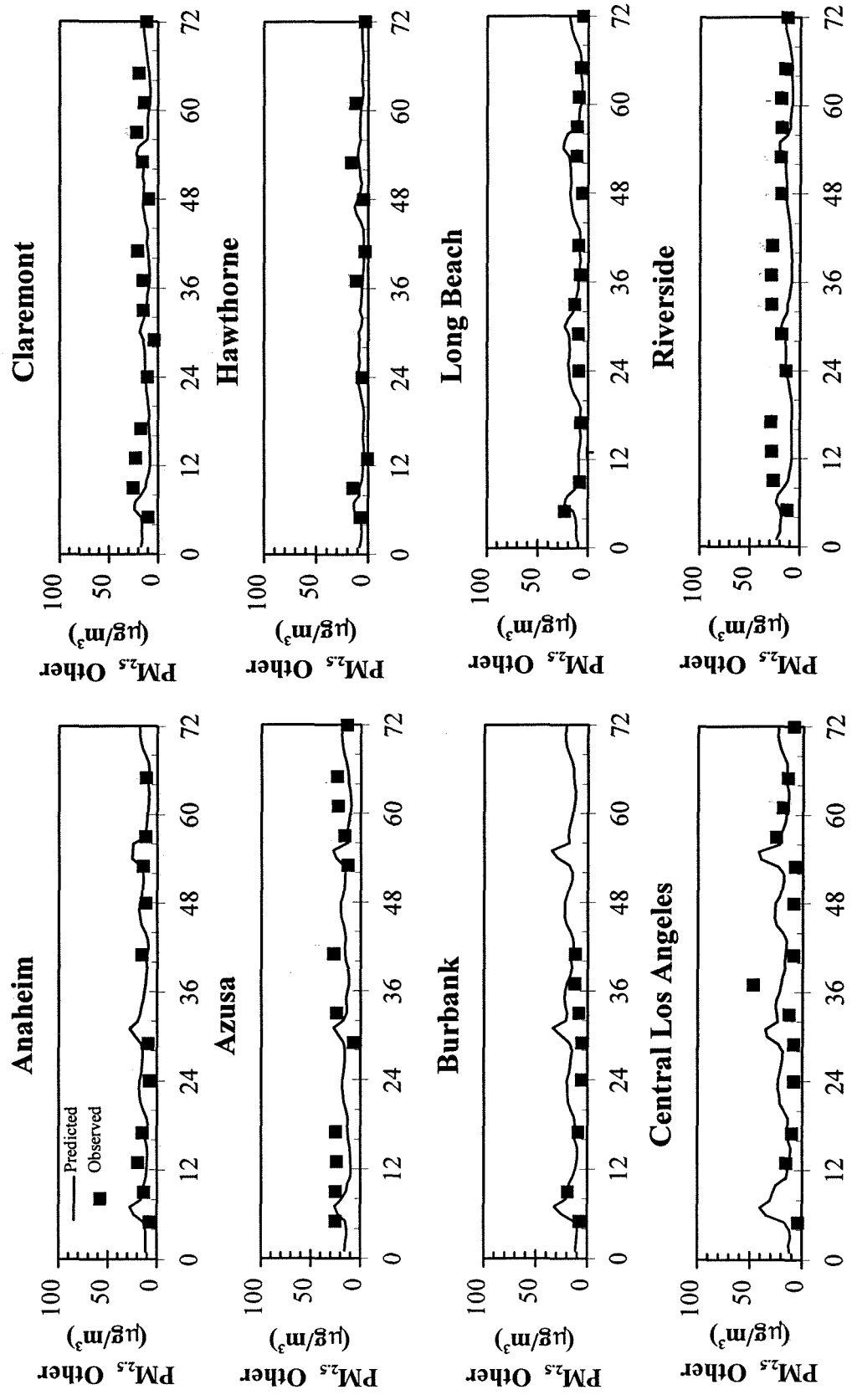

Fig. B.11 Time-series of predicted and observed $PM_{2.5}$ crustal species at various locations during 27-29 August 1987.

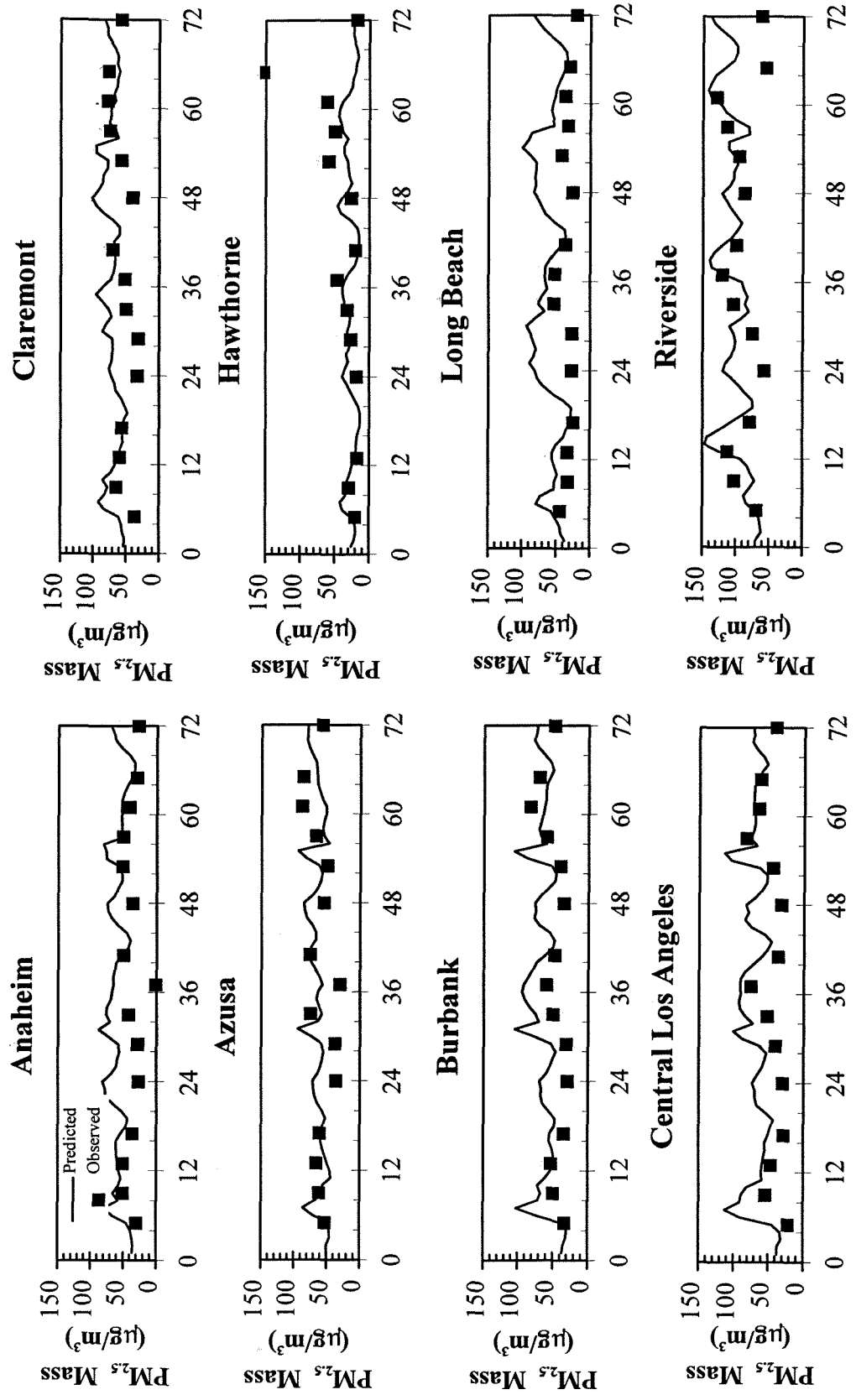

Fig. B.12 Time-series of predicted and observed $PM_{2.5}$ total mass at various locations during 27-29 August 1987.

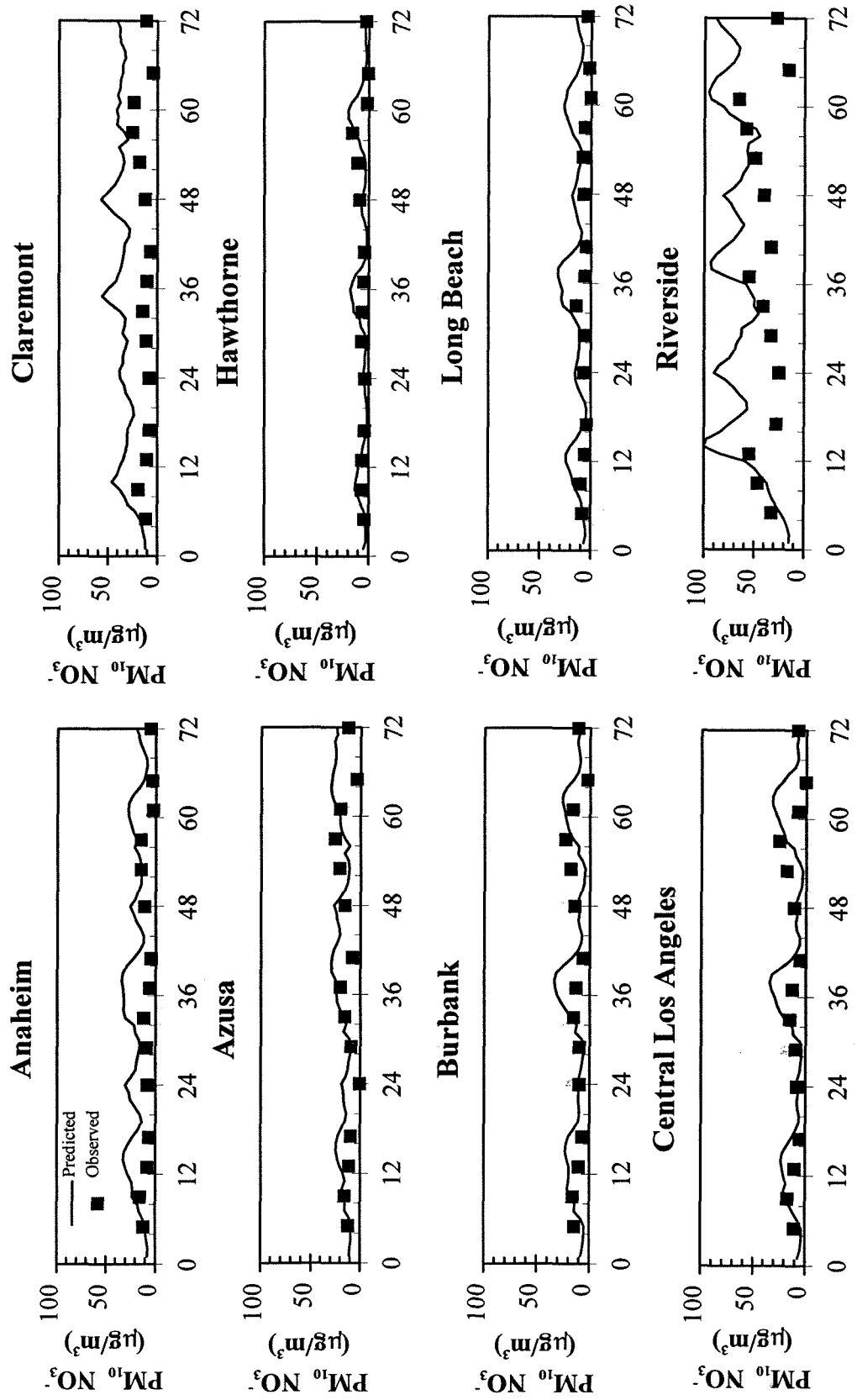

Fig. B.13 Time-series of predicted and observed PM_{10} nitrate at various locations during 27-29 August 1987.

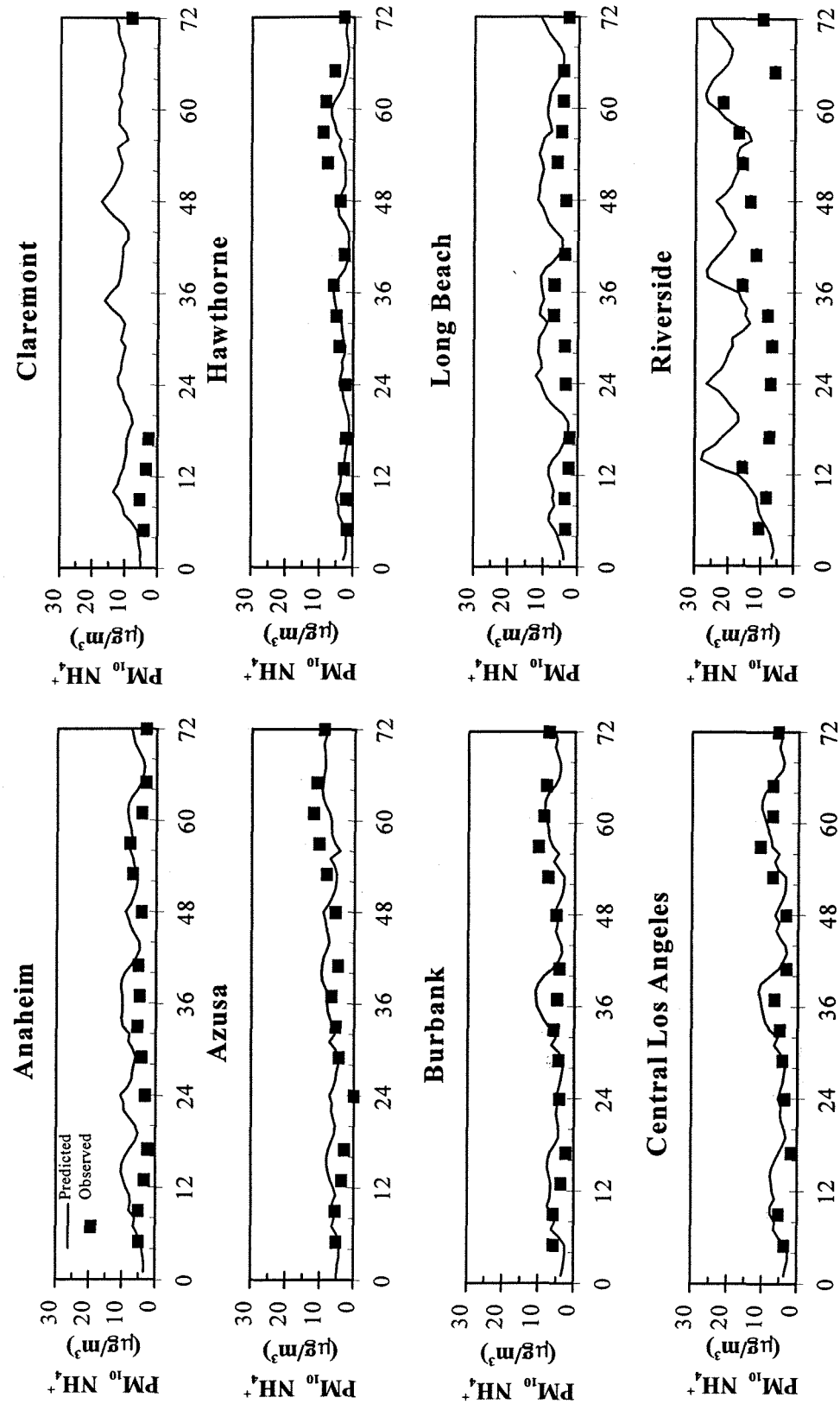

Fig. B.14 Time-series of predicted and observed PM_{10} ammonium at various locations during 27-29 August 1987.

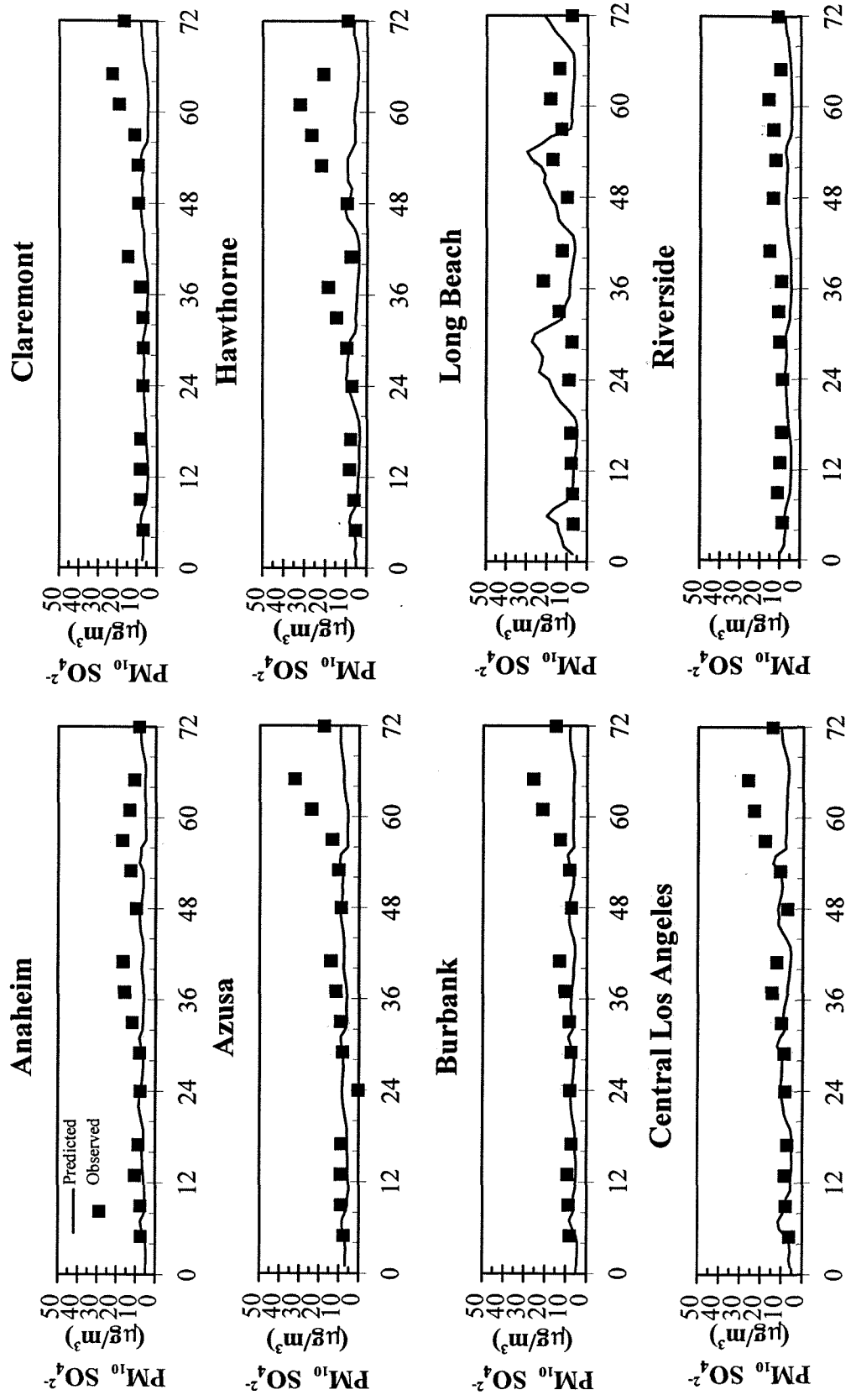

Fig. B.15 Time-series of predicted and observed PM_{10} sulfate at various locations during 27-29 August 1987.

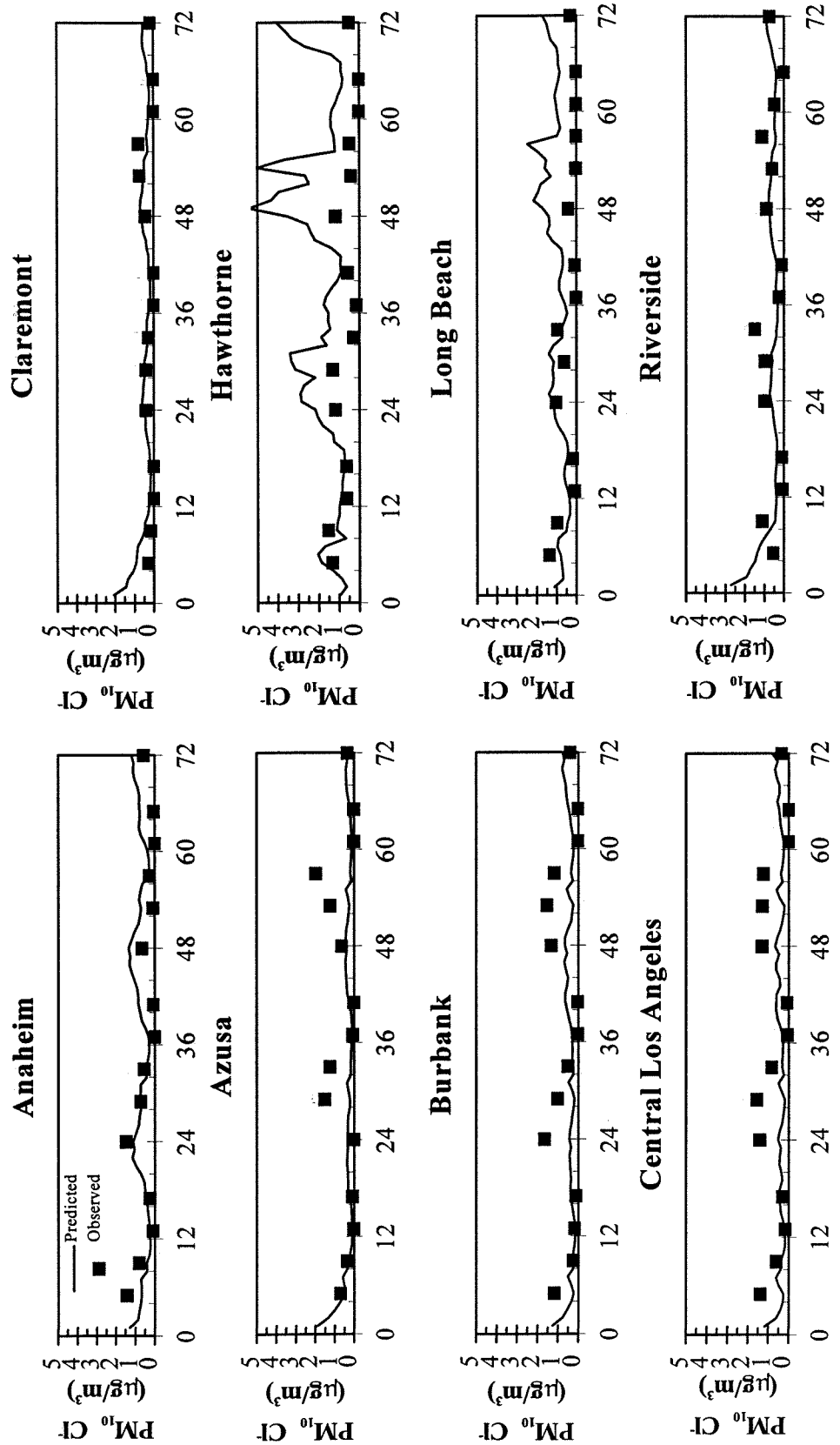

Fig. B.16 Time-series of predicted and observed PM_{10} chloride at various locations during 27-29 August 1987.

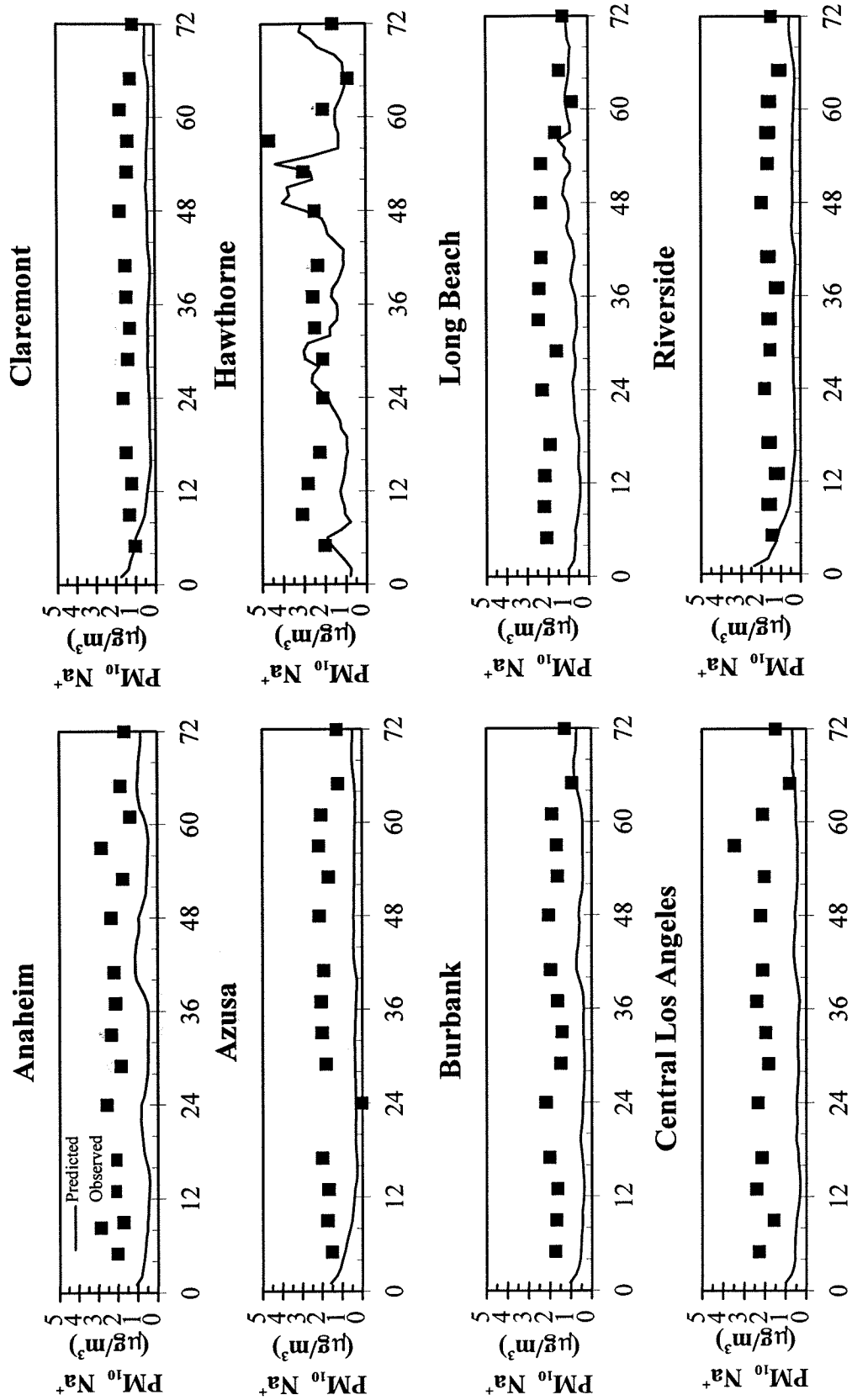

Fig. B.17 Time-series of predicted and observed PM_{10} sodium at various locations during 27-29 August 1987.

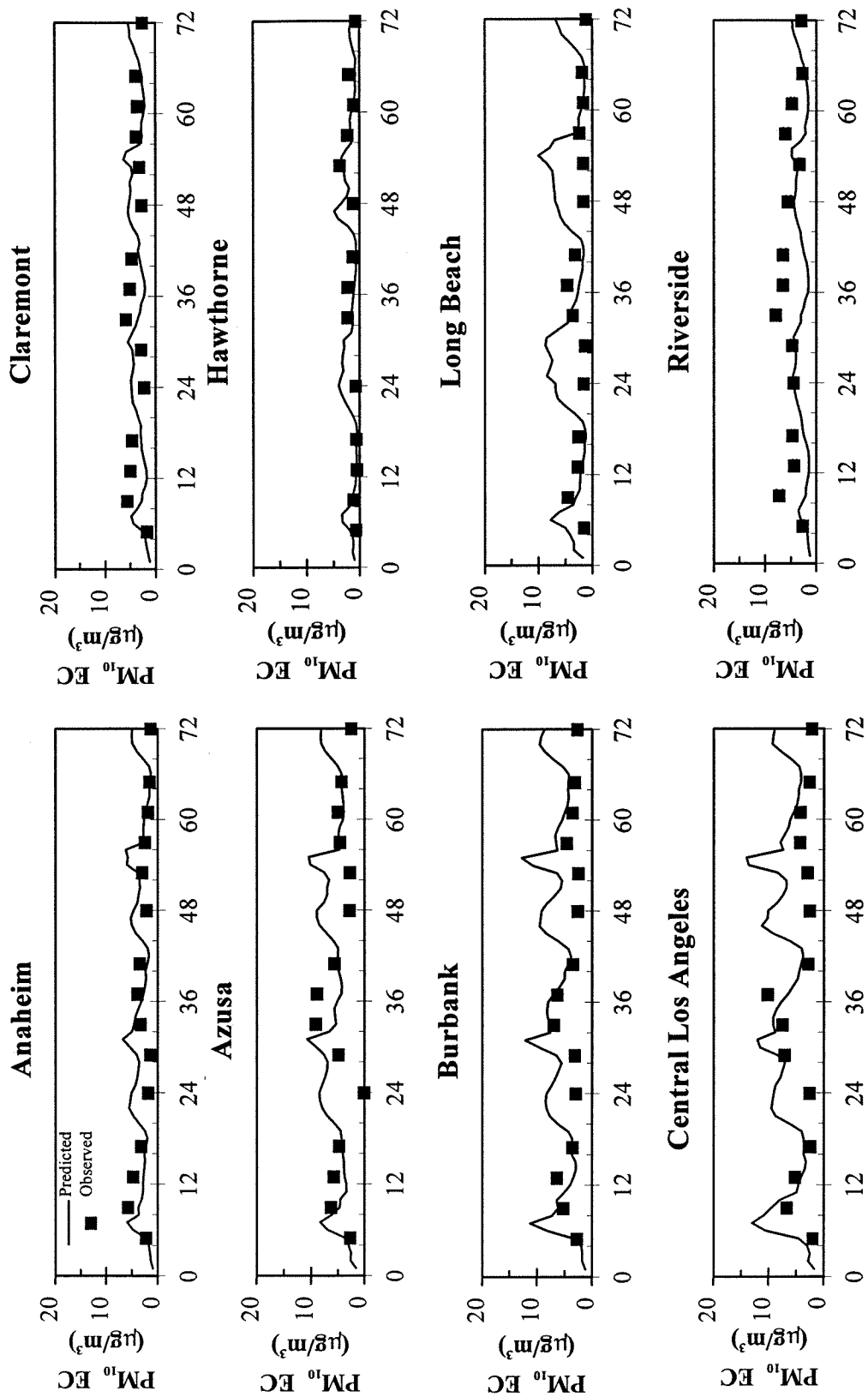

Fig. B.18 Time-series of predicted and observed PM_{10} elemental carbon at various locations during 27-29 August 1987.

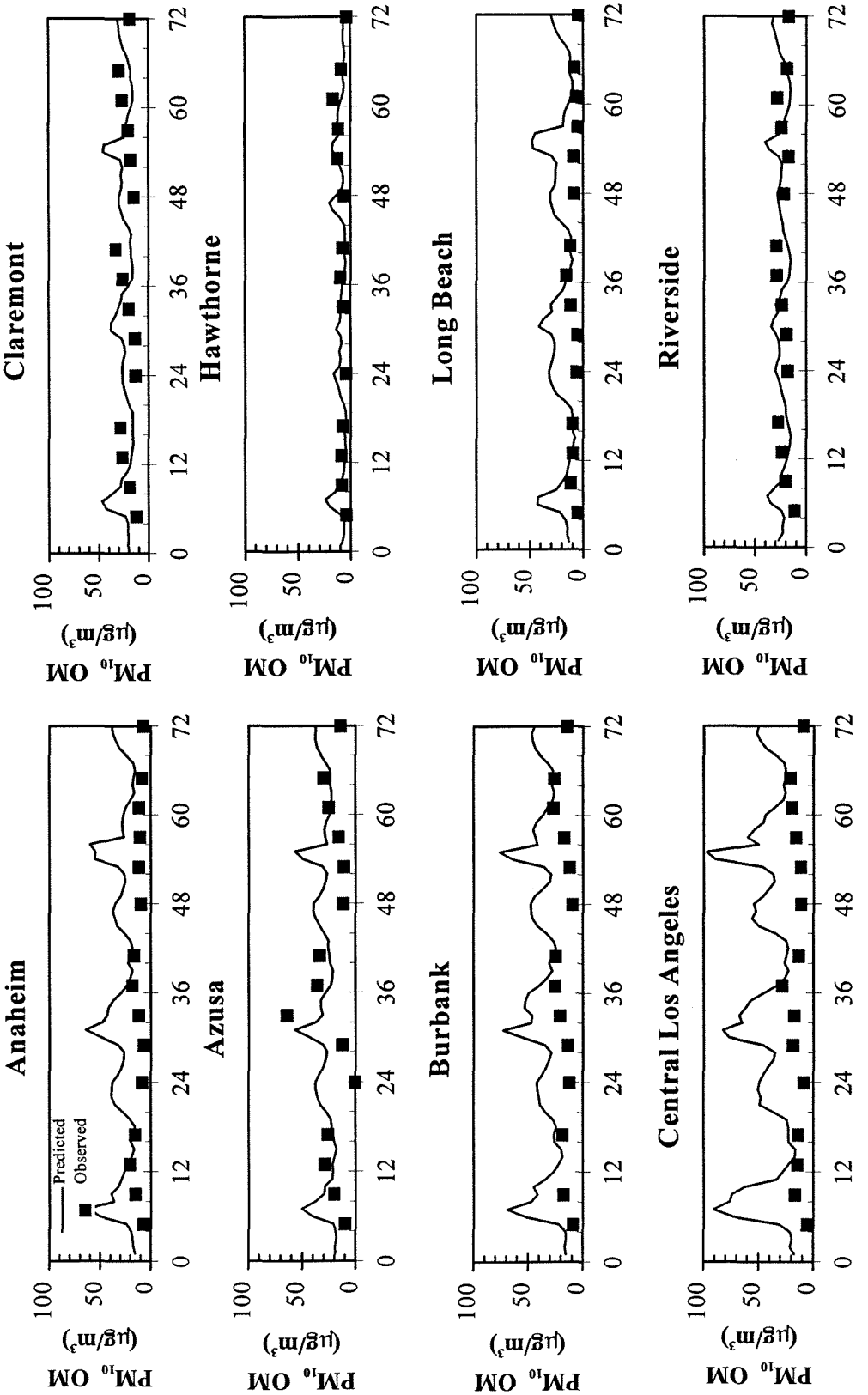

Fig. B.19 Time-series of predicted and observed PM_{10} organic matter at various locations during 27-29 August 1987.

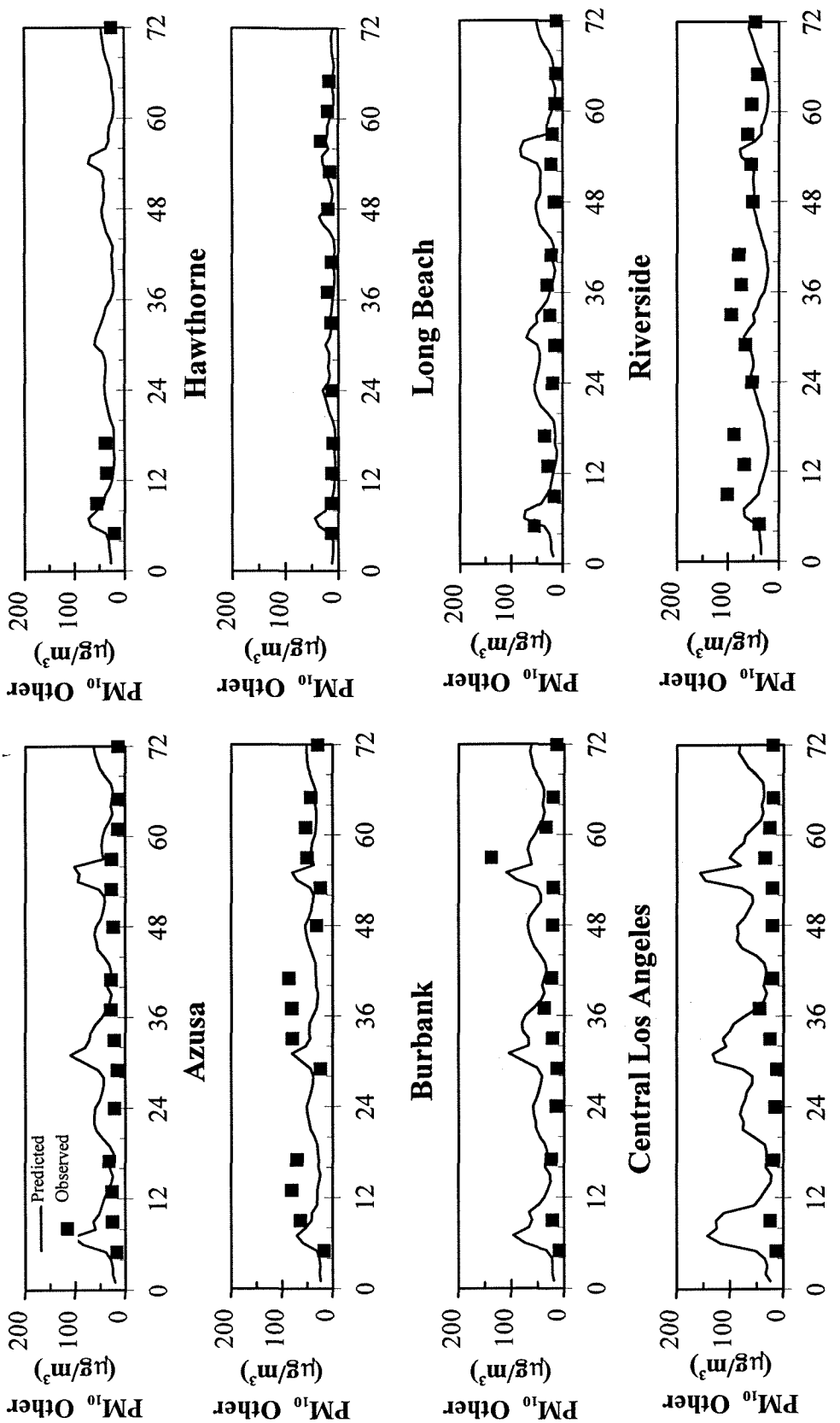

Fig. B.20 Time-series of predicted and observed PM_{10} crustal species at various locations during 27-29 August 1987.

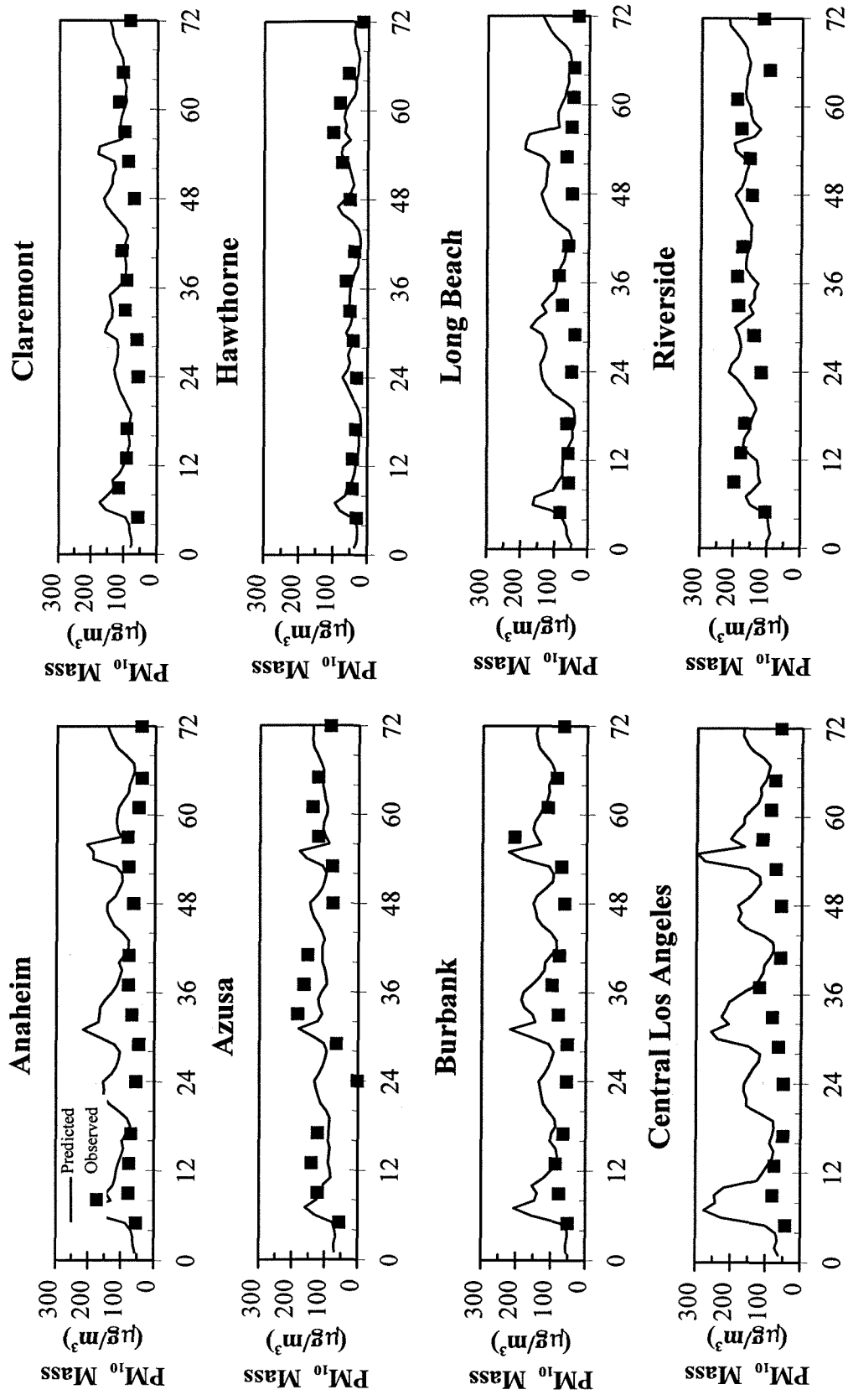

Fig. B.21 Time-series of predicted and observed PM_{10} total mass at various locations during 27-29 August 1987.